PHYSICAL CONDITIONS IN LOW-LUMINOSITY ACTIVE GALACTIC NUCLEI

Thesis by

Alexei Vladimir Filippenko

In Partial Fulfillment of the Requirements

for the Degree of

Doctor of Philosophy

California Institute of Technology

Pasadena, California

1984

(Submitted May 18, 1984)

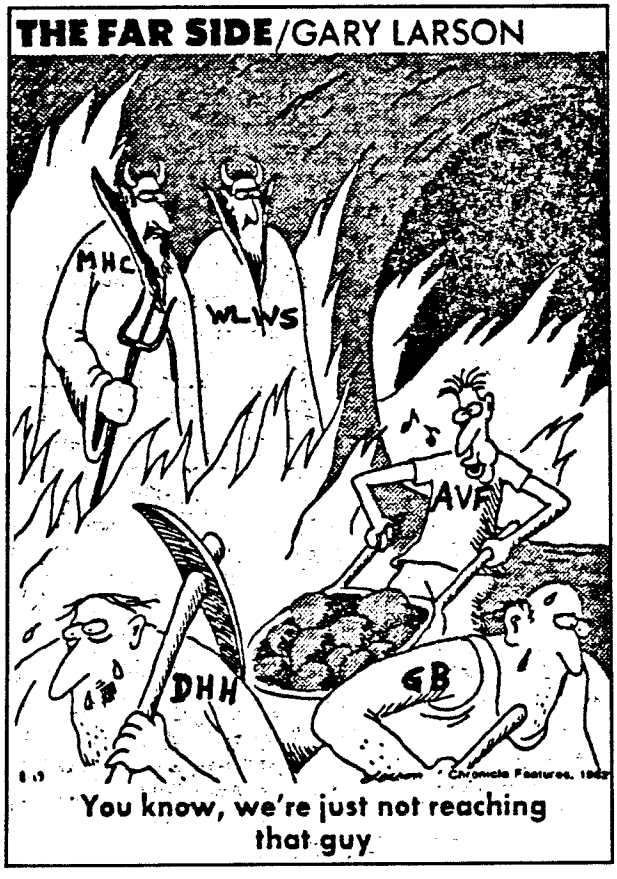
THE FAR SIDE/GARY LARSON
MHC
WLWS
AVF
DHH
GB
You know, we're just not reaching that guy

Маме и Папе,

которые подарили мне
маленький телескоп
одиннадцать лет тому назад
и познакомили меня
с чудесами вселенной.

"I'm afraid you've got a bad egg, Mr. Jones."

"Oh no, my Lord, I assure you! Parts of it are excellent!"

"Punch," Vol. CIX, p. 222 (1895)

ACKNOWLEDGEMENTS

I have spent nearly five years at Caltech, and wish to thank many individuals for making almost every day enjoyable. Someone will undoubtedly be omitted, but rest assured that you are not forgotten.

Foremost among those who influenced me is my thesis advisor, HMP Sargent. Wal taught me much of what is not available in the classroom: he provided tips on becoming a pundit, chasing crumpet, pouring beer, and understanding Sumo wrestling. He also affected my development as a scientist, and a large part of any success I may achieve will be a direct product of his advice and teachings. Maybe someday Wal will convince me that baseball is a finer sport than tennis, and that I shouldn't drink milk; this will probably not happen, however, until he agrees that tables of the Popsicle Angle are far more convenient than his (admittedly clever) toy, and that emission-line profiles in active galaxies, although obviously lacking the grandeur and romance of QSO absorption lines, can nevertheless be as exciting as I claim.

Bev Oke expressed great interest in my work and frequently gave useful advice. His course on galaxies taught me the necessary basics, and subsequent discussions sharpened my thinking on a number of matters (including the pernicious effects of Wood's anomalies in spectrographs). I will always enjoy associating with him.

Peter Goldreich's friendship is a special one since we share an active interest in tennis. Our (countably) infinite number of matches were most enjoyable and provided an important outlet which helped maintain my sanity. Peter also gave me sound scientific advice, and clarified some mysterious aspects of pulsars.

Speaking of pulsars, I must thank Tony Readhead and Marty Ewing for their patience while our project showed little progress due to my neglect. Part of the blame rests with V. Radhakrishnan ("Rad"), whose enthusiasm inspired me to spend much time theorizing about these curious objects. I do hope to complete our work in the "near" future.

Jesse Greenstein sets an example that everyone would do well to follow. The enormous energy with which he conducts research, and his overall approach to Life and Science, are truly wonderful.

I owe many thanks to Richard Feynman, whose contagious enthusiasm inspired a fellow student (Jeff Richman) and me to think carefully about the fundamental principles of general relativity, as well as measurement theory and the interpretation of quantum mechanics. Schrödinger's cat, the Bell inequality, and charged particles in gravitational fields filled my dreams during my first two years, and I will always consider our conversations a highlight of my graduate career.

Many other pundits were influential in one way or another. Peter Young's friendship and brilliance will never escape my memory; I only wish I could have helped him somehow. Fred Lo nominated me for the Miller Fellowship at UC Berkeley (which I accepted), and Peter Wannier introduced me to Fibonacci numbers in pinecones. Marshall Cohen and Bob Brucato kept me amused with queries and theories from the general public. Words of wisdom were provided by Roger Blandford, Jim Gunn, Al Moffet, Jeremy Mould, and Maarten Schmidt. Allan Sandage published marvelous descriptions of the spectra of many galaxies, from which I chose particularly interesting objects for further study.

Jules Halpern, my collaborator on several projects, introduced me to X-ray astronomy and helped me develop an intuitive, physical grasp of

photoionization models. He played an important role in my completion of this research, and kept me smiling when the going was rough. Other postdocs who offered useful advice include John Tonry, Greg Bothun, David Tytler, Dayton Jones, Steve Unwin, Wojciech Zurek, Jim Applegate, and my apartment-mate Todd Boroson. Thanks also to all the Santa Barbarians, who provided much friendship and assistance while running the other half of the Caltech/Carnegie circus.

Stan Peale taught, guided, and inspired me when I was an undergraduate at UC Santa Barbara. He was one of the main reasons why I chose to pursue research in astrophysics, and I hope to maintain our close friendship. David Cannell and Jim Hartle, from whom I learned much physics, also deserve a great deal of credit. My other comrades in Santa Barbara, including Mike Hanna and Victor von Salza, provided considerable entertainment whenever I returned.

Having spent a large number of memorable nights obtaining data at the Mt. Wilson, Las Campanas, and Palomar Observatories, I offer my sincerest thanks to the Directors (George Preston, Gerry Neugebauer, Maarten Schmidt) and Time Allocation Committees, the staff (cooks, electronics technicians, mechanical wizards), the Astro-electronics Lab, and everyone else associated with those picturesque mountain tops. Especially appreciated was the assistance of Juan Carrasco and Al Lilge (Big Eye), Bob Griffith, Skip Staples, and Dave Tennant (Pig Eye), Roger Higson (Hig Eye), Jim Frazer and Howard Lanning (Old Eye), and Angel Guerra and Fernando Peralta (South Eye). My apologies go to Bill Qualls for being such a dud and sleeping during most of the Palomar trips, to Larry Blakeé for shaving off my mustache, and to Ardith Birdsell for the milk incident. Steve Shectman, Gary Yanik, Ken Clardy, Bev Oke, Jim

Gunn, Fred Harris, Barbara Zimmerman, and Todd Boroson were among those most involved with the instruments and software. PHOBOS, DEIMOS, and their peripherals were of primary importance in reducing and analyzing the data, so I thank Judy Cohen, Kimo Yap, Mike Lesser, Dan Zirin (the Great ZAR), Peter Parnicky, and especially Tim Pearson and Keith Shortridge for keeping them healthy and willing most of the time.

A number of other people were particularly kind to me. Lilo Hauck always offered words of encouragement and had more confidence in me than I deserved. Marilynne Rice pulled me out of hot water several times, and Rhea Goodwin arranged some of the logistics for my travels. Ann Palfreyman and Linda Soha, as well as my paycheck-keepers Lorna Thayer and Jill King, were always pleasant to see. Helen Holloway amused me with interesting stories about the past, while Margaret Katz kept me from starving by providing lots of edible treats before colloquia. Finally, librarian Helen Knudsen was indispensable when I needed to find things like the "Publications of the Bohemian/Transylvanian Relativistic Observatory."

I feel especially fortunate to have taken three trips to Las Campanas, which were precursors to excitement and adventure too great (perhaps) for even a Jedi. How can I ever forget the thrill of being an accused terrorist at Machu-Picchu, tromping around in the Amazon Jungle among deadly snakes, discovering that feet freeze readily at elevations of over 5600 m, seeing penguins and huge iguanas side by side on the Galapagos Islands, and being bitten by a possibly rabid dog in Quito?

I am very grateful to the Fannie and John Hertz Foundation for providing full tuition and a nice salary throughout my graduate career. The Fellowship relieved me of much guilt when I asked Wal and others to

pay for travel expenses, page charges, and assorted goodies.

Graduate students spend a majority of their "spare" time together, and my association with protopundits and trolls in the dungeons of Robinson made life especially enjoyable. In particular, I wish to mention Don Schneider, who rarely lost a doughnut bet but was great fun to bait with outrageous or suggestive remarks; Roger Linfield, who introduced me to the cartoon which now forms the frontispiece of this thesis; Richard Simon, who warned me what Caltech is like even before I applied; Matt Malkan, who got the shock of his life in Beverly Hills one evening; Doug Rabin, who was remarkably good-natured the time I stole the basketball away from him; Richard Wade, with whom I had a pleasant stroll through the streets of Copenhagen (nudge, nudge, know what I mean?); John Hoessel, from whom I learned about Dimetrodons as well as big-time astronomy in the real world; Abi Saha, whose eyes will probably never recover from staring at RR Lyrae stars at the plate limit; Ken Young, who introduced me to the joys of the Anarchist Cookbook; Alain Porter, the new caretaker of the quote board and to whom I wish much success with strawberries and life; Mike Rich, who could make a lot of money by drawing cartoons but instead will probably end up marrying Kron 3; Jeff Pier, who claimed that I was anointed even before the memo appeared; Keith Horne, who introduced me to the pitfalls of asteroid occultations and almost convinced me to visit Ethiopia; Richard Gomer ("El Mysterioso"), who should combine his talents by studying muscular spasms of protozoa in giant molecular clouds; Graham Berriman, whose British heritage and wit provided me with valuable training in understanding the English Army; Dave Hough, who could have been a good kid except that he went into VLBI; James

Fillmore, who urged me to talk to a certain person; Bill Sebok, who would gladly tell you more about computers than you ever wished to hear; Howard Yee, whose knowledge of diseases I wouldn't trust too much; Rick Edelson, who is an excellent example of a stochastic process; Russell Redman and Kirk Borne, who sympathized while I was working on Jackson problems; Tom Lockhart and Michael Ashley, who chose to leave before it was too late; Kevin Lind, who should never have held a copy of MTW during his mug shot; Steve Kent, who built the P60 SIT Spectrograph and will go down in history for his "glitch"; John Biretta, who made the same mistake I did in attempting two theses; Steve Lichten, who got more personal telephone calls than all other students combined; Pawan Kumar, who will someday find a cosmic connection between solar oscillations and M87; and Jim McCarthy, who is attempting to achieve the impossible by building a good Echelle spectrograph. To all of you, and to all I've left out, I give my heartfelt thanks.

During the past year, someone very special entered my life and helped me finish this thesis. Barrie Trinkle provided much love, support, and happiness, for which I will always be grateful.

Finally, I thank my family for bringing me up in a good home, stressing the value of scholastic achievement and integrity, and encouraging me to satisfy my curiosity about the world through scientific investigation. My parents, grandparents, and brother always helped in every way, and this thesis is the least I can do to show them it was all worthwhile. Although the telescope through which Ivan and I often peered at the universe was very small, it inspired discussions and ignited a flame within me that will probably last a lifetime.

ABSTRACT

Physical conditions in the nuclei of emission-line galaxies are investigated by analyzing their continua and optical emission lines.

The strength and shape of the nonstellar continuum is derived for nine Seyfert galaxies. As in QSOs, it is described by a power law with slope ~ -1.1, and in the most luminous objects it flattens at blue and UV wavelengths. Even at minimum brightness it has no short-wavelength cutoff near 1 μm, eliminating the possibility that the near-infrared flux is dominated by thermal emission from hot dust grains.

A detailed analysis at optical and X-ray energies demonstrates that gas in the nucleus of NGC 7213 is photoionized by nonstellar radiation, even though it also exhibits the spectral characteristics of galaxies thought to be heated by shocks. After careful removal of the strong stellar component, it is shown how these "shock" features are actually more consistent with photoionization. The key is a large range of densities (~ 10^3-10^7 cm^{-3}) in the narrow-line clouds, and a fairly low ionization parameter.

Similar studies of three additional galaxies confirm these results and strengthen the hypothesis that gas in LINERs ("low ionization nuclear emission-line regions") is photoionized rather than shock-heated. A tight correlation is found between the width of forbidden lines and their critical density. Moreover, much of the ionizing radiation is probably produced by a hot (T ~ 10^4-10^5 K) accretion disk.

A sensitive survey indicates that ~ 30-40% of LINERs exhibit weak, broad Hα emission. The emission-line intensity ratios are consistent

with photoionization by a nonstellar continuum, indicating the presence of activity similar to (but much milder than) that of QSOs in a significant fraction of all nearby galaxies.

Relative intensities of emission lines in the narrow-line X-ray galaxy NGC 7314 are typical of type 2 Seyferts, but their widths (FWHM ~ 120-150 km s^{-1}) are remarkably small. Thus, nonstellar radiation need not be associated with rapid motions among the narrow-line clouds. The profile of the broad Hα emission suggests that gas flows ballistically away from the nucleus. Dust, which heavily reddens radiation from broad-line clouds, is probably located within or near the clouds themselves.

TABLE OF CONTENTS

INTRODUCTORY NOTE

This thesis represents an attempt to understand the physical conditions and processes which exist in the nuclei of emission-line galaxies. In particular, various emission-line profiles and intensity ratios are analyzed in order to determine the nature of the excitation mechanism in galaxies exhibiting low-luminosity Seyfert characteristics and in "low ionization nuclear emission-line regions" (LINERs). The research was inspired by articles I read and by discussions with galaxy pundits.

Much of the work was done in collaboration with my colleagues at Caltech. Matt Malkan initiated the project described in Chapter 1, while Jules Halpern contributed significantly to Chapters 2 and 3. Wal Sargent and I are trying to determine the faint end of the luminosity function of active galactic nuclei, and our first results are given in Chapter 5. Finally, Jesse Greenstein obtained data with the Multichannel Spectrophotometer for the stars in Appendix 2.

Each chapter is written as a self-contained article for publication. Chapter 1 and Appendix 1 are reprinted from The Astrophysical Journal (1983, 275, 477-492) and the Publications of the Astronomical Society of the Pacific (1982, 94, 715-721), respectively. Chapters 2 and 3 are scheduled to appear in the 1984 October 15 issue of The Astrophysical Journal. Appendix 2 will be published in the 1984 July issue of the Publications of the Astronomical Society of the Pacific. Chapter 4 has been submitted to The Astrophysical Journal. Chapters 5 and 6 will be submitted to The Astrophysical Journal Supplement Series and The Astronomical Journal, respectively.

CHAPTER 1

The Stellar and Nonstellar Continua of Seyfert Galaxies: Nonthermal Emission in the Near-Infrared.

Matthew A. Malkan and Alexei V. Filippenko

Reprinted from The Astrophysical Journal (1983, 275, 477-492).

When you have eliminated the impossible,

whatever remains, however improbable,

must be the truth.

"The Sign of the Four" (1890)

Sir Arthur Conan Doyle

THE ASTROPHYSICAL JOURNAL, 275:477–492, 1983 December 15

THE STELLAR AND NONSTELLAR CONTINUA OF SEYFERT GALAXIES: NONTHERMAL EMISSION IN THE NEAR-INFRARED

MATTHEW A. MALKAN AND ALEXEI V. FILIPPENKO
Palomar Observatory, California Institute of Technology
Received 1983 March 24; accepted 1983 May 26

ABSTRACT

Spectra having high resolution and excellent signal-to-noise ratios have been obtained for the nuclei of nine Seyfert galaxies. In Seyfert 1 nuclei the Mg I λ5175, Na I D λ5892, and Ca II λ8542 stellar absorption lines are extremely weak, indicating that galactic starlight does not contribute a significant fraction of the observed continuum. The relative amount of light (in a given aperture) due to the unresolved nucleus of each galaxy has been measured from direct images made with a silicon intensified target (SIT). Knowing the fraction of nuclear light which comes from stars, we deduced the total stellar and nonstellar continuum fluxes in the spectral range λλ5000–8600. Within a 10″ aperture stars contribute a sixth or less of the visual continuum in Mrk 335 and Mrk 509, one-fourth to two-fifths of that in NGC 4151, 5548, and 7469, and three-fifths of that in NGC 1275, 3227, and 4051. These fractions are accurate to 10%–15%. The starlight has colors which are typical of those in the disks of normal spiral galaxies. The nonstellar continuum is similar to that of quasars—it drops from the near-infrared to the visual like a power law with slope $\alpha \sim -1.1$ to -1.2, and in the brighter galaxies it flattens in the blue. Even at minimum brightness, the nonstellar flux has no short-wavelength cutoff near 1 μm, eliminating the possibility that the near-infrared flux is dominated by thermal emission from hot dust grains.

In an appendix, we report several weak emission lines that have not been previously seen in the spectra of active galactic nuclei. Some interesting characteristics of the broad permitted lines, as well as differences in the widths of various forbidden lines, are also mentioned.

Subject headings: galaxies: nuclei — galaxies: Seyfert — galaxies: stellar content — spectrophotometry

I. INTRODUCTION

Nearby Seyfert galaxies have been extensively investigated because they are bright and easy to observe. Their relatively faint nonstellar continuum is more difficult to study, however, because of substantial contamination from starlight. In particular, the spectral shape of the nonstellar continuum has not been unambiguously measured in any low-luminosity Seyfert galaxy; rather, many workers have simply *assumed* that it is similar to that of luminous quasars.

Direct imaging cannot in itself determine the galactic contribution, since much of the starlight may lie within the seeing disk and is inseparable from the pointlike (unresolved) nonstellar light. Nor is low-resolution spectrophotometry of the continuum adequate, as it cannot distinguish a large stellar component with a weak blue nonstellar continuum from a smaller stellar component with a strong red nonstellar continuum (Malkan and Oke 1983). The most effective spectroscopic indicators of a stellar population are prominent absorption lines such as the G band (λ4304), the Mg I *b* triplet (λ5167, λ5173, λ5184), and the Ca II near-infrared triplet (λ8498, λ8542, λ8662). These lines are presumably absent in any nonstellar continuum, and their strengths in normal galaxies are well known. The strong Na I D (λ5890, λ5896) and Ca II H (λ3968) and K (λ3934) lines can also be useful, but they may be contaminated by interstellar absorption in the host galaxy (Osterbrock 1978, 1983).

Osterbrock (1978, 1983) gave estimates or upper limits to the starlight components of many Seyfert 1 spectra from the strength of the Ca II K line. However, the slit size was small (2″.7 × 4″.0), so these measurements refer only to the nucleus. Direct imaging is required to estimate the starlight contribution seen in large apertures. In addition, the nonstellar light in Seyfert 1 galaxies is much bluer than that of stars, and it is therefore essential to measure the stellar flux at longer wavelengths, where its relative strength is greater. Finally, since the nonstellar continuum often varies by more than a magnitude on time scales of a month (Penston *et al.* 1974), images and spectra should be obtained contemporaneously. Malkan and Oke (1983) used this combination of slit spectroscopy and direct imaging of the Seyfert galaxies Mrk 3, Mrk 6, and NGC 1068. Their spectra

had reasonably good signal-to-noise ratios, but only 7 Å resolution, and it is not easy to separate weak absorption lines from adjacent emission lines.

In this paper, digital images of nine Seyfert galaxies are combined with coudé spectra having excellent signal-to-noise ratios and high resolution in order to more precisely estimate the stellar flux and to determine the nature of the remaining continuum. The observations are presented in § II, and the methods used to analyze them are outlined in § III. Section IV discusses the host galaxies, whereas § V examines properties of the nonstellar continuum. A brief summary of our main conclusions is given in § VI.

II. OBSERVATIONS

Direct images were obtained with the SIT Area Photometer (Kent 1979) on the Palomar 1.5 m telescope, as listed in Table 1. The data come in the form of a 256×256 array of square pixels, each 0".7 on a side, giving a $3' \times 3'$ field of view. To maximize the dynamic range, the photocathode was run at a relatively low gain, corresponding to a saturation level of 10,000 photons per pixel. The required integration times for our bright objects were still only 10–600 s, and two or three consecutive exposures of each galaxy were usually taken. The light passed through square filters selected to exclude significant contamination from emission lines. Most images were obtained through either a Gunn violet (v) filter (Thuan and Gunn 1976), with $\lambda_0 = 4000$ Å and $\Delta\lambda = 400$ Å, or a Wratten 88A filter, which gives $\lambda_0 = 7900$ Å, $\Delta\lambda = 1200$ Å, corresponding approximately to the i magnitude defined by Wade *et al.* (1980). A few images were obtained through narrow-band ($\Delta\lambda = 100$ Å) filters centered on either 6615 Å or 6760 Å, which were kindly loaned by Dr. H. C. Arp. For each galaxy, the filter was selected to avoid the strong Hα + [N II] emission lines; thus the 6760 Å filter was used for low-redshift galaxies, and the 6615 Å filter for objects of higher redshift. Comparison with the absolute spectrophotometric scans of de Bruyn and Sargent (1978) shows that contamination from line emission in all these filters was negligible.

An average zero-level picture was removed from each frame, and pixel-to-pixel sensitivity variations were eliminated by flattening with a lengthy exposure of the illuminated dome ceiling. The sky measured in a large (typically $\gtrsim 1'$) annulus centered on the galaxy was subtracted from each exposure. Since this correction was well determined, and generally less than 10% of the central brightness of the galaxy, it is a small source of uncertainty in the derived surface brightness profiles. The photometric zero points were set by several measurements of defocused standard stars and are accurate to 10%. Spatial distortions in the SIT frames were negligible in the regions of interest.

Spectra having ~ 1.6 Å resolution were obtained with a photon-counting Varo-Reticon detector (Shectman and Hiltner 1976) at the coudé focus of the Mount Wilson 2.5 m Hooker telescope. A small aperture ($\sim 1''.6 \times 3''.7$) isolated light from the nuclear seeing disk. An image

TABLE 1

JOURNAL OF OBSERVATIONS (UT)

Galaxy	Coudé Spectroscopy	Direct Imaging	Optical Spectrophotometry	Infrared Photometry
NGC 1068 ...	1982 Jan 4 (Mg)	1981 Oct 16	...	...
	1982 Nov 14 (Na)	1982 Mar 7	...	...
	1981 Oct 24 (Ca)	...	...	...
NGC 1275 ...	1981 Oct 22,23 (Mg)	1981 Oct 9,10,14,16	...	...
NGC 3227 ...	1981 Mar 29 (Mg)	1981 Apr 1	...	...
	1982 Nov 14,15 (Mg)	...	...	...
	1981 Jan 10 (Na)	...	...	...
NGC 4051 ...	1981 Mar 28 (Mg)	1981 Apr 1	1979 Jun 12	1978 Feb 22
	1982 May 22 (Mg)	1982 May 20	...	1980 Mar 25
	1982 Apr 19 (Na)	...	...	1980 Mar 30
	1982 May 21 (Na)	...	...	...
NGC 4151 ...	1981 Mar 29 (Mg)	1981 Apr 1	1980 Mar 9	1980 Feb 11
	1982 May 22 (Mg)	1982 Mar 7	1979 Apr 16	1980 Mar 30
	1982 Apr 19 (Na)	1982 May 20	...	1979 Apr 13
	1982 Apr 20 (Ca)	...	...	1979 May 6
NGC 5548 ...	1981 Mar 30 (Mg)	1981 Apr 1	1980 Mar 9	1980 Mar 30
	1982 May 22 (Mg)	1982 Mar 7	...	1980 Apr 15
	1982 May 21 (Na)	1982 May 21	...	...
NGC 7469 ...	1981 Oct 22 (Mg)	1981 Aug 9	1980 Sep 30	1980 Oct 25
	1982 Nov 14 (Na)	1981 Oct 10,15,17	1979 Jun 12	1979 Jun 29
Mrk 335	1981 Oct 23 (Mg)	1981 Aug 9	...	...
	1982 Nov 15,16 (Na)	1981 Oct 10,15,16	...	...
Mrk 509	1982 May 21 (Na)	1981 Aug 9, Oct 14,16	...	...

derotator was not used because of the unacceptably large light losses it would have caused. The sky was measured in an identical aperture displaced by ~ 6″, and appropriate corrections were applied when light from the galactic disk contaminated the sky spectrum. Owing to the very steep surface brightness profiles in Seyfert galaxies, these corrections were generally very small, but in several cases (e.g., NGC 1068) we obtained additional sky spectra a few arc minutes away from the object to achieve greater accuracy. Standard stars (Oke and Gunn 1983) were used to calibrate the instrumental response, and all observations were divided by the spectrum of an intrinsically featureless continuum from a tungsten lamp to remove local variations in the detector sensitivity. Wavelengths were calculated from Fe–Ar arcs taken several times throughout the night. There were gradual drifts in the wavelength scale, but the calibration should be accurate to ~ 0.3 Å. Atmospheric absorption lines were removed by comparison with the spectra of early B stars.

III. ANALYSIS

a) Direct Images

The radial surface brightness profiles for each object were derived by azimuthally averaging the signal as a function of distance from the image center. Repeated measurements on different nights show that these curves are accurate to 0.1 mag for radii up to 15″. The same information is also available as the integrated fluxes within a series of concentric circles centered on the peak brightness of the galaxy. A typical example of these two forms (differential and integral) of displaying the data is shown for NGC 5548 in Figures 1 and 2. The following analysis does not assume the galaxies are azimuthally symmetric: we simply refer all measurements to circular apertures for convenient comparison with other observations.

The galaxy profiles were then compared with those of field stars on the same frames to determine the resolved fraction of galaxy light. That is, a stellar (unresolved) seeing profile was scaled to match the galaxy profile in the central few arc seconds. Any remaining galaxy light above this profile is resolved and presumed to arise from stars, as shown in Figures 1 and 2. The scaled seeing profiles match the inner parts of the galaxy profiles with high precision: the residuals are only 2%–3%, smaller than the width of the lines in Figure 1.

The limiting source of error in this procedure was the accuracy with which the seeing profile could be determined at the time each Seyfert nucleus was measured. When a single frame had more than one bright stellar image, their surface brightness profiles were always very similar, with full widths at half-maximum (FWHM) ~ 1.″4–1.″9. On average, the seeing profile was independent of wavelength. However, there were small but

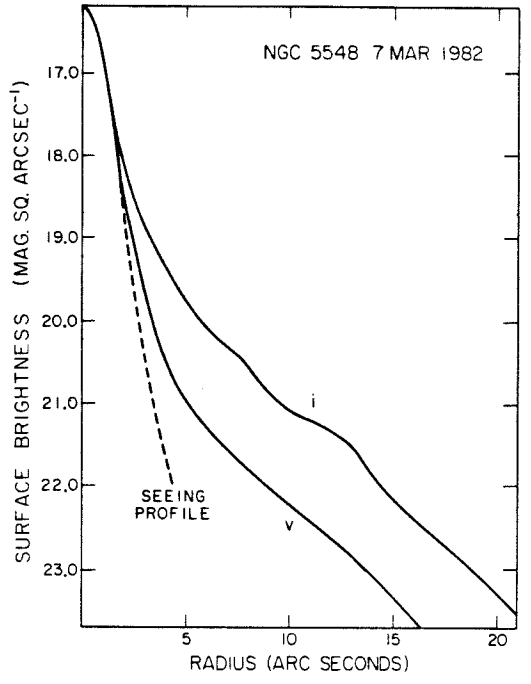

FIG. 1.—Surface brightness profiles of NGC 5548, observed through *v* and *i* filters. The violet and infrared fluxes are comparable in the predominantly nonstellar nucleus. At larger radii, the infrared/violet flux ratio increases, leveling off at the much redder color typical of a galaxy. The dashed line is a seeing profile, scaled to match the center of the *i* brightness distribution in NGC 5548. In other words, it shows the portion of light in NGC 5548 which is unresolved.

detectable changes in the profile of a single star observed in two consecutive exposures, and gradual changes in the seeing occurred throughout the course of a night. Roughly half of the program galaxies did not have a bright field star in the same frame, so we compared these with stellar images observed either immediately before or after the galaxy. Owing to the seeing fluctuations, our estimates of the unresolved fractions are only accurate to 10%–15%. That is, two stellar images obtained in the same part of a night were often not identical. Compared with the sharper image, the poorer one had up to 10%–15% of its light "resolved." This dominant source of error was reduced by averaging the results of several frames. Possible errors in the photometric zero points would not alter the *fractions* of resolved light we found by this procedure.

Our estimates of the fraction of resolved light in NGC 5548 and NGC 7469 agree with those obtained by de Bruyn (1982) in 1978 June. In several cases, galaxies were imaged on more than one night. Even when their nuclear brightness varied, we found the same amount of starlight present, to within 0.10–0.20 mag. This is a

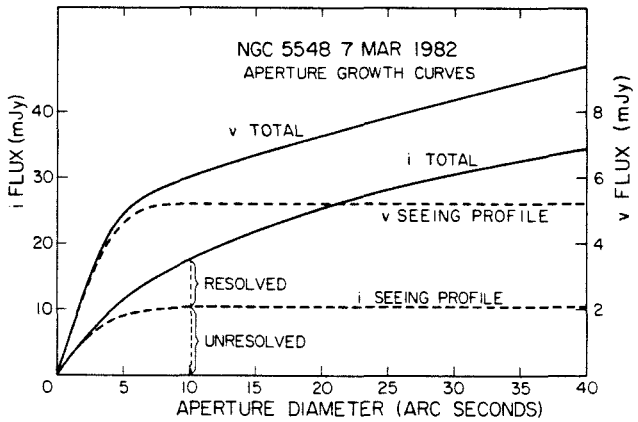

FIG. 2.—The integrated flux as a function of diameter enclosed by a circular aperture centered on the nucleus of NGC 5548. The scale for the violet fluxes is on the right; the infrared fluxes are plotted on a scale which is a factor of 5 larger. The dashed lines show seeing profiles (derived from images of field stars) normalized to match the galaxy growth curves at the smallest diameters. They correspond to the fraction of the light which is unresolved: 5.4 mJy at 4000 Å and 10.8 mJy at 7900 Å. The sharp bend in the v curve indicates that the nucleus of NGC 5548 dominates at 4000 Å; the image at 7900 Å is more extended because the starlight is much redder than the light from the nucleus.

reasonable measure of the total uncertainties associated with the estimates of starlight fluxes, which are listed in Table 2. The errors for NGC 3227 are somewhat larger since it was imaged on only one night.

b) Spectra

The unresolved continuum comes from the pointlike nonstellar nucleus and the starlight of the central part of the galaxy which falls within the seeing disk. Our spectra were used to estimate the ratio of unresolved stellar to nonstellar flux, under the assumption that the fraction of light in the nucleus due to stars is simply the ratio of the observed equivalent width of a stellar absorption line to its average value in the spectrum of an ordinary galaxy.

Figures 3–5 illustrate all of the spectra included in our analysis, with the exception of some repeat observations. The relative flux per unit frequency interval is plotted as a function of wavelength, and both scales are linear. Wavelengths have been reduced to the rest system of the observed galaxy. Since small apertures and long integration times were used, in some cases atmospheric dispersion produced substantially unequal light losses in different portions of a spectrum (Filippenko 1982). Therefore, to flatten the continuum for accurate measurements of absorption lines, every spectrum was normalized by fitting a cubic spline through the continuum and dividing the flux in each bin by the local value of the spline. This technique artificially removes any broad intrinsic spectral shape, so the true relative intensities of regions separated by more than ~100 Å

TABLE 2

FLUXES AT 5400 Å (mJy)

	WITHIN 10″ APERTURE		TOTAL STARLIGHT WITHIN APERTURE OF:			
GALAXY	Stellar	Nonstellar[a]	15″	20″	25″	30″
NGC 1068 ...	65	17	100	140	180	220
NGC 1275 ...	5.2	2.9	9.3	13	15	17
NGC 3227 ...	7.6	5.2	14	19	25	...
NGC 4051 ...	7.3	5.7	10	13	16	19
NGC 4151 ...	14	21/29[b]	21	28	34	40
NGC 5548 ...	3.4	6.9	5.6	7.4	9.0	10
NGC 7469 ...	6.8	7.5/12[b]	7.9	10	13	15
Mrk 335.....	1.5	7.4	...	...	...	...
Mrk 509.....	1.5	8.6	...	...	...	...

[a] The nonstellar flux (f_ν) is approximately a power law with slope −1.1 to −1.2 in all cases.

[b] The two nonstellar fluxes refer to measurements when the continuum was faint and when it was bright.

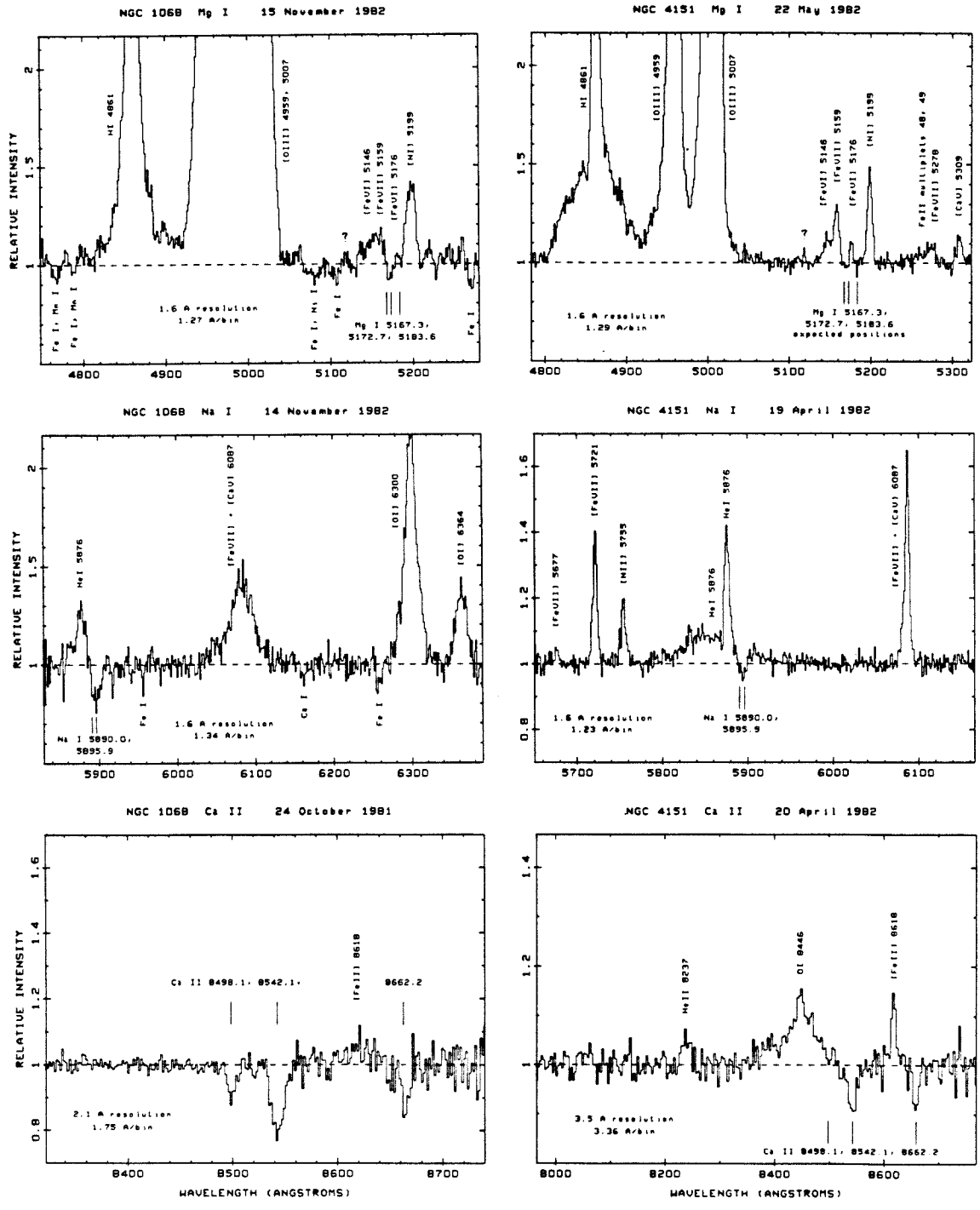

FIG. 3.—Coudé spectra, shifted to zero redshift, of NGC 1068 and NGC 4151 near the Mg *b*, Na D, and Ca II near-infrared absorption lines. The continuum has been normalized to unity in each case, and relative intensities refer to flux per unit frequency interval. Very low and high flux levels are not plotted in order to emphasize the continuum. The emission feature indicated by a question mark is an unidentified line at $\lambda \sim 5120$ Å.

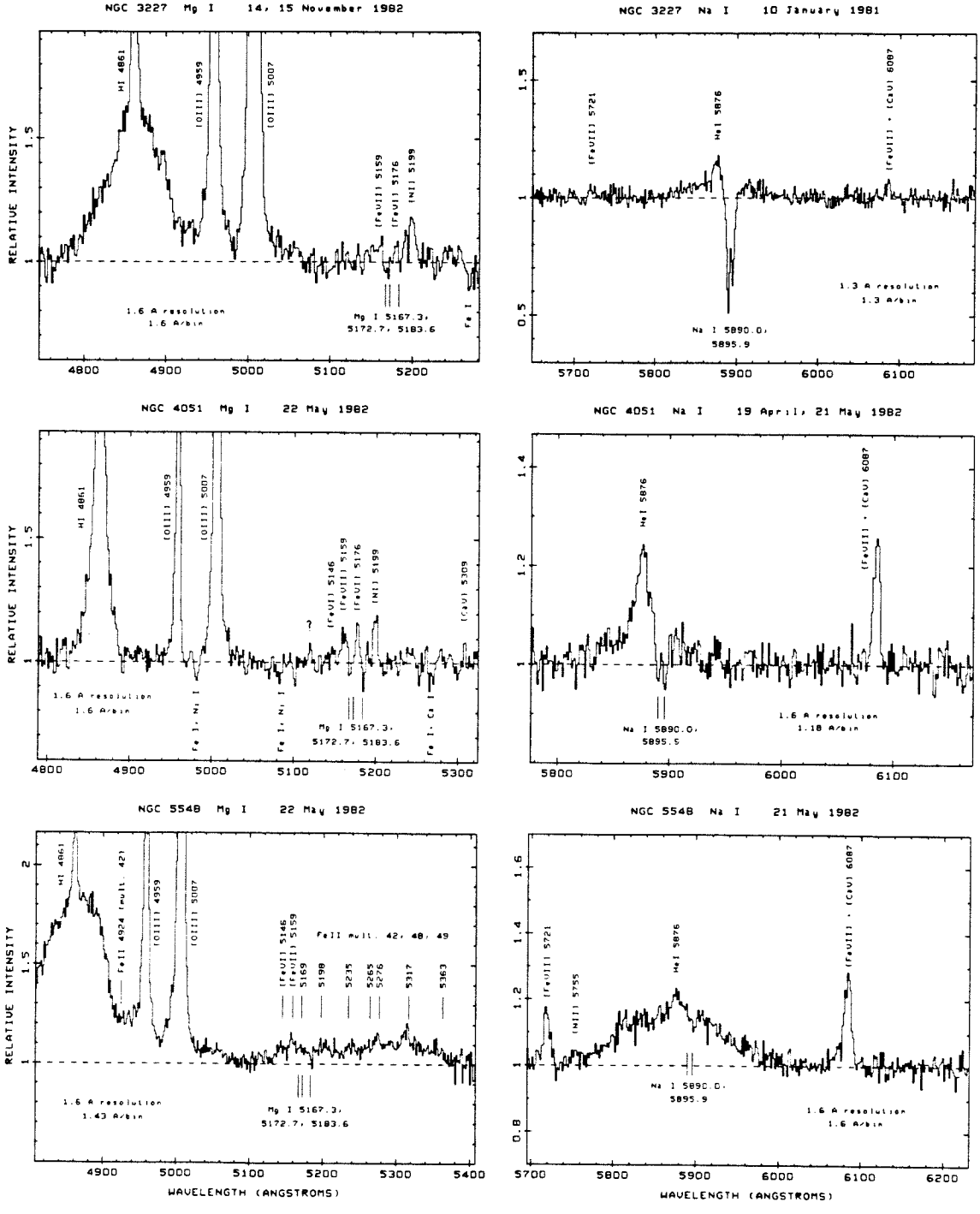

FIG. 4.—Same as Fig. 3, but for NGC 3227, 4051, and 5548 near Mg *b* and Na D

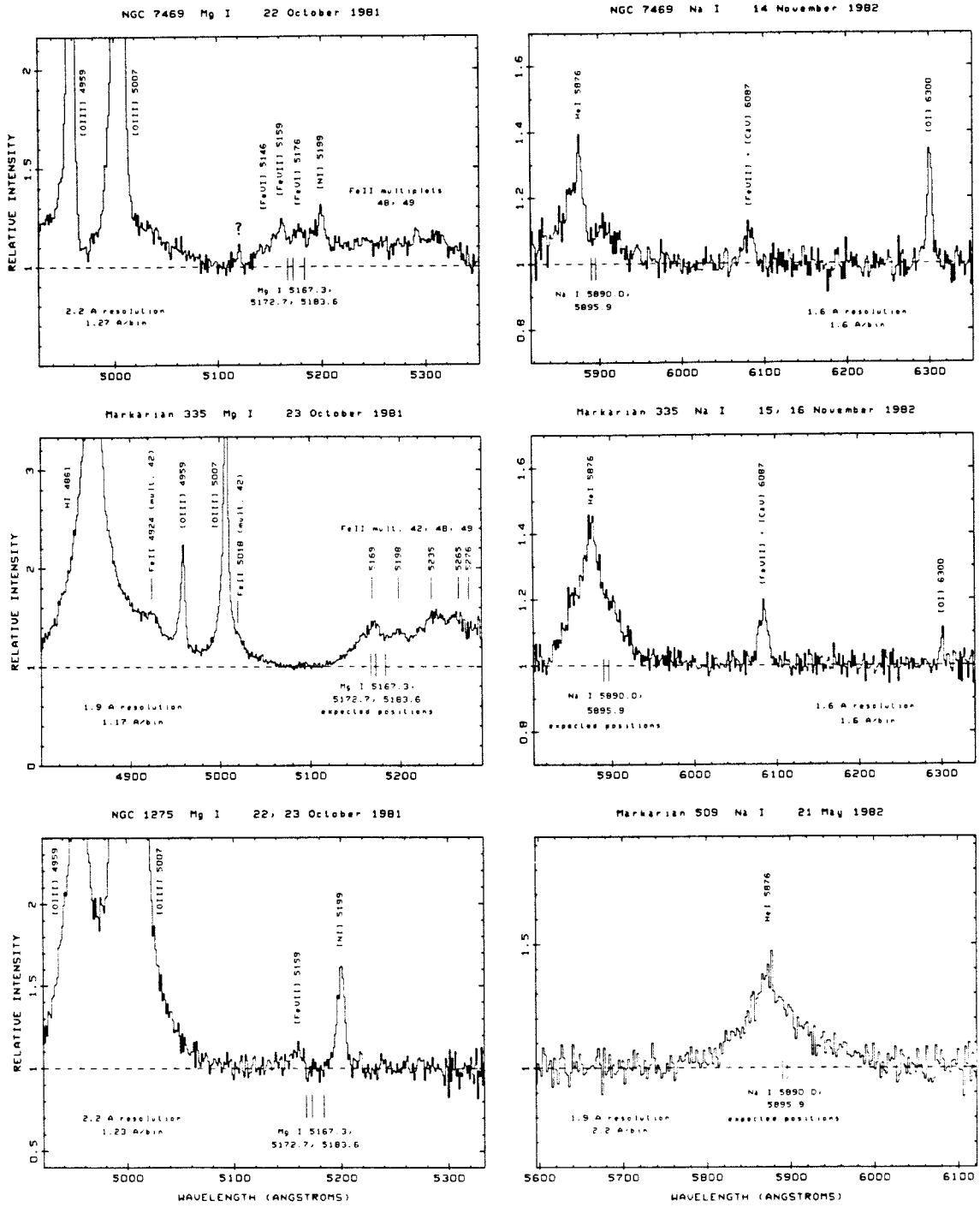

FIG. 5.—Same as Fig. 3, but for NGC 1275, NGC 7469, and Mrk 335 near Mg *b*, and for NGC 7469, Mrk 335, and Mrk 509 near Na D

are not displayed exactly. Note that in most spectra the relative scale is adjusted to emphasize the continuum, so very low or high flux levels are not plotted.

Although they are potentially useful indicators of starlight, the G band and the Ca II H and K lines were not observed because of the increasing proportion of nonstellar light and, in particular, the decreasing detector sensitivity at short wavelengths. Similarly, the Ca II near-infrared triplet could be measured in only the brightest nearby galaxies NGC 1068 and NGC 4151, as the efficiency of the system plummets longward of ~ 8000 Å.

Prominent emission and absorption lines (or the expected position of absorption lines) are marked on the spectra. The equivalent widths of absorption features were measured in the standard manner, but some difficulties were encountered with Mg *b* and Na D. For example, galaxies such as NGC 1068, 3227, 4051 and 4151 exhibit strong forbidden lines of nitrogen and highly ionized iron which contaminate the Mg *b* absorption, as well as narrow He I λ5876 near the Na D doublet. These emission lines could be removed to first order because the high spectral resolution adequately isolated them from the absorption lines. Permitted lines of Fe II presented an additional problem near Mg *b*, as can be seen in Mrk 335, NGC 5548, and NGC 7469. The spectra were compared with those published by Phillips (1977, 1978), and once again our high spectral resolution was necessary for accurate measurement of the absorption lines. Finally, a suitable correction was made to the equivalent width of Na D in objects which show broad He I λ5876 emission, and in spectra from which broad Na D emission (due to high-pressure sodium vapor lamps) could not be completely subtracted.

Our assumption that the spectra measure only unresolved nuclear light is conservative, since light from the galactic disk entered near the ends of the long (3″.7) aperture. Furthermore, if some off-nuclear light entered the aperture because of guiding errors or atmospheric dispersion, the strengths of absorption lines would be overestimated. Despite these effects, the absorption lines in most of the spectra are extremely weak, indicating that the unresolved light is almost entirely nonstellar.

Since some Na D absorption may arise from the interstellar medium of the host galaxy, the true equivalent width of the stellar absorption could be even smaller than the values listed in Table 3. NGC 3227 has extremely strong, narrow Na D absorption (Fig. 4), which seems inconsistent with its very weak Mg *b* lines. NGC 4051 also exhibits an easily resolved Na D doublet, in contrast to the stellar Na D absorption in the bulge of NGC 1068 (Fig. 3). The nucleus of NGC 3227 is obscured by $A_V \sim 1.4$ mag, and NGC 4051 could have half as much extinction (Malkan 1983*a*). We suspect that most of the Na D absorption in these two objects (and possibly in others as well) is interstellar. Na D absorption due to our Galaxy did not present any difficulties, since $cz \gtrsim 1000$ km s^{-1} for all of the Seyfert galaxies observed.

The equivalent widths of stellar absorption lines in the spectra of Seyfert nuclei are given in Table 3. Our measurements may be somewhat generous: the true widths could be less, but they certainly do not exceed the ones listed by more than ~ 25%, so it is unlikely that the contribution due to stars has been significantly underestimated. Since the absorption lines are very weak in most of the objects, we were concerned primarily with the danger of underestimating the starlight contribution; such an error would have an important impact on our conclusions. The small equivalent widths listed for the Mg *b* lines are in good agreement with the Ca K widths measured by Osterbrock (1978) in these objects

TABLE 3

COUDÉ SPECTROSCOPY: EQUIVALENT WIDTHS (Å)

Galaxy	Mg I *b*	Na I D	Ca II λ8542[a]
Average spiral[b] ...	4.5 ± 2.1	3.7 ± 1.6	3.2 ± 0.5
NGC 1068	1.7	2.9	3.0
NGC 1275	0.25	...	...
NGC 3227	0.75	4.2	...
NGC 4051	0.8	1.1	...
NGC 4151	0.2	0.8	1.1
NGC 5548	0.2	0.3	...
NGC 7469	0.3	0.7	...
Mrk 335.....	< 0.1	< 0.2	...
Mrk 509.....	...	< 0.25	...

NOTE: — The symbol < means line not detected or only marginally detected—upper limit given.

[a] Ca II refers to the width of one component of the triplet, at 8542 Å; the other two lines (8498, 8662 Å) were more difficult to measure.

[b] Average spiral: Mg *b* and Na D from Hartwick and Cowley 1980 and Stauffer 1983. Ca II from Cohen 1978.

c) Stellar and Nonstellar Fluxes

In order to determine the amount by which galactic absorption lines have been diluted by a nonstellar featureless continuum, we must know the intrinsic strengths of the lines. The spectra measured light from roughly the central kiloparsec of each object, where the bulge dominates the contribution from the disk component in early- and intermediate-type spiral galaxies. Since the integrated spectra of galactic bulges are dominated by red giants, the strengths of stellar absorption lines do not vary greatly from galaxy to galaxy. Cohen (1978) found that the near-infrared Ca II triplet lines have relatively constant equivalent widths in different galaxies and exhibit no spatial variations in a given object. The equivalent widths of Mg *b* and Na D in Table 3, taken from Hartwick and Cowley (1980) and Stauffer (1983), are averages over all types of spiral galaxies. The larger variations seen in the *b* and D lines are due to metallicity differences and dilution from the blue continuum of hot young stars.

Although these variations in equivalent width are a nonnegligible source of error in our analysis, it is likely that the stellar population in the nuclei of Seyfert galaxies more closely resembles that of elliptical or early-type spiral galaxies than that of late-type spirals. Thus, the *effective* scatter in the width of a line is probably smaller than indicated in Table 3. For example, late-type spiral galaxies exhibit relatively weak Mg *b* absorption, but their stellar population is probably not representative of Seyfert 1 nuclei since features such as Fe I λ5269, whose strengths should be comparable to that of Mg *b* (Osterbrock 1983), are not visible (except weakly in NGC 1068 and NGC 3227).

The direct imaging gives R, the ratio of resolved to total light within a 10″ aperture (as illustrated in Fig. 2). To compare estimates made at different wavelengths, we assume that the starlight spectrum is that of the "standard galaxy" of Yee and Oke (1978), in which the ratios of flux at 4000, 5200, 6600, and 8000 Å are 0.33:1.0:1.5:2.3. As illustrated by Malkan and Oke (1983), it is a good match to the integrated spectra of early-type galaxies and to the central regions of later-type spiral galaxies, which are dominated by bulge light from red giants.

The starlight flux at 5200 A in a 10″ aperture is given by

$$F_*(5200) = C_*(\lambda)\,F(\lambda)\left[R + (1-R)(\mathrm{EW}_{\mathrm{obs}}/\mathrm{EW}_*)\right],$$

where the measurements of *total* flux $F(\lambda)$, R, and absorption equivalent width ($\mathrm{EW}_{\mathrm{obs}}$) are made at a wavelength λ. The quantity $C_*(\lambda)$ is the standard galaxy color $F_*(5200)/F_*(\lambda)$, and EW_* is the equivalent width of the absorption line in the case of pure starlight. The first term, $C_*(\lambda)F(\lambda)R$, is the resolved (extended) flux, which is, by assumption, entirely stellar. The second term is the portion of the unresolved nucleus which is starlight, as manifested by absorption lines in our spectra. In all objects the first term is larger than the second, since ($\mathrm{EW}_{\mathrm{obs}}/\mathrm{EW}_*$) is typically 0.05–0.20 and tends to be smallest when R is small (e.g., in Mrk 335 and Mrk 509).

Errors in the photometric zero points [leading to incorrect $F(\lambda)$] and those in the galaxy color $C_*(\lambda)$ propagate linearly as errors in the estimated stellar flux. We confirm in § IV that the galaxy colors are indeed very similar to those of our standard galaxy, so the second source of error is negligible. For the values listed in Tables 2 and 3, it is evident that the dominant source of error comes from 10%–15% uncertainties in R, although the second term tends to offset errors in the first. As long as a portion of the seeing disk is contaminated by starlight (i.e., as long as $\mathrm{EW}_{\mathrm{obs}}/\mathrm{EW}_*$ exceeds zero), the resolved flux ratio (R) tends to increase as the seeing improves, but this improvement in the seeing also decreases $\mathrm{EW}_{\mathrm{obs}}/\mathrm{EW}_*$. If the seeing is *identical* during the direct and spectroscopic observations, its effects cancel. On the other hand, if it is much *worse* during the direct observations, the starlight flux is underestimated. It is probable that any differences in our observations were actually in the opposite sense: the direct images were generally obtained under slightly better seeing conditions than the spectra (if we include guiding errors in the effective "seeing"). In the next section we confirm that seeing did *not* lead to an underestimate of the stellar flux.

The additional photometric errors and uncertainties in EW_* lead to estimates of stellar and nonstellar flux in Table 2 that are accurate to 15%–20%. Aperture growth curves were used to calculate the total amount of visual continuum flux from stars in 10″–30″ apertures (Table 2).

IV. THE HOST GALAXIES

Having separated the stellar and nonstellar continuum in each Seyfert nucleus, we can now compare the host galaxies with others which lack active nuclei. As Yee (1983) concluded for 11 Seyfert 1 galaxies, the nuclear colors (dominated by nonstellar light) are much bluer than those of starlight. But it is relatively easy to measure the colors at radii larger than 5″, where contamination from the unresolved nucleus is negligible. The starlight colors measured 5″–30″ from the nuclei of NGC 4051, 4151, 5548, and Mrk 335 are approximately the same as those of the standard galaxy. Colors were not measured in NGC 3227 and Mrk 509.

The type 2 Seyfert galaxy in our sample, NGC 1068, shows little color change from the nucleus to a radius of ~ 7″. At larger radii (8″–17″), the color becomes bluer than that of a standard galaxy by 0.2 mag in $v - r$. This is due to the contribution from bright rings of H II regions and their associated young stars, which are

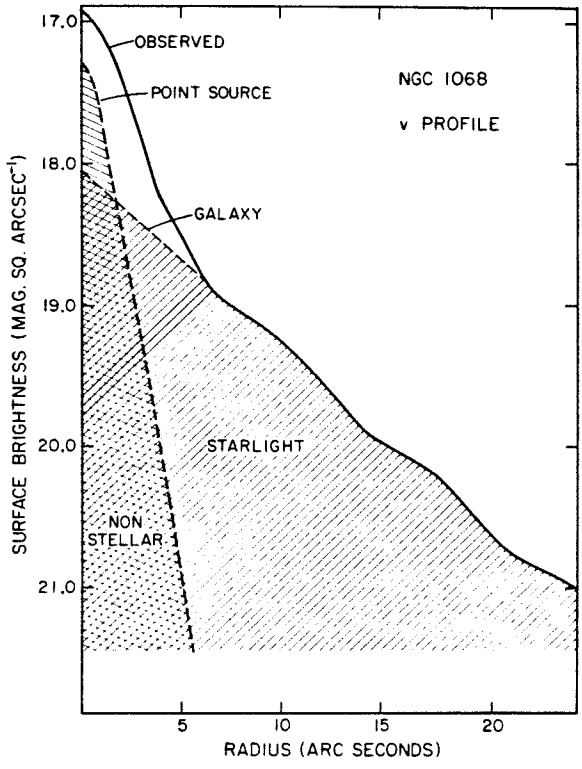

FIG. 6.—The observed violet surface brightness profile of NGC 1068, and its decomposition into an unresolved nonstellar component (*hatched region bounded by the dashed line labeled "point source"*) and a galactic starlight component (*hatched region bounded by the dashed line labeled "galaxy"*). The sum of the nonstellar and stellar components is equal to the observed profile (*solid line*). Integrating the galaxy curve and assuming a normal starlight color yields the stellar flux estimates given in Table 2. At the nucleus ($r \sim 0$) stars make up about a third of the light at v, in excellent agreement with the spectroscopic results.

evident on photographs having short exposure times (Alloin *et al.* 1981). The FWHM of the Na D and Ca II near-infrared lines is 470 ± 40 km s^{-1}, and the corresponding velocity dispersion (200 ± 20 km s^{-1}) is at the high end of observed values in bulges of spiral galaxies (cf. Kormendy and Illingworth 1982).

We checked our estimates of the stellar flux *in the nucleus* at several different wavelengths to see if they are consistent with the light from a standard galaxy. In all cases except NGC 1275, the inferred galaxy colors are the same as those of the standard galaxy to within 0.1–0.2 mag. NGC 1275 is unusual in that $v - g$ does not change by more than 5% from the nucleus out to a radius of 15″. Thus, its nucleus and the nearby starlight both have roughly the same blue color, $v - g \sim 0.25$, which is several tenths of a magnitude bluer than the standard galaxy. The additional blue light around the nucleus of NGC 1275 probably comes from a population of young stars, as has already been revealed by previous observations of Balmer absorption lines in off-nuclear spectra (Minkowski 1968).

We agree with Yee (1983) that the starlight in most Seyfert galaxies has the colors of typical spiral disks. That is, it is only slightly bluer than an elliptical galaxy. Malkan, Margon, and Chanan (1983) found the same result from imaging quasars of low redshift selected from X-ray surveys.

The surface brightness profiles allow one critical check for consistency with the spectroscopy. As illustrated in Figures 6 and 7 for NGC 1068 and NGC 4151, we can use the images to estimate the total stellar flux by a method which is completely independent of the spectroscopy. Guided by the portion of the profile outside $r = 3''$, which is entirely starlight, we smoothly extrapolate (as indicated by the thin dashed line) the galaxy flux to $r = 0''$, much as Yee (1983) did in his analysis. We then compare the inferred central surface brightness of the stars with the observed central surface brightness to find what fraction of the nuclear light is stellar. Approximately a third of the v light in the nucleus of NGC 1068 is predicted to be stellar, and in NGC 4151 stars should contribute a tenth of the v light and a third of the

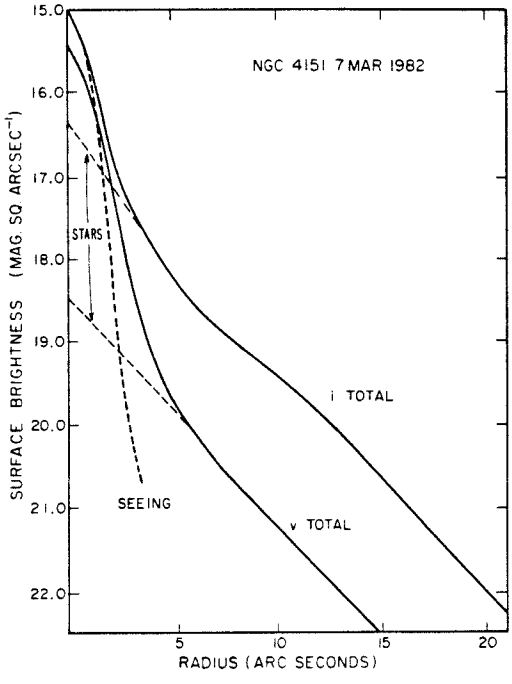

FIG. 7.—The observed v and i surface brightness profiles of NGC 4151. The starlight component is shown extrapolated into the nucleus by the thin dashed lines. The i seeing profile is shown by the heavy dashed line.

i light. These predictions are in excellent agreement with the observed absorption-line strengths, confirming our assumptions that the seeing was similar during the direct and spectroscopic observations, and that the intrinsic strengths of absorption lines in the stars were normal.

V. THE NONSTELLAR CONTINUUM

The estimates of starlight flux in the preceding section allow us to isolate the spectra of the nonstellar continuum. Several of the galaxies in this program have been observed nearly simultaneously at infrared and optical wavelengths. The observing dates are given in Table 1. Optical spectrophotometry was obtained through a 10″ aperture by de Bruyn, Sargent, and Readhead (1982) with the multichannel spectrometer (Oke 1969) on the Hale 5 m telescope. Near-infrared photometry (1.2–3.5 μm) was obtained with the Las Campanas du Pont 2.5 m and Mount Wilson 1.5 m reflectors, or taken from previous studies by Rieke (1978), McAlary *et al.* (1983), Cutri *et al.* (1981), Rudy *et al.* (1982), McAlary, McLaren, and Crabtree (1979), and Balzano and Weedman (1981). Our new infrared photometry is presented in Table 4. Most of the measurements were made with 8″–12″ apertures, so that only very minor corrections were required before combining the infrared with the optical observations, as has been done in Fig. 8. The data are plotted as vertical bars. We also include measurements made at 10 μm, although generally these were not simultaneous with the other observations. If there is significant variability at 10 μm in any of these galaxies, this portion of the composite spectra should be considered more uncertain.

In Mrk 335 and Mrk 509, the correction for starlight included in a 10″ aperture is 15% or less and can almost be ignored completely. The corrected nonstellar continua look very similar to the multichannel spectra published by de Bruyn and Sargent (1978). However, starlight comprises a significant fraction of the light within 5″ of the nucleus in all of the other Seyfert galaxies. Figure 8 shows the infrared and optical spectra of NGC 4051, 4151, 5548, and 7469 obtained through a 10″ aperture. Channels containing strong emission lines were excised. The dashed line shows the estimated flux due to stars (from Table 2), and the solid line is the remaining nonstellar light (which is the difference between the bars and the dashed line). Although optical and infrared photometry is available for NGC 1275, we did not attempt a subtraction because, as discussed above, we suspect its starlight is bluer than that of the standard galaxy. For two galaxies, NGC 4151 and NGC 7469, combined infrared and optical data are available

TABLE 4

NEW INFRARED MAGNITUDES

Galaxy	J(1.2 μm)	H(1.6 μm)	K(2.2 μm)	L(3.5 μm)	N(10.6 μm)	Aper.	Date	Tel.[a]
NGC 1068	...	...	...	...	0.96 ± 0.16	9	1979 Sep 6	M60
NGC 1275	...	...	9.83 ± 0.08	...	4.14 ± 0.24	12/9[b]	1979 Sep 7	M60
NGC 7469	...	...	9.14 ± 0.08	...	4.12 ± 0.19	12/9[b]	1979 Sep 6	M60
	10.97 ± 0.03	10.08 ± 0.03	9.34 ± 0.03	8.25 ± 0.05	...	11	1980 Jun 29	L100
	10.54 ± 0.03	9.80 ± 0.03	9.14 ± 0.03	8.00 ± 0.05	...	18	1980 Jun 29	L100
	10.35 ± 0.03	9.57 ± 0.03	9.00 ± 0.03	...	...	63	1980 Aug 1	C36
Mrk 335	...	...	...	...	5.47 ± 0.21	9	1979 Sep 7	M60
Mrk 509	11.99 ± 0.03	11.14 ± 0.03	10.18 ± 0.03	8.70 ± 0.05	...	10	1980 Jul 3	L100

[a] M = Mount Wilson, L = Las Campanas, C = Cerro Tololo. Numbers refer to telescope mirror diameter (inches).
[b] Larger aperture refers to measurement at shorter wavelength.

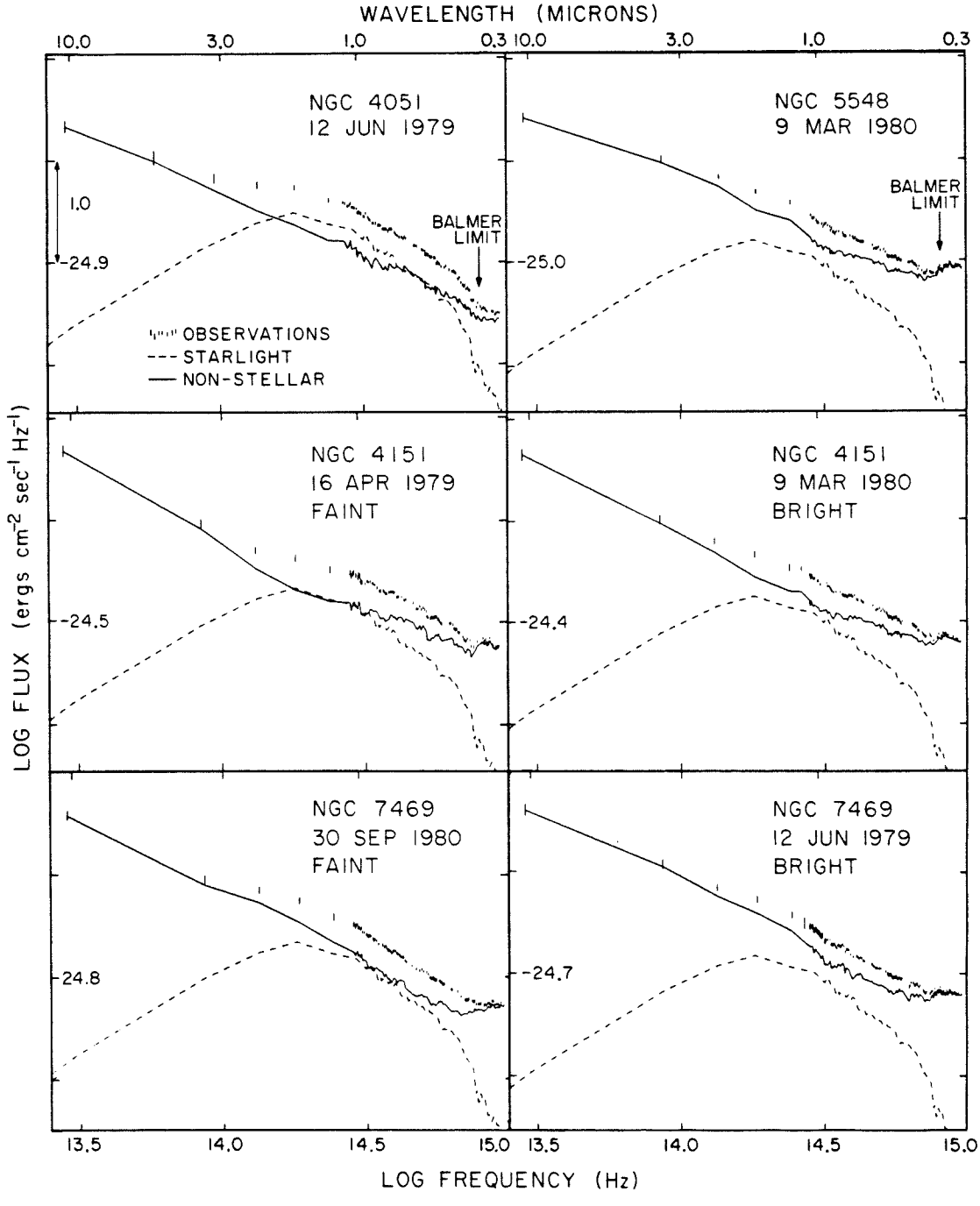

FIG. 8.—Decomposition of the spectra of NGC 4051, 4151, 5548, and 7469 at optical and infrared wavelengths. Bars represent the total observed fluxes in a 10″ aperture. The dashed line shows the amount of flux due to starlight, as given in Table 2, and the solid line is the remaining nonstellar flux found by subtracting the dashed line from the observed fluxes. Arrows indicate the frequency of the Balmer limit. All objects have a marked contribution from blended Balmer lines and continuum which reaches its maximum value at 3650 Å. The spectra on the left side have low-luminosity nonstellar components, which resemble a power law of slope −1.2, but with slight downward curvature. Those on the right have brighter nonstellar components which are more similar to the spectrum of Mrk 509.

for two epochs—one in which the nuclei were near their maximum brightness, and one when they were near minimum. NGC 4051 has never shown optical variations greater than ~ 0.3 mag.

All of the nonstellar spectra exhibit a decrease in slope near 4000 Å ($\log \nu = 14.875$) and then level off at ~ 3650 Å ($\log \nu = 14.915$). Malkan and Sargent (1982; hereafter MS) have already seen this feature in six Seyfert galaxies. The exact wavelength coincidence lead them to attribute it to blended Balmer lines and strong emission in the Balmer continuum. Our results strengthen their view that it is always present in the spectra of Seyfert galaxies.

In Figure 9 we have shifted the nonstellar spectra on top of each other, in two distinct groups. The "faint" group includes NGC 4151 and NGC 7469 near minimum, and NGC 4051. These spectra are slightly steeper and show no indication of any flattening before the Balmer jump which could be attributed to thermal emission (MS). The "bright" group includes NGC 4151 and NGC 7469 near maximum, and NGC 5548. Their nonstellar spectra are almost identical to the spectrum of Mrk 509, which is plotted for comparison. They show a small but significant flattening in the visual, considerably *before* the blending of Balmer lines merges into the Balmer continuum. This characteristic "ultraviolet excess" (or "blue bump") is present in nearly all luminous Seyfert 1 galaxies and quasars. It has been analyzed in detail by MS and by Malkan (1983*b*), who found that it is best interpreted as thermal emission from optically thick accreting gas. The two least luminous Seyfert galaxies studied by MS were NGC 4151 and NGC 5548, for which only an upper limit on the strength of the thermal ultraviolet emission could be established. The present measurements of starlight in NGC 4151 and NGC 5548 provide a more precise estimate of their nonstellar spectra, and it is now evident that when they are bright, they also flatten around 5500 Å (Fig. 9). Thus, the less luminous Seyfert nuclei can show the same signature of optically thick thermal ultraviolet emission that MS concluded was present in all brighter objects.

All the nonstellar spectra slope down from 10 μm to the visual roughly like power laws ($f_\nu \propto \nu^\alpha$) with slopes (α) of -1.1 to -1.2. This characteristic shape is commonly seen in most broad emission-line objects, as discussed by MS. A closer look reveals that the spectra are not exactly described by power laws but usually have a slight downward curvature, as mentioned by Malkan (1983*b*) and others. The logarithmic slope from 0.8 to 2.5 μm is one- or two-tenths steeper than the slope from 2.5 to 10 μm. It seems reasonable to expect

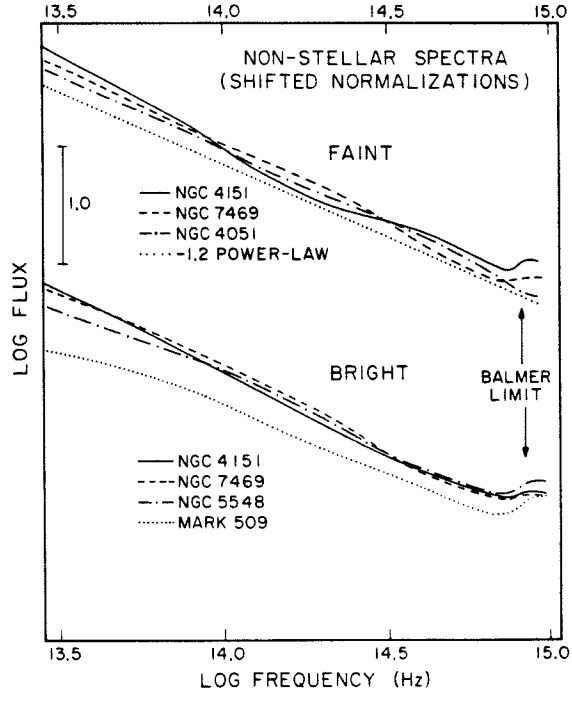

FIG. 9.—The nonstellar spectra from Fig. 8, rescaled for easy comparison with each other. The "faint" spectra fall steadily all the way to the Balmer limit and are not very different from the $f_\nu \propto \nu^{-1.2}$ power law shown for comparison. The "bright" nonstellar spectra are almost identical to that of Mrk 509, which has a detectable flattening in the blue well before the Balmer limit.

this curvature to continue to longer and shorter wavelengths. The 10–100 μm spectra of Seyfert 1 nuclei should show noticeable curvature and an overall slope which is flatter than -1.0. Note that on the scale of Figure 9, even a 10% error in the relative calibration of optical and infrared fluxes would still have no discernible effect on our results.

Our estimate of stellar flux in NGC 1068 is slightly higher than that obtained by Malkan and Oke (1983). Since it is based on better observations, it supersedes the previous value. The estimate of starlight flux in NGC 4151 is lower than that of Schmidt and Miller (1980), probably because they assumed the nonstellar light was a flat power law ($f_\nu \propto \nu^{-0.33}$).

Rieke (1978, 1981) has made estimates of the starlight flux in NGC 4151 and in several other low-luminosity Seyfert nuclei to examine their nonstellar infrared spectra. In NGC 4151, he assumed that the red spectrum at minimum light is entirely due to stars. Our spectra of the nucleus of NGC 4151 at minimum do not confirm this, since all of its absorption lines are far too weak to arise from pure undiluted starlight. Thus, Rieke's estimate of the stellar flux in 4151 is $\sim 50\%$ too high. Consequently, the nonstellar spectrum of NGC 4151 at minimum is not qualitatively different from that at maximum brightness: both fall smoothly from 2–3 μm to the visual, roughly with a power-law slope of -1.1 to -1.2. There is no short-wavelength break around 1 μm. If the bulk of the 2 μm flux comes from hot dust grains, as has been suggested by Rieke (1978) and reiterated by other investigators (Rieke and Lebofsky 1979; Angel and Stockman 1980), such a thermal Boltzmann cutoff in the nonstellar spectrum should be observable. Since it is not seen in any of our Seyfert 1 spectra, which instead have an approximately power-law shape (as in quasars), we conclude that *the bulk of their 2 μm flux is not thermal.*

Careful photometric monitoring by Lebofsky and Rieke (1980) shows that the blue and infrared variations in NGC 4151 and in the low-redshift quasar III Zwicky 2 are sometimes not instantaneously correlated. If (as MS argue) the blue light is predominantly thermal, while the red is nonthermal, they may not always vary synchronously. Rieke's measurements also show that the nonstellar infrared continuum may steepen slightly when it fades.

Although our results severely restrict the role that thermal dust emission could play in contributing to the near-infrared flux, they do not conclusively rule out the possibility that thermal emission may become important at longer wavelengths in many Seyfert 1 nuclei. For example, the "power law" seen at shorter wavelengths could turn over beyond 3 μm if the right amount of thermal emission from dust at $T \sim 500$ K were present to preserve the linearity of the resulting spectrum. Yet it seems implausible that the thermal and nonthermal fluxes would always be so well balanced: one should expect to see some spectra with a sharp (exponential) increase to longer wavelengths, as well as some with a turnover at 10 μm. This conflicts with the great uniformity of most infrared spectra of Seyfert 1 nuclei and quasars.

The starlight fluxes derived for NGC 1068 in the blue and red agree fairly well with those estimated by Malkan and Oke (1983). However, our high-quality near-infrared spectrum shows that the Ca II lines are probably seen at full strength in the nucleus of NGC 1068. At most, 10% of the near-infrared continuum within a 10″ aperture is nonstellar, indicating that the "power law" seen by Malkan and Oke (1983) at shorter wavelengths has flattened by 8000 Å. Since the nonstellar light is bluer than the starlight, the increase in polarization at shorter wavelengths is probably due to the nonstellar component (cf. Visvanathan and Oke 1968; Miller 1983). Our failure to detect dilution from nonstellar light at 8500 Å in NGC 1068 indicates that at least some Seyfert 2 galaxies do not have the same near-infrared power law that is generally present in type 1 Seyferts. It is not possible to ascertain whether the nonthermal component extends into the infrared in Seyfert 2 nuclei because this portion of their spectra is dominated by thermal emission from dust with a maximum temperature of 300–800 K (Malkan and Oke 1983). The same complication arises in the unusually red spectra of a few heavily reddened Seyfert 1 galaxies such as Mrk 231, which have very steep infrared spectra that are predominantly thermal (Rieke 1976).

VI. SUMMARY

Coudé spectroscopy and direct imaging have been combined to estimate the starlight fluxes in the nuclei of nine nearby Seyfert galaxies. The starlight colors agree with those expected in early-type spiral galaxies. The nonstellar continuum in low-luminosity Seyfert 1 nuclei is similar to that of very luminous Seyfert galaxies and quasars. It falls from the infrared to the visual roughly as a power law with a slope of -1.1 to -1.2. Except in the least luminous Seyfert nuclei studied, there is also a flattening before the Balmer limit, which has been attributed to optically thick thermal emission. Even at minimum brightness, there is no spectral steepening at wavelengths less than 1 μm, ruling out a thermal origin for the bulk of the 2 μm emission.

During the many nights required to obtain the data, expert assistance was provided by Howard Lanning and Jim Frazer at Mount Wilson, Skip Staples and Bob Griffith at Palomar, and Oscar Duhalde, Fernando Peralta, and Angel Guerra at Las Campanas. We are grateful to A. G. de Bruyn, A. C. S. Readhead, and W. L. W. Sargent for private communication of unpub-

lished data, as well as Abi Saha and James Fillmore for some of the computer programs used in the analysis. Informative discussions with J. B. Oke, G. H. Rieke, W. L. W. Sargent, and D. P. Schneider are appreciated, and we thank H. K. C. Yee for particularly illuminating conversations. This work was supported by the Fannie and John Hertz Foundation through two graduate fellowships, and by the National Science Foundation through grant AST-8216544 to W. L. W. Sargent.

APPENDIX

LINE PROFILES AND NEW EMISSION LINES

The data obtained for this investigation have also been used in a study of the emission lines in Seyfert galaxies. Although a detailed analysis will be presented elsewhere (Filippenko and Malkan 1983), a few conclusions are briefly discussed here.

Several new emission lines have been identified in the coudé spectra. One is He II λ8237, in NGC 4151 (Fig. 3). Careful examination of Figure 1 in Grandi (1978) reveals that the feature may also be present in NGC 1068, NGC 4051, and Mrk 335, but this must be confirmed with spectra of higher quality. In principle, He II λ8237 can be used together with He II λ4686 as a reddening indicator; the signal-to-noise ratio in our data, however, is not sufficiently large.

A stronger and more puzzling line in NGC 4151 is at $\lambda \sim 8617$ Å. It is narrow, and therefore probably corresponds to a forbidden transition. Several spectra obtained by J. B. Oke (1983) confirm the presence of this line. The most likely identification is [Fe II] λ8617, which is also visible in the Eta Carinae nebula (Thackeray 1953) and in the Orion nebula (Grandi 1975; Danziger and Aaronson 1974). A considerably broader feature appears at approximately the same wavelength in NGC 1068 (Fig. 3), but the width is consistent with that of other forbidden lines in this object.

Still another line which (to our knowledge) has not been previously reported in Seyfert galaxies appears at $\lambda \sim 5120$ Å in NGC 4051, 4151, 7469, and possibly 1068. Although its exact identification is unknown, it is probably a forbidden line from a highly ionized species, since [Fe VII] emission is strong in these galaxies. The feature also appears in NGC 6741 and IC 418 (Aller and Walker 1970), two planetary nebulae which exhibit lines from multiply ionized elements, but surprisingly it may be absent in other high-excitation planetary nebulae (Kaler 1976).

With high spectral resolution, we can investigate line profiles and small differences in the width and redshift of lines which represent a wide range of excitation. Such studies will provide information concerning the kinematics and geometry of the gas and dust in Seyfert nuclei. For example, the width of the [Fe VII]+[Ca V] λ6087 line in NGC 1068 and NGC 7469 is considerably greater than that of [O I] λ6300, and in Mrk 335 the widths differ by a factor of 2–3. A similar increase in line width with increasing ionization potential of the corresponding ion has been noticed in several other Seyfert galaxies (Osterbrock 1981; Pelat, Alloin, and Fosbury 1981) and indicates that the cloud velocity dispersion is greatest near the central source of ionizing radiation. Moreover, the difference between the redshift of emission and absorption lines in NGC 1068, which was first noticed by Burbidge, Burbidge, and Prendergast (1959), is confirmed, and slight discrepancies are evident in other objects as well.

A search for broad wings in the emission lines has also been conducted. For example, NGC 1068 may have a very faint, broad component of Hβ which qualitatively resembles that of Seyfert 1 galaxies. Similarly, the Hβ profile in NGC 5548 has three distinct components: one corresponds to the narrow forbidden lines, another has a width which is typical of that in type 1 Seyfert galaxies, whereas the third may extend redward of [O III] λ5007 and is reminiscent of the extremely broad wings seen in broad-line radio galaxies (Osterbrock, Koski, and Phillips 1976). Finally, it is possible that very weak wings are present in the [O III] λ4959, 5007 lines of NGC 4151, but this must be confirmed in future investigations.

REFERENCES

Aller, L. H., and Walker, M. F. 1970, *Ap. J.*, **161**, 917.
Alloin, D., Laques, P., Pelat, D., and Despiau, R. 1981, *Astr. Ap.*, **95**, 394.
Angel, J. R. P., and Stockman, H. S. 1980, *Ann. Rev. Astr. Ap.*, **18**, 321.
Balzano, V. A., and Weedman, D. W. 1981, *Ap. J.*, **243**, 756.
Burbidge, E. M., Burbidge, G. R., and Prendergast, K. H. 1959, *Ap. J.*, **130**, 26.
Cohen, J. G. 1978, *Ap. J.*, **221**, 788.
Cutri, R. M., *et al.* 1981, *Ap. J.*, **245**, 818.
Danziger, I. J., and Aaronson, M. 1974, *Pub. A.S.P.*, **86**, 208.
de Bruyn, A. G. 1982, private communication.
de Bruyn, A. G., and Sargent, W. L. W. 1978, *A.J.*, **83**, 1257.
de Bruyn, A. G., Sargent, W. L. W., and Readhead, A. C. S. 1982, private communication.
Filippenko, A. V. 1982, *Pub. A.S.P.*, **94**, 715.
Filippenko, A. V., and Malkan, M. A. 1983, in preparation.
Grandi, S. A. 1975, *Ap. J. (Letters)*, **199**, L43.
_____. 1978, *Ap. J.*, **221**, 501.
Hartwick, F. J., and Cowley, A. 1980, *Ap. J.*, **235**, 755.
Kaler, J. B. 1976, *Ap. J. Suppl.*, **31**, 517.
Kent, S. M. 1979, *Pub. A.S.P.*, **91**, 394.

Kormendy, J., and Illingworth, G. 1982, *Ap. J.*, **256**, 460.
Lebofsky, M. J., and Rieke, G. H. 1980, *Nature*, **284**, 410.
Malkan, M. A. 1983*a*, *Ap. J. (Letters)*, **264**, L1.
_____. 1983*b*, *Ap. J.*, **268**, 582.
Malkan, M. A., Margon, B., and Chanan, G. 1983, *Ap. J.*, submitted.
Malkan, M. A., and Oke, J. B. 1983, *Ap. J.*, **265**, 92.
Malkan, M. A., and Sargent, W. L. W. 1982, *Ap. J.*, **254**, 22 (MS).
McAlary, C. W., McLaren, R. A., McGonegal, R. J., and Maza, J. 1983, *Ap. J. Suppl.*, **52**, 341.
McAlary, C. W., McLaren, R. A., and Crabtree, D. R. 1979, *Ap. J.*, **234**, 471.
Miller, J. S. 1983, preprint.
Minkowski, R. 1968, *A.J.*, **73**, 836.
Oke, J. B. 1969, *Pub. A.S.P.*, **81**, 11.
_____. 1983, private communication.
Oke, J. B., and Gunn, J. E. 1983, *Ap. J.*, **266**, 713.
Osterbrock, D. E. 1978, *Proc. Nat. Acad. Sci.*, **75**, 540.
_____. 1981, *Ap. J.*, **246**, 696.
_____. 1983, *Pub. A.S.P.*, **95**, 12.
Osterbrock, D. E., Koski, A. T., and Phillips, M. M. 1976, *Ap. J.*, **206**, 898.
Pelat, D., Alloin, D., and Fosbury, R. A. E. 1981, *M.N.R.A.S.*, **195**, 787.
Penston, M. V., *et al.* 1974, *M.N.R.A.S.*, **169**, 357.
Phillips, M. M. 1977, *Ap. J.*, **215**, 740.
_____. 1978, *Ap. J. Suppl.*, **38**, 187.
Rieke, G. H. 1976, *Ap. J. (Letters)*, **206**, L15.
_____. 1978, *Ap. J.*, **226**, 550.
_____. 1981, *Ap. J.*, **250**, 87.
Rieke, G. H., and Lebofsky, M. J. 1979, *Ann. Rev. Astr. Ap.*, **17**, 477.
Rudy, R. J., Jones, B., Levan, P. D., Smith, H. E., Willner, S. P., and Tokunaga, A. T. 1982, *Ap. J.*, **257**, 570.
Schmidt, G. D., and Miller, J. S. 1980, *Ap. J.*, **240**, 759.
Shectman, S., and Hiltner, W. A. 1976, *Pub. A.S.P.*, **88**, 960.
Stauffer, J. 1983, *Ap. J.*, **264**, 14.
Thackeray, A. D. 1953, *M.N.R.A.S.*, **113**, 211.
Thuan, T. X., and Gunn, J. E. 1976, *Pub. A.S.P.*, **88**, 543.
Visvanathan, N., and Oke, J. B. 1968, *Ap. J. (Letters)*, **152**, L165.
Wade, R. A., Hoessel, J. G., Elias, J. H., and Huchra, J. P. 1980, *Pub. A.S.P.*, **91**, 35.
Yee, H. K. C. 1983, *Ap. J.*, **272**, 473.
Yee, H. K. C., and Oke, J. B. 1978, *Ap. J.*, **226**, 753.

ALEXEI V. FILIPPENKO and MATTHEW A. MALKAN: Department of Astronomy, 105-24, California Institute of Technology, Pasadena, CA 91125

CHAPTER 2

NGC 7213: A Key to the Nature of LINERs?

Alexei V. Filippenko and J. P. Halpern

To be published in The Astrophysical Journal, 1984 Oct 15.

The most incomprehensible thing about the world is that it is comprehensible.

Albert Einstein

ABSTRACT

New optical spectra show that the nucleus of the S0 galaxy NGC 7213 resembles those of type 1 Seyferts: emission lines such as [Ne V]λ3426, He II λ4686, and broad Hα are visible, and a nonstellar component accounts for a substantial portion of the continuum at blue and ultraviolet wavelengths. On the other hand, many of the emission-line intensity ratios suggest heating due to shocks, since they are similar to those in Heckman's "low ionization nuclear emission-line regions" (LINERs). Lines from neutral and singly-ionized species are prominent, and high temperatures seem to be implied by the unusually large strength of [O III]λ4363. This investigation demonstrates that the spectral characteristics are much more consistent with photoionization by a nonstellar continuum than with shock heating.

To avoid serious errors in line strengths, the strong stellar component is accurately removed by subtraction of an appropriate template galaxy. Widths of the remaining emission lines range from ~ 200 to ~ 2000 km s^{-1} (FWHM), indicating that clouds having different bulk velocities exist in the narrow-line region. Large differences are seen even in lines which arise from the same species, such as [O II]λ3726,3729 (~ 300 km s^{-1}) and [O II]λ7319,7330 (~ 1000 km s^{-1}). Since the latter (auroral) pair is enhanced in gas of high density (~ 10^6 cm^{-3}) while the former (nebular) lines are dominant where densities are low (~ 10^3 cm^{-3}), physically distinct clouds having vastly different densities are present and contribute unequally to the nebular and auroral components of [O II]. This conclusion also applies to the transauroral and nebular lines of [S II], and is supported by a tight

correlation between line width and critical density ($\underline{v} \propto \underline{n}_e(\underline{crit})^{1/5}$) for 16 forbidden lines.

The observed ratio $\underline{R} \equiv \underline{I}([O\ III]\lambda 4959+5007)/\underline{I}([O\ III]\lambda 4363) = 6.65$ cannot be reproduced at any reasonable temperature unless $\underline{n}_e \gtrsim 10^{5.5}$ cm^{-3}. If $\underline{T}_e \sim 16000$ K (as in hot photoionized gas), then $\underline{n}_e \sim 10^{6.4}$ cm^{-3}, and values exceeding 10^7 cm^{-3} are likely if the enhancement of auroral over nebular components in clouds of very high density is considered. This is much larger than the value of ~ 500 cm^{-3} implied by the $\underline{I}([S\ II]\lambda 6716)/\underline{I}([S\ II]\lambda 6731)$ intensity ratio, and exceeds the density normally ascribed to the narrow-line regions of Seyfert galaxies (10^3–10^5 cm^{-3}). Given the great range of densities in NGC 7213, models involving photoionization by a nonstellar continuum are able to reproduce the observed spectrum. High temperatures are not implied by the [O III] ratio, and a rather low ionization parameter can give rise to strong emission from neutral and singly-ionized species. Moreover, the observed relationship between cloud velocity and density, which is consistent with clouds in Keplerian orbits and a nearly radius-independent ionization parameter, can be understood in terms of the two-phase model of quasar emission-line regions developed by Krolik, McKee, and Tarter. The individual clouds must be optically thick to the Lyman continuum so that each of them includes every ionization stage up to a certain level. High velocities and densities are found closer to the nucleus than low values.

These results may be relevant to LINERs as a class, since the small value of $\underline{R}$ which is sometimes observed could be indicative of high densities rather than high temperatures. This would eliminate the major argument in favor of shock heating in LINERs, whose observed spectra are

adequately explained by photoionization models in all other respects.

Subject headings: galaxies:individual (NGC 7213)--galaxies:nuclei--
galaxies:Seyfert--line profiles--spectrophotometry--
radiation mechanisms

I. INTRODUCTION

NGC 7213 is a nearby S0 galaxy associated with an X-ray source (Halpern and Filippenko 1984, hereafter Paper II). Phillips (1979) showed that its nucleus exhibits broad Hα emission characteristic of Seyfert 1 galaxies, but that the Hα luminosity of $\sim 2 \times 10^{41}$ erg s^{-1} ($H_0 = 50$ km s^{-1} Mpc^{-1}) is low for type 1 Seyferts. He also noted the absence of obvious broad Hβ emission and the prominence of the stellar continuum.

The narrow-line spectrum is of unusually low excitation; [O III]λ5007, [O II]λ3727, and [O I]λ6300 have comparable intensities, and strong [S II]λ6716,6731 and [N II]λ6548,6583 are visible as well. Heckman (1980) identified these properties in a large number of galactic nuclei (including NGC 7213) known as "LINERs," and such objects received further attention from Stauffer (1982) and Keel (1983a,b). The spectra of LINERs resemble that of NGC 1052, an E3/S0 galaxy in which shock heating (Dopita 1977; Shull and McKee 1979) was proposed to explain the low-excitation lines (Koski and Osterbrock 1976; Fosbury *et al.* 1978). Consequently, the emission in LINERs is generally attributed to shocks (e.g., Baldwin, Phillips, and Terlevich 1981). On the other hand, many LINERs are strong X-ray sources (Halpern and Steiner 1983), and their spectra have recently been reproduced equally well with models involving photoionization by a power-law continuum and a low number of ionizing photons per nucleon, or "ionization parameter" (Ferland and Netzer 1983; Halpern and Steiner 1983). In addition, careful measurements of [O III]λ4363 in NGC 1052 (Keel and Miller 1983; Rose and Tripicco 1984) imply a lower temperature than found in previous investigations,

indicating that shocks might not be necessary. Thus, the origin of activity in these galaxies remains unclear.

Features common to both Seyfert galaxies and LINERs make NGC 7213 an important object for closer scrutiny. Moreover, Figure 2 in Phillips (1979) indicates that some forbidden lines have different profiles and might provide insight into the physical conditions. In order to shed light on the line excitation mechanism, new X-ray and optical spectra were obtained. X-ray data and the overall continuum from radio through X-ray energies are described in Paper II, whereas a detailed analysis of the optical emission lines is presented here.

Section II describes the observations and presents a brief overview of the spectrum. The stellar component is carefully subtracted in §III, and §IV subsequently discusses the measurement of various emission lines in detail. Important physical parameters are derived in §V. The Seyfert characteristics of NGC 7213 are reviewed in §VI, and its shock features are reconciled with photoionization models. The arguments may apply to other LINERs as well. Section VII explores theoretical models that can help explain the relationships discovered among the emission lines, and major conclusions are summarized in §VIII.

II. THE OPTICAL SPECTRUM

a) Observations and Reductions

NGC 7213 was observed on 1982 August 16-18 UT with the Intensified Reticon (Shectman and Hiltner 1976) attached to the Boller and Chivens Cassegrain spectrograph at the Las Campanas 2.5 m duPont reflector. Two Bausch and Lomb gratings, each having 1200 grooves mm^{-1}, were used in

first order to obtain 3 spectra at $\lesssim 2.5$ Å resolution. The integration times (s) and wavelength ranges were (1800, 1400, 3000) and ($\lambda\lambda$3100-4985, 4455-6355, 5675-7570), respectively. A GG420 filter blocked out second-order light in the red spectrum. Sky subtraction was achieved by measuring the object and sky simultaneously through each of the two entrance apertures (2" x 4") separated by 27.4". Outer regions of the galaxy produced very little contamination of the sky aperture.

Wavelength calibration was made possible by recording the spectra of various comparison arcs, and a dispersion of ~ 0.15 Å was obtained by fitting a fifth-order polynomial to the centroids of unblended emission lines. Measurements of atmospheric lines showed that zero-point offsets were likewise very small ($\lesssim 0.2$ Å). The Reticon was exposed to a featureless continuum for a long period of time to facilitate the calibration of pixel-to-pixel variations in the detector sensitivity, and a series of integrations made with different intensity levels demonstrated that continuum coincidence losses were negligible.

Calibration of the overall spectral response on the AB_{79} scale of Oke and Gunn (1983) was achieved by comparison with the faint standard stars GD-248 and G158-100 (Filippenko and Greenstein 1984), which are nearly featureless. Since they are located near the celestial equator, the long dimension of the entrance aperture was aligned along the atmospheric refraction to minimize relative light losses (Filippenko 1982a). The observations of NGC 7213 were made when the air mass was $\lesssim 1.1$, so a single orientation (E-W) was chosen to ensure that nearly identical regions of the galaxy were sampled each night. At all times the seeing was ~ 1", and 2 of the 3 nights were photometric. Application of a constant scaling factor to data from the cloudy night

produced excellent agreement in continuum shape with the other spectra. The derived absolute flux is uncertain by ~ ± 25%, however, since the standards were measured through a 2" x 4" aperture (as was NGC 7213).

b) Brief Overview

The entire optical spectrum of the central 340 x 680 pc^2 of NGC 7213 (H_o = 50 km s^{-1} Mpc^{-1}), obtained by adding together the three separate spectra, is presented in Figure 1. Data points in overlapping sections were combined in proportion to their statistical weights. A Gaussian with 4.4 Å full width at half-maximum was used to smooth the displayed spectrum, so an unresolved emission line should appear as a spike with thickness comparable to the markers which identify interesting features. Telluric absorption lines were not removed. A Galactic extinction A_V = 0.05 mag ($A_V \sim 3.2E_{B-V}$), which is an average of the values derived from Burstein and Heiles (1982) and from Heiles and Cleary (1979), was adopted to deredden the spectrum. The Whitford (1958) reddening law was used by fitting a quadratic polynomial over the range λλ3000-8000 to points tabulated by Lequeux *et al.* (1979) and Burgess (1958).

Generally speaking, the spectrum resembles that obtained by Phillips (1979). Forbidden lines of neutral, singly-, and doubly-ionized atoms are prominent, and Hα exhibits both narrow and broad components, the latter significantly redshifted with respect to other features. A corresponding broad Hβ line is weak. The strong underlying continuum is indicative of an old stellar population, but it does not dominate the spectrum to the extent noted previously by Phillips (1979) because of the smaller aperture used here.

An obvious feature is the large range in width of the forbidden lines. [O I]λ6300 is roughly twice as broad as either of the [S II]λ6716,6731 lines, for example, and [O III]λ5007 is considerably broader than the blended [O II]λ3726,3729 doublet. Even more remarkable is that in some cases <u>different</u> lines arising from the <u>same</u> ions have disparate widths, as can be seen by comparing [O II]λ3726,3729 with [O II]λ7319,7330. This clearly indicates that the lines are <u>not</u> produced by the same gas; rather, clouds having different bulk velocities must be present, each one contributing to the emission-line spectrum in a manner dictated by local physical conditions.

Lines of Ne^{+4} and He^{+}, as well as the broad Balmer profiles, suggest that a nonstellar continuum similar to that in active galactic nuclei of high luminosity comprises a significant fraction of the flux at blue and ultraviolet wavelengths. Moreover, Paper II shows that a decomposition of the continuum into a "standard" giant elliptical galaxy (Yee and Oke 1978) and a power-law spectrum ($f_\nu \propto \nu^{-\alpha}$) results in a nonstellar component which accounts for at least 50% of the flux at λ3300. The best fit is obtained if the observed continuum of NGC 7213 is initially dereddened by $A_V \sim 0.61$ mag; in this case, the nonstellar component ($\alpha = 1.1$) dominates over the starlight at wavelengths shorter than λ3950 (see Paper II).

III. THE EMISSION LINES

a) Subtraction of the Stellar Continuum

The intensities and profiles of emission lines are strongly affected by absorption lines from the bulge stars of NGC 7213, as shown in Figure 1. Since "two-dimensional" data taken through a long slit

were not available, the starlight was removed by subtracting the spectrum of a different galaxy instead. IC 4889, the adopted template, is a bright $SO_{1/2}(5)$ galaxy (Sandage and Tammann 1981), and its spectral type, metallicity, and stellar velocity dispersion are quite similar to those in NGC 7213. Weak Hα, [N II]λ6548,6583, and [O II]λ3727 are the only emission lines visible.

Data were obtained at Las Campanas on 1983 August 13-14 UT in the manner used for NGC 7213, and a composite was formed from two separate spectra of the nucleus. Blueward of ~ 4500 Å the resolution (FWHM) is $\lesssim 2.5$ Å in the composite, but redward the contribution of a second spectrum with $\lesssim 5$ Å resolution is significant. Since the velocity dispersion in IC 4889 is roughly 200 km s^{-1}, the absorption lines are resolved in each individual spectrum, and the effective resolution is approximately uniform in the composite. The data were dereddened under the assumption that the Galaxy produces $A_V \sim 0.10$ mag in the direction of IC 4889 (Burstein and Heiles 1982).

Although spectra of IC 4889 and NGC 7213 closely resemble each other, the apparent metallicity of the former is higher than that of the latter. This is partly due to the nonstellar component in NGC 7213 (Paper II), and comparable metallicities were found after its removal. To decrease remaining discrepancies, the flux in all pixels within a given section of IC 4889 was scaled by an appropriate amount, and a "featureless" component whose shape represents the absorption-free continuum was added or subtracted in order to bring the flux density back to the level of the true continuum. Thus, absorption lines in the modified spectrum had roughly the same equivalent width as corresponding lines in NGC 7213.

It was also necessary to adjust the continuum of IC 4889 so that its shape is nearly identical to that of NGC 7213. Differences may have been caused by subtracting an incorrect amount of nonstellar component from the spectrum of NGC 7213, or by incomplete removal of the reddening in either galaxy. The adjustment was made by i) dividing the spectra into several sections of width ~ 400 Å, ii) marking regions in both spectra where emission lines are present (or suspected to be present) in NGC 7213, iii) fitting a quadratic or cubic to the unmarked points in each section, and iv) rescaling the continuum of IC 4889 at every pixel with the local ratio of the two fits. The spectrum of the template was subsequently subtracted from that of the object. Since the same regions were excluded from the polynomial fits in both galaxies, and since the order of the fit in a given section was also the same, this approach was objective and produced a reliable removal of the stellar component. As a check, many regions devoid of emission were treated as though they actually do contain emission hidden among the numerous absorption lines, and no spurious features were discovered. Longward of ~ 5500 Å the signal-to-noise ratio of the template was not sufficiently high to be of great use in the subtraction.

Figure 2 illustrates the results. Emission lines only barely noticeable in the original spectrum rise prominently above the flat baseline. Excellent examples are [N I]λ5198+5200, whose small width provides a striking contrast with [O III], and He II λ4686. Not only is the broad component of Hβ clearly visible, but a similar one is present in Hγ and possibly Hδ. There is no evidence of the Fe II emission often seen in Seyfert 1 galaxies (Phillips 1978). Noise in the net spectrum is somewhat greater than $2^{1/2}$ times that in either of the original

spectra due to small differences in the velocity dispersion, metallicity, and spectral type of each galaxy.

b) Measurements of Emission Lines

Various parameters were measured from the net spectrum shown in Figure 2c, and from the red portion of the original spectrum. Wavelengths were determined by minimizing the absolute value of the convolution of each line with the derivative of a suitable Gaussian (Schneider and Young 1980). Since some emission lines (e.g., [O III]λ5007) exhibit weak, very narrow components in addition to broader blue wings, Gaussians having small dispersions were used to obtain accurate wavelengths for the peaks of lines, whereas larger dispersions gave better estimates of the line centroids. In all measurements the redshift of the galaxy ($\underline{v}$ = 1769 km s^{-1}), as given by Sandage and Tammann (1981), was removed. This systemic velocity is consistent with the value of 1789 km s^{-1} recently derived by cross-correlations of absorption-line spectra (Sadler 1984).

Intensities were obtained by integrating the flux in all pixels between the endpoints of each line. In many cases these were compared with values determined from the Gaussian which best approximates the given profile. For each line a weighted average based on an appraisal of the two methods was adopted. Full widths at half-maximum (FWHM) were also determined manually and from fits with symmetric functions, and are reasonably well defined. The full width at zero-intensity (FWZI), however, was usually measured less precisely, as it strongly depends on the signal-to-noise ratio in the wings of a line.

The results of various measurements are given in Table 1. Listed

for each line is the laboratory wavelength, the difference between the laboratory wavelength and that of the line centroid, the difference between the laboratory wavelength and that of the line peak, the dereddened (A_V = 0.05 mag and A_V = 0.61 mag) intensity relative to I([O III]λ5007), the FWHM, the FWZI, and the number of km s^{-1} $Å^{-1}$ at the line. Many of the quantities were derived by the use of special techniques discussed in the next section.

IV. DETAILED ANALYSIS OF BLENDS

a) [O I], [N II], Hα, [S II]

Figure 3a illustrates Hα and the remarkable differences in the widths and profiles of [O I]λ6300,6364 and [S II]λ6716,6731. The absence of emission from highly ionized Fe elsewhere in the spectrum argues against contamination of [O I]λ6364 by [Fe X]λ6374, and the similar profiles of [O I]λ6300 and [O I]λ6364 suggest that [S III]λ6312 is also not strong. Moreover, the relative intensity of the two [O I] lines agrees with theoretical predictions.

The continuum was artificially removed in Figure 3b by fitting cubic splines through selected points, since IC 4889 exhibits weak emission lines of Hα and [N II]λ6548,6583. Absorption features such as the TiO band blueward of [O I]λ6300, the Ca + Fe line at ~ λ6495, and the B band were excised, but no attempt was made to account for Hα absorption in NGC 7213. Gaussians were fit to [S II] and subtracted from the spectrum, and the [O I] profiles were approximated with cubic splines. Figure 3d shows Hα after removal of [N II]. It was assumed that i) I([N II]λ6583)/I([N II]λ6548) = 3.0, ii) Δλ = 35.4 Å, and iii) the lines are Gaussians whose width is equal to the average of the

[S II] emission, as suggested by their appearance and by the expectation that roughly the same clouds produce these lines.

The narrow and broad components of Hα merge smoothly, and it is difficult to distinguish unambiguously between them. Two local maxima are visible, and the absence of strong absorption in this spectral region, together with the similar appearance of Hβ (Figure 3f), makes it likely that the secondary peak is intrinsic to the profile. Figure 3d also illustrates the decomposition of the profile into 6 individual Gaussians (e.g., Pelat and Alloin 1980, 1982). The overall fit is excellent (Figure 3e), and the relevant parameters of each component are given in Table 2. The physical significance of all these Gaussians is questionable, however, since the FWHM of Hβ is noticeably smaller than that of Hα. If the decomposition of Hα is repeated with the physically reasonable requirement that one component resemble the core of Hβ, a total of 7 Gaussians is necessary to produce a fit whose accuracy is comparable to that of the 6-component fit. Failure to remove stellar Hα affects fluxes by only a few percent and does not change this result, as Balmer lines are generally weak in E and S0 galaxies. Thus, great physical significance should not be ascribed to all of the individual components. Only a few general conclusions, such as the existence of an asymmetrical broad component and the variation in Balmer decrement with velocity (Shuder 1982), can be drawn with confidence.

Some evidence for temporal variations may be found by comparing Figure 3 with previously published results. In particular, the "valley" visible in Hα and Hβ is not present in the spectrum taken by Phillips (1979) in 1978. This rather small change is well within the theoretically allowed variability, especially for such a low-luminosity

active nucleus.

b) Hβ, [O III]

Inspection of Figures 1 and 2a suggest the presence of a broad Hβ component similar to that seen in Hα. Parameters of this line are difficult to measure due to prominent Mg b absorption, but subtraction of the template reveals a relatively clean profile.

Contamination of [O III]λ4959 was removed by fitting a cubic spline through points thought to represent the red wing of Hβ. The spline was required to vanish at the bottom of the "valley" between the [O III] lines (Figure 2c) and to have a continuous first derivative. As a check, this technique produced I([O III]λ5007)/I([O III]λ4959) = 2.83, which is close to the theoretical prediction (2.96). In addition, the [O III]λ4959 and [O III]λ5007 profiles are remarkably similar: a narrow component is present at essentially the systemic velocity of 1769 km s^{-1}, but the bulk of the emission is blueshifted by ~ 180 km s^{-1}, as in many of the other forbidden lines.

c) [O III], Hγ

The blending caused by large intrinsic widths of Hγ and [O III]λ4363, together with the proximity of strong absorption (Figure 4a), make it difficult to measure the individual lines unless the underlying continuum is subtracted (as in Figure 4c). A broad component of Hγ is visible, and a narrow "spike" appears as well. The former corresponds to those seen in Hα and Hβ, and the latter has a counterpart in Hα (Gaussian C in Table 2), but not in Hβ. A narrow component probably also exists in Hβ, but it is not visible due to an imperfect match between the strengths of Balmer absorption lines in

NGC 7213 and IC 4889.

One of the most important diagnostics of physical conditions is [O III]λ4363. Estimates of its shape and intensity were obtained by assuming that the profiles of Hγ and Hβ are identical. Hβ was shifted so that its peak coincides with that of Hγ, and was subsequently scaled to produce the best overall fit to the broad component. An inherent assumption is that [O III]λ4363 does not have very extended wings that merge with those of Hγ. A scaling factor of 0.32 (Figure 4d) produced a satisfactory fit and leads one to believe that the profiles of Hγ and Hβ are very similar. In Figure 4e, Hγ was subtracted from the blended line, leaving [O III]λ4363 and a small residual of narrow Hγ emission which was removed in Figure 4f.

Table 1 shows that [O III]λ4363 is remarkably strong and also somewhat broader than the related [O III]λ4959,5007 lines. These measurements play an important role in subsequent discussions, and it must be stressed that they were probably not overestimated. It is likely, however, that the derived strength of [O III]λ4363 was too large in a number of previous studies of LINERs, since Figure 4b clearly demonstrates a high point in the normal stellar continuum precisely at the position expected for [O III]λ4363. Failure to properly account for the underlying stellar absorption lines therefore leads to serious errors in the measured flux of [O III]λ4363, as emphasized by Keel and Miller (1983) and by Rose and Tripicco (1984).

d) [S II], Hδ, [Ne III], Hε

A puzzling blend composed of [S II]λ4069,4076 and Hδ is seen in Figure 5a. There is no clear separation between [S II] and the extended

red wing, whose centroid appears ~ 10–15 Å blueward of its expected position if it is Hδ. Weak [Fe V]λ4071.5 might be present, but this is improbable in view of the absence of additional Fe lines having comparable strength (Osterbrock 1981).

The puzzle disappears when the stellar component, which contains a high point at ~ λ4088, is subtracted from NGC 7213. The blend breaks up into several recognizable lines: [S II]λ4069, an Hδ line of comparable width, and a very weak, poorly-determined broad component of Hδ which corresponds to the wings seen in Hα, Hβ, and Hγ. The lines can be fit well by Gaussians. Of course, a portion of the [S II] profile is due to emission at λ4076, which is calculated to be a factor of ~ 4 weaker than [S II]λ4069.

Figure 5a also shows how [Ne III]λ3967 and Hε are hidden in the strong Ca II H (λ3968) absorption line. There is a hint of He I λ3889 + Hζ emission redward of [Ne III]λ3869 as well, and these weak lines are clearly visible in Figure 5c. The derived strength of [Ne III]λ3967 is roughly 0.30 that of [Ne III]λ3869, in agreement with theory. A broad component of Hε is probably present, but its small flux cannot be measured due to comparable uncertainties in the procedure used to remove the stellar component from this troublesome spectral region.

V. INTERPRETATION OF THE EMISSION LINES

To investigate the ionization mechanism in NGC 7213, it is necessary to disentangle physically distinct regions by examining the various widths and intensity ratios in Table 1; otherwise, conclusions drawn from the data may be invalid. With this in mind, the relevant electron densities and temperatures are now determined. Unless

otherwise stated, all line intensities are dereddened with the Galactic extinction A_V = 0.05 mag, since the value of 0.61 mag derived from an analysis of the optical continuum may be inconsistent with the X-ray measurements (Paper II).

a) Atomic Data

Theoretical emission-line intensity ratios were calculated as a function of n_e and T_e using detailed balance in ions having 5 low-lying levels in the ground state configuration (Kafatos and Lynch 1980). Temperature-dependent collision strengths from the following sources were used: Péquignot and Aldrovandi (1976) for [O I], Pradhan (1976, 1978) for [O II] and [S II], Baluja, Burke, and Kingston (1981) for [O III], Seaton (1975) for [N II], Pradhan (1974) for [Ne III], and Giles (1979) for [Ne V]. Sources for the transition probabilities were Garstang (1968) for [O I] and [Ne III], Nussbaumer and Rusca (1979) for [N II] and [Ne V], Nussbaumer and Storey (1981) for [O III], Mendoza and Zeippen (1982) for [S II], and Zeippen (1982) for [O II].

The critical density (n_e^i(crit)) for each level i, above which collisional de-excitation of the level is important (Osterbrock 1974), was calculated from

$$n_e^i(\text{crit}) = \sum_{j<i} A_{ij} \Big/ \sum_{j \neq i} q_{ij} \quad , \qquad (1)$$

where A_{ij} is the transition probability (from level i to level j) and q_{ij} is the collisional (de)excitation rate.

b) Line Widths

Table 1 demonstrates that the forbidden lines in NGC 7213 display a

great range in width. An impressive example is provided by [O II]λ3726,3729 and [O II]λ7319,7330, which show that lines from the same species receive different relative contributions from various clouds. The same can be said for [S II]λ6716,6731 and [S II]λ4069,4076, as well as for [O III]λ4959,5007 and [O III]λ4363. This obviously complicates the derivation of densities, temperatures, and reddenings from emission-line intensity ratios.

Line width increases systematically with the ionization potential (χ) of the corresponding ion in a few active galaxies (e.g., Osterbrock 1981; Pelat, Alloin, and Fosbury 1981), and others are known in which the ionization level is correlated with n_e (e.g., Phillips 1978; Osterbrock, Koski, and Phillips 1976). An increase in n_e and the bulk motions of clouds with decreasing distance from the central source of radiation is the probable cause of this. Although such an effect also appears to be present in NGC 7213 (Figure 6), lines from the same species but with markedly different widths suggest that χ is not the fundamental parameter. Rather, a physical variable which in many cases increases with χ, but is also able to distinguish between transitions from different upper levels in a given species, would be better.

A parameter satisfying these requirements is the critical density. Indeed, Figure 7 illustrates the close relationship between the width of a forbidden line and $n_e(crit)$ for the upper level from which the corresponding electron transition occurs. Lines associated with $n_e(crit) \sim 10^6$ cm^{-3} are broader than those having small ($\sim 10^3$ cm^{-3}) values, and both the FWHM and FWZI obey the same relation ($v \propto (n_e(crit))^{1/5}$), obtained with unweighted linear least-squares fits. Since there are few points at low $n_e(crit)$, several of which are

associated with large errors, a weighted analysis essentially uses only the points at high n_e(crit) and gives a linear fit which is less plausible than an unweighted one. Balmer lines are not plotted since the effects of radiative transfer greatly complicate the interpretation of n_e(crit), but it is obvious from Table 1 that the observed general trend continues if $n_e \sim 10^9$ cm^{-3} is assumed for the broadest components.

Most of the scatter in Figure 6 is absent in Figure 7, and the final correlation coefficients (r) of the fits are ~ 0.72 and ~ 0.92, respectively. As usual, $r = 1.0$ represents a perfect correlation, whereas $r = 0.0$ for completely uncorrelated data. It is possible that for a given value of n_e(crit) the average width of lines produced by species having high χ (e.g. [Ne V], [O III]) is slightly greater than that of lines from species with low χ, but the number of lines is not sufficiently high to allow a statistically significant conclusion. Thus, in NGC 7213 the critical density is clearly the primary discriminant, while χ has only secondary importance.

Pelat, Alloin, and Fosbury (1981) suggested that the forbidden lines in the Seyfert galaxy NGC 3783 may obey a similar relationship between n_e(crit) and width, but they did not measure lines produced by low-ionization species having large critical density (such as [O I]λ6300,6364, [S II]λ4069,4076, and [O II]λ7319,7330). Instead, every line in their sample associated with a large n_e(crit) is also characterized by high χ, and similarly for low values of χ and n_e(crit). Hence, the correlation they obtained between width and χ was roughly as strong as that obtained between width and n_e(crit), and it was not clear which of the two parameters is fundamental.

The emissivity of gas is proportional to n_e^2 below n_e(crit) and to

n_e above it. Thus, a given line is emitted most efficiently from gas whose density is close to n_e(crit), so emission lines can act as tracers of n_e if the range is sufficiently large. Figure 7 implies that many clouds with different bulk motions and densities exist in the narrow-line region of NGC 7213. Dense clouds appear to be moving the fastest, although it is not known a priori whether this motion is turbulent or systematic.

Of course, the existence of distinct regions having widely different densities and velocities has long been accepted as the explanation for the presence of narrow forbidden and permitted lines, together with broad permitted lines, in the spectra of Seyfert nuclei. It is reasonable that in at least some galaxies substantial density variations also exist among clouds which produce the narrow components. In fact, forbidden lines of unequal width have been noticed in a number of LINERs and radio galaxies (Heckman 1980; Danziger, Fosbury, and Penston 1977), but NGC 7213 is the first example in which lines arising from the same species are significantly different.

c) Physical Conditions

The widths can be used to distinguish between different clouds. [O II]λ3726,3729 and [S II]λ6716,6731 are comparable in width, so they probably arise from roughly the same gas. If $T_e = 10^4$ K, the observed ratio $I([S\ II]\lambda6716)/I([S\ II]\lambda6731) = 0.99 \pm 0.03$ corresponds to $n_e \sim 470 \pm 60$ cm^{-3}, in which case $I([O\ II]\lambda3726)/I([O\ II]\lambda3729)$ is predicted to be $\sim 0.97 \pm 0.04$. Although the [O II] doublet is unresolved, this value is consistent with its symmetrical profile. Densities which differ greatly from ~ 500 cm^{-3} are excluded — the

intensity ratio is ~ 0.74 when $\underline{n}_e$ = 100 cm^{-3} and ~ 1.23 when $\underline{n}_e$ = 1000 cm^{-3}, and the [O II] profile should then be noticeably asymmetrical.

Clouds which give rise to the narrow "nebular" ([O II]λ3726,3729 and [S II]λ6716,6731) doublets cannot possibly produce the "auroral" ([O II]λ7319,7330) and "transauroral" ([S II]λ4069,4076) lines simultaneously, as shown in Figure 8 for [O II]. The two blends are drawn on the same velocity scale and are decomposed into their two major constituents (each having the same width), under the assumptions that $\underline{I}$([O II]λ7319)/$\underline{I}$([O II]λ7330) = 1.27 and $\underline{I}$([O II]λ3726)/$\underline{I}$([O II]λ3729) = 1.00. The former ratio is almost completely independent of $\underline{n}_e$ and $\underline{T}_e$, whereas the latter represents the best fit to the data and is consistent with the ratio 0.97 ± 0.04 derived above. Clearly, the components of the nebular doublet are considerably narrower than the individual auroral lines, and therefore cannot be produced by the same ions.

If the broad [O II]λ7319,7330 lines are produced by gas near its critical density (~ 5.9 x 10^6 cm^{-3}), then Figure 9 shows that the corresponding components of [O II]λ3726,3729 should be a factor of ~ 26 less intense if log $\underline{T}_e$ = 4.0 (point A), and ~ 47 times weaker if log $\underline{T}_e$ = 4.2 (point B), assuming $\underline{A}_V$ = 0.0 mag. The absence of this broad component in Figure 8c is therefore not surprising. Similarly, if the narrow nebular emission is produced in gas with $\underline{n}_e$ ~ 470 cm^{-3}, then the flux of this line should be ~ 40 times greater than that of the corresponding narrow [O II]λ7319,7330 if log $\underline{T}_e$ = 4.0 (point C), and a factor of ~ 20 greater if log $\underline{T}_e$ = 4.2 (point D). This component is difficult to detect in Figure 8a due to the low signal-to-noise ratio,

but the top half of the profile may be slightly too narrow in comparison with the bottom half and the Gaussian fit.

The same reasoning applies to [S II]. If the broad transauroral lines are produced by gas near $\underline{n}_e(\underline{crit}) \sim 1.7 \times 10^6$ cm^{-3}, the corresponding components of [S II]λ6716,6731 should be factors of ~ 33 and ~ 48 weaker ($\underline{A}_V = 0.0$) if log $\underline{T}_e = 4.0$ and log $\underline{T}_e = 4.2$, respectively (Figure 10), and are undetectable in Figure 3b. Moreover, if the narrow nebular doublet is produced by gas with $\underline{n}_e \sim 470$ cm^{-3}, then its strength should be ~ 12 times greater than the narrow component of the transauroral lines if log $\underline{T}_e = 4.0$ and a factor of ~ 7 greater if log $\underline{T}_e = 4.2$. Nonzero reddening would lead to even larger factors. Figure 5 indicates that [S II]λ4069 might have a very small narrow core, but this cannot be established with certainty.

Of course, if substantial quantities of gas exist at densities <u>between</u> 10^3 cm^{-3} and 10^6 cm^{-3}, one should expect to see many components of various widths in the profile of a given line. In practice, these usually cannot be distinguished because they blend with one another and have roughly the same profile. A superposition of components with different widths and intensities is probably present in [O I]λ6300,6364, however, as Figure 3b shows that the wings are much more extended than those in a single Gaussian.

Additional evidence for the presence of densities $\gtrsim 10^6$ cm^{-3} is found from careful examination of the nebular [O III]λ4959,5007 and auroral [O III]λ4363 lines. Assume for the time being that all of the [O III] lines originate in the same clouds. Then a density estimate for the O^{++} zone can be obtained from the ratio $\underline{R} \equiv \underline{I}([O\ III]\lambda 4959+5007)/\underline{I}([O\ III]\lambda 4363)$, even though this is normally

used as a measure of the temperature (Osterbrock 1974). Indeed, Figure 11 shows that the observed value ($\underline{R}$ = 6.65) cannot be achieved unless $\underline{n}_e$ is at least $\sim 10^{5.5}$ cm^{-3}, for any reasonable temperature. Within the range $10000 \leq \underline{T}_e \leq 25000$ K ($4.0 \leq \log \underline{T}_e \leq 4.4$) the density must be between 10^6 and 10^7 cm^{-3}. If $\underline{T}_e$ = 16000 K ($\log \underline{T}$ = 4.2), which is near the high end in Seyfert galaxies (Koski 1978), then $\underline{n}_e = 10^{6.4}$ cm^{-3}. The derived density becomes still higher if relative intensities of emission lines are corrected with $\underline{A}_V$ = 0.61 mag, as suggested by the continuum decomposition (Paper II). This startling result clearly demonstrates that enormous differences in density must exist in the forbidden-line gas of NGC 7213.

Similar arguments could be applied to [N II]λ5755 and [O I]λ5577, but these nondetections do not provide useful additional constraints on $\underline{n}_e$ and $\underline{T}_e$. The situation could change if an absorption template were accurately subtracted from this spectral region.

It is important to mention that high $\underline{n}_e$ in the O^{++} zone exists in several broad-line radio galaxies (Osterbrock, Koski, and Phillips 1976) and low-redshift QSOs (Baldwin 1975): the small value of $\underline{R}$ in 3C 390.3, 3C 382, PKS 0837-12, and PKS 1217+02 indicate that $\underline{n}_e \gtrsim 10^6$ cm^{-3}. These galaxies are cases of extreme activity, and their Balmer lines are generally broader than those in classical type 1 Seyferts. There has previously been no conclusive evidence that such large densities are also found in the narrow-line regions of less luminous Seyferts or in LINERs, however. The observed ratios $\log \{\underline{I}([O\ III]\lambda 4959+5007)/\underline{I}([Ne\ III]\lambda 3869+3967)\} = 0.47$ and $\log \underline{R} = 0.82$, for example, place NGC 7213 in the lower left corner of Figure 1 in Heckman and Balick (1979), suggesting $\underline{n}_e \sim 10^{6.6}$ cm^{-3} and

T_e ~ 13000 K. Almost all other objects in Figure 1 have a lower density, and the two exceptions are peculiar in that the derived T_e seems unreasonably low ($T_e \lesssim 7500$ K).

The density estimate for the O^{++} zone was made under the assumption that all 3 of the [O III] lines are produced in the same clouds, but Table 1 and Figure 7 show that [O III]λ4363 is broader than the nebular lines. Since regions with $n_e \sim 10^7$ cm^{-3} produce more [O III]λ4363 (n_e(crit) ~ 3 x 10^7 cm^{-3}) relative to [O III]λ4959,5007 (n_e(crit) ~ 7.9 x 10^5 cm^{-3}) than those with $n_e \sim 10^6$ cm^{-3}, a single value of the density cannot, strictly speaking, be obtained from the observed ratio R. The quoted value of $10^{6.4}$ cm^{-3} is biased toward high densities, and a more reasonable interpretation is that $n_e \gtrsim 10^7$ cm^{-3} in clouds which produce most of the auroral line, whereas $n_e \lesssim 10^6$ cm^{-3} in those from which a majority of the nebular emission arises.

The existence of a region with $n_e \sim 10^7$ cm^{-3} (as for [O III]λ4363) implies that Balmer emission should be enhanced relative to [O III]λ4959,5007 in NGC 7213 (Péquignot 1984). This occurs because n_e is considerably greater than n_e(crit) for [O III]λ4959,5007. Thus, while Balmer emission is proportional to n_e^2 at $n_e \sim 10^7$ cm^{-3}, nebular [O III] is only proportional to n_e, so the former should be stronger relative to the latter than in the low-density ($n_e \sim 10^3$-10^5 cm^{-3}) clouds normally found in the narrow-line regions of active galactic nuclei. Figure 2c shows that this is true in NGC 7213: [O III]λ4959+5007 is roughly a factor of 4.4 stronger than the corresponding component of Hβ, noticeably smaller than the value of 10–20 generally found in Seyfert 2 galaxies (Koski 1978) and in the narrow-line regions of type 1 Seyferts. Of course, part of this

decrease in [O III] is also due to the low ionization parameter generally associated with LINERs.

These results unambiguously demonstrate that large density variations among clouds of gas in the narrow-line region of NGC 7213 play an important role in determining the emission-line spectrum, and it is inferred that other galaxies, such as NGC 1052 (Keel and Miller 1983), might be similarly affected. Lines of a given element which arise from different stages of ionization may not necessarily be directly compared in photoionization and shock models, and in classification schemes (e.g., Heckman 1980; Baldwin, Phillips, and Terlevich 1981). Even different lines produced by the same ion can originate in regions having substantially different physical conditions. Evidence for this based on relative intensities has been presented in several previous investigations (e.g., Heckman and Balick 1979), but NGC 7213 is by far the most convincing case to date since it also exhibits a variety of profiles. Thus, one must exhibit caution when deducing physical parameters such as reddening (Malkan 1983a), density, and temperature. It is also not a simple task to use the line strengths in photoionization models, since most of these are too simplistic (e.g., constant density or pressure) to allow for the different observed conditions in NGC 7213.

d) Geometry and Kinematics

In NGC 7213 line widths are correlated primarily with the density rather than the ionization state. Such a situation can arise if individual clouds of differing densities are all optically thick to Lyman continuum radiation, since several different stages of ionization

are represented in each cloud.

If clouds move freely in the potential well of a massive central object, and if they are in pressure equilibrium with a hot confining medium (§VIIa), then the densest ones should be closest to the nucleus and have the greatest velocities. Figure 7 and the measured wavelengths of emission lines are consistent with this, but dust must be present in the clouds to provide selective obscuration. In particular, narrow lines such as [S II]λ6716,6731, as well as the very weak, narrow components of broader lines (e.g., [O III]λ4959,5007) share the systemic (absorption line) velocity of NGC 7213, whereas Table 1 shows that the broad components of forbidden lines (especially those associated with high ionization potentials) are systematically blueshifted. One interpretation is that the dense clouds have substantial radial motions. Suppose that dust survives in the neutral and singly-ionized zones, but not in the hot regions where [Ne III], [O III], and [Ne V] are produced. The high-ionization lines will be seen preferentially from the illuminated faces of clouds beyond the continuum source. If most of the clouds are approaching the nucleus or emit primarily during the inward leg of a Keplerian orbit (as in the model of Carroll and Kwan 1983: §VIIc), then the high-ionization lines will be blueshifted. [O I], on the other hand, which is produced throughout the neutral, dusty region will have no preferred direction. Lines of [O II] and [S II] may or may not exhibit net blueshifts, depending on the distribution of dust and on the cloud kinematics; in NGC 7213, the auroral and transauroral components are slightly blueshifted, while the nebular ones are not, emphasizing once again that not all lines are emitted from the same clouds (§Vc). It is also possible that the narrow peaks of emission

lines, including those of [O III] mentioned above, might be produced in a "reservoir" of low-density gas which is far from the nucleus, moves rather slowly, and does not suffer from as much obscuration by dust.

e) The Balmer Decrement

It is not possible to obtain separate Balmer decrements for each of the Gaussian components of Hα in Figure 3e. The flux within the entire profile of a Balmer line is therefore computed, with the exception of the very narrowest component of Hα (Gaussian C in Table 2) and Hγ (the "spike" in Figure 4c). The observed decrement (Galactic $A_V = 0.05$ mag removed) is

$$I(H\alpha)/I(H\beta)/I(H\gamma)/I(H\delta) = 6.20/1.00/0.35/0.12 .$$

If the Balmer lines are produced purely by recombination, then at an average density of 10^7 cm^{-3} and a temperature of 1.5×10^4 K the Case B decrement should be (Brocklehurst 1971)

$$I(H\alpha)/I(H\beta)/I(H\gamma)/I(H\delta) = 2.76/1.00/0.47/0.26 ,$$

which differs significantly from the observed one. A standard assumption is that dust reddens the lines, in which case $I(H\alpha)/I(H\beta)$, $I(H\gamma)/I(H\beta)$, and $I(H\delta)/I(H\beta)$ imply $A_V \sim 2.2$, 2.0, and 3.5 mag, respectively. The last of these is very uncertain due to the weakness of Hδ, but the first two show good agreement, so $A_V = 2.1$ mag is adopted. This exceeds the value $A_V = 0.61$ mag obtained for the continuum. Such a discrepancy is common, particularly in broad-line radio galaxies (Osterbrock, Koski, and Phillips 1976).

At high densities, however, self-absorption (Netzer 1975) and collisional excitation (Kwan and Krolik 1981) also produce substantial deviations from recombination theory. They probably play some role in

NGC 7213, since an extrapolation of the optical nonstellar continuum beyond the Lyman limit is inadequate to produce the observed Balmer emission (corrected with $A_V = 2.1$ mag). In particular, the Hα flux expected with the $(\alpha, A_V) = (1.1, 0.61)$ continuum decomposition discussed in §IIb (and derived in Paper II) and a covering fraction $\lesssim 0.3$ (Paper II) is $\lesssim 3.0 \times 10^{-13}$ erg s^{-1} cm^{-2}, which is a factor of $\gtrsim 30$ smaller than the dereddened ($A_V = 2.1$) observed flux.

On the other hand, if part of the difference between the observed and theoretical decrements is not caused by dust, or if the covering fraction is larger, the calculated shortage of ionizing photons becomes less severe. Moreover, there is no guarantee that the simple extrapolation used above is valid, especially in light of Péquignot's (1984) recent arguments favoring a pronounced maximum in the continuum blueward of the Lyman limit in the LINER NGC 1052. Evidence for a similar feature in NGC 7213 is provided by the possible "UV bump" (Paper II), which may be due to thermal radiation from a hot ($T \sim 8 \times 10^4$ K) accretion disk (Malkan 1983b; Péquignot 1984). Hence, there may in fact be very little discrepancy between theory and observations.

It is interesting to note that NGC 7213 is consistent with Shuder's (1981) strong correlation between the flux of Hα and that of the nonthermal continuum at λ4800 in radio galaxies, type 1 and 2 Seyfert galaxies, and QSOs. This provides good evidence for photoionization, even though the NGC 7213 data, corrected for Galactic extinction ($A_V = 0.05$ mag), show a deficit of nonthermal flux in comparison with the average of Seyferts. The deficit is within the range observed by Shuder (1981), however, and is reduced substantially if an extinction of

0.61 mag (Paper II) rather than 0.05 mag is assumed. The "UV bump" discussed above and advocated by Malkan (1983b) and Péquignot (1984) can probably account for the remaining discrepancy.

f) Ultraviolet Emission Lines

Wu, Boggess, and Gull (1983) noted that the I(C IV λ1550)/I(C III] λ1909) ratio of 1.9 in NGC 7213 is unusually low in comparison with the average of 5 for Seyfert 1 galaxies. The strength of these lines relative to Hβ (Table 1) suggests that they are produced in a region whose ionization parameter (U) is $\sim 10^{-2}$ (Halpern 1982), as expected for the broad-line region. It would be important to measure their widths and compare them with the optical forbidden lines to test this hypothesis.

VI. LINERs: PHOTOIONIZATION OR SHOCKS?

Photoionization models involving nonstellar power laws have enjoyed considerable success at explaining the emission lines in Seyfert galaxies and QSOs (e.g., Boksenberg and Netzer 1977; Ferland 1981), especially following the incorporation of improved cross sections for charge-exchange reactions (Butler, Heil, and Dalgarno 1980). In some cases, however, the strong [O III]λ4363 line relative to [O III]λ4959+5007 is thought to imply temperatures too large to be compatible with photoionized gas. The prototype is NGC 1052, which Fosbury et al. (1978) concluded is heated by shocks. Based on their spectral similarity to NGC 1052, Heckman's (1980) LINERs are also often regarded as shock heated (Baldwin, Phillips, and Terlevich 1981). On the other hand, the strengths of several lines in the spectrum of

NGC 1052 are inconsistent with this (Ferland and Netzer 1983). Moreover, Halpern and Steiner (1983) and Ferland and Netzer (1983) demonstrate that photoionization models having remarkably few free parameters provide adequate agreement with observations if $\underline{U}$ is low enough. In fact, they see a continuity between the characteristics of Seyferts and LINERs which can be reproduced by a systematic variation of $\underline{U}$. LINERs, for example, show strong emission from neutral and singly-ionized species due to relatively low values of $\underline{U}$ and/or high covering fractions.

This simplicity is a tremendous virtue of the power-law hypothesis. Nevertheless, it has been questioned because of its apparent inability to explain the derived temperatures. But a frequently overlooked fact is that high temperatures result only under the assumption that the density in the O^{++} region is comparable to that deduced from the [O II]λ3726,3729 and [S II]λ6716,6731 doublets, which is typically $\sim 10^3$-10^4 cm^{-3}. In NGC 7213 this is clearly not the case: $\underline{n}_e$ is between 10^6 and 10^7 cm^{-3}, and it must be emphasized that the observed [O III] intensity ratio cannot be reproduced at any reasonable temperature if $\underline{n}_e \lesssim 10^{5.5}$ cm^{-3} (Figure 11). Photoionization models therefore can account for the [O III] intensity ratio in NGC 7213, since an excessive $\underline{T}_e$ is not implied. Moreover, the lines produced by elements in low stages of ionization also have a well-understood origin, as their relative intensity ratios do not markedly differ from those in LINERs and Seyfert galaxies.

Although shock models can also reproduce many of the observed relative intensities of lines, they do not readily (if at all) explain the presence of [Ne V]λ3426 and broad Balmer emission, and the power-law

component visible in the optical spectrum also should be absent. Moreover, Paper II demonstrates that the X-ray spectrum of NGC 7213 is represented by $f_\nu \propto \nu^{-0.72 \pm 0.12}$, which is similar to that in many Seyfert galaxies. The compact, flat-spectrum nuclear radio source, "UV bump," and characteristic shape of the continuum from IR through X-ray wavelengths are additional features that have counterparts in other active extragalactic objects (Paper II). Finally, after accounting for the range in gas densities only He II λ4686 appears considerably weaker than the value predicted by photoionization models, but this is often a puzzle even in classical Seyferts. A possible solution has been discussed by Péquignot (1984), whose calculations include the effects of a sharp decrease in the number of ionizing photons at energies above ~ 3-4 ryd.

Thus, there can be little doubt that gas near the nucleus of NGC 7213 is ionized predominantly by nonstellar radiation, although Filippenko (1982b) originally conjectured that shocks may be significant. Of course, some shock heating is almost certainly present given the high observed velocities of clouds, but the effects of the ionizing continuum are probably dominant. The spectrum differs from that of normal Seyfert galaxies due to the lower ionization parameter and wider range of densities in its narrow-line region. In particular, clouds with $n_e \sim 10^6$-10^7 cm^{-3} produce strong [O I]λ6300,6364, [O III]λ4363, and other lines associated with high values of n_e(crit).

An important point to remember is that obvious differences in line width provided the major indication that several distinct regions contribute to the emission-line spectrum in NGC 7213. The analysis was straightforward because lines originating in regions having different

densities were not used to derive physical parameters. A number of the LINERs studied by Heckman (1980) show similar behavior (Filippenko 1984), so NGC 7213 is not unique. Furthermore, Péquignot (1984) actually uses measured intensity ratios to predict that the gas density in the nucleus of NGC 1052 is stratified in the manner reported here (see § VII). There is no a priori reason to suppose, however, that such a clear demarcation of various clouds must occur in every LINER. In particular, regions of high and low n_e need not have markedly different velocities. If the narrow-line clouds are moving ballistically away from the nucleus, for example, then the equation of mass continuity implies that $n_e \propto r^{-2}$ (where r is the distance from the nucleus), whereas the velocity is roughly independent of r. Hence, other galaxies may contain clouds having dissimilar density whose relative contributions to particular emission lines are not equal, but until now there was no compelling reason for this assumption.

In light of the simplicity of the photoionization hypothesis and its success at explaining the wide range of behavior seen in active galactic nuclei, it would be worthwhile to conduct detailed investigations of many LINERs. If the same conclusions can be drawn for a substantial number of cases, then it is possible that a majority of active galaxies are powered by nonstellar radiation produced near a massive central object, as suspected by Keel (1983a), Ferland and Netzer (1983), and Halpern and Steiner (1983).

VII. THEORY

a) General Considerations

A successful model for the forbidden lines in NGC 7213 must account

for the correlation between their width and critical density, FWHM $\propto n_e(\mathrm{crit})^{0.19\pm0.02}$. The following discussion is based on the assumption that photoionization by a nonstellar continuum is the major source of energy input, as argued in §VI. It is also assumed that the FWHM of a line represents the bulk motion of clouds whose density is equal to the critical density for that line. Figure 7 therefore indicates that

$$\left(\frac{v}{10^3}\right) = \left(\frac{n}{10^6}\right)^{1/5} \qquad (2)$$

represents an approximate relation between cloud velocity and density if the units of n and v are cm^{-3} and $\mathrm{km\ s}^{-1}$, respectively.

Consider clouds in Keplerian orbits, for which $v \propto r^{-1/2}$. One can transform r via $U \propto Ln^{-1}r^{-2}$, where U is the ionization parameter and L is the ionizing luminosity. As long as L is constant over a dynamical timescale, $v \propto (nU)^{1/4}$. Equation (2) is therefore consistent with Keplerian orbits in which U is constant or a very slowly varying function of r. In particular, U must change by less than a factor of 10 while n varies by 10^4.

Approximate constancy of U is an important result of the two-phase model of emission-line regions in QSOs (Krolik, McKee, and Tarter 1981, hereafter KMT), since it reproduces the narrow range actually observed. The broad-line clouds are confined in pressure equilibrium with a hot intercloud medium which is Compton heated by a hard X-ray continuum, and two-phase equilibrium is possible only for a narrow range of U dictated by the atomic physics. This model will be extended to the narrow-line region of NGC 7213, and the existence of a hot confining medium will be demonstrated. Much of what follows parallels discussions in KMT and in

Krolik and Vrtilek (1984).

For calculational convenience, the ionizing continuum is represented by a power law with an exponential cutoff at high energies. Specifically,

$$f_\nu = f_o \left(\frac{\nu}{\nu_o}\right)^{-1} \exp\left(-\frac{\nu}{\nu_m}\right) \quad \text{erg cm}^{-2}\,\text{s}^{-1}\,\text{Hz}^{-1} , \qquad (3)$$

where ν_o = 1 ryd, $\nu_m = 10^4$ ryd, and f_o is the flux density at the Lyman limit (observed at the earth). U is the dimensionless ratio of ionizing photon density to nucleon density n at the face of a cloud:

$$U = \frac{d^2}{cnr^2} \int_{\nu_o}^{\infty} \frac{f_\nu}{h\nu}\, d\nu \approx \frac{f_o d^2}{chnr^2} , \qquad (4)$$

where d is earth's distance from the object. The dynamical time scale is

$$t_{dyn} = \frac{r}{V} = \frac{d}{V}\left(\frac{f_o}{chnU}\right)^{1/2} . \qquad (5)$$

For NGC 7213, d = 35.4 Mpc and $f_o \sim 0.67$ mJy (extrapolating the power law in Figure 1b of Paper II to the Lyman limit), so

$$t_{dyn} \approx 2\times 10^{11} \left(\frac{10^3}{V}\right)\left(\frac{10^6}{n}\right)^{1/2}\left(\frac{10^{-3}}{U}\right)^{1/2} \text{ s.} \qquad (6)$$

In the absence of a confining mechanism, a cloud of radius a will expand at roughly the sound speed with time scale $t_{exp} = a/c_s$. Thus,

$$t_{exp} \approx 6\times 10^{9} \left(\frac{10^4}{T}\right)^{1/2}\left(\frac{N_H}{10^{22}}\right)\left(\frac{10^6}{n}\right) \text{ s.} \qquad (7)$$

where $N_H \sim an$ is the column density. If $T = 10^4$ K and $N_H \sim 10^{22}$ cm^{-2}

(Kwan and Krolik 1981; Halpern and Steiner 1983), and if $\underline{U} = 3 \times 10^{-3}$ is typical for LINERs (Halpern and Steiner 1983), then $\underline{t}_{exp}$ is shorter than $\underline{t}_{dyn}$ for $\underline{n} \gtrsim 60$ cm^{-3}. Clouds would therefore not survive even one crossing time in the absence of a confining mechanism.

Cold clouds may be confined by a hot intercloud medium (referred to by the subscript $\underline{h}$) provided that $\underline{n}_{\underline{h}}\underline{T}_{\underline{h}}$ is large enough. Its minimum density may be derived by assuming that evaporation of the clouds themselves is the only source of gas. Suppose spherical clouds of radius $\underline{a}$ are uniformly distributed with filling factor $\underline{F}_{\underline{f}}$ (or covering fraction $\underline{F}_{\underline{c}} = 3\underline{r}\underline{F}_{\underline{f}}/4\underline{a}$). The equilibrium intercloud density $\underline{n}_{\underline{h}}$ is given by

$$v_h n_h / r = F_f n / t_{exp} \quad , \qquad (8)$$

where $\underline{v}_{\underline{h}}$ is the velocity with which the intercloud gas leaves the system. Substituting $\underline{F}_{\underline{c}}$ and equation (7) into equation (8), it is found that

$$n_h \approx 2 \times 10^4 \, F_c \left(\frac{T}{10^4}\right)^{1/2} \left(\frac{n}{10^6}\right)\left(\frac{10^3}{v_h}\right) \quad \text{cm}^{-3} \, . \qquad (9)$$

A medium of this density would be sufficient to confine the narrow-line clouds provided it could be heated to $\underline{T}_{\underline{h}} \gtrsim 10^6$ K. The required heat input to the confining medium can be provided by photoionization, which for $\underline{T}_{\underline{h}} \sim 10^6$ K has the rate $\Gamma_p \sim 10^{-23}$ erg cm^3 s^{-1} (KMT). The heating time is then

$$t_{heat} = \frac{3kT_h}{n_h \Gamma_p} \approx 4 \times 10^9 \left(\frac{T_h}{10^6}\right)\left(\frac{10^4}{n_h}\right) \quad \text{s} \, , \qquad (10)$$

which is comparable to $\underline{t}_{exp}$ but much shorter than the crossing time.

This heating mechanism represents a point of departure from models of the broad-line region. Gas cannot be heated to the Compton equilibrium temperature of $\sim 10^8$ K since the heating time for the Compton process is much longer than the dynamical time scale of the narrow-line region. Instead, the equilibrium $\underline{T}_h$ may be estimated by balancing the photoionization heating and dynamical times. Combining equations (2), (6), and (10), and invoking pressure equilibrium between the hot medium and cold clouds ($\underline{nT} = \underline{n}_h \underline{T}_h$) yields

$$T_h \approx 7 \times 10^6 \left(\frac{n}{10^6}\right)^{3/20} \left(\frac{10^{-3}}{U}\right)^{1/4} \left(\frac{T}{10^4}\right)^{1/2} \quad K. \qquad (11)$$

Therefore the temperature range of the hot medium is approximately $2 \times 10^6 \lesssim \underline{T}_h \lesssim 9 \times 10^6$ K if $10^3 \lesssim \underline{n} \lesssim 3 \times 10^7$ cm^{-3} and $\underline{U} = 3 \times 10^{-3}$. Note that "coronal" emission lines of [Fe X] and [Fe XIV] should be negligible since the gas is much more highly ionized than thermal plasma of similar temperature.

The allowed range of ionization parameter in pressure equilibrium is determined by the atomic physics and the spectral shape of the continuum radiation, so it should be comparable for the broad- and narrow-line regions. For QSOs, KMT found $0.3 < \Xi < 10$, where Ξ is proportional to the ratio of radiation pressure to gas pressure and may be somewhat lower in LINERs (as suggested by the discussion in subsection b). For the spectrum of equation (3),

$$\Xi = \frac{d^2}{cnkTr^2} \int_{\nu_0}^{\nu_1} f_\nu \, d\nu \approx \frac{f_0 \nu_0 d^2}{cnkTr^2} \ln\left(\frac{\nu_1}{\nu_0}\right), \qquad (12)$$

where $\nu_0 = 1$ ryd and $\nu_1 = 10^3$ ryd. Since the cloud temperature $\underline{T} \sim 10^4$ K, equations (4) and (12) can be used to obtain

$$U = \frac{kT\Xi}{h\nu_0} \Big/ \ln\left(\frac{\nu_1}{\nu_0}\right) \approx 0.01 \, \Xi \, . \qquad (13)$$

Hence, $3 \times 10^{-3} < \underline{U} < 10^{-1}$, in reasonable agreement with observations.

The angular size of the emission-line region can be derived from equation (5):

$$\theta = \frac{r}{d} \approx 1.2 \left(\frac{10^3}{n}\right)^{1/2} \left(\frac{10^{-3}}{U}\right)^{1/2} \text{ arc sec.} \qquad (14)$$

This predicts that the region should be unresolved for $\underline{n} \gtrsim 10^3$ cm^{-3}.

b) Comparison with Existing Models

A constant $\underline{U}$, in conjunction with any kinematic model involving Keplerian orbits, produces a $\underline{v} \propto \underline{n}^{1/4}$ dependence, and it is encouraging that the observations agree so closely with this "dimensional" argument. Shock models, on the other hand, have difficulty explaining this behavior; they predict no correlation, or at best a continuity, in the velocity of clouds which produce the [O I], [O II], and [O III] lines (among others).

Several detailed models of the narrow-line region have recently been proposed. One of these (Carroll and Kwan 1983, hereafter CK) considers clouds in gravitational infall (parabolic orbits) and explicitly predicts that the line width should increase with $\underline{n}_e(\underline{crit})$. The assumptions of the model include confinement by an isothermal medium and $\underline{n} \propto \underline{r}^{-2}$, so that $\underline{U}$ remains constant with $\underline{r}$. In addition, the clouds remain optically thick at all radii so that all ionization stages up to a certain level are present at all velocities. Clouds at $\underline{n} \sim 10^6$ cm^{-3}, for example, cannot be optically thin to the Lyman continuum, because then [O I]λ6300,6364 could not be produced at high velocities. Outflow models tend to produce optically thin clouds, so in this case line width might correlate better with ionization state than with critical density.

The line widths predicted by CK agree well with the observed velocity widths, except that CK assume a relatively strong, narrow component (FWHM ~ 250 km s^{-1}) in each line, which is supposed to arise in a reservoir of low-density gas. The net effect is to drastically reduce the variation of FWHM relative to that of the FWZI. No significant differences between FWHM and FWZI are observed in Figure 7, which argues against a large reservoir of low-density gas. The line intensity ratios predicted by the model are also not in good agreement with observations of NGC 7213, since parameters of the model were obviously adjusted to best fit the "average" Seyfert galaxy, whose ionization level is higher than that of LINERs. Note, however, that the predicted ratio I([O III]λ5007)/I([O III]λ4363) = 5 for the infalling clouds alone (neglecting the narrow-line reservoir) agrees perfectly with the observations (Table 1).

CK successfully explain the blueshifted centroids of forbidden lines, which are especially prominent among [Ne V], [Ne III], and [O III]. Although the clouds are in Keplerian orbits, emission during outflow is much weaker than that from the inward leg. If the clouds contain appreciable quantities of dust, then infalling clouds on the far side of the continuum source will be preferentially seen, resulting in a net blueward asymmetry. As discussed in § V*d*, this asymmetry need not be present in all of the lines. It is also entirely consistent with a constant value of U, particularly since various lines are emitted by different clouds. Furthermore, U can vary by up to a factor of ten in NGC 7213 (§ VII*a*), thereby producing additional stratification in the line-emitting zones.

The CK model applies only if gravity dominates over radiation

pressure, and hints that the property which distinguishes NGC 7213 and other LINERs from "normal" Seyfert galaxies may be an abnormally low ratio of ionizing flux to central mass. For an optically thick cloud it is necessary that

$$M > L_{ion} / (4\pi c G m_H N_H) \quad g, \qquad (15)$$

where m_H is the mass of a hydrogen atom and L_{ion} is the luminosity between 1 and ~ 100 ryd. Thus,

$$\frac{M}{M_\odot} > 1.2 \times 10^7 \left(\frac{10^{22}}{N_H}\right)\left(\frac{L_{ion}}{10^{43}}\right) , \qquad (16)$$

and $M \sim 2 \times 10^7\ M_\odot$ would be sufficient for gravity to dominate in NGC 7213 ($L_{ion} \sim 1.5 \times 10^{43}$ erg s^{-1}). The mass derived assuming Keplerian orbits and $U = 3 \times 10^{-3}$ is $\sim 4 \times 10^8\ M_\odot$, consistent with Equation (16). This simple argument neglects other forces, such as drag by the hot intercloud medium.

Krolik and Vrtilek (1984, hereafter KV) discuss a dynamical model which consists of an outflowing hot wind in a logarithmic potential. The clouds are assumed to be entrained in the wind, and line profiles are generated for both adiabatic and non-adiabatic flows. Although KV do not explicitly consider the effects of n_e(crit) in calculating line profiles, some restrictions can be placed on the parameters of their model. Only the adiabatic solutions agree with the observations in that they decelerate with increasing r, and a consequence of this is that the temperature of the hot medium cannot increase with radius. In addition, the flow is likely to be supersonic everywhere since the sound speed in a gas having $T_h = 10^6$ K is only ~ 100 km s^{-1}. The adiabatic, supersonic

solutions have the property that $\underline{U}$ is nearly independent of $\underline{r}$, whereas $\underline{v}$ decreases slowly. These are exactly the conditions which are inferred from the observed line widths, so that the KV model could in principle be made consistent with the data. Since KV display only one supersonic model, adjustments in additional parameters will be necessary in order to test for quantitative agreement. It also remains to be seen if the outflowing clouds can remain optically thick over a sufficient range in radius to maintain species having low ionization at both low and high velocity.

A similar model is presented by Carleton (1984). Gas which produces the broad lines flows radially into the narrow-line regions (or vice versa), and the emission of the gas is integrated over its lifetime. Carleton (1984) correctly predicts that the widths of forbidden lines should increase with $\underline{n_e}(\underline{crit})$, and the calculated profiles of emission lines resemble those in NGC 7213 (especially is the case of [O I]λ6300,6364). These predictions are also made by Péquignot (1984), and the density stratification on which his models are based is strongly supported by the observations of NGC 7213.

To conclude, it appears that simple kinematic arguments can account for the general behavior of velocity width versus critical density. Detailed fitting of the line strengths and profiles may in the future discriminate between the various dynamical models which have been proposed. At present, the model by CK seems to most naturally explain the data in a quantitative manner.

VIII. SUMMARY

New optical spectra of the nearby S0 galaxy NGC 7213 are analyzed.

Due to the presence of a very strong stellar component, a major effort is made to accurately subtract the optical spectrum of an appropriate template galaxy, yielding the uncontaminated emission-line spectrum. Failure to properly remove the absorption lines in previous studies of similar galaxies is probably responsible for overestimates of the strength of weak lines such as [O III]λ4363, which is situated at a high point in the normal stellar continuum.

The following conclusions are drawn in this study:

1) Many of the main characteristics of type 1 Seyfert galaxies are exhibited by the nucleus of NGC 7213. These include broad Balmer emission and forbidden lines of highly ionized species. In addition, Paper II reports the presence of a power-law X-ray spectrum, significant nonstellar flux at optical wavelengths, and possibly a "UV bump." By analogy with classical active extragalactic objects, photoionization is clearly the gas excitation mechanism. On the other hand, the great strength of [O III]λ4363 relative to [O III]λ4959+5007 is reminiscent of the high temperatures seen in shock-heated gas, and initially seems inconsistent with photoionization by a nonstellar continuum. Furthermore, prominent emission from neutral and singly-ionized species suggest that the gas may be heated by shocks.

2) The observations are reconciled with photoionization models by the discovery that densities of order 10^6-10^7 cm^{-3} exist in the narrow-line region. At such high densities, auroral [O III]λ4363 emission is greatly enhanced even at the usual temperature of photoionized gas ($\sim 10^4$ K). Moreover, strong lines from many species of low ionization are produced if the ionization parameter is small and the density is high.

3) Low-density clouds are also present in the emission-line region, as shown by the relative intensities of the nebular [O II] and [S II] doublets. These lines are much narrower than the auroral and transauroral components of the same species, whose widths are comparable to those of [O III]. This implies that clouds having very different bulk motions and densities exist near the nucleus of NGC 7213. Such diversity in the narrow-line region is unprecedented in the study of active galactic nuclei.

4) There is a strong correlation between the width of an emission line and the critical density of the upper level from which the corresponding electron transition occurs. Since any line is most efficiently produced at densities near or just above the critical value if a sufficiently large range of densities is present, this supports the conclusion in (3).

5) The observed relationship between velocity width and density ($v \propto n^{1/5}$) is consistent with clouds moving in Keplerian orbits while maintaining a nearly constant ionization parameter. This can be understood by a natural extension of the two-phase model of QSO emission-line regions. Strong density stratification is a feature of several other theoretical studies as well.

6) The Balmer decrement indicates $A_V = 2.1$ mag in the absence of other effects. A simple extrapolation of the nonstellar continuum (derived in Paper II) to UV wavelengths is inadequate by roughly a factor of 10 to produce the dereddened Balmer intensities even if the covering fraction is unity, so collisional excitation and radiative transfer probably alter the Case B decrement. Additional ionizing photons from the "UV bump" can alleviate any remaining discrepancy.

7) This investigation may contain the key to the nature of LINERs, whose spectra have been well explained by photoionization models except for the high temperature ($T_e \gtrsim 25000$ K) sometimes derived from the nebular to auroral [O III] intensity ratio. Due to this discrepancy, and to the strong lines from neutral and singly-ionized species, emission in LINERs has often been attributed to heating by shocks. On the other hand, if high densities and large ranges in density are present, as in the case of NGC 7213, the temperature of the ionized gas need not be high to explain the relative line intensities. Photoionization by a nonstellar continuum is then the most likely mechanism of gas excitation, and the low-ionization lines indicate that the ionization parameter is lower than in classical Seyfert galaxies.

It is a pleasure to thank S. A. Shectman, G. Yanik, and K. Clardy for the design, construction, and maintenance of the hardware and software associated with the Intensified Reticon detector at Las Campanas Observatory. The enthusiastic help of night assistants A. Guerra and F. Peralta, and of day assistants H. Solis and W. Robinson, is greatly appreciated. Useful discussions were enjoyed with W. L. W. Sargent, J. B. Oke, M. Elvis, N. P. Carleton, D. P. Schneider, M. A. Malkan, and W. C. Keel. An anonymous referee made many valuable remarks. Thanks are due to P. J. Young for the data reduction program (LOLITA) and to T. J. Pearson for much of the software used to produce the figures. Some of the results in this paper were presented by A. V. F. at a workshop on "Ionization Mechanisms in Emission-Line Nuclei of Galaxies" (Pagel and Edmunds 1983). The Fannie and John Hertz Foundation provided financial assistance to A. V. F.

through a graduate fellowship, and additional support was obtained from NSF grant AST-8216544 to W. L. W. Sargent and NASA grant NGL 05-002-134 to J. B. Oke. Observations were made as part of the cooperative agreement between the Carnegie Institution of Washington and Caltech.

TABLE 1

Properties of Emission Lines in NGC 7213

1 Line (* blend)	2 λ(lab) (Å)	3 Δλ(cen.) (Å)	4 Δλ(peak) (Å)	5 I/I(N2) (A_V = 0.05)	6 I/I(N2) (A_V = 0.61)	7 FWHM (Å)	8 FWZI (Å)	9 km $s^{-1}A^{-1}$
CIV	1549.5	...	...	6.80[a]	13.2[a]	...	...	193
CIII]	1908.7	...	...	3.59[a]	6.93[a]	...	...	157
[Ne V] *	3345.83	-3.93[b]	...	0.046±0.021	0.061	17.9±4.5	46.0±14.5	89.6
[Ne V]	3425.87	-1.27	...	0.142±0.026	0.184	22.3±2.6	61.9±8.8	87.5
[O II] *	3726.05 + 3728.80	-0.40[c]	0.08[c]	0.429±0.011	0.516	7.1±0.5	20.1±2.5	80.4
[Ne III]	3868.76	-2.16	-0.46	0.342±0.021	0.410	15.9±0.9	50.1±4.3	77.5
He I * + Hζ *	3888.65 3889.05	...[d]	...	0.091±0.028	0.108	15.5±2.0	45.0±7	77.1
[Ne III]* + Hε *	3967.47 3970.07	...[e]	...	0.140±0.026	0.164	17.3±2.6	43.0±10.6	75.6
[S II] *	4068.60 + 4076.35	-0.70[f]	...	0.217±0.022	0.251	17.0±2.0	46.0±7	73.7
Hδ *	4101.73	-1.61[g]	...	0.165±0.066[h]	0.190	11.0±3.0	24±9	73.1
Hγ *	4340.46	-0.70[g]	0.40	0.516±0.052[h]	0.571	25±9	190±40	69.1
[O III] *	4363.21	-4.21	...	0.203±0.020	0.224	23.3±3.6	67.0±12	68.7
He II	4685.75	-0.95	...	0.064±0.032	0.067	25.5±6	63±15	64.0
Hβ	4861.33	-1.43[g]	-0.33	1.435±0.060[h]	1.462	28±10	250±40	61.7
[O III]	4958.92	-2.32	0.08	0.353±0.020	0.355	20.5±2.0	56.0±8.4	60.5
[O III]	5006.85	-3.45	-0.05	1.000±0.025	1.000	19.4±1.0	64.9±4.5	59.9
[N I] *	5197.94 + 5200.41	-0.51[c]	...	0.044±0.015	0.043	3.5±0.8	11.0±2	57.7
He I	5875.64	-0.7	...	<0.09[i]	<0.08[i]	15±10	40±25	51.0
[O I]	6300.32	-0.52	-0.12	0.825±0.029	0.705	14.5±1.1	59.9±3.8	47.6
[O I]	6363.81	0.29	0.59	0.278±0.019	0.236	13.8±2.0	53.9±7.0	47.1
[N II][j] *	6548.06	0.32	...	0.160±0.024	0.133	7.2±1.5	23.5±4.6	45.8

(Table 1, continued)

Hα *	6562.79	0.21[k]	-0.19	9.04±0.04[l]	7.50[l]	45±20	420±50	45.7
[N II] *	6583.39	0.32	...	0.479±0.072	0.396	7.2±1.5	23.5±4.6	45.5
[S II]	6716.42	0.50	...	0.267±0.006	0.218	7.4±0.5	23.8±1.3	44.6
[S II]	6730.78	0.22	...	0.269±0.006	0.220	7.0±0.5	22.9±1.3	44.5
[O II] *	7319.1 + 7330.2	-1.19[c]	...	0.371±0.037	0.288	25.2±2.9	65.0±9.3	40.9

Notes to Table 1

Column 1: Identification of species. Asterisks indicate major blends.

Column 2: Lab wavelength, in air (vacuum λ for CIV, CIII]). Bowen (1960) source of most lines.

Column 3: λ(observed centroid) - λ(lab). Typical error ~ ± 0.5 Å, worse for weaker lines. Systemic velocity $\underline{v}$ = 1769 km s^{-1} removed.

Column 4: λ(observed peak) - λ(lab), given only if differs significantly from Column (3).

Column 5: Dereddened (A_V = 0.05 mag) flux relative to [O III]λ5007 ≡ N2 = 2.119 x 10^{-13}erg $s^{-1}cm^{-2}$.

Column 6: Dereddened (A_V = 0.61 mag) flux relative to [O III]λ5007 ≡ N2 = 3.768 x 10^{-13}erg $s^{-1}cm^{-2}$. Relative errors similar to those in Column (5).

Column 7: Full width at half-maximum (instrumental width removed).

Column 8: Full width at zero-intensity (instrumental width removed).

Column 9: Km s^{-1} $Å^{-1}$ at the given λ, for comparison of line widths and velocity shifts.

[a]Derived from Wu, Boggess, and Gull (1983).

[b]Δλ calculated relative to [Ne V], but contamination by [Ne III]λ3342.5 possible.

[c]Close doublet. Δλ calculated relative to average laboratory λ.

[d]He I badly blended with Hζ; uncertain relative strengths. Δλ not calculated.

[e][Ne III] blended with Hε; uncertain relative strengths. Δλ not calculated.

[f][S II] doublet unresolved. Δλ relative to average lab λ, assuming I(4069)/I(4076) = 4.

[g]Refers to component with width comparable to that of [O III]λ5007.

[h]20-25%, 20-25%, and ~ 40% of this total flux in Hβ, Hγ, and Hδ (respectively) is due only to the component described in (g).

[i]Upper limit -- line may be detected, but large uncertainty.

[j]Parameters of [N II]λ6548 fixed relative to [N II]λ6583.

[k]Refers to Gaussian D in Table 2.

[l]Hα absorption removed to first order, but not with template galaxy IC 4889.

TABLE 2

Parameters of Hα Decomposition[a]

Gaussian	Relative amplitude	λ (Å)	FWHM (Å)[b]	Flux[c] (10^{-14}erg $s^{-1}cm^{-2}$)
A	1.00	6481	42.4	4.21
B	2.07	6516.5	25.9	5.27
C	7.81	6562.6	5.65	4.27
D	15.0	6563	50.6	73.6
E	4.91	6585	184	86.8
F	3.14	6645	50.6	15.0

[a]See Figure 3d.

[b]Instrumental resolution (FWHM ~ 2.5 Å) not removed.

[c]Dereddened, A_V = 0.05 mag.

REFERENCES

Baldwin, J. A. 1975, Ap. J., 201, 26.

Baldwin, J. A., Phillips, M. M., and Terlevich, R. 1981, Pub. A.S.P., 93, 5.

Baluja, K. L., Burke, P. G., and Kingston, A. E. 1981, J. Phys. B., 14, 119.

Boksenberg, A., and Netzer, H. 1977, Ap. J., 212, 37.

Bowen, I. S. 1960, Ap. J., 132, 1.

Brocklehurst, M. 1971, M.N.R.A.S., 153, 471.

Burgess, A. 1958, M.N.R.A.S., 118, 477.

Burstein, D., and Heiles, C. 1982, A. J., 87, 1165.

Butler, S. E., Heil, T. G., and Dalgarno, A. 1980, Ap. J., 241, 442.

Carleton, N. P. 1984, private communication.

Carroll, T. J., and Kwan, J. 1983, Ap. J., 274, 113 (CK).

Danziger, I. J., Fosbury, R. A. E., and Penston, M. V. 1977, M.N.R.A.S., 179, 41P.

Dopita, M. A. 1977, Ap. J. Suppl., 33, 437.

Ferland, G. J. 1981, Ap. J., 249, 17.

Ferland, G. J., and Netzer, H. 1983, Ap. J., 264, 105.

Filippenko, A. V. 1982a, Pub. A.S.P., 94, 715.

--------. 1982b, Bull. A.A.S., 14, 947.

--------. 1984, Ap. J., submitted.

Filippenko, A. V., and Greenstein, J. L. 1984, Pub. A.S.P., submitted.

Fosbury, R. A. E., Mebold, V., Goss, W., and Dopita, M. A. 1978, M.N.R.A.S., 183, 549.

Garstang, R. H. 1968, in IAU Symposium 34, Planetary Nebulae, ed. D. E. Osterbrock and C. R. O'Dell (Dordrecht: Reidel) p. 138.

Giles, K. 1979, M.N.R.A.S., 187, 49P.

Halpern, J. P. 1982, Ph.D. thesis, Harvard University.

Halpern, J. P., and Filippenko, A. V. 1984, Ap. J., submitted (Paper II).

Halpern, J. P., and Steiner, J. E. 1983, Ap. J. (Letters), 269, L37.

Heckman, T. M. 1980, Astr. Ap., 87, 152.

Heckman, T. M., and Balick, B. 1979, Astr. Ap., 79, 350.

Heiles, C., and Cleary, M. N. 1979, Aust. J. Phys. Suppl. No. 47, 1.

Kafatos, M., and Lynch, J. P. 1980, Ap. J. Suppl., 42, 611.

Keel, W. C. 1983a, Ap. J., 269, 466.

---------. 1983b, Ap. J. Suppl., 52, 229.

Keel, W. C., and Miller, J. S. 1983, Ap. J. (Letters), 266, L89.

Koski, A. T. 1978, Ap. J., 223, 56.

Koski, A. T., and Osterbrock, D. E. 1976, Ap. J. (Letters), 203, L49.

Krolik, J. H., McKee, C. F., and Tarter, C. B. 1981, Ap. J., 249, 422 (KMT).

Krolik, J. H., and Vrtilek, J. 1984, preprint (KV).

Kwan, J., and Krolik, J. H. 1981, Ap. J., 250, 478.

Lequeux, J., Peimbert, M., Rayo, J. F., Serrano, A., and Torres-Peimbert, S. 1979, Astr. Ap., 80, 155.

Malkan, M. A. 1983a, Ap. J. (Letters), 264, L1.

Malkan, M. A. 1983b, Ap. J., 268, 582.

Mendoza, C., and Zeippen, C. 1982, M.N.R.A.S., 198, 127.

Netzer, H. 1975, M.N.R.A.S., 171, 395.

Nussbaumer, H., and Rusca, C. 1979, Astr. Ap., 72, 129.

Nussbaumer, H., and Storey, P. J. 1981, Astr. Ap., 99, 177.

Oke, J. B., and Gunn, J. E. 1983, Ap. J., 266, 713.

Osterbrock, D. E. 1974, Astrophysics of Gaseous Nebulae. (San Francisco: W. H. Freeman and Co.).

Osterbrock, D. E. 1981, Ap. J., 246, 696.

Osterbrock, D. E., Koski, A. T., and Phillips, M. M. 1976, Ap. J., 206, 898.

Pagel, B. E. J., and Edmunds, M. G. 1983, Nature, 304, 488.

Pelat, D., and Alloin, D. 1980, Astr. Ap., 81, 172.

--------. 1982, Astr. Ap., 105, 335.

Pelat, D., Alloin, D., and Fosbury, R. A. E. 1981, M.N.R.A.S., 195, 787.

Péquignot, D. 1984, Astr. Ap., 131, 159.

Péquignot, D., and Aldrovandi, S. M. U. 1976, Astr. Ap., 50, 141.

Phillips, M. M. 1978, Ap. J. Suppl., 38, 187.

--------. 1979, Ap. J. (Letters), 227, L121.

Pradhan, A. K. 1974, J. Phys. B., 7, L503.

--------. 1976, M.N.R.A.S., 177, 31.

--------. 1978, M.N.R.A.S., 184, 89P.

Rose, J. A., and Tripicco, M. J. 1984, Ap. J., submitted.

Sadler, E. M. 1984, A. J., 89, 23.

Sandage, A. R., and Tammann, G. A. 1981, A Revised Shapley-Ames Catalog of Bright Galaxies. (Carnegie Institution of Washington, Washington, D.C.)

Schneider, D. P., and Young, P. J. 1980, Ap. J., 238, 946.

Seaton, M. J. 1975, M.N.R.A.S., 170, 475.

Shectman, S. A., and Hiltner, W. A. 1976, Pub. A.S.P., 88, 960.

Shuder, J. M. 1981, Ap. J., 244, 12.

--------. 1982, Ap. J., 259, 48.

Shull, J. M., and McKee, C. F. 1979, Ap. J., 227, 131.

Stauffer, J. R. 1982, Ap. J., 262, 66.

Whitford, A. E. 1958, A.J., 63, 201.

Wu, C.-C., Boggess, A., and Gull, T. R. 1983, Ap. J., 266, 28.

Yee, H. K. C., and Oke, J. B. 1978, Ap. J., 226, 753.

Zeippen, C. J. 1982, M.N.R.A.S., 198, 111.

FIGURE CAPTIONS

Figure 1: The dereddened optical spectrum of the central 2" x 4" of NGC 7213, smoothed with a 4.4 Å (FWHM) Gaussian, is shown on a logarithmic wavelength (linear velocity) scale. As in all other spectra illustrated here, the systemic velocity of 1769 km s^{-1} (Sandage and Tammann 1981) was removed. Intensities are linear, but the absolute calibration is uncertain by ~ ± 25%. Over the range ~ λλ3700–6800 the S/N ratio is so high that most features are real.

Figure 2: Spectra of (a) NGC 7213, (b) a template galaxy, and (c) the emission-line component of NGC 7213 obtained by subtracting (b) from (a), are plotted on a logarithmic wavelength (linear velocity) scale. All 3 spectra in each half are shown on the same ordinate scale, but the zero-point offsets differ to improve clarity, and the scale of the bottom half is twice that of the top. The nonstellar continuum is absent in (a), and the metallicity and general continuum shape of IC 4889 were adjusted to roughly match those of NGC 7213. The Galactic extinction ($A_V = 3.2E_{B-V} = 0.05$ mag) was removed in the emission-line spectrum (c). [O II]λ3727 emission in IC 4889 is not shown in (b).

Figure 3: (a) The spectrum of NGC 7213 near Hα is shown on a linear velocity scale. In (b) the stellar continuum and obvious absorption lines (except Hα) are removed. Note the markedly different profiles of [O I] and [S II], which are removed in (c). [N II] is excised next (d), leaving only the asymmetrical Hα. A least-squares fit with the minimal number of Gaussians necessary to yield acceptable residuals (e) is also shown (see Table 2). Each of the 6 components cannot be physically

significant, however, since the Hβ profile (f) has a narrower core.

Figure 4: Spectra (a), (b), and (c) represent a small section of Figure 2. [O III]λ4363 and Hγ are blended in (a), and are contaminated by absorption lines. The template galaxy (b), which lacks emission lines, is drawn on the same relative intensity scale but offset for clarity. It is subtracted from NGC 7213 in (c), revealing the presence of broad Hγ emission that has a close counterpart in the Hβ profile (d). Hβ is scaled so that the red and blue wings match those of Hγ, and in (e) it is subtracted from the blend. What remains is largely [O III]λ4363, but a small, narrow Hγ line is also visible. After removing the remaining Hγ (f), a Gaussian is fit to [O III]λ4363. The approximation is satisfactory, as shown by the residuals (g).

Figure 5: The top 3 spectra represent a portion of Figure 2. Strong absorption lines preclude accurate measurement of most emission in NGC 7213 (a), but IC 4889 (b) provides a close approximation to the stellar component. The net emission-line spectrum of NGC 7213 is shown in (c), revealing the [Ne III]λ3968 + Hε blend which was previously hidden by Ca II H absorption. Similarly, although a high point in the stellar continuum blends [S II]λ4069+4076 and Hδ in (a), the emission lines are well resolved in (c), and a broad component of Hδ is visible as well. Gaussians (d) are used to represent the emission lines, leaving very small residuals (e).

Figure 6: Log FWHM is plotted against $\log\chi$ for each forbidden line, where χ is the ionization potential of the corresponding species. Widths and errors are taken from Table 1. An unweighted linear

least-squares fit formally indicates the presence of a correlation (correlation coefficient $\underline{r}$ = 0.72). Several lines from the same species but with markedly different widths (e.g., [O II], [S II]), however, demonstrate that the correlation is not of fundamental significance, and that χ is at most a secondary parameter.

Figure 7: Log FWHM (filled squares) and log FWZI (open circles) are plotted against log $\underline{n}_e(\underline{crit})$ for each forbidden line, where $\underline{n}_e(\underline{crit})$ is the critical density of the upper level from which the corresponding transition occurs. Widths and errors are taken from Table 1, and uncertainties in theoretically calculated critical densities may be of order $\pm$ 25%. Unlike Figure 6, in which there is considerable scatter, the least-squares fits indicate high correlation coefficients ($\underline{r}$ = 0.92). Note that lines from the same species but with markedly different widths strengthen the correlation. Since gas emits a line most efficiently when it is near $\underline{n}_e(\underline{crit})$ for that line, clouds with different bulk motions and densities must exist in the narrow-line region.

Figure 8: [O II]λ7319+7330 (a) and [O II]λ3726+3729 (c) are plotted on the same velocity and relative intensity scales. The blends are decomposed into their two major constituents, each having the same width. The true width of a line is obtained by removing the instrumental resolution from the observed width. Components of the blue doublet are considerably narrower than the individual red lines, and cannot be produced by the same clouds.

Figure 9: The logarithm of the theoretical intensity ratio of nebular

to auroral [O II] emission (A_V = 0.0) is plotted as a function of log T_e for a range of densities. Dashed lines represent the low- and high-density limits. Points A and B show that the intensity of broad [O II]λ3726,3729 lines from clouds which give rise to the broad auroral lines in NGC 7213 is negligible at reasonable temperatures. Similarly, points C and D indicate that the narrow components of [O II]λ7319,7330 should be difficult to detect.

Figure 10: The theoretical ratio of nebular to transauroral [S II] emission (A_V = 0.0) is plotted in the same manner as in Figure 9, and the interpretation of points A, B, C, and D is similar as well.

Figure 11: The theoretical intensity ratio of nebular to auroral [O III] emission (R) is plotted as a function of log T_e for a range of densities and zero reddening. Dashed lines approximate the low- and high-density limits. In NGC 7213, the observed value R = 6.65 cannot be produced at any temperature unless $n_e \gtrsim 10^{5.5}$ cm^{-3} in clouds which produce the [O III] emission. At T ~ 16000 K, the average density is ~ $10^{6.4}$ cm^{-3}, and the true values are probably $\gtrsim 10^7$ cm^{-3} and $\lesssim 10^6$ cm^{-3} in regions which produce most of the auroral and nebular lines, respectively. The average density can vary between 10^6 and 10^7 cm^{-3} for the large range $4.0 \leq \log T_e \leq 4.4$.

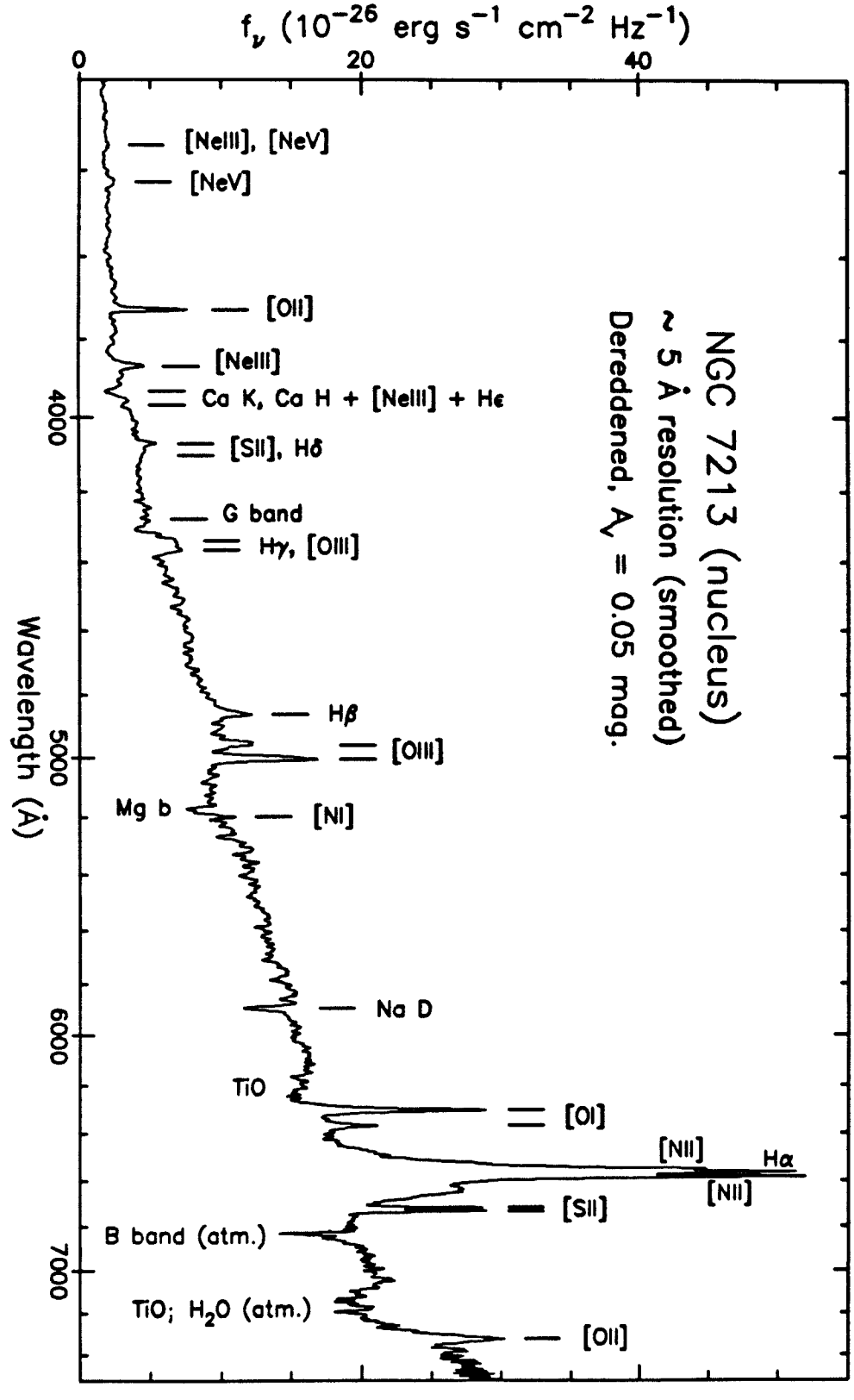
f_ν (10^{-26} erg s^{-1} cm^{-2} Hz^{-1})
0
20
40
Wavelength (Å)
4000
5000
6000
7000
NGC 7213 (nucleus)
~ 5 Å resolution (smoothed)
Dereddened, A_V = 0.05 mag.
[NeIII], [NeV]
[NeV]
[OII]
[NeIII]
Ca K, Ca H + [NeIII] + Hε
[SII], Hδ
G band
Hγ, [OIII]
Hβ
[OIII]
Mg b
[NI]
Na D
TiO
[OI]
[NII]
Hα
[NII]
[SII]
B band (atm.)
TiO; H_2O (atm.)
[OII]

Figure 1

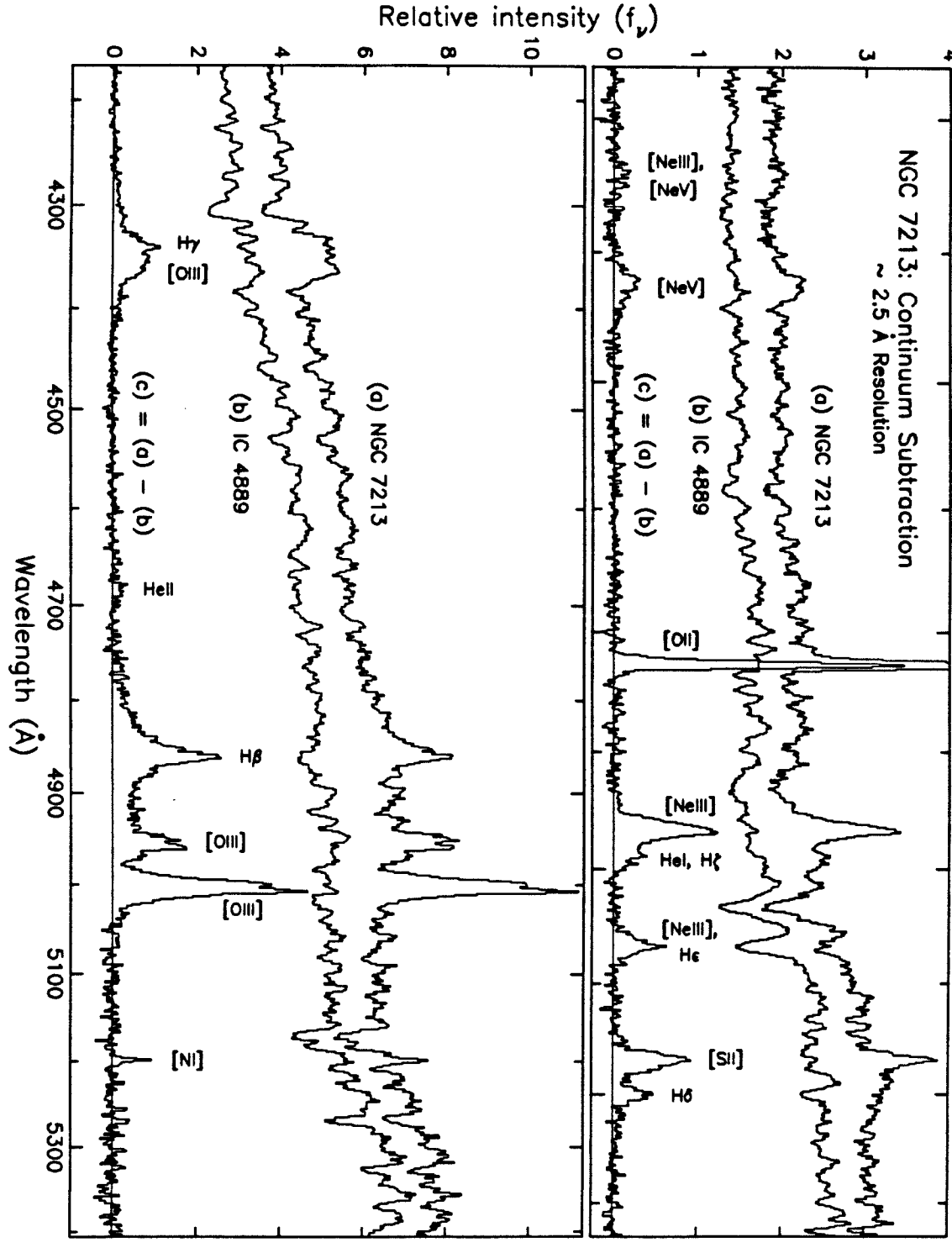
Relative intensity (f_ν)
NGC 7213: Continuum Subtraction
~ 2.5 Å Resolution
(a) NGC 7213
(b) IC 4889
(c) = (a) − (b)
[NeIII], [NeV]
[NeV]
[OII]
[NeIII]
HeI, Hζ
[NeIII], Hε
[SII]
Hδ
(a) NGC 7213
(b) IC 4889
(c) = (a) − (b)
Hγ [OIII]
HeII
Hβ
[OIII]
[OIII]
[NI]
Wavelength (Å)

Figure 2

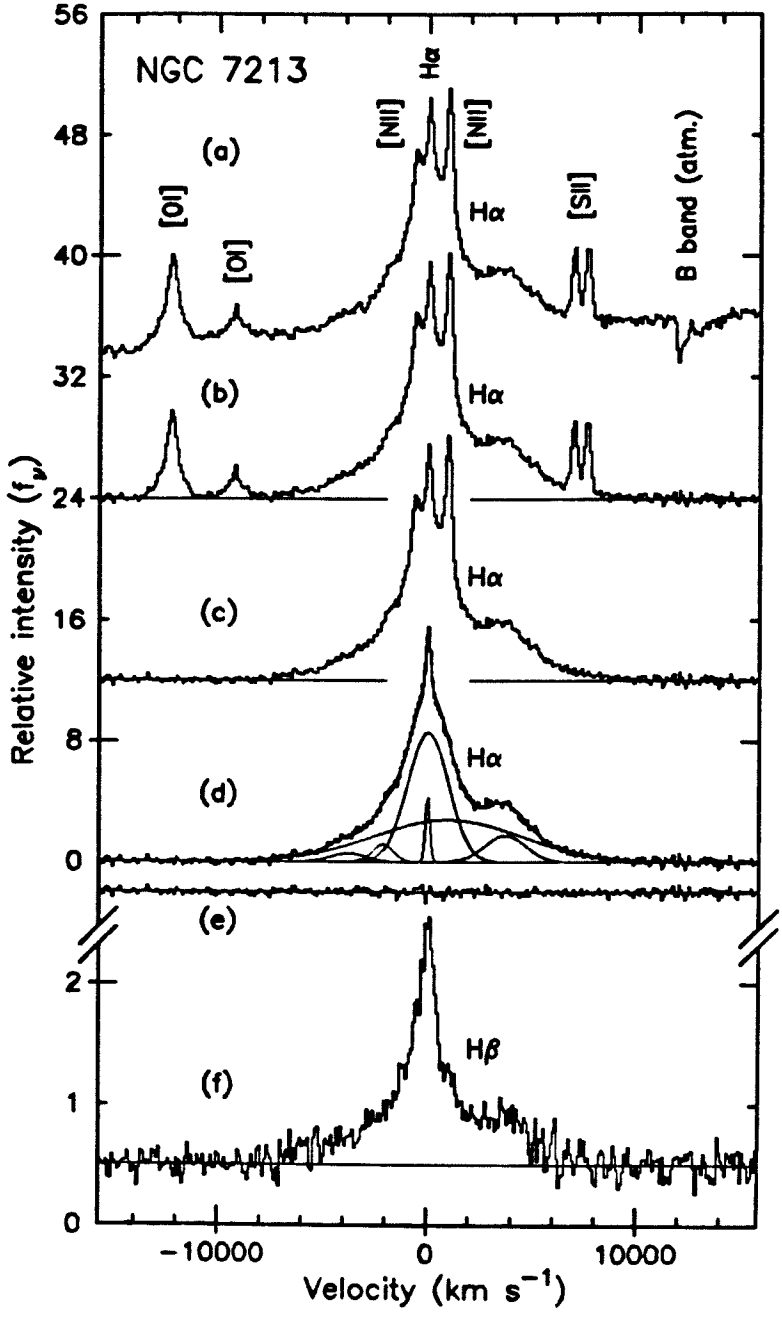
NGC 7213
Hα
[NII]
[NII]
[OI]
[OI]
[SII]
B band (atm.)
(a)
(b)
(c)
(d)
(e)
(f)
Hα
Hα
Hα
Hα
Hβ
Relative intensity (f_ν)
56
48
40
32
24
16
8
0
2
1
0
−10000
0
10000
Velocity (km s^{-1})

Figure 3

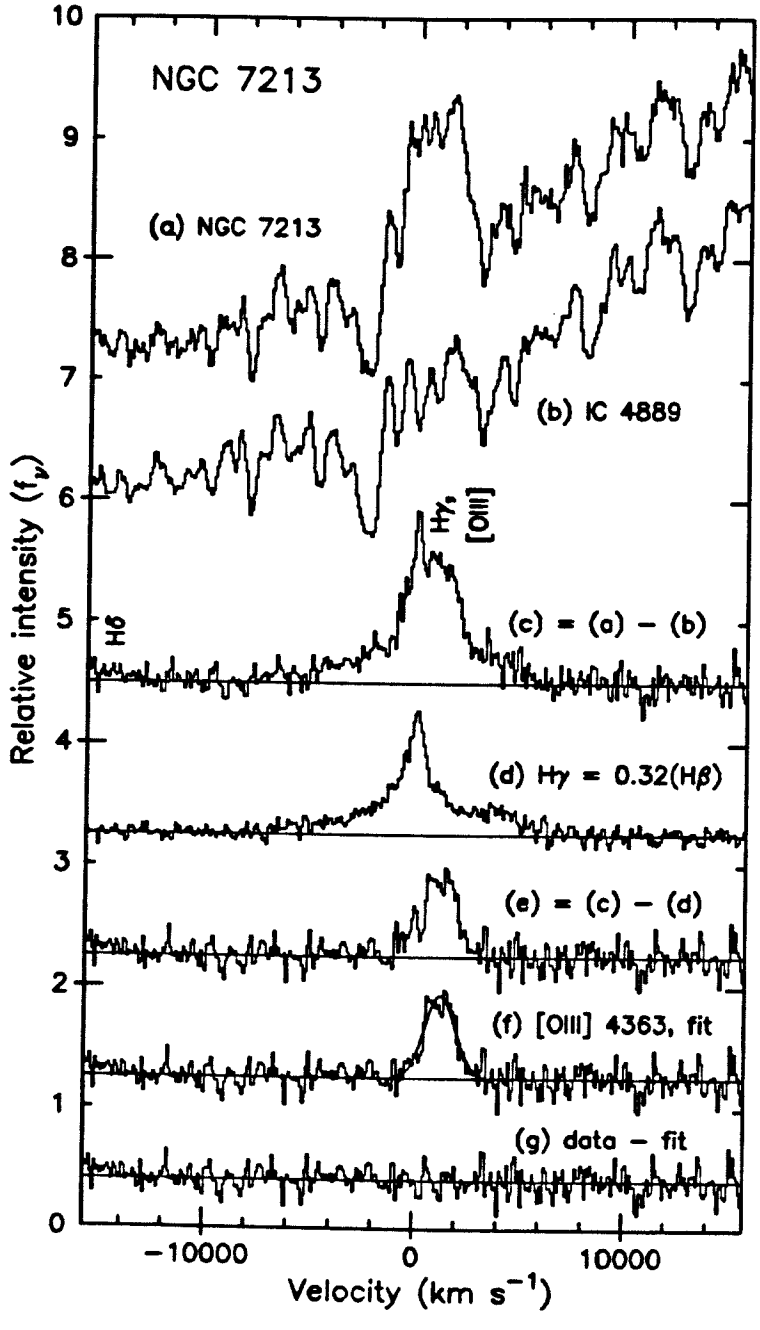
NGC 7213
(a) NGC 7213
(b) IC 4889
Hγ, [OIII]
Hδ
(c) = (a) − (b)
(d) Hγ = 0.32(Hβ)
(e) = (c) − (d)
(f) [OIII] 4363, fit
(g) data − fit
Relative intensity (f_ν)
Velocity (km s^{-1})
−10000
0
10000
0
1
2
3
4
5
6
7
8
9
10

Figure 4

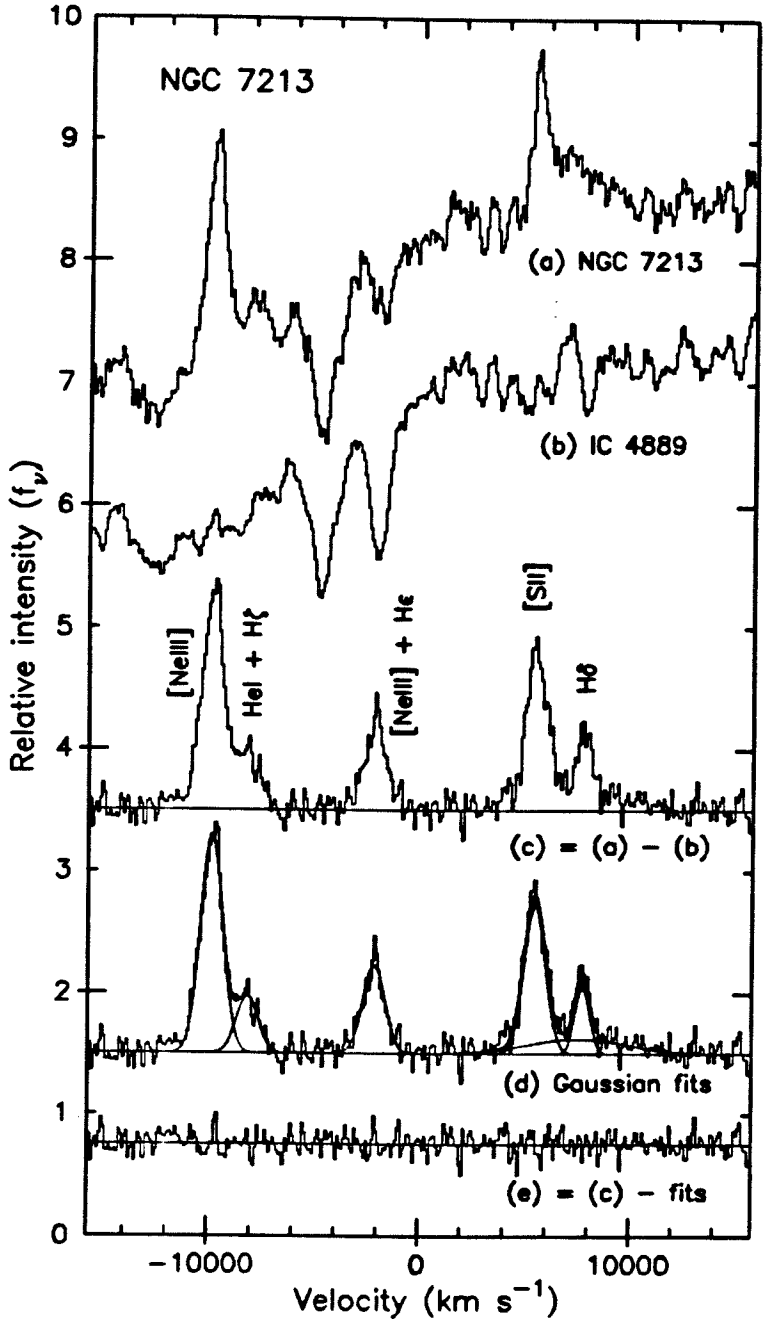
NGC 7213
(a) NGC 7213
(b) IC 4889
[NeIII]
HeI + Hζ
[NeIII] + Hε
[SII]
Hδ
(c) = (a) − (b)
(d) Gaussian fits
(e) = (c) − fits
Relative intensity (f_ν)
Velocity (km s^−1)
−10000
0
10000
0
1
2
3
4
5
6
7
8
9
10

Figure 5

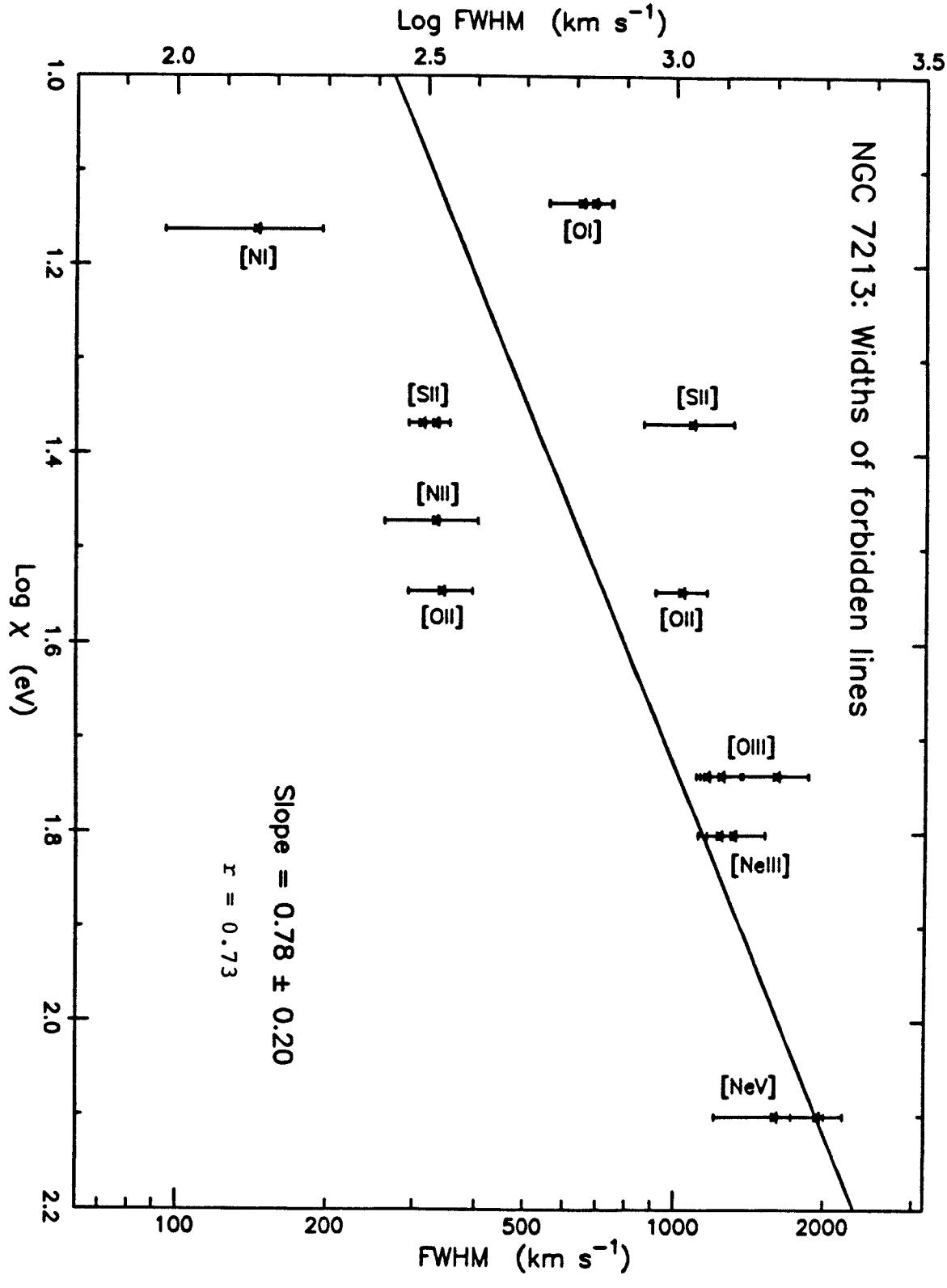
Log FWHM (km s^{-1})
2.0
2.5
3.0
3.5
1.0
1.2
1.4
1.6
1.8
2.0
2.2
Log χ (eV)
NGC 7213: Widths of forbidden lines
[NI]
[OI]
[SII]
[SII]
[NII]
[OII]
[OII]
[OIII]
[NeIII]
[NeV]
Slope = 0.78 ± 0.20
r = 0.73
100
200
500
1000
2000
FWHM (km s^{-1})

Figure 6

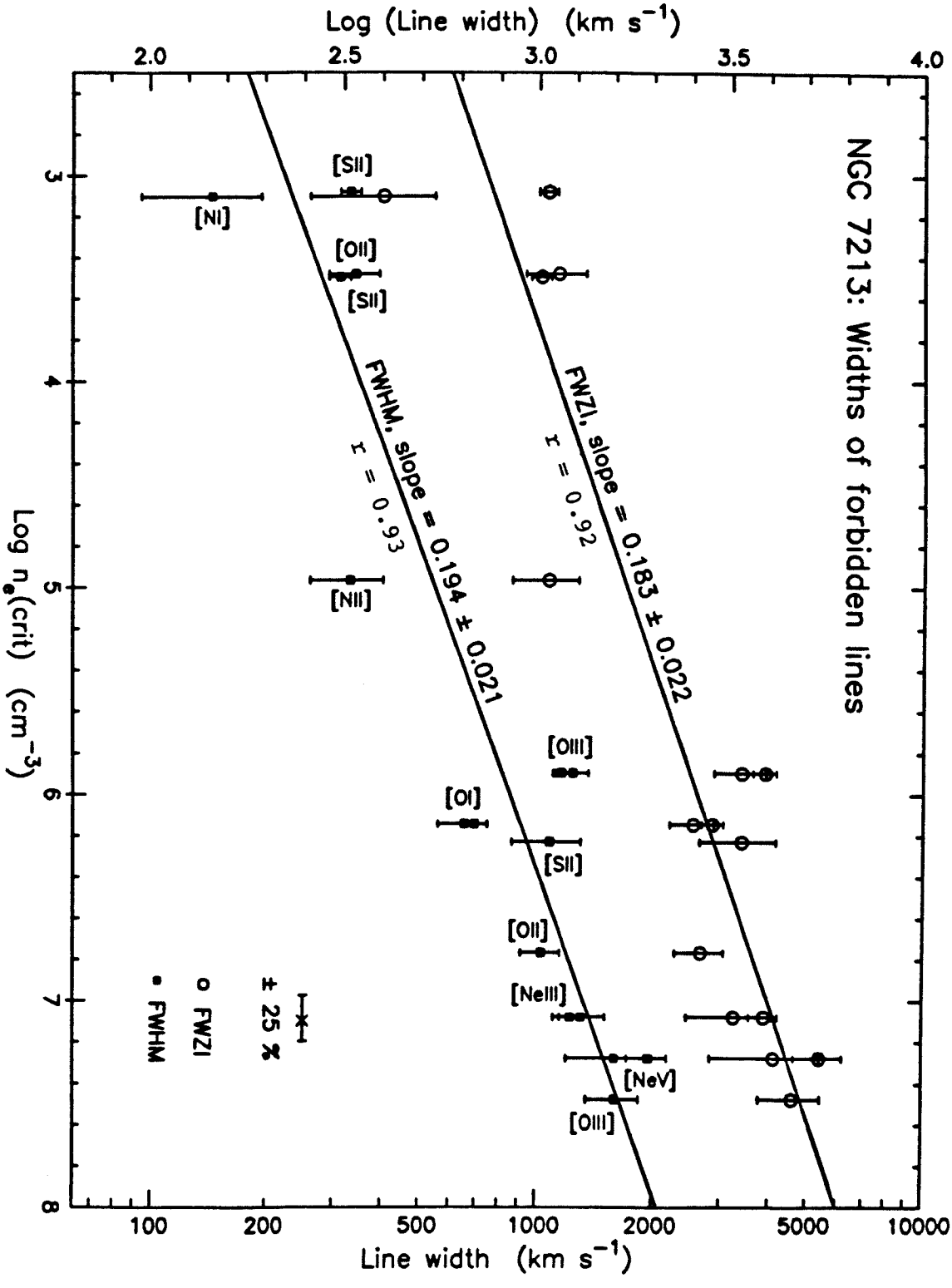
Log (Line width) (km s^{-1})
2.0
2.5
3.0
3.5
4.0
NGC 7213: Widths of forbidden lines
FWHM, slope = 0.194 ± 0.021
r = 0.93
FWZI, slope = 0.183 ± 0.022
r = 0.92
[SII]
[NI]
[OII]
[SII]
[NII]
[OIII]
[OI]
[SII]
[OII]
[NeIII]
[NeV]
[OIII]
• FWHM
o FWZI
± 25 %
Log n_e(crit) (cm^{-3})
3
4
5
6
7
8
100
200
500
1000
2000
5000
10000
Line width (km s^{-1})

Figure 7

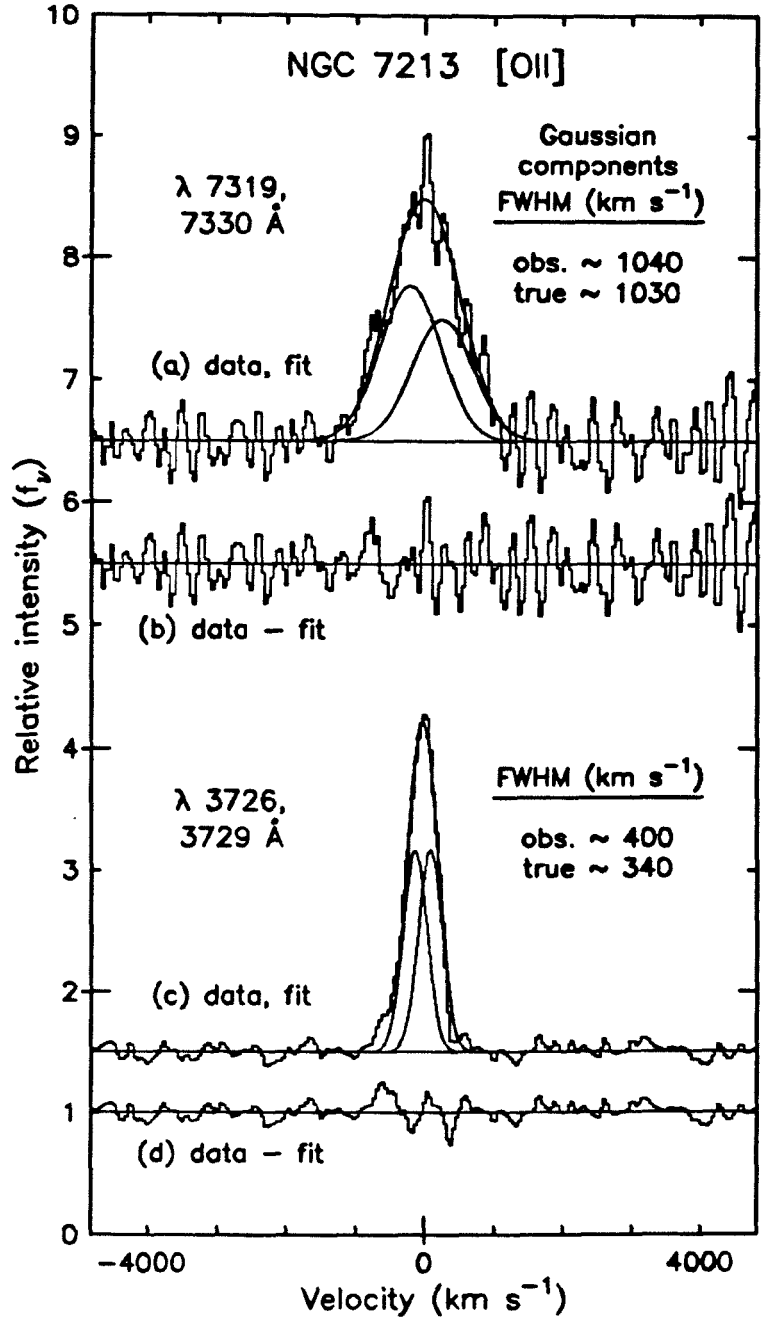
NGC 7213 [OII]
λ 7319,
7330 Å
Gaussian
components
FWHM (km s^{-1})
obs. ~ 1040
true ~ 1030
(a) data, fit
(b) data − fit
λ 3726,
3729 Å
FWHM (km s^{-1})
obs. ~ 400
true ~ 340
(c) data, fit
(d) data − fit
Relative intensity (f_ν)
Velocity (km s^{-1})
0
1
2
3
4
5
6
7
8
9
10
−4000
0
4000

Figure 8

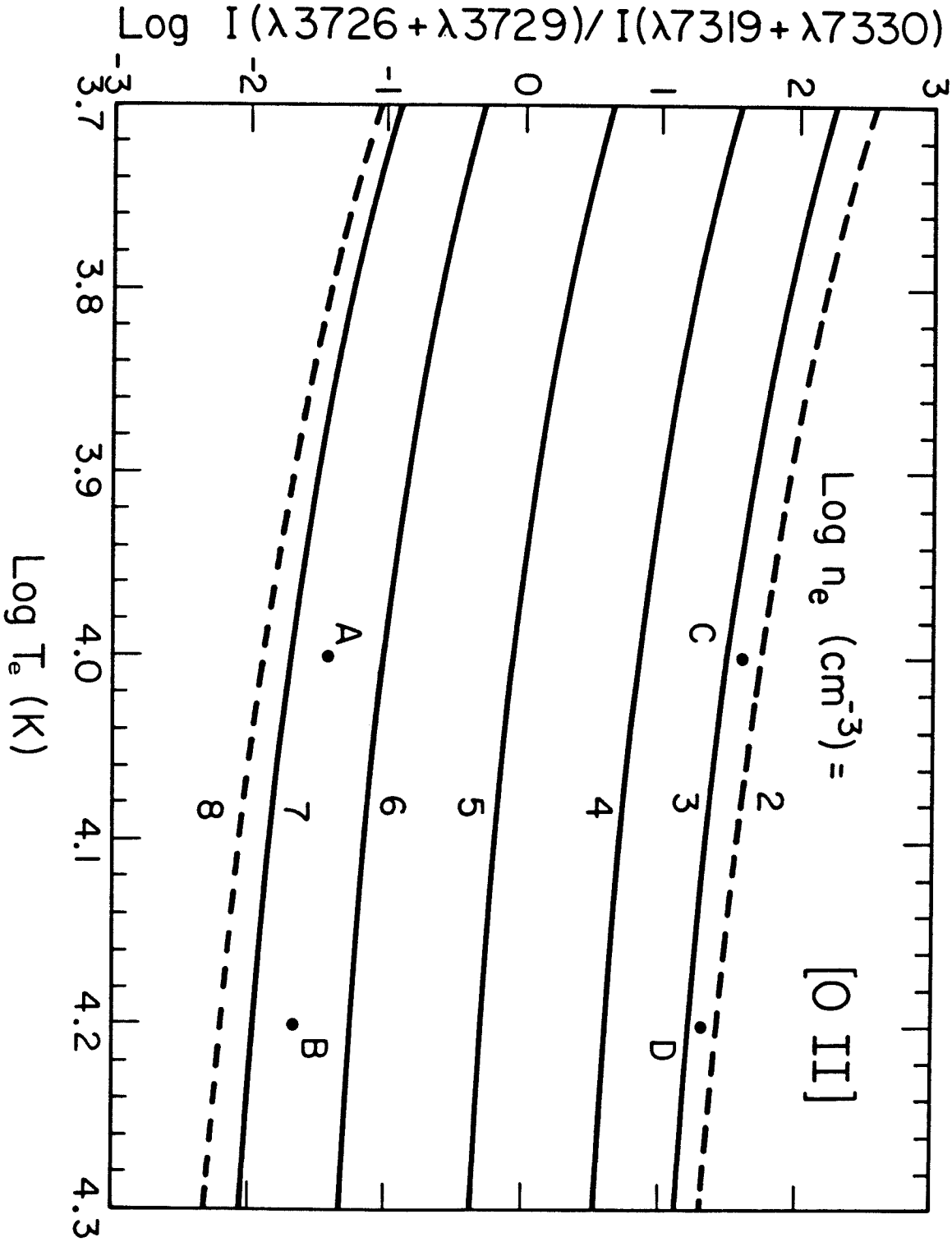
Log I(λ3726 + λ3729)/ I(λ7319 + λ7330)
-3
-2
-1
0
1
2
3
Log Te (K)
3.7
3.8
3.9
4.0
4.1
4.2
4.3
Log ne (cm-3) =
[O II]
2
3
4
5
6
7
8
A
B
C
D

Figure 9

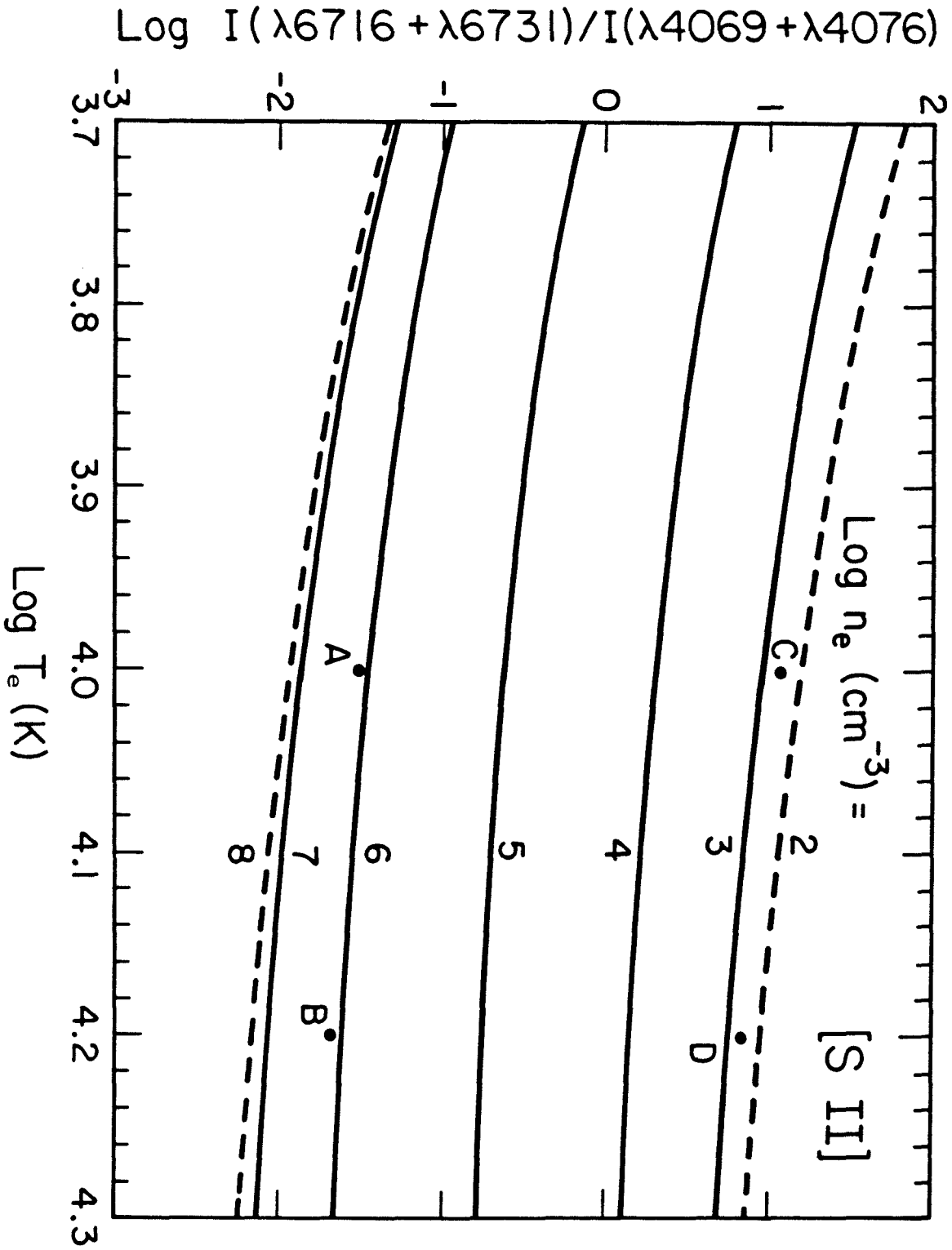
Log I(λ6716+λ6731)/I(λ4069+λ4076)
-3
-2
-1
0
1
2
3.7
3.8
3.9
4.0
4.1
4.2
4.3
Log Te (K)
Log ne (cm-3) =
[S II]
A
B
C
D
8
7
6
5
4
3
2

Figure 10

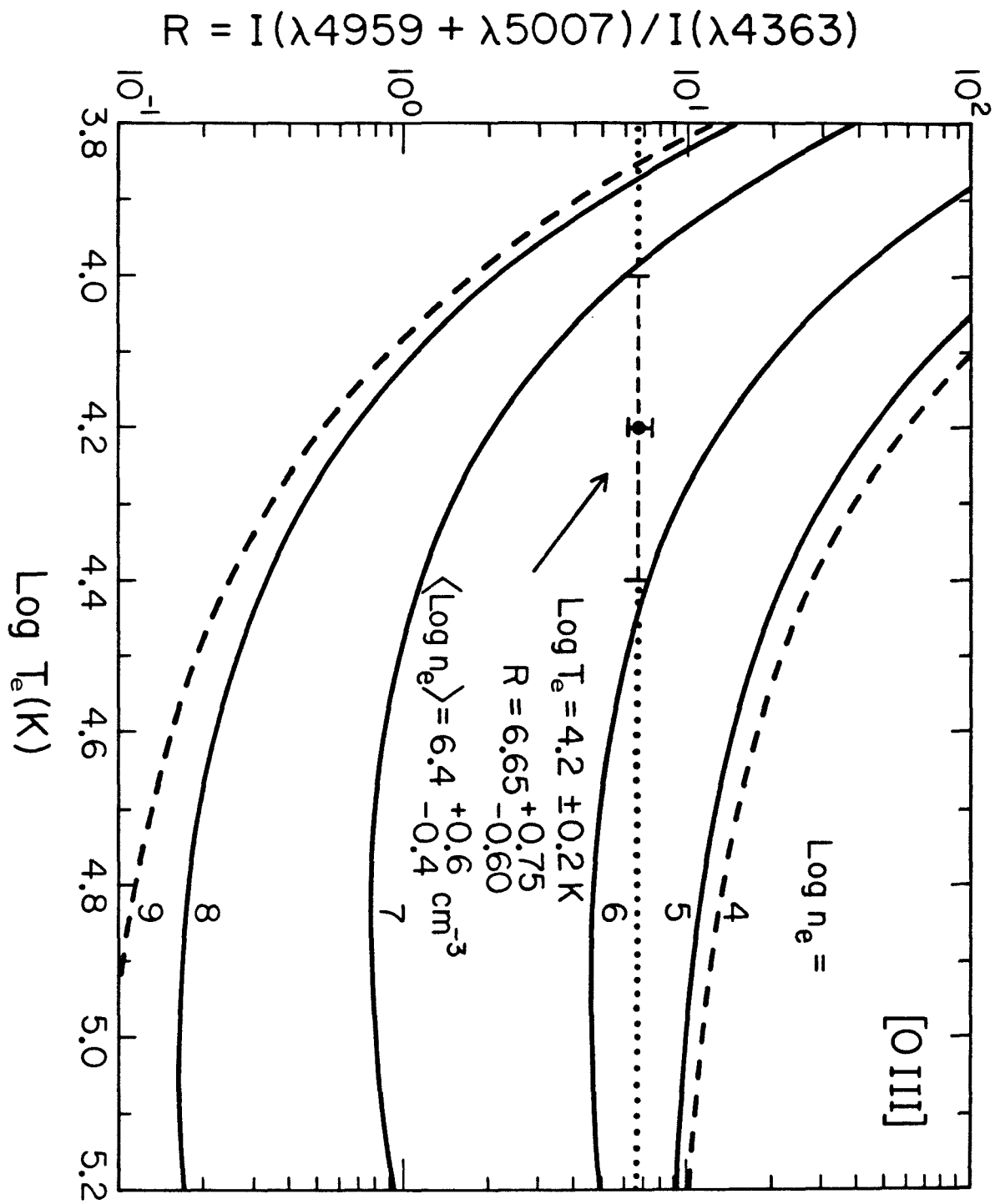
R = I(λ4959 + λ5007)/I(λ4363)
10^-1
10^0
10^1
10^2
3.8
4.0
4.2
4.4
4.6
4.8
5.0
5.2
Log Te(K)
9
8
7
6
5
4
Log ne =
[O III]
⟨Log ne⟩= 6.4 +0.6 -0.4 cm^-3
Log Te = 4.2 ±0.2 K
R = 6.65 +0.75 -0.60

Figure 11

CHAPTER 3

The Nonstellar Continuum of the Seyfert Galaxy NGC 7213.

J. P. Halpern and Alexei V. Filippenko

To be published in The Astrophysical Journal, 1984 Oct 15.

Deep in the human unconscious is a pervasive need

for a logical universe that makes sense.

But the real universe is always one step beyond logic.

"The Sayings of Maud'Dib"

by the Princess Irulan

Dune, Frank Herbert

ABSTRACT

Optical spectrophotometry of the nearby Seyfert galaxy NGC 7213 reveals that nonstellar radiation accounts for at least 50% of the observed continuum at λ3300. A formal decomposition of the continuum into a power law of index 1.1 (where $f_\nu \propto \nu^{-\alpha}$) and the spectrum of a giant elliptical galaxy suggests that the true nonstellar flux may be substantially larger if reddening is allowed. The derived visual extinction (A_V) is ~ 0.61 ± 0.2 mag, of which only ~ 0.05 mag is likely to be Galactic.

X-ray spectra obtained with the IPC and MPC on the Einstein Observatory are approximated by a power law with $\alpha = 0.72 \pm 0.12$ and $N_H \lesssim 2.5 \times 10^{20}$ cm^{-2}. The equivalent A_V of $\lesssim 0.12$ mag is less than that found from the optical analysis. This discrepancy might be resolved by the emission of substantial bremsstrahlung radiation at temperatures less than 1 keV from a hot medium which confines the forbidden-line clouds.

Published observations at radio, IR, and UV wavelengths are combined with the new data to produce the overall continuum, which is similar to that of other type 1 Seyferts. A "UV bump" may be present. Since NGC 7213 has one of the highest ratios of X-ray to optical luminosity among active galactic nuclei, it extends a previously established trend to low-luminosity objects. The ionizing continuum of NGC 7213 is of great importance in attempts to explain the optical characteristics of LINERs, which it resembles because of the low-ionization emission lines and flat-spectrum radio source.

Subject headings: galaxies:individual (NGC 7213)--galaxies:nuclei--galaxies:Seyfert--spectrophotometry--X-rays:sources--X-rays:spectra

I. INTRODUCTION

Marshall et al. (1979) found that the nearby (v = 1769 km s^{-1}) S0 galaxy NGC 7213 lies within the error box of the HEAO A-2 X-ray source H2209-471, but the large size of the box (~ 0.6 x 2.8 deg^2) rendered the association of the two objects uncertain. Subsequent optical spectrophotometry by Phillips (1979) demonstrated the presence of broad Hα emission similar to that found in Seyfert 1 galaxies, making identification with the X-ray source highly probable. On the other hand, Phillips (1979) saw no evidence for a substantial nonstellar continuum at optical wavelengths. The X-ray luminosity of ~ 3 x 10^{42} erg s^{-1} (H_o = 50 km s^{-1} Mpc^{-1}) in the 2-10 keV band (Marshall et al. 1979) is smaller than that of most type 1 Seyferts and narrow-line X-ray galaxies (Halpern 1982; Mushotzky 1982), but larger than that of type 2 Seyferts (Kriss 1982). A second HEAO A-2 scan obtained 6 months after the first showed that the intensity of the source had increased by ~ 70% at a confidence level of ~ 2σ (Piccinotti et al. 1982), providing additional support for the association with a compact Seyfert nucleus. NGC 7213 was detected during pointed observations with the HEAO 1 scanning modulation collimator (Dower et al. 1980), and Kriss (1982) reported a luminosity of 1.1 x 10^{43} erg s^{-1} in the 0.5-4.5 keV band with the Imaging Proportional Counter on the Einstein Observatory. The Hα luminosity of ~ 2 x 10^{41} erg s^{-1}, however, is low for a Seyfert 1 galaxy (Phillips 1979).

The optical spectrum exhibits features common not only in type 1 Seyferts, but in Heckman's (1980) "low ionization nuclear emission-line

regions" (LINERs) as well. Although emission in LINERs has often been attributed to heating by shocks, a detailed analysis of the forbidden lines by Filippenko and Halpern (1984, hereafter Paper I) shows how the spectral characteristics of NGC 7213 can be reconciled with photoionization by nonstellar radiation. An important key is the discovery of clouds having densities of order 10^6–10^7 cm^{-3} in the narrow-line region.

In this paper, the optical continuum of NGC 7213 is decomposed into stellar and nonstellar components, and the spectrum at X-ray energies is derived from observations made with the Monitor Proportional Counter (Gaillardetz et al. 1978) and Imaging Proportional Counter (Giacconi et al. 1979) on the Einstein Observatory. Ultraviolet, infrared, and radio observations published elsewhere are then combined with the new data to produce the overall continuum.

II. THE OPTICAL CONTINUUM

a) Standard Galaxy plus Power Law

Paper I describes the optical observations in detail. Briefly, spectra having 2.5 Å resolution were obtained with the Intensified Reticon on the 2.5 m duPont reflector at Las Campanas Observatory. Although relative intensities are accurately calibrated over most of the observed range, the absolute flux is uncertain by ~ ± 25% because of the small size of the aperture (2" x 4").

Prominent emission of [O I], [O II], [O III], [S II], [Ne III], and HI are visible, and the strong absorption lines in the underlying continuum reveal the dominance of an old stellar population typical of those seen in the bulge of other S0 and Sa galaxies. On the other hand,

emission lines produced by such highly ionized species as Ne^{+4} indicate that nonstellar radiation may form a substantial fraction of the optical flux. Furthermore, the continuum is considerably bluer than that of galaxies which exhibit no signs of unusual activity, and the broad Balmer lines resemble those in quasars and type 1 Seyferts.

The continuum of NGC 7213 was therefore decomposed into a standard galaxy and a power-law spectrum ($f_\nu \propto \nu^{-\alpha}$) which is presumably of nonthermal origin (e.g., electron synchrotron radiation). A more general analysis (e.g., Malkan and Sargent 1982; Malkan 1983) was not possible because of the very limited wavelength range of the data, but the procedure was similar to that done by Goodrich and Osterbrock (1983), Yee and Oke (1978), and others. The galactic component was represented by the "average" giant elliptical used in a study of radio galaxies by Yee and Oke (1978). Such an object is a fairly good approximation to the bulge of S0 and Sa galaxies; its main drawback is that the continuum is probably somewhat redder than the integrated starlight in the nucleus of NGC 7213. This leads to a slight overestimate of the nonstellar component and/or an underestimate of the reddening. The spectrum of the standard galaxy was transformed from the AB_{69} magnitude scale to the recent AB_{79} scale (Oke and Gunn 1983), since AB_{79} was used to flux-calibrate spectra of NGC 7213.

Regions containing emission lines were ignored, and the resolution was degraded to that of the standard galaxy. Only the index (α) and the ratio of nonstellar flux to total flux at λ5460 ($\log \nu$ (Hz) = 14.740) were varied in a least-squares fit to the dereddened spectrum of NGC 7213. It was discovered, however, that the decomposition is not sensitive to α, since nonstellar radiation is not sufficiently dominant

and the wavelength range is small. Therefore, α was chosen to be close to 1.1, which is the value found for a sample of QSOs and Seyfert galaxies (Malkan and Sargent 1982; Malkan and Filippenko 1983). In particular, Table 1 lists the results obtained with α set to 0.8, 1.1, 1.4, and 1.7, and Table 2 gives the relative strengths of both components at selected wavelengths for $\alpha = 1.1$.

Figure 1a illustrates the best spectral decomposition with $\alpha = 1.1$ when the continuum of NGC 7213 is dereddened by $A_V = 0.05$ mag (where $A_V \sim 3.2 E_{B-V}$), the Galactic extinction (Burstein and Heiles 1982; Heiles and Cleary 1979). At λ5460 the nonstellar component accounts for only ~ 11.4% of the flux, while at λ3250 it is roughly the strength of the standard galaxy. The overall fit is reasonably good, but the deviations suggest that better agreement could be obtained if the continuum of NGC 7213 were dereddened by a moderate amount.

Additional fits were performed, this time with the reddening of NGC 7213 and the ratio of the nonstellar flux to the total flux at λ5460 as free parameters (Table 1). If $\alpha = 1.1$, the best fit is obtained with a continuum reddening corresponding to $A_V \sim 0.61$ mag in NGC 7213. The results are tabulated in Table 2 and plotted in Figure 1b. It is apparent that the fit is better than with $A_V = 0.05$ mag, especially at the relatively sharp "break" near λ3950. At λ5460 the nonstellar component now accounts for ~ 23.5% of the flux, and its contribution equals that of the standard galaxy at ~ λ3950. Over the range $\lambda\lambda$3202-6272 it accounts for fully 33% of the total flux.

If the observed blue excess were of stellar origin, it would require the presence of 1.3×10^5 B0 or 2.4×10^4 O5 main sequence stars, but emission lines typical of star-burst galaxies (e.g.,

Weedman et al. 1981) would then be expected. Slight errors in the flux calibration, as well as differences between the spectra of giant elliptical galaxies and the bulge of NGC 7213, also cannot account for the enormous nonstellar flux in the blue and near-UV. At λ3200, it is a magnitude brighter than the stellar component, whereas the errors are likely to be within ± 0.3 mag. Moreover, no nonstellar component was found when the same procedure was performed on the normal S0 galaxy IC 4889, in agreement with the absence of other signs of activity in this object.

b) Reddening

Note that A_V = 0.61 mag applies to all of the observed continuum; the nonstellar radiation is assumed not to experience any additional extinction as it travels out from the nucleus. Of course, it is also possible that only the nonstellar component is substantially reddened (e.g., by dust close to the nucleus). A least-squares decomposition indicates that this is unlikely, however, since acceptable fits (which are nevertheless formally worse than that in Figure 1b) require the power law to experience $A_V \sim 1.8$-1.9 mag. The nonstellar contribution is then nearly equal to that of stars over the range λλ4000-6000, which is incompatible with the relatively strong absorption lines observed in NGC 7213. The amount of dilution provided at various wavelengths in the $(\alpha, A_V) = (1.1, 0.61)$ decomposition is consistent with the observed equivalent widths, although there is a range of acceptable dilution due to differences in line strengths among elliptical galaxies and the bulges of spirals. In addition, photographs indicate the presence of dust in the outer portions of NGC 7213 (Phillips 1979), so there might

be dust between the earth and nucleus as well. In reality, somewhat different amounts of reddening may apply to the stellar and nonstellar components, but here it will be assumed that a single value is correct for the entire continuum.

Table 1 shows that the derived extinction $A_V \sim 0.61$ mag ($E_{B-V} \sim 0.19$ mag) depends on the particular choice of spectral index; it can differ by $\pm$ 0.1 mag for a plausible range in α. It also changes with the range of wavelengths used in the analysis, and an error of $\pm$ 0.1 mag is not inconceivable. Finally, for a given α the fit is satisfactory for values of A_V in a range of roughly $\pm$ 0.1 mag. Thus, a reasonable approximation to the error in A_V is $\pm$ 0.2 mag.

III. X-RAY OBSERVATIONS

NGC 7213 was observed by Einstein on three occasions in 1979 and 1980, with intervals of ~ 6 months between observations. The dates and integration times are given in Table 3.

a) Monitor Proportional Counter (MPC)

The MPC is mounted on the outside of Einstein, and is coaligned with the imaging telescope. It is an argon-filled, non-imaging detector with an effective area of 667 cm^2 and a 1.5 deg (full width at zero-intensity) square collimator. A complete description of the methods used for data reduction, including background subtration, is given by Halpern (1982, 1984).

Table 3 lists the count rates in the 2-6 keV band and the 2-10 keV fluxes. NGC 7213 was not the primary target of the second observation, but nevertheless was the dominant source in the field of view. The count rate and flux in this case include a multiplicative factor of 1.63

to correct for off-axis transmission of the collimator. Variability by a factor of ~ 3 is evident, and the luminosity spans a range which includes the earlier HEAO A-2 values.

The pulse height data were fit with a standard power-law spectrum and absorption due to intervening neutral gas. Specifically,

$$\frac{dN}{dE} = A\, E^{-(\alpha+1)}\, e^{-\sigma(E) N_H} \quad \text{photons cm}^{-2}\,\text{s}^{-1}\,\text{keV}^{-1}, \qquad (1)$$

where $\sigma(E)$ is the Brown and Gould (1970) opacity, N_H is the equivalent neutral hydrogen column density, and A is a normalizing factor. The derived spectral parameters and 90% error bars are listed in Table 3. For the 1980 observation, the spectral parameters were derived from MPC and IPC data taken simultaneously (see below). Since there is independent evidence from the IPC that the column density is extremely low ($N_H \lesssim 5 \times 10^{20}$ cm^{-2}), absorption in the MPC band is expected to be negligible. Therefore, the spectral index for the first two observations was recomputed under the assumption $N_H = 0$, resulting in nearly identical values for the best fit, but slightly smaller formal errors.

b) Imaging Proportional Counter (IPC)

The soft X-ray luminosity measured by the IPC on day 136 of 1980 was 1.1×10^{43} erg s^{-1} in the 0.5-4.5 keV band (Kriss 1982). This is nearly equal to the 2-10 keV luminosity of 1.02×10^{43} erg s^{-1}, and a simple calculation shows that these values would be equal if a spectral slope $\alpha \sim 0.7$ with no absorption extends throughout both energy bands. The IPC and MPC data can in principle be fit simultaneously, yielding spectral parameters over the combined energy band, but this is

cumbersome due to the significantly different behavior of the two detectors. Temporal and spatial variations exist in the gain of the IPC, and the precise values for this observation have not yet been determined. The gain of the MPC, on the other hand, is quite stable. Since it was necessary to vary the assumed IPC gain about the nominal value, the IPC pulse height data were fit separately using the same model as in equation (1). The following is a brief description of the procedure.

NGC 7213 appeared in the center of the IPC image, and source counts were determined from a circle of radius 180" about the X-ray centroid. The background was obtained in an annulus between radii of 320" and 440" concentric with the source, and properly scaled by area. It contributes no more than 5% of the count rate in any one channel, and represents only 1.3% of the total. The net (background subtracted) count rate in channels corresponding nominally to 0.12-4.65 keV is 2.69 ± 0.04, and the effective exposure of 1517 seconds includes a 5% correction for dead time. Standard corrections were also applied for counts lost in scattering by the mirrors and in the wings of the IPC point response function.

Grids of model spectra were generated for several assumed values of BAL, which is a measure of the gain as determined by the mean pulse height channel of the 1.5 keV aluminum line. These values were within $\pm$ 1 of the nominal 16.6 for this day of observation. Figure 2 shows the IPC 90% contours superimposed on the MPC 90% contour determined from data obtained simultaneously. The dashed line indicates the envelope of acceptable fits when the gain was allowed to vary, and should therefore be taken as an indication of the total uncertainty in the present

analysis. Figure 3 displays the theoretical spectra which produced the best fits for the IPC and MPC.

IV. INTERPRETATION

a) Column Density and Spectral Index

Under the assumption that a single power law applies throughout the observed energy band, the narrow range of overlap in Figure 2 between the IPC and MPC constrains α to 0.72 ± 0.12 and N_H to $< 2.5 \times 10^{20}$ cm^{-2}. It should be emphasized that the existence of a region of overlap is a necessary but not sufficient condition for a constant spectral slope, since the normalizations must also agree. In fact, the best agreement occurs for $\alpha = 0.7$ and $N_H = 2 \times 10^{20}$ cm^{-2}, where $A = 0.0170$ photons cm^{-2} s^{-1} keV^{-1} is found for both the MPC and IPC. Most other points within the overlap region also require normalizations that agree to within $\pm$ 10%, which is as good as can be expected given the uncertainties in relative calibration. On the other hand, the true spectrum between 0.25 and 2 keV is probably not much steeper than 0.85 or much flatter than 0.6, even though this seems to be allowed by the IPC contours in Figure 2. Such a curved spectrum would produce discrepant total count rates between the MPC and IPC when forced to fit in the region of overlap.

An independent constraint on the column density comes from the measurements at 21 cm in the Galaxy. Values of N_H in the line of sight to extragalactic sources are never observed to be less than $\sim 10^{20}$ cm^{-2}, even near the galactic poles (Dickey, Salpeter, and Terzian 1978). Several observations within 1° of NGC 7213 by Heiles and Cleary (1979) yield $1.6 \times 10^{20} \lesssim N_H \lesssim 2.1 \times 10^{20}$ cm^{-2}. This is in agreement with the

joint X-ray confidence region, and rules out IPC spectra flatter than $\alpha \sim 0.6$ since N_H would be too low. It is also evident from the X-ray spectrum that any column density intrinsic to NGC 7213 must be small. The implications of this last point will be discussed in the next subsection.

The spectral parameters listed in Table 3 are consistent with the results of Mushotzsky (1982), who found that α generally falls between 0.6 and 0.8 in Seyfert galaxies. Mushotzky (1982) also indicates that $N_H < 5 \times 10^{21}$ cm^{-2} for NGC 7213. Although the first and third MPC observations have comparable statistical uncertainties based on the total source counts, the signal-to-noise ratio was a factor of 3 larger in the latter case because the source was stronger (and the integration time shorter). Hence, the third observation is expected to be least susceptible to systematic errors involving background subtraction, and the simultaneous IPC data can be used to restrict the range of spectral parameters. $N_H \lesssim 2.5 \times 10^{20}$ cm^{-2} and $\alpha = 0.72 \pm 0.12$ are therefore adopted as the best estimates for the spectral parameters in the 0.25-10 keV band, but slight deviations from a power law shape cannot be ruled out.

b) Covering Fraction and Visual Extinction

The shape of the X-ray spectrum also demonstrates that the covering fraction of emission-line clouds is small. For the broad-line clouds, expected column densities of several times 10^{22} cm^{-2} (Kwan and Krolik 1981) would cause a low-energy cutoff near 3 keV, as is observed in NGC 4151. Models of narrow-line clouds require $N_H \sim 2.5 \times 10^{21}$ cm^{-2} (Halpern and Steiner 1983) for typical Seyfert galaxies, but there is

probably quite a large spread. In particular, column densities 10 times larger than average could explain cases such as NGC 7213 in which the $\underline{I}([O\ I]\lambda6300)/\underline{I}([O\ II]\lambda3727)$ ratio is large (Halpern 1982). All these estimates are much higher than the upper limit $\underline{N}_H \sim 2.5 \times 10^{20}$ cm^{-2} derived from the X-ray data for NGC 7213, and point to a low covering fraction. Moreover, for interstellar material with normal extinction properties, such a low column density is associated with $\underline{A}_v$ of at most ~ 0.12 mag (Gorenstein 1975). This is in direct conflict with the optical analysis presented in § II, which suggests that $\underline{A}_v = 0.61 \pm 0.2$ mag. It is interesting that the sense of this disagreement is opposite that in most narrow-line X-ray galaxies, in which the X-ray column density is too large compared with other reddening indicators (Maccacaro, Perola, and Elvis 1982; Mushotzky 1982).

The absence of low-energy X-ray absorption, however, applies only to the earth's line of sight, and is not necessarily representative of the global covering fraction as measured by the equivalent widths of emission lines. In addition, the expected functional form of the X-ray absorption given in equation (1) is strictly correct only for a uniform, cold absorber which completely covers the source. If the source were only partially occulted, a spectrum having low resolution might appear only slightly flatter, without a noticeable low-energy turnover. This would be especially true if the absorbing medium were characterized by a broad distribution in $\underline{N}_H$.

Nevertheless, the fact that the IPC and MPC data agree with a spectral index of 0.7, both individually and in their relative normalization, is a strong indication that the covering fraction is

small. The index is not flatter than average, and there is no evidence for a turnover at low energies except due to material in the Galaxy. Given the estimated uncertainties of ~ 10% in relative calibration between the IPC and MPC, it appears that any covering fraction due to broad- or narrow-line clouds in the line of sight must be no more than ~ 30%, and possibly much less.

c) Thermal Emission

There is an alternative resolution to the discrepancy between the X-ray and optical extinction. Suppose that the power law at X-ray energies is in fact absorbed by $N_H \sim 1.3 \times 10^{21}$ cm^{-2} (corresponding to $A_V = 0.61$ mag), but that an additional source of thermal emission at temperatures less than 1 keV fills in the low-energy absorption. Specifically, Paper I shows that the thermal bremsstrahlung emission may be expected from a hot medium (referred to by the subscript h) which confines the forbidden-line clouds. The radius of the emitting region is

$$r = d\left(\frac{f_o}{chnU}\right)^{1/2} , \qquad (2)$$

where d is the distance to NGC 7213, f_o is the flux density of the ionizing continuum at the Lyman limit, n is the cloud density, and U is the ionization parameter. The integrated emission is (Tucker 1975)

$$\frac{dN}{dE} \approx \frac{1.4 \times 10^{-11}}{E d^2} \int_{r_{min}}^{r_{max}} r^2 n_h^2 T_h^{-1/2} e^{-E/kT_h} dr \quad \text{photons cm}^{-2}\,\text{s}^{-1}\,\text{keV}^{-1} . \qquad (3)$$

Since T_h is only approximately known, a constant value of $\sim 10^7$ K is assumed, as expected if the narrow-line clouds are very dense (Paper I).

Invoking pressure equilibrium between the two phases, and combining equations (2) and (3), yields

$$\frac{dN}{dE} \approx \frac{1.5 \times 10^{-6}}{E} \left(\frac{10^{-3}}{U}\right)^{3/2} \left(\frac{T}{10^4}\right)^{2} \left(\frac{10^7}{T_h}\right)^{5/2} e^{-E/kT_h} \int_{n_{min}}^{n_{max}} n^{-1/2}\, dn \quad \text{photons cm}^{-2}\text{s}^{-1}\text{keV}^{-1}. \quad (4)$$

If the upper limit is taken to be $\underline{n} \sim 3 \times 10^7$ cm^{-3}, a flux of $\sim 1.3 \times 10^{-3}$ photons cm^{-2} s^{-1} keV^{-1} near the characteristic energy of ~ 0.9 keV is found. This is $\sim 7\%$ of the observed flux (Figure 3), and would not greatly affect the X-ray spectrum. If $\underline{T_h}$ were a factor of 3 smaller, however, bremsstrahlung at ~ 0.3 keV would contribute an excess comparable to the observed flux. Unless properly taken into account, this could substantially decrease the derived value of $\underline{N_H}$, and it may resolve the discrepancy between the optical ($\underline{A_V} = 0.61$) and X-ray ($\underline{A_V} \lesssim 0.12$) results.

Since the X-ray spectrum of NGC 7213 is typical of type 1 Seyfert galaxies, one might doubt that the above hypothesis actually explains the difference in derived values of $\underline{A_V}$. Do any other Seyfert galaxies show evidence of thermal emission, or is NGC 7213 a very special case? Unfortunately, the poor spectral resolution of the Einstein data does not permit one to distinguish between power-law and thermal spectra over a large range of assumed parameters. In fact, power-law slopes cannot be unambiguously derived at X-ray energies if thermal emission is a possible contributor. There is a distribution of slopes among Seyfert galaxies, and it may well be that the steeper ones contain contamination from thermal emission. One interpretation of the extended X-ray emission in NGC 4151 discussed by Elvis, Briel, and Henry (1983) was thermal bremsstrahlung from a confining medium in the narrow-line

region. Similarly, extended thermal emission superimposed on an absorbed power law is a plausible alternative to the "leaky absorber" explanation of the soft X-ray excesses observed (Reichert et al. 1983) in a number of Seyfert galaxies. Thus, it is not unlikely that thermal emission from a hot intercloud medium is sufficient to explain much of the discrepancy between the derived values of A_V in NGC 7213, especially in light of the particularly favorable conditions provided by the narrow-line clouds of high density (Paper I).

Note that the total column density of the hot medium in NGC 7213 is $\sim 10^{23}$ cm^{-2}. Elements of medium weight, particularly O, must be almost entirely stripped of electrons in order not to cause significant absorption of the soft X-rays. The Thomson scattering depth is only ~ 0.07, so scattering in the hot medium is negligible.

V. THE OVERALL CONTINUUM

Measurements of NGC 7213 in the infrared bands J, H, K, L, and N were made by Frogel and Elias (as reported by Phillips 1979), Glass (1981), Glass, Moorwood, and Eichendorf (1982), McAlary et al. (1983) and Ward et al. (1982). The International Ultraviolet Explorer was used by Wu, Boggess, and Gull (1983) to study NGC 7213 at UV wavelengths. These data were combined with the X-ray observations and new optical spectra to produce the overall continuum from X-ray through infrared wavelengths (Figure 4). NGC 7213 is also a Parkes radio source (PKS 2206-474) with a flux density of 0.23 Jy at 2.7 GHz (Bolton et al. 1977). It must be emphasized that the measurements were made at different times and through different apertures, which greatly complicates the interpretation of the spectrum.

The continuum is similar to that seen in type 1 Seyfert galaxies, although a significant stellar component is present at optical and near-infrared wavelengths. Data at 10 μm and possibly 3.5 μm are the only IR points which are not contaminated by stellar light. Glass, Moorwood, and Eichendorf (1982) concluded that $\alpha \sim 1.1$ and $\underline{A}_V \sim 0.6$ mag in NGC 7213, from an analysis of IR, optical, and UV data. However, these values are based on the assumption that 40% of the dereddened K (2.2 μm) flux in a 9" aperture is due to the power-law component. This is twice as much nonstellar flux as found in the present study, so the agreement in α and $\underline{A}_V$ may be fortuitous. Their power law passes through the 10.3 μm point at ~ 250 mJy, but is incompatible with the new optical data since it exceeds the total dereddened flux blueward of 4000 Å. This restriction probably arises because the optical data presented here were taken through a smaller aperture than that used by Phillips (1979). Hence, the nonthermal component is likely to be comparable to the one derived from the least-squares fits in § II (and shown again in Figure 4). The flux at 10 μm may therefore contain a significant contribution from thermally-emitting dust at temperatures of several 100 K.

There is also a discrepancy among the IR measurements themselves. The J and H fluxes taken through a 9.1" aperture are more than a factor of 2 larger than the corresponding fluxes in a 7" aperture. This is difficult to understand in terms of any reasonable distribution of stellar light, and may require a substantial variation in the nonstellar flux. On the other hand, variability seems to be excluded by the agreement of all the measurements at L. A reconciliation of the various IR measurements would obviously be desirable.

One representation of the overall continuum shape is given by the spectral index β_{ox} between 4000 Å and 2 keV (Grindlay *et al.* 1980), which is 1.06 ± 0.08 in NGC 7213. With the $(\alpha, A_V) = (1.1, 0.61)$ decomposition derived in § II, it is found that β_{ox} of the *nonthermal component alone* is 1.04 ± 0.08, not significantly different from the "raw" number given above. These values (whose error bars are due almost entirely to the observed range of X-ray variability) are near the low end of the distribution for type 1 Seyferts and X-ray selected active galactic nuclei (Kriss 1982), and NGC 7213 therefore has one of the highest ratios of X-ray to optical luminosity among active galactic nuclei. It has been shown (Zamorani *et al.* 1981; Reichert *et al.* 1982; Tananbaum and Avni 1982) that the ratio of X-ray to optical luminosity is inversely related to total luminosity for X-ray or optically selected QSOs. This correlation extends to Seyfert galaxies (Kriss 1982), and NGC 7213 suggests that it is also true in objects having still lower luminosity.

The UV flux lies substantially above an extrapolation of the optical data. This could simply reflect variability between the epochs of the UV and visual observations (which would be interesting in itself), but alternatively it may indicate the presence of the "UV bump" often seen in quasars and Seyfert 1 galaxies (Malkan and Sargent 1982; Oke, Shields, and Korycansky 1984). Excess emission in the far UV decreases the derived deficit of ionizing photons (based on the strength of the Balmer lines) which exists if the power-law component alone is used (Paper I). The X-ray spectrum follows the common pattern in which the slope is flatter than the optical power law, and there must be at least 2 changes in slope if the spectra are to join continuously in the

far UV.

Sadler (1984) recently published new radio observations of a complete sample of southern E and S0 galaxies. The flux density of NGC 7213 is 0.187 $\pm$ 0.017 Jy at 2.7 GHz and 0.228 $\pm$ 0.010 Jy at 5.0 GHz. The power-law spectrum between 2.7 and 5.0 GHz is therefore inverted ($\alpha = -0.3$), whereas a majority of galaxies have steep ($\alpha \gtrsim 0.5$) spectra. Heckman (1980) found that many of the LINERs in his sample have compact nuclear radio sources, so NGC 7213 is more like a LINER than a Seyfert galaxy in this respect.

VI. SUMMARY

Phillips (1979) first identified broad Hα emission in NGC 7213, supporting the claim that this galaxy is associated with the HEAO A-2 source H2209-471. X-ray observations presented here show that the spectral index is typical of Seyfert galaxies. Moreover, the overall continuum resembles those in classical active extragalactic objects, as evidenced by the possible UV bump, the flat radio spectrum, and the optical nonstellar continuum. There can be little doubt that gas near the nucleus is photoionized by a nonstellar continuum.

This is an important conclusion since NGC 7213 also exhibits the optical characteristics of LINERs (Heckman 1980), whose emission lines have often been attributed to heating by shocks. If the "shock" features of NGC 7213 can be reconciled with photoionization models, it is possible that the entire class of LINERs consists of objects in which the basic physical processes are similar to those in QSOs and type 1 Seyfert galaxies. An extensive analysis of the optical emission lines is presented in Paper I, where it is shown that shocks are indeed not

necessary to explain the observed features.

The small X-ray column density disagrees with the reddening of $\underline{A}_V = 0.61$ mag determined from the optical spectrum. However, there may be thermal emission at temperatures of $\sim 5 \times 10^6$ K which is sufficient to fill in the soft X-ray turnover and create an approximation to a single power law. Thermal emission from a hot medium which confines the narrow-line clouds may make a substantial contribution to the soft X-ray flux of Seyfert galaxies. X-ray spectra having higher resolution are needed to look for line emission or continuum features which may be indicative of a spectrum containing both thermal and power-law components.

The able assistance of the electronics technicians and telescope operators at Las Campanas Observatory is greatly appreciated. Permission to make use of the MIT IPC observation of NGC 7213 was kindly granted by G. Kriss. An anonymous referee made several helpful remarks concerning the analysis and presentation of the data. This research was supported in part by NASA grant NGL 05-002-134 to J. B. Oke, and by the Fannie and John Hertz Foundation in the form of a graduate fellowship to A. V. F.

TABLE 1

Parameters of Continuum Decomposition

Power law slope α[a]	A_V (mag)[b,e]	$\left(\frac{\text{Power law}}{\text{Total}}\right)_{\lambda 5460}$[c,f]	$\left(\frac{\text{Power law}}{\text{Total}}\right)_{\lambda\lambda 3202-6272}$[d,f]
0.8	0.05[a]	0.094	0.15
1.1	0.05[a]	0.114	0.17
1.4	0.05[a]	0.135	0.19
1.7	0.05[a]	0.157	0.21
0.8	0.63	0.202	0.30
1.1	0.61	0.236	0.33
1.4	0.57	0.263	0.35
1.7	0.53	0.300	0.38

[a]Fixed parameter.

[b]Free or fixed parameter.

[c]Free parameter.

[d]Flux derived from final decomposition.

[e]$E_{B-V} = A_V/3.2$ used to deredden continuum of NGC 7213 prior to decomposition.

[f]Flux ratio (where total flux = power law + standard galaxy fluxes).

TABLE 2

Relative Fluxes of Continua[a], $\alpha = 1.1$

λ (Å)	$\left(\frac{\text{Power law}}{\text{Total}}\right)^{b}$ $A_V = 0.05$ mag[c]	$\left(\frac{\text{Power law}}{\text{Total}}\right)^{b}$ $A_V = 0.61$ mag[c]
3202	0.536	0.735
3500	0.434	0.648
4000	0.229	0.417
4500	0.152	0.302
5000	0.139	0.280
5460	0.114	0.236
6000	0.102	0.214
6272	0.107	0.223

[a]See Figure 1.

[b]Flux ratio (where total flux = power law + standard galaxy fluxes).

[c]$E_{B-V} = A_V/3.2$ used to deredden continuum of NGC 7213 prior to decomposition.

TABLE 3

Einstein Observations of NGC 7213

Day	Year	Exp. Time (s)	counts s^{-1} (2-6 keV)[a]	F_x (2-10 keV) (10^{-11} erg $cm^{-2}s^{-1}$)	A	α[b]	N_H[c] ($10^{21}cm^{-2}$)	L_x (2-10 keV)[d] (10^{42} erg s^{-1})	M/I[e]
112	1979	7493	1.01±0.10	2.20	0.0068	0.85±0.11	<8.0	3.29	M
295	1979	975	0.81±0.16[f]	1.67	0.0075	1.1±0.6	<20	2.50	M
136	1980	1516	2.97±0.12	6.80	0.0170	0.72±0.12	<0.25	10.2	M,I

[a] 1 MPC count = 1.05 UFU.

[b] 90% error bars.

[c] Upper limits.

[d] Intrinsic (unabsorbed) luminosity, H_o = 50 km s^{-1} Mpc.

[e] Instrument used: M denotes MPC, I denotes IPC.

[f] Includes correction factor of 1.63 for off-axis collimator response.

REFERENCES

Bolton, J. G., Savage, A., and Wright, A. E., 1977, Aust. J. Phys., Astrophys. Suppl. No. 41, 25.

Brown, R. L., and Gould, R. J. 1970, Phys. Rev. D, 1, 2252.

Burstein, D., and Heiles, C. 1982, A. J., 87, 1165.

Dickey, J. M., Salpeter, E. E., and Terzian, Y. 1978, Ap. J. Suppl., 36, 77.

Dower, R. G., Griffiths, R. E., Bradt, H. V., Doxsey, R. E., and Johnston, M. D. 1980, Ap. J., 235, 355.

Elvis, M., Briel, U. G., and Henry, J. P. 1983, Ap. J., 268, 105.

Filippenko, A. V., and Halpern, J. P. 1984, Ap. J., submitted (Paper I).

Gaillardetz, R., Bjorkholm, P., Mastronardi, R., Vanderhill, M., and Howland,D. 1978, IEEE Trans. Nucl. Sci., NS-25, 437.

Giacconi, R., et al. 1979, Ap. J., 230, 540.

Glass, I. S. 1981, M.N.R.A.S., 197, 1067.

Glass, I. S., Moorwood, A. F. M., and Eichendorf, W. 1982, Astr. Ap., 107, 276.

Goodrich, R. W., and Osterbrock, D. E. 1983, Ap. J., 269, 416.

Gorenstein, P. 1975, Ap. J., 198, 95.

Grindlay, J. E., Steiner, J. E., Forman, W. R., Canizares, C. R., and McClintock, J. E. 1980, Ap. J. (Letters), 239, L43.

Halpern, J. P. 1982, Ph.D. thesis, Harvard University.

--------. 1984, Ap. J., 281, 000.

Halpern, J. P., and Steiner, J. E. 1983, Ap. J. (Letters), 269, L37.

Heckman, T. M. 1980, Astr. Ap., 87, 152.

Heiles, C., and Cleary, M. N. 1979, Aust. J. Phys. Suppl. No. 47, 1.

Kriss, G. A. 1982, Ph.D. thesis, Massachusetts Institute of Technology.

Kwan, J., and Krolik, J. H. 1981, Ap. J., 250, 478.

Maccacaro, T., Perola, G. C., and Elvis, M. 1982, Ap. J., 257, 47.

Malkan, M. A. 1983, Ap. J., 268, 582.

Malkan, M. A., and Filippenko, A. V. 1983, Ap. J., 275, 477.

Malkan, M. A., and Sargent, W. L. W. 1982, Ap. J., 254, 22.

Marshall, F. E., Boldt, E. A., Holt, S. S., Mushotzky, R. F., Pravdo, S. H., Rothschild, R. E., and Serlemitsos, P. J. 1979, Ap. J. Suppl., 40, 657.

McAlary, C. W., McLaren, R. A., McGonegal, R. J., and Maza, J. 1983, Ap. J. Suppl., 52, 341.

Mushotzky, R. F. 1982, Ap. J., 256, 92.

Oke, J. B., and Gunn, J. E. 1983, Ap. J., 266, 713.

Oke, J. B., Shields, G. A., and Korycansky, D. G. 1984, Ap. J., 277, 64.

Piccinotti, G., Mushotzky, R. F., Boldt, E. A., Holt, S. S., Marshall, F. E., Serlemitsos, P. J., and Shafer, R. A. 1982, Ap. J., 253, 485.

Phillips, M. M. 1979, Ap. J. (Letters), 227, L121.

Reichert, G. A., Mason, K. O., Thorstensen, J. R., and Bowyer, S. 1982 Ap. J., 260, 437.

Reichert, G. A., Petre, R., Mushotzky, R. F., and Holt, S. S. 1983, Bull. A.A.S. 15, 675.

Sadler, E. M. 1984, A. J., 89, 53.

Tananbaum, H., and Avni, Y. 1982, Ap. J. (Letters), 262, L17.

Tucker, W. H. 1975, Radiation Processes in Astrophysics. (Cambridge: MIT Press).

Ward, M., Allen, D. A., Wilson, A. S., Smith, M. G., and Wright, A. E.

1982, M.N.R.A.S., 199, 953.

Weedman, D. W., Feldman, F. R., Balzano, V. A., Ramsey, L. W., Sramek, R. A., and Wu, C.-C. 1981, Ap. J., 248, 105.

Wu, C.-C., Boggess, A., and Gull, T. R. 1983, Ap. J., 266, 28.

Yee, H. K. C., and Oke, J. B. 1978, Ap. J., 226, 753.

Zamorani, G. et al. 1981, Ap. J., 245, 357.

FIGURE CAPTIONS

Figure 1: The smoothed continuum of NGC 7213 is decomposed into a nonstellar power law plus an old stellar population (represented by a "standard" giant elliptical galaxy). Magnitude $AB = -2.5\log(f_\nu) - 48.6$, where f_ν is in ergs s^{-1} cm^{-2} Hz^{-1}. In (a) the continuum is dereddened under the assumption that Galactic $A_V = 0.05$ mag, where $A_V = 3.2E_{B-V}$. A noticeably more satisfactory fit (b) is obtained if an additional extinction $A_V = 0.56$ mag is present in NGC 7213.

Figure 2: Contours of acceptable fits (90% confidence) to the 1980 May 15 Einstein MPC and IPC data are shown. The numbers 15.6, 16.6, and 17.6 refer to different assumed gains of the IPC, where 16.6 is the nominal BAL (see text). The dashed line encompasses the total range of allowed fits to the IPC data.

Figure 3: Theoretical spectra which represent the best fits to the 1980 May 15 Einstein IPC (light bars) and MPC (dark bars) data are illustrated. Spectral parameters and errors refer to the overlap region of the 90% contours shown in Figure 2.

Figure 4: Data covering the overall continuum of NGC 7213 are displayed. Note that the radio, IR, optical, UV, and X-ray measurements were taken through different effective apertures and at different epochs. Frogel and Elias obtained the 10 μm point at 0.19 Jy (filled circle with tick marks), as reported by Phillips (1979), and "N" refers collectively to all 4 observations near 10 μm. The point at 8.3 μm has much larger error bars than other measurements. Solid lines represent the new optical and X-ray spectra reported in this paper. Open crosses

and the dashed line show the optical and UV data dereddened by $\underline{A}_V = 0.61$ mag, but the IR data have not been dereddened. The dash-dot line is the power-law component ($\alpha = 1.1$) derived from a least-squares fit to the optical data only, and happens to extrapolate through the observation at 8.3 μm obtained by Glass, Moorwood, and Eichendorf (1982). A possible inconsistency among the IR points is discussed in the text, and an excess typical of Seyfert 1 galaxies is indicated by the UV flux. The flatness of the X-ray slope in comparison with the optical power law requires that there be at least two breaks in the unobserved UV spectrum.

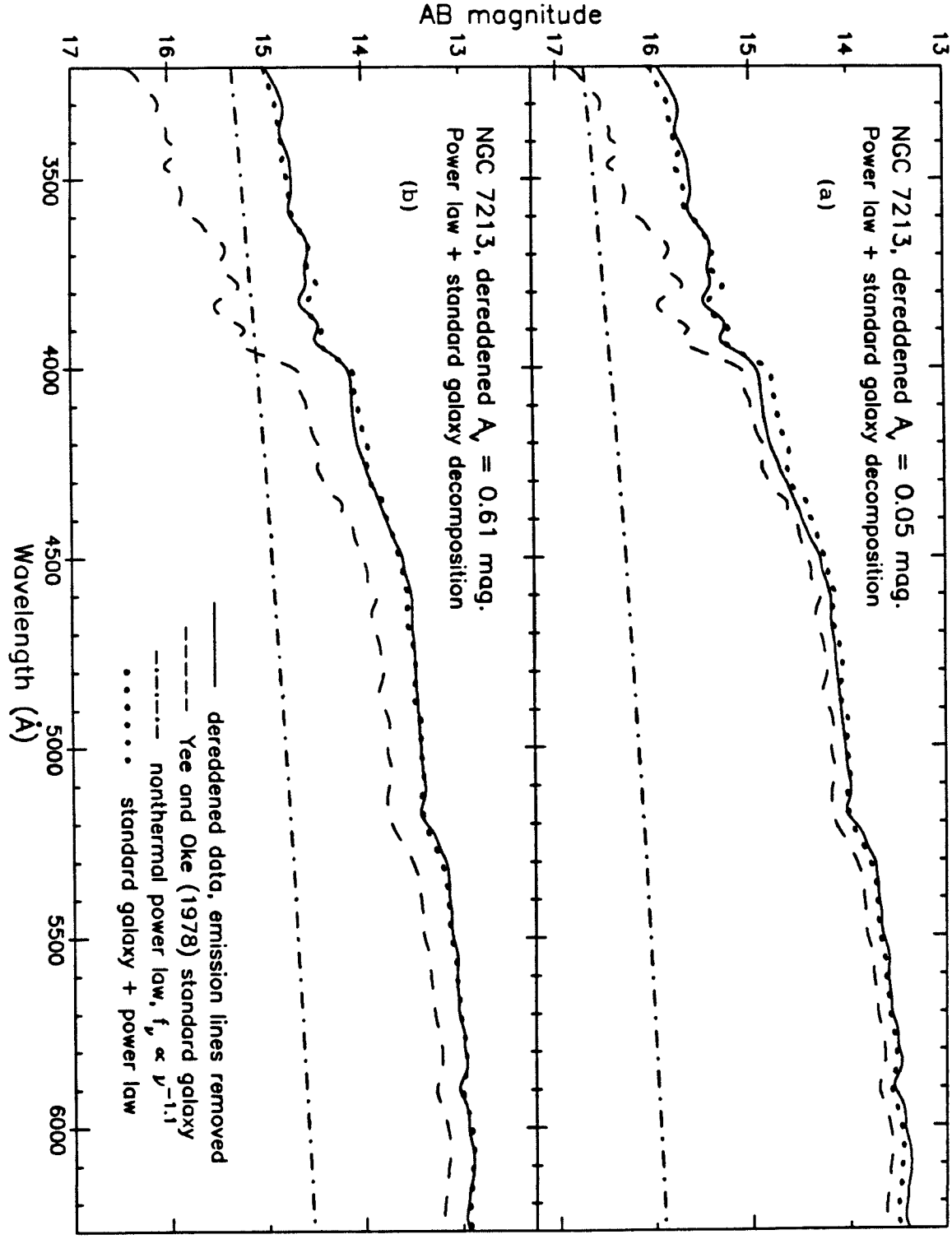
NGC 7213, dereddened A_v = 0.05 mag.
Power law + standard galaxy decomposition
(a)
NGC 7213, dereddened A_v = 0.61 mag.
Power law + standard galaxy decomposition
(b)
AB magnitude
Wavelength (Å)
dereddened data, emission lines removed
Yee and Oke (1978) standard galaxy
nonthermal power law, $f_\nu \propto \nu^{-1.1}$
standard galaxy + power law

Figure 1

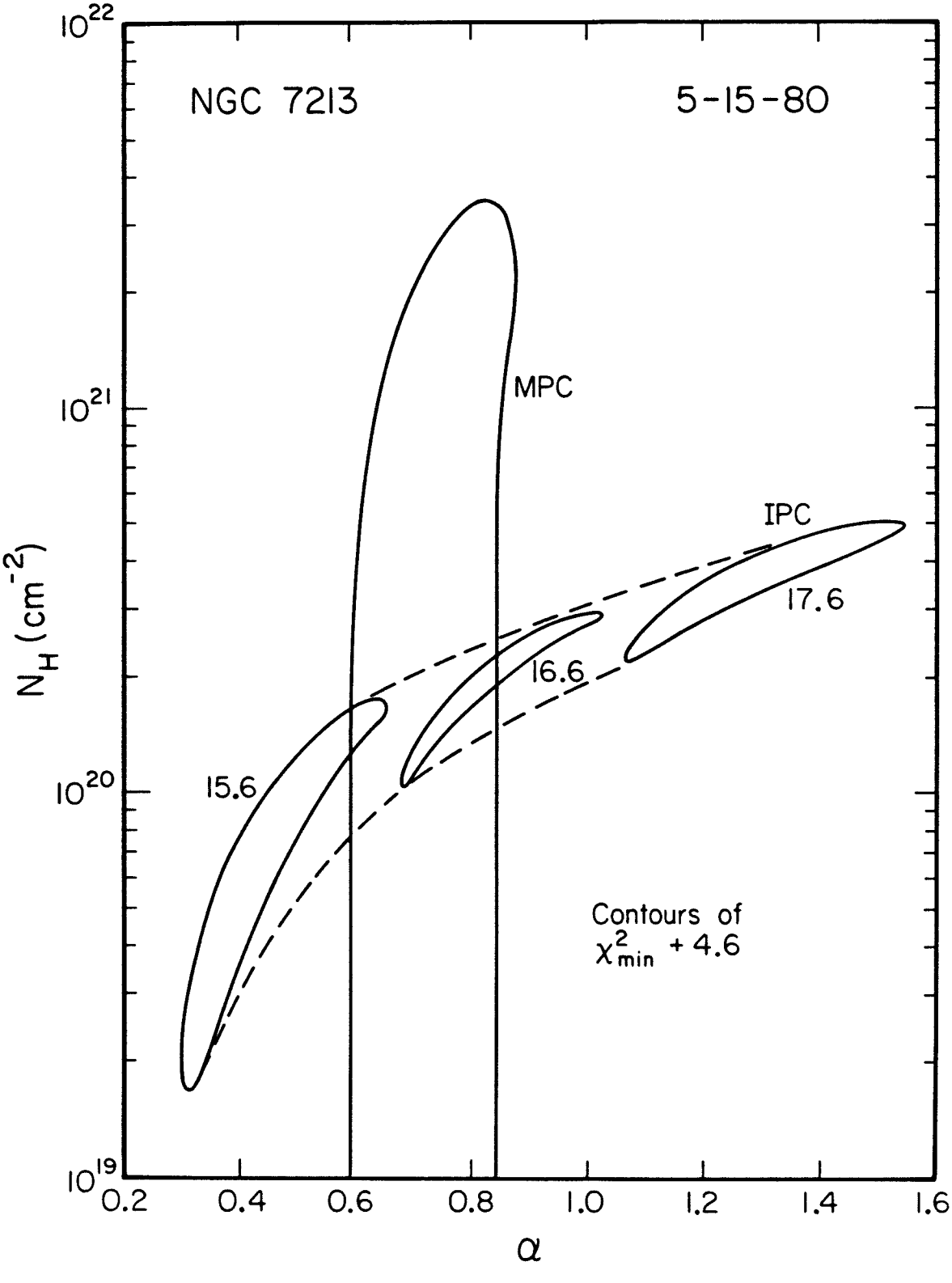
NGC 7213
5-15-80
MPC
IPC
17.6
16.6
15.6
Contours of
χ^2_{min} + 4.6
N_H (cm^{-2})
10^{22}
10^{21}
10^{20}
10^{19}
0.2
0.4
0.6
0.8
1.0
1.2
1.4
1.6
α

Figure 2

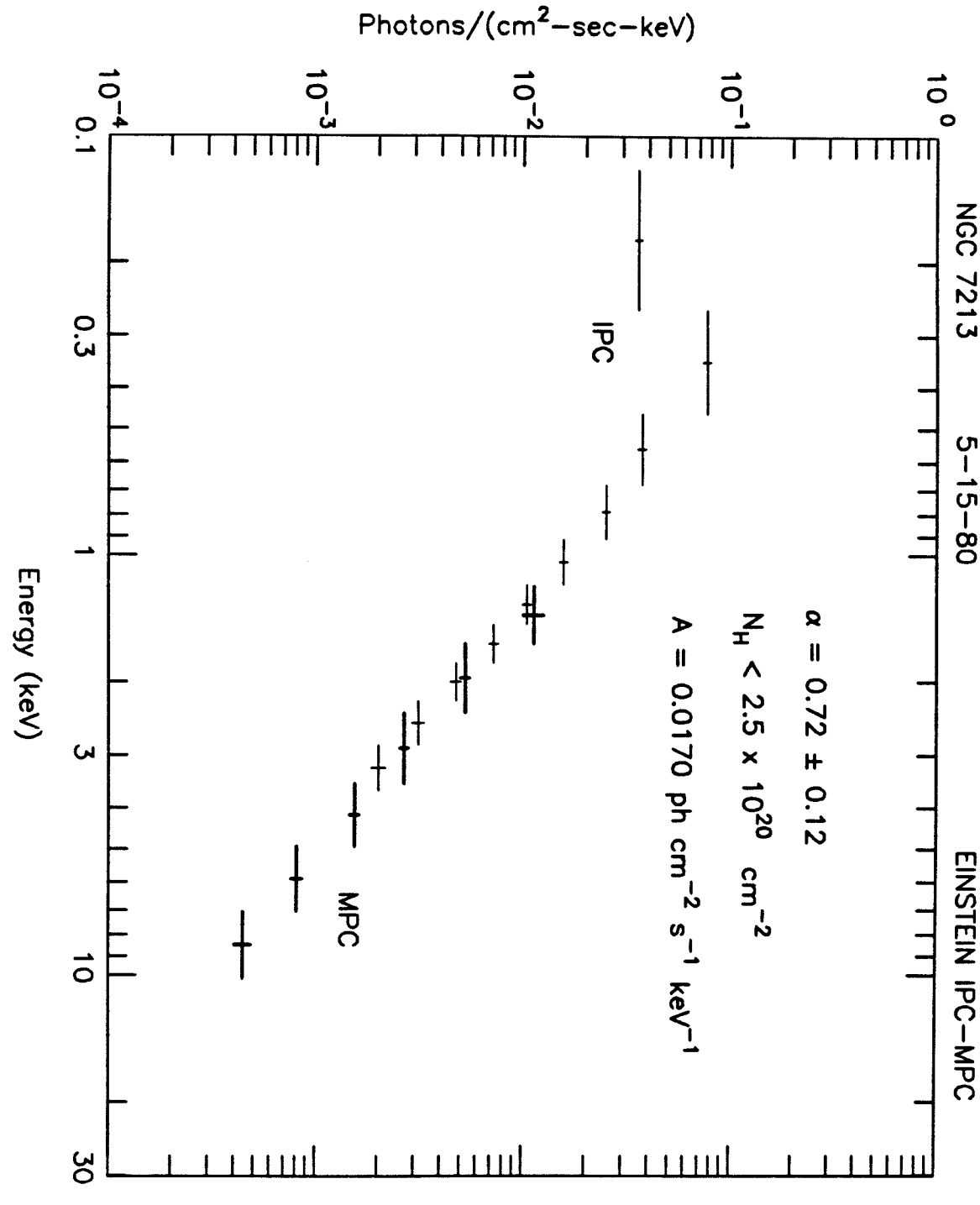
Photons/(cm²-sec-keV)
10⁰
10⁻¹
10⁻²
10⁻³
10⁻⁴
NGC 7213
5-15-80
EINSTEIN IPC-MPC
IPC
MPC
α = 0.72 ± 0.12
N_H < 2.5 x 10²⁰ cm⁻²
A = 0.0170 ph cm⁻² s⁻¹ keV⁻¹
Energy (keV)
0.1
0.3
1
3
10
30

Figure 3

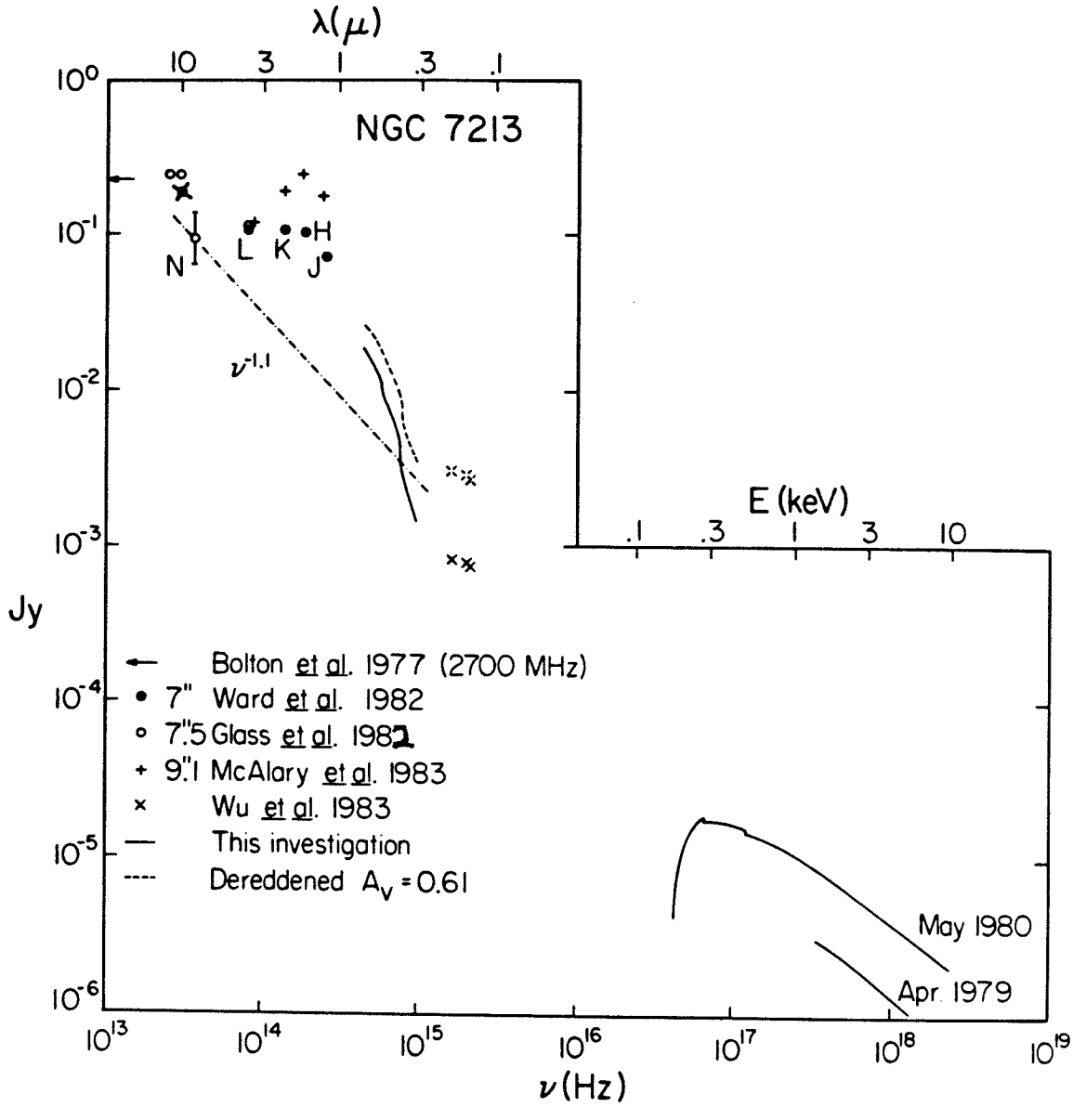
λ(μ)
10
3
1
.3
.1
NGC 7213
N
L
K
H
J
$\nu^{-1.1}$
E (keV)
.1
.3
1
3
10
Jy
Bolton et al. 1977 (2700 MHz)
7" Ward et al. 1982
7".5 Glass et al. 1982
9".1 McAlary et al. 1983
Wu et al. 1983
This investigation
Dereddened $A_V = 0.61$
May 1980
Apr. 1979
ν(Hz)

Figure 4

CHAPTER 4

New Evidence for Photoionization as the Dominant Excitation Mechanism in LINERs.

Alexei V. Filippenko

Submitted for publication, The Astrophysical Journal

For out of olde feldes, as men seyth,
Cometh al this newe corn for yer to yere;
And out of olde bokes, in good feyth,
Cometh al this newe science that men lere.

"The Parliament of Fowls"
Geoffrey Chaucer

ABSTRACT

Optical spectrophotometry of the nearby QSO MR 2251-178 and the powerful radio galaxies Pictor A and PKS 1718-649 is presented. MR 2251-178 and Pictor A have featureless continua and broad Balmer emission (FWZI ~ 20000 km s^{-1}), as well as prominent forbidden lines spanning a wide range of ionization potentials (e.g., [O I], [Fe VII]). Both objects are undoubtedly photoionized by the nonstellar radiation. A nonstellar component is convincing only at blue and UV wavelengths in Pks 1718-649. Careful subtraction of the starlight reveals He II λ4686 emission. Its strength, and especially that of [Ne V]λ3426, argue strongly against shock heating as the main excitation mechanism. Gas near the nucleus is therefore photoionized, but the ionizing radiation must be substantially more intense than predicted by the power law at optical wavelengths. The profile of Hα has weak, broad wings (FWZI ~ 4500 km s^{-1}).

In all three objects, the width of a forbidden line increases with its critical density for collisional deexcitation. This implies a considerable range in density (10^3-10^7 cm^{-3}) among the clouds of gas in the narrow-line region, as discussed by Filippenko and Halpern for the prototype NGC 7213. The densest clouds are optically thick to the Lyman continuum, close to the nucleus, and move most rapidly.

Several previous studies concluded that Pictor A and Pks 1718-649, whose strong lines of low ionization satisfy the criteria of LINERs, are heated by shocks; at low densities the great observed strength of [O III]λ4363 relative to [O III]λ5007 implies temperatures incompatible with photoionization. Serious inconsistensies with photoionization

models are unlikely, however, if the wide range of densities reported here is taken into account. The presence of similar properties in galactic nuclei having active components of high (MR 2251-178), medium (Pictor A), and low (PKS 1718-649) luminosity suggests that the physical processes in most, if not all, classical AGNs and LINERs may be fundamentally the same.

Subject headings: galaxies:nuclei--galaxies:Seyfert--line profiles--radiation mechanisms--quasars--X-rays:sources.

I. INTRODUCTION

A large effort has been made in theoretical models to reproduce the spectral characteristics of active galactic nuclei (AGNs), including QSOs, type 1 and type 2 Seyfert galaxies, and most recently Heckman's (1980) "low ionization nuclear emission-line regions" (LINERs). Based on the clear presence of nonthermal ionizing radiation in QSOs and the most luminous Seyfert 1 galaxies, the models incorporated power-law continua of various strengths to explain the observed intensity ratios of optical emission lines. Early attempts were moderately successful (see Davidson and Netzer 1979, and references therein), but the agreement improved noticeably when the importance of charge-transfer reactions (e.g., Butler, Heil, and Dalgarno 1980) was recognized. In fact, some studies (Ferland and Netzer 1983; Halpern and Steiner 1983) even attempted to unify all AGNs by varying essentially one parameter, the ratio of ionizing photons to nucleons at the face of a cloud. Objects having a high "ionization parameter" (e.g., type 1 Seyferts) display a rich emission-line spectrum including lines from highly-ionized species, whereas those characterized by a low value (e.g., LINERs) are dominated by emission from neutral and singly-ionized atoms.

Despite the success of these models, several problems are evident. One of the most important is that the strengths of transauroral and auroral lines (noteably [O III]λ4363) are often too large in comparison with the corresponding nebular lines ([O III]λ4959+5007) in LINERs. This led some investigators to ascribe the emission to shock heating (e.g., Fosbury *et al.* 1978; Koski and Osterbrock 1976), since the

intensity ratios are a natural consequence of the high temperatures produced by shocks. Another problem is that the observed He II λ4686 emission in LINERs is too weak relative to Hβ. Although collisional enhancement of Balmer lines may be partly responsible, it is unlikely that the effect can be more important in LINERs than in classical Seyferts. Shock models, on the other hand, do not predict strong He II λ4686.

Recent studies have shown, however, that photoionization may in fact be more successful than shock heating in producing the observed emission in LINERs. Keel and Miller (1983), Filippenko and Halpern (1984, hereafter FH), and Rose and Tripicco (1984) have emphasized the importance of properly accounting for the prominent stellar continuum when measuring weak emission lines. [O III]λ4363, for example, lies on top of a "high point" between stellar absorption lines; consequently, its strength has often been overestimated. The new, lower values remove some to the conflict with simple photoionization models, and more detailed theoretical studies incorporating a range of densities in the narrow-line region (NLR) eliminate the remaining discrepancies (Péquignot 1984). These calculations also postulate that much of the ultraviolet (UV) continuum is produced by a hot (T ~ 80000 K) accretion disk (Malkan 1984), resulting in relatively weak He II λ4686.

A detailed analysis of the bright galaxy NGC 7213 (FH; Halpern and Filippenko 1984) agrees well with the predictions and may provide a key to the nature of LINERs. Gas near the nucleus of NGC 7213 is clearly photoionized by nonstellar radiation, but the optical spectrum also exhibits characteristics of shock-heated gas such as strong [O III]λ4363 and low-ionization emission lines. FH show that these features can be

understood without shocks if clouds covering a wide range of densities (10^3–10^7 cm^{-3}) exist in the NLR. The very different widths of forbidden lines demonstrate conclusively that this is indeed the case.

It is tempting to speculate that at least some nearby galaxies harbor a massive black hole which is running out of "fuel" (Gunn 1979). These might be LINERs: NGC 7213 shows that their characteristics are explainable in terms of photoionization rather than shocks, and that the dominant physical processes may be fundamentally the same as those in QSOs. A greater number of objects must be investigated, however, before drawing definitive conclusions.

This paper presents observations which strongly support the above arguments. Density stratification in the NLR is evident in Pks 1718–649 (a classical LINER), Pictor A (an N galaxy with features of type 1 Seyferts and LINERs), and MR 2251–178 (a nearby QSO), demonstrating that the physical conditions in objects spanning a wide range in the ratio of nuclear (unresolved) to disk (resolved) luminosity can be comparable to those in NGC 7213. Unless otherwise noted, a Hubble constant of 50 km s^{-1} Mpc^{-1} is assumed.

II. OBSERVATIONS

The data were obtained in August 1983 with the Boller and Chivens Cassegrain spectrograph on the 2.5 m du Pont reflector at Las Campanas Observatory. A journal of observations is given in Table 1. Shectman's (1981) Intensified Reticon detector, an improved version of the original instrument (Shectman and Hiltner 1976), was used to obtain the spectra. Bausch and Lomb gratings with 600 and 1200 grooves/mm provided typical resolutions (in first order) of roughly 5 and 2.5 Å, respectively. The

wavelength scale was determined by fitting a fifth-order polynomial to the positions of unblended emission lines in comparison spectra (Fe, Ar, Ne) obtained before and after each observation.

To minimize the effects of atmospheric dispersion when using a small (2" x 4") entrance aperture (Filippenko 1982), its long dimension was aligned along the parallactic angle corresponding to the midpoint of each observation. The relatively large separation between the "object" and "sky" apertures (27.4") ensured that light from the outer portions of the objects did not contribute significantly to the sky measurements. Calibration of the overall response of the spectrograph was achieved with faint, relatively featureless standard stars (Filippenko and Greenstein 1984). Coincidence losses were negligible due to the faintness of all objects, except in the case of MR 2251-178 ($\S$ Vc).

No filters were used, so second-order contamination longward of ~ λ6400 is present. This is generally not serious since galaxies are much fainter at blue and UV wavelengths than in the red. An exception is MR 2251-178, whose strong "UV bump" ($\S$ Vc) produces serious second-order contamination redward of ~ λ6000. In addition, note that the standard stars (G158-100 and G24-9) are bluer than the integrated light of galactic bulges, resulting in greater second-order contamination and hence an overestimate of the spectrograph's sensitivity at the red end. Pictor A and Pks 1718-649 therefore exhibit a noticeable decrease in flux density longward of ~ λ6400; their emission-line intensities must be viewed with caution in this region.

Local variations in the response of the detector were calibrated with lengthy exposures of the featureless continuum from a hot tungsten lamp. Stability of these "flatfields" from one night to the next was

excellent (~ 1-2%).

III. PKS 1718-649

a) Background

Pks 1718-649 is a D galaxy (m_V ~ 15.5) which exhibits a powerful, inverted radio spectrum from 408 to 2700 MHz and strong optical emission lines (Savage 1976; Fosbury *et al.* 1979, hereafter FMGV). Faint spiral arms surrounding the bright bulge are visible in deep photographs, suggesting the classification of SAB(s)bP in the system of de Vaucouleurs and de Vaucouleurs (1964). H I accounts for fully 6% of the object's total mass. FMGV reported that the optical spectrum is of unusually low ionization: lines of [O I], [O II], and [S II] are particularly prominent. The similarity with the LINER NGC 1052, together with the absence of a blue nonstellar excess, led them to conclude that the emission-line spectrum is the result of shock heating.

FMGV noticed that [O I]λ6300 is significantly broader than other unblended emission lines, and also more than a factor of three stronger than [O I]λ6364. They decided that it is blended with [S III]λ6312, but this is unlikely considering the weakness of [S III] in Seyferts and other emission-line galaxies. A more plausible conclusion is that the [O I] lines are intrinsically broad, and that the one at λ6364 appears too weak due to underlying Fe I λ6355, 6359 absorption (Filippenko and Sargent 1984). The resemblance to NGC 7213 (FH) suggests that Pks 1718-649 may provide additional clues to the LINER phenomenon.

b) The Stellar and Nonstellar Continua

In overall appearance the spectrum resembles that of FMGV. Close

inspection, however, reveals a faint blue excess which is not produced by the old stellar population. To quantify it, the continuum was decomposed into the spectrum of a giant elliptical galaxy (Yee and Oke 1979) and a power law ($f_\nu \propto \nu^{-\alpha}$), as described by FH. Ignoring regions contaminated by emission lines, least-squares fits were performed to obtain the reddening and the ratio of nonstellar to total flux at λ5460. An accurate determination of the spectral index was impossible due to the dominance of starlight and the small wavelength range, but $\alpha = 1.5 \pm 0.5$ produced good results. This is somewhat steeper than in most QSOs and type 1 Seyfert galaxies (Malkan and Sargent 1982; Malkan and Filippenko 1983), but is fairly representative of type 2 Seyferts (Koski 1978).

The results are shown in Figure 1a. A faint nonstellar component contributes only ~ 6% of the observed flux at λ5460. Its relative prominence increases at shorter wavelengths, and near λ3200 it is roughly half the strength of starlight. Dilution of the Ca II K (λ3934) and H (λ3968) absorption lines is calculated to be small (~ 13-14%). These results are sensitive to the range of wavelengths and to the value of α used in the decomposition, but the general conclusions remain unchanged.

Using the usual reddening curve (Whitford 1958), the derived reddening corresponds to $A_V = 3.2 E_{B-V} = 0.70$ mag. This is larger than the expected Galactic value of 0.27 mag (Burstein and Heiles 1982). Dust in the nuclear region (FMGV) can probably account for the observed excess.

c) Emission Lines

Old stars dominate the spectrum and affect measurements of emission lines, producing unacceptable inaccuracies in crucial diagnostic lines such as [O III]λ4363 and He II λ4686. The starlight was therefore removed with a template devoid of emission. As in NGC 7213, the S0 galaxy IC 4889 was a particularly suitable choice because the metallicity and stellar velocity dispersion in its nucleus are similar to those of Pks 1718-649.

FH describe the procedure in detail. First, the nonstellar component was subtracted from the dereddened spectrum of Pks 1718-649 (Figure 2a). The overall spectral shape of IC 4889 was then adjusted to match that of the object (thereby artificially removing differences in reddening, etc.), and its metallicity was decreased slightly. Finally, weak [O II]λ3727 was excised, resulting in the spectrum shown in Figure 2b. Subtraction of the template from the object produced the net emission-line spectrum (Figure 2c). Regions blueward of λ3600 and redward of λ5150 were excluded because of poor signal-to-noise (S/N) ratios in either Pks 1718-649 or IC 4889.

Benefits of the subtraction are obvious. [Ne III]λ3967 + Hε, previously hidden in deep Ca II H absorption, are present. Similarly, the [S II]λ4069 + Hδ and [O III]λ4363 + Hγ blends are much easier to analyze. Even He II λ4686, which was not suspected in the original data (Figure 2a), is visible.

Emission lines in Figure 2c have different widths, and in several cases (e.g., [O III]λ5007, Hβ) strong wings make the profiles appear distinctly non-Gaussian. These results are confirmed by the data in the vicinity of Hα (Figure 3a). [O I]λ6300 is significantly broader than the combined [S II]λ6716+6731 doublet, and its profile exhibits wings of

greater prominence than a Gaussian having the same full width at half-maximum (FWHM).

An even broader component is apparent in the Hα + [N II] blend, especially on the red side. Comparison with the nearby [S II] emission (which is produced under roughly the same physical conditions as [N II]) indicates that this component is almost certainly Hα. A full width at zero-intensity (FWZI) of ~ 4500 Å makes it qualitatively similar to (but less intense and narrower than) that in classical type 1 Seyferts. Together with the nonstellar continuum, it suggests that in some ways Pks 1718-649 may be one of the weakest Seyfert 1 galaxies discovered to date. Spectra of many other LINERs also contain very faint, broad Hα emission (Filippenko and Sargent 1984).

To facilitate quantitative analysis of the data, the intensity, FWHM, and full width at 10%-intensity (FW10) of each emission line was carefully measured. The traditional FWZI was generally not chosen because it is difficult to determine and is very dependent on the S/N ratio. All intensity measurements are listed in Table 2. Typical errors are generally ~ 5-10% for strong, unblended lines, 10-20% for blends or weaker lines, and up to 100% for the faintest features (denoted by a colon). These values do not include possible inaccuracies in the overall calibration of the spectrum. Widths are given in Table 3.

In a few cases special procedures were used to deblend lines. The assumed strength and width of [N II]λ6583 were varied to yield a smooth Hα profile. Comparison of Hα and Hβ showed excellent agreement except in the reddest portion of the broad wing; it was therefore legitimate to remove Hγ from [O III]λ4363 by appropriately scaling the Hβ profile.

Hδ was subtracted from the wing of [S II]λ4069,4076 in a similar manner.

The only major discrepancy between the new intensity ratios and those measured by FMGV occurs in $\underline{I}$([N II]λ6548+6583)/$\underline{I}$(Hα). Since FMGV used three Gaussians of equal width to decompose the blend in their relatively low-resolution data (~ 10 Å), too much Hα flux was attributed to [N II]. Many other differences, including FMGV's nondetection of weak emission such as He II λ4686, can be explained by contamination from underlying absorption lines. Note that their absolute flux of Hβ is a factor of ~ 2.8 larger than that quoted here, but the entrance apertures are different and neither study claims photometric accuracy.

Table 2 indicates the presence of [Ne V]λ3426. Since appreciable [Ne V] is not produced by shocks or in normal H II regions around OB stars, it is highly likely that gas is photoionized by the nonstellar continuum described in § III$\underline{b}$. The detection of He II λ4686 supports this conclusion. Although an extrapolation of the derived power law past the Lyman limit fails by nearly a factor of 10 to produce the dereddened Hα flux of 2.0×10^{-13} erg s^{-1} cm^{-2}, such a calculation is probably oversimplified; most bright QSOs and type 1 Seyferts have much more radiation at UV wavelengths than expected from a comparison with the optical power law (e.g., Malkan and Sargent 1982; Oke, Shields, and Korycansky 1984). If such an excess also exists in Pks 1718-649, it may account for the observed flux of Hα.

After correcting for extinction ($\underline{A}_V$ = 0.70 mag), the nonthermal monochromatic luminosity at λ4800 is ~ 2.4×10^{27} erg s^{-1} Hz^{-1} and the luminosity of Hα emission is 1.8×10^{41} erg s^{-1} (of which at most one-third can be produced in the "broad-line region"). Transforming to $\underline{H}_o$ = 75 km s^{-1} Mpc^{-1}, these values place Pks 1718-649 among type 2

Seyferts of low luminosity in Figure 2 of Shuder (1981). Using the mean $\underline{I}(L_x)/\underline{I}(H\alpha)$ ratio of ~ 40 for active galaxies (Elvis, Soltan, and Keel 1984) and the observed flux of Hα corrected for Galactic extinction ($\underline{A}_V$ = 0.27 mag), the predicted X-ray flux in the 2-10 keV range is ~ 8×10^{-12} erg s^{-1} cm^{-2}, which is below the completeness limit (3.1×10^{-11}) of the Piccinotti *et al.* (1982) sample.

The ratio $\underline{R} \equiv \underline{I}([O\ III]\lambda 4959+5007)/\underline{I}([O\ III]\lambda 4363)$ is ~ 12.7, which is remarkably small and implies that $\underline{T}_e \sim 7 \times 10^4$ K if $\underline{n}_e \sim 10^4$ cm^{-3}. $\underline{T}_e$ becomes still larger if the density obtained from the [S II]λ6716,6731 doublet (~ 250 cm^{-3}) is used. Even if the data are not dereddened, R = 14.3 makes the derived value of $\underline{T}_e$ very high ($> 5.5 \times 10^4$ K). Such temperatures are incompatible with photoionization models, which always predict $\underline{T}_e \lesssim 20000$ K, but they may be prevalent in shock-heated gas.

A reconciliation with photoionization can be made if one does not assume that the density in the O^{++} zone is low. At high $\underline{n}_e$ (~ 10^6 cm^{-3}), collisional deexcitation of the [O III]λ4959,5007 lines is greater relative to that of [O III]λ4363 because the former are associated with a smaller critical density than the latter; $\underline{R}$ therefore shifts to low values. Although Ferland and Netzer (1983) considered high densities improbable in LINERs, FH discovered undeniable evidence for them in NGC 7213: the correlation between line width and $\underline{n}_e(\underline{crit})$ is considerably better than that between line width and ionization potential, and even lines emitted by the *same* species (such as [O II]λ3726,3729 and [O II]λ7319,7330) have different widths. Since a line is produced most efficiently by gas near its $\underline{n}_e(\underline{crit})$, different lines act as effective tracers of the density in NGC 7213.

The same arguments are directly applicable to Pks 1718-649. Figure 4a illustrates the dependence of FW10 on the ionization potential (χ) for 12 different forbidden lines. Estimates of the errors are shown along with the actual measurements. A correlation may be present, but the scatter is large. If χ is replaced with n_e(crit), on the other hand (b), the correlation coefficient rises from 0.28 to 0.91, and a correlation is certain. Similar results were obtained for the FWHM of lines, as summarized in Table 4. Note that the ionization potential used in this paper and by FH corresponds to the actual ion under consideration, rather than to the next less ionized species as in some studies (e.g., Pelat, Alloin, and Fosbury 1981; De Robertis and Osterbrock 1984). Also, the critical densities were calculated with assumed temperatures ranging from 10000 K (for low-ionization lines) to 20000 K (for [Ne V]).

An important point is that lines from the same species and characterized by different values of n_e(crit), such as the blue and red [S II] doublets as well as [O III]λ4959,5007 and [O III]λ4363, greatly strengthen the correlation between width and n_e(crit). Pelat, Alloin, and Fosbury (1981), who analyzed the type 1 Seyfert NGC 3783, also suggested that line width increases with n_e(crit), but their correlation between width and χ was equally good because they had no lines that were capable of unambiguously discriminating between χ and n_e(crit).

Thus, clouds of high density (10^6-10^7 cm^{-3}) clearly play a major role in determining the emission-line spectrum of Pks 1718-649. These densities are a factor of 10 to 100 higher than even the highest ones normally found in the NLR of Seyfert galaxies and adopted in photoionization models. Exceptions to this are several broad-line radio

galaxies (Osterbrock, Koski, and Phillips 1976) and quasars (Baldwin 1975). As discussed in detail by FH, regions of high density enhance auroral and transauroral lines such as [O III]λ4363 and [S II]λ4069,4076 relative to the nebular emission and mimic the effects of high T_e. No conflicts exist with the temperatures required by photoionization models. The simultaneous presence of low densities (derived from the [S II] doublet) precludes the use of simple, single-density models.

Several other properties of the emission lines should be mentioned. [O III]λ4959 and [O III]λ5007 are blueshifted by 40-50 km s^{-1} with respect to low-ionization lines, which share the systemic (absorption-line) velocity of ~ 4290 km s^{-1}. This can easily be explained in models which incorporate dust in the narrow-line clouds (FH). Not much dust is necessary to produce such a small difference, and very little intrinsic reddening of the emission lines is indicated by the observed Balmer decrement. After dereddening the emission lines by A_V = 0.70 mag (derived in § III*b*), Table 2 shows that $I(H\alpha)/I(H\beta)/I(H\gamma)/I(H\delta)$ = 3.65/1.00/0.48/0.27, close to the theoretical decrement (Brocklehurst 1971) of 2.84/1.00/0.47/0.26. Only $I(H\alpha)/I(H\beta)$ is discrepant, but the difference is primarily due to the broad component in the Hα profile.

IV. PICTOR A

a) Background

Pictor A is a 16th-magnitude elliptical galaxy at a distance of ~ 210 Mpc. Conspicuous optical emission lines (Schmidt 1965) and the object's association with a strong double-lobed radio source led to its classification as an N galaxy. Although the spectral index of the

extended radio structure is ~ 0.9, Pictor A also exhibits a compact unresolved core having a flat or even inverted spectrum. Its infrared colors are consistent with a nonstellar continuum of power-law shape (Glass 1981), and it is a source of hard X-rays (Marshall et al. 1979). A bright, almost unresolved nucleus is visible in photographs of short exposure, while deeper images show a smooth elliptical shape (e ~ 0.7) with no irregularities or filaments. The optical emission lines have both narrow and broad components (Danziger, Fosbury, and Penston 1977, hereafter DFP); in particular, the broad wings of Hα have FWZI greater than 20000 km s^{-1}, and the profile of [O I]λ6300 is much wider than those of [S II]λ6716,6731. This is very similar to NGC 7213, and inspired the detailed study discussed below.

b) Analysis of the Data

A new optical spectrum, convolved with a Gaussian having 5.3 Å FWHM to yield a resolution of ~ 7 Å, is presented in Figure 5. The object's redshift (cz = 10520 km s^{-1}) was obtained by averaging the observed wavelengths of [O I], [S II], Hα, Hβ, and Hγ. High-ionization lines ([O III]λ4959,5007, [Ne III]λ3869) exhibit small relative blueshifts (~ 60 km s^{-1}), as in Pks 1718-649 and many other active galactic nuclei (e.g., Grandi 1978; Wilson 1979). Widths and intensities of emission lines were carefully determined (Tables 2 and 3) with the techniques described in § III and by FH. DFP only measured peak intensities in the central cores of lines, resulting in a number of discrepancies with the ratios in Table 2.

As in type 1 Seyferts and quasars, the continuum is nearly featureless: Ca II K has an equivalent width of only ~ 1 Å, and that of

the G-band (λ4304) is $\lesssim$ 1.5 Å. The continuum is therefore predominantly of nonstellar origin. High-ionization lines such as He II λ4686, [Ne III], and [Fe VII] indicate that it continues blueward to energies of at least ~ 100 eV, photoionizing gas near the nucleus. Hα emission is very broad (FWZI $\gtrsim$ 20000 km s^{-1}), with logarithmic wings to first order ($\underline{I}(\Delta\lambda) \sim C_1 \log(\Delta\lambda) + C_2$, where C_1 and C_2 are constants). Comparison with the data of DFP shows that its intensity and profile vary with time. Broad emission is also visible in Hβ and He II λ4686, as emphasized in Figure 6.

A quantitative decomposition of the optical continuum (§ III) is illustrated in Figure 1b. The best fit is obtained when the data are dereddened by $\underline{A}_V$ = 0.17 mag, and a value of ~ 1.1 is derived for α. Unlike the case in Pks 1718-649, the nonstellar component dominates starlight by a wide margin: at λ4000, stars account for ~ 9% of the total flux, and even in the red their contribution is only ~ 20%. Objects with a less prominent nonstellar component than in Pks 1718-649, or a stronger one than in Pictor A, would be difficult to illustrate in a manner analogous to that used here, so Figure 1 nicely represents two rather extreme cases.

Simple extrapolation of the power-law continuum to UV energies predicts an Hα flux of 9.93×10^{-14} erg s^{-1} cm^{-2} if Hα is produced entirely by recombination of photoionized gas. This is nearly a factor of three smaller than the observed (dereddened) intensity. As in Pks 1718-649, a "UV bump" may account for the deficit, and its presence is likely in view of the great similarity between Pictor A and other Seyfert 1 galaxies. Furthermore, much of the Balmer emission may be due to collisional enhancement in the high-density clouds ($\underline{n} \sim 10^9$ cm^{-3})

which presumably exist in the broad-line region. A rather steep Balmer decrement, $\underline{I}(H\alpha)/\underline{I}(H\beta)/\underline{I}(H\gamma)/\underline{I}(H\delta) = 4.75/1.00/0.43/0.21$, supports this hypothesis (Kwan and Krolik 1981).

The continuum and rich emission-line spectrum of Pictor A demonstrate that gas is undoubtedly photoionized by nonstellar radiation. On the other hand, the great relative intensity of [O I]λ6300 puts Pictor A into the LINER class at least in some respects (Heckman 1980), and heating due to shocks is often thought to be the primary ionization mechanism in these objects. In fact, comparison with the supernova remnant N49 (Osterbrock and Dufour 1973), the Cygnus Loop (Miller 1974), and the models of Cox (1972) led DFP to conclude that gas in Pictor A is heated by shocks. Their hypothesis was supported by the anomalously intense [O III]λ4363, from which they derived a temperature too high (~ 30000 K) to be compatible with photoionization. How, then, can these results be consistent with the conclusions drawn from the new data?

Casual inspection of Figure 5 hints that the answer is exactly the same as for Pks 1718-649 and NGC 7213 (FH): the [O I]λ6300 line is broader than the entire [S II]λ6716+6731 blend, suggesting that clouds of different density and velocity may exist in the nuclear region. Figures 7a and 7b provide compelling evidence that this is indeed the case, since line widths are once again much better correlated with $\underline{n}_e(\underline{crit})$ than with χ.

Relevant parameters of the unweighted, linear least-squares fits are given in Table 4. A correlation between line width and χ is probably present, but this is to be expected even if $\underline{n}_e(\underline{crit})$ is the fundamental parameter since χ generally increases with increasing

$n_e(crit)$ for strong optical emission lines. Outstanding exceptions are [O I]λ6300 and [S II]λ4069, and it is precisely these lines (together with [O III]λ4363) that produce such a clear distinction between the two relations in Figure 7.

Under the assumption that each line is emitted by clouds whose density is equal to the appropriate value of $n_e(crit)$, Table 4 shows that FWHM $\propto n^{0.103\pm0.015}$ in Pictor A. A larger slope is obtained if the FW10, rather than FWHM, is measured: FW10 $\propto n^{0.161\pm0.022}$. These findings agree well with the model of optically thick clouds in gravitational infall proposed by Carroll and Kwan (1983; see also Kwan and Carroll 1982), which explicitly predicts that width should increase with density. In this model, a reservoir of low-density gas produces relatively strong, narrow cores in the emission lines and reduces the variation of FWHM relative to that of FWZI (or FW10). The low-density gas is not always significant, however, as evidenced by Pks 1718-649 and NGC 7213 (FH).

It is interesting that corresponding points in Figures 4b and 7b have approximately the same positions relative to the line of best fit. The points representing [O III], [O I], and [S II] near $\log[n_e(crit)] \sim 6$ are good examples, and others are visible as well. Measurement errors are unlikely to produce the effect. It may even be consistent with the model of Carroll and Kwan (1983), which does not predict a strictly linear relation between $\log(v)$ and $\log(n)$.

The comparable widths of [N II]λ6583 and lines characterized by low critical densities ($\sim 10^3$ cm^{-3}) suggest that [S II]λ6724, [O II]λ3727, and [N I]λ5200 are all produced mainly in the low-density reservoir ($n_e \sim 10^3$–10^4 cm^{-3}), which does not participate in the gravitational

infall (Carroll and Kwan 1983). [N II]λ6583 is probably not an additional member of this group, since it is produced mainly in clouds of considerably higher density. Linear fits to [N II] and the other high-density points (omitting those of low-density mentioned above) in the correlation between FWHM and n_e(crit) give somewhat steeper slopes than those in Table 4: Pictor A has a slope of 0.15 rather than 0.10, while in Pks 1718-649 it is 0.17 (instead of 0.11). As discussed by FH, a slope of 0.20-0.25 is expected if clouds move in Keplerian orbits while maintaining a nearly constant ionization parameter, U. Approximate constancy of U is an important result of the two-phase model of QSO emission-line regions developed by Krolik, McKee, and Tarter (1981), and a natural extension of this model to the NLR was possible in NGC 7213 (FH). The similar behavior of the emission lines in Pks 1718-649 and Pictor A provide additional evidence for the confinement of clouds by a hot intercloud medium, although in these galaxies U is not quite as constant.

The ratio I([O III]λ4959+5007)/([O III]λ4363), derived after careful subtraction of Hγ using the scaled profile of Hβ, is ~ 14. This is much smaller than the value obtained by DFP (who did not attempt to accurately deblend the line from Hγ) and indicates a temperature of at least 5.5×10^4 K if $n_e \sim 10^4$ cm^{-3}. If the [S II]λ6716,6731 lines are used to derive the density, as was done by DFP, then $n_e \sim 450$ cm^{-3} and the temperature implied by the [O III] ratio is still higher. At a density of $\sim 10^6$ cm^{-3}, on the other hand, the temperature is only 15000 K, as required by photoionization models.

Pictor A thus exhibits a great range of densities, just as NGC 7213 and Pks 1718-649. Instead of the distinct narrow-line (low density) and

broad-line (high density) regions often mentioned in connection with type 1 Seyferts, a more or less continuous range is present. Values $\gtrsim 10^7$ cm^{-3} are indicated by some forbidden lines, and the density must be still higher ($> 10^8$ cm^{-3}) in high-velocity clouds which produce the broad wings in permitted lines. Oddly enough, DFP saw "no evidence for the existence of a high-density component," even though their spectra clearly show wings in the [O I] profiles (compared with the nearby [S II] lines) and extremely broad Balmer emission.

V. MR 2251-178

a) Background

MR 2251-178 was the first QSO to be initially identified from X-ray observations (Ricker *et al.* 1978). At the time of discovery, it was only the second QSO known to emit X-rays. Its optical flux varies on time scales of a few months (Ricker *et al.* 1979), and a weak, unresolved radio source is present at ~ 5 GHz. Spectrophotometry by Canizares, McClintock, and Ricker (1978) revealed a strong emission-line spectrum dominated by broad permitted lines (FWZI ~ 20000 km s^{-1}). The derived redshift was 0.0638 ± 0.0015, making MR 2251-178 very nearby compared with most QSOs. It was originally called a QSO rather than a type 1 Seyfert galaxy because of its high luminosity and stellar appearance on plates from the Palomar Observatory Sky Survey.

Phillips (1980) showed that MR 2251-178 is associated with a cluster of ~ 50 galaxies, and that faint nebulosity surrounds the unresolved core. Detailed spectrophotometry by Bergeron *et al.* (1983, hereafter BBDT) demonstrated the additional presence of a giant envelope of photoionized gas around the QSO and its parent galaxy. Independent

measurements indicate that $\underline{I}$([O III]λ4959+5007)/$\underline{I}$(O III]λ4363) is between 7 and 9 in the nucleus (Canizares, McClintock, and Ricker 1978; BBDT), substantially lower than the normal ratio (~ 25–50) for photoionized gas in AGN. Furthermore, BBDT's spectrum shows two relatively distinct components in some of the forbidden lines, suggesting that clouds of different density may exist in the NLR.

The new spectrum, obtained through an 8″ x 8″ aperture under photometric conditions, is illustrated in Figure 8. Only [O III]λ5007 was noticeably affected by coincidence losses (~ 8%), although small inaccuracies may also exist in some of the other very strong emission lines. The instrumental resolution was ~ 5.4 Å, but the data in Figure 8 were smoothed with a Gaussian to yield a final value of ~ 7 Å. The spectrum was dereddened under the assumption of a normal reddening law and a Galactic $\underline{A}_V$ of 0.05 mag (Burstein and Heiles 1982). A redshift of 0.06397 ± 0.00005 was calculated from the emission lines and removed. No systematic differences in redshift between high- and low-ionization lines were evident to within ~ ± 15 km s^{-1}.

Hβ has a FWZI of at least 25000 km s^{-1}; it may be closer to 30000 km s^{-1} if the contribution of broad He II λ4686 is small. This indicates gas velocities of order 10% that of light, and implies $M \sim 10^{10}$ $M_\odot$ for the central object if the clouds are typically at radii of ~ 0.1 pc.

Starlight is almost completely absent. The only measureable absorption feature is Ca II K, whose equivalent width (~ 0.2 Å) demonstrates that stars contribute $\lesssim$ 2% of the flux near λ4000. Since a large aperture was used, the strength of the line is increased by the galactic nebulosity surrounding the QSO itself; the ratio of nonstellar

to stellar flux in the unresolved nucleus is $\gtrsim 100$. Complementing the featureless continuum is a prominent UV excess.

Properties of emission lines were measured in the usual manner (Tables 2 and 3). Agreement with the results of BBDT is generally satisfactory, except for the weakest features and badly blended lines. A distinct, broad component of He II λ4686 is probably present but cannot be deblended from Hβ. The Balmer decrement is steeper than reported by BBDT, and the Balmer lines themselves are weaker relative to [O III]λ5007 and to the continuum. The equivalent width of Hβ is ~ 130 Å, compared with the previously published (BBDT) value of ~240 Å. Thus supports previous claims of optical variability in MR 2251-178.

As suspected, the forbidden lines display a range of profiles (Figure 9). The [O II]λ3727 blend is narrow and does not exhibit appreciable wings. [O III]λ5007 (averaged with [O III]λ4959 in Figure 9), on the other hand, has significant extensions to the blue and red. The strength of the broad component relative to the narrow core is still larger in the [Ne III] and [Ne V] lines. Unlike the case in some high-ionization Seyfert galaxies recently studied by De Robertis and Osterbrock (1984), [O III]λ4363 is broader than [O III]λ5007 and once again demonstrates that $\underline{n_e}$(crit) (rather than χ) is the fundamental parameter.

Note that the deblending of [O III]λ4363 from Hγ (Figures 9e and 9f) is uncertain. Hγ was assumed to have a symmetrical core, since a scaled version of Hβ could not be used due to marked differences in unblended portions of the two profiles; the Balmer decrement clearly varies with velocity. The [O III] intensity ratio R is ~ 10, somewhat higher than the approximate measurements by BBDT and by Canizares,

McClintock, and Ricker (1978).

Figure 10 displays the intensity ratio R as a function of velocity in the line profiles. Defining the peaks of the emission lines as zero, it is clear that the strength of [O III]λ4363 relative to [O III]λ5007 increases dramatically in the extended wings. Under the simplifying assumption of constant temperature (T_e = 15000 K) in the photoionized gas, this means that the density of clouds increases monotonically with their velocity. Higher densities ($\gtrsim 5 \times 10^6$ cm^{-3}) probably occur at even greater velocities than could be shown in Figure 10 (due to the limited S/N ratios); similarly, the lowest densities ($\sim 10^6$ cm^{-3}) represent only an upper limit because of contamination from dense, high-velocity clouds moving transversely to the line of sight. The increase of cloud velocity with density is confirmed by the strong correlation between width and n_e(crit) for lines produced by different species (Table 4). Thus, MR 2251-178 exhibits the same behavior as Pks 1718-649 and Pictor A.

VI. DISCUSSION

The emission-line spectra of Seyfert galaxies were explained reasonably well by early photoionization models involving prominent nonstellar continua, especially following the incorporation of accurate rates for charge-transfer reactions. A poor match was found, however, with the observed characteristics of low-ionization galaxies (LINERs). Instead, their spectral resemblance to supernova remnants suggested that shock heating may be the dominant excitation mechanism.

Ferland and Netzer (1983) compared predictions of shock models with the average spectrum of LINERs and found reasonably good agreement,

except for several important inconsistencies in the prototype, NGC 1052. Representative shock models in Table 5 show that a good fit is also difficult to achieve in Pks 1718-649 and Pictor A. Shocks with higher velocities must be postulated to explain the great strength of [O III]λ4363, for example, but they would produce too much He II λ4686 and He I λ5876. Moreover, the presence of strong [Ne V] and [Fe VII] (Table 2) is incompatible with shocks.

In light of these and other developments, emphasis has recently shifted back to photoionization models. Extensive calculations (Ferland and Netzer 1983; Halpern and Steiner 1983) suggest a continuity between classical AGNs and objects exhibiting milder nuclear activity. It might even be possible to reproduce the entire range of observed characteristics mainly by varying the photon flux. Typical results listed in Table 5, however, demonstrate that these models are also inadequate. Temperatures derived from the observed intensity ratio of the [O III] lines are incompatible with photoionization, and the models predict too much He II λ4686. Relative photon fluxes must be greater in order to produce significant [Ne V]λ3426 (Halpern 1982), but then the calculated intensities of [O I]λ6300 and several other lines are too small.

The continua of MR 2251-178 and Pictor A are completely dominated by nonstellar radiation which extends far beyond the Lyman limit (as evidenced by the strong flux at X-ray energies). There can be no doubt that the emission lines are produced by photoionization, and yet they exhibit the exact problems discussed above! The same can be said for NGC 7213 (FH) and probably even for Pks 1718-649, although the relative strength of their ionizing continuum is not as great as in MR 2251-178

and Pictor A. Clearly, then, an understanding of how all this is possible may resolve the same difficulties in the interpretation of LINERs.

The observations discussed here show that a partial solution is provided by a great range of densities among clouds of gas in the NLR. Values as low as 500 cm^{-3} and as high as $\sim 10^7$ cm^{-3} must be present. This is much larger than the range found in most type 2 Seyferts (Koski 1978), but it may be common in LINERs (Filippenko and Sargent 1984) and broad-line radio galaxies (Osterbrock, Koski, and Phillips 1976). Dense gas contributes strongly to auroral and transauroral lines such as [O III]λ4363 and [S II]λ4069,4076, mimicking the effects of high temperatures. The actual temperature can easily be compatible with photoionization models, so shocks need not be invoked.

The observed correlation between line width and critical density in all three galaxies suggests that clouds move through the NLR in Keplerian orbits. Detailed models (Carroll and Kwan 1983) based on this idea show that most of the emission is produced by clouds falling toward the nucleus, and the predictions are in excellent quantitative agreement with the new results. High densities in the individual clouds make them optically thick to the Lyman continuum, so that each of them includes every ionization stage up to a certain level. Strong [O I] is produced in a vast region of partially ionized (~ 10%) hydrogen (Halpern 1982).

A model developed by Péquignot (1984) concentrates on emission-line intensity ratios in greater detail. Péquignot (1984) concludes that the spectral characteristics of NGC 1052 require a density stratification of the type reported here; single-density models fall far short of providing adequate agreement (as in Table 5). Moreover, he suggests

that the observed He II λ4686 is too weak compared with the predictions of simple photoionization models incorporating a power-law continuum because the ionizing radiation is produced primarily by a hot ($\underline{T} \sim 10^{4-5}$K) accretion disk rather than by nonthermal processes. The ionizing flux drops rapidly at energies higher than ~ 4 ryd, in contrast with a power-law spectrum. Sufficient He II λ4686 emission is present even in galaxies such as NGC 7213 (FH) and Pks 1718-649 (Figure 2a), in which none at all is visible prior to the removal of a template containing only absorption lines.

Some difficulties still remain, but these do not seem fundamental or insurmountable. The predicted strength of [N I]λ5200, for example, is too large (Table 5). This may be partially resolved by adopting a higher minimum density in the clouds, since $\underline{n_e}$(crit) is very small. Furthermore, the charge-exchange reaction $N^+ + H \longrightarrow N^0 + H^+$ is slow, so the abundance of neutral nitrogen can be greatly affected by other physical processes (such as ionization from an excited level of N^+) which are not properly treated in the models.

VII. CONCLUSIONS

These data demonstrate that a variety of AGN have narrow-line clouds which cover a great range in density and velocity, and the actual values of the physical parameters are in all cases similar. Virtually the same conclusions were drawn in the analysis of a classical LINER (Pks 1718-649), a type 1 Seyfert galaxy with a strong stellar continuum and strong low-ionization lines (NGC 7213), a classical Seyfert 1 galaxy with some LINER characteristics (Pictor A), and a nearby QSO (MR 2251-178). The respective flux of Hβ from the nuclei of these

objects is very roughly 3, 5, 27, and 1560 in units of 10^{40} ergs s^{-1}, and the intensity of a blue nonstellar continuum follows a comparable progression. Since Balmer emission and nonstellar radiation are indicators of "activity" in galactic nuclei, the results reported here suggest that physical conditions and processes are similar in all these objects.

In particular, they imply that photoionization, rather than shock heating, is the dominant excitation mechanism even in LINERs. To test this, a very sensitive search for weak nonstellar continua, [Ne V]λ3426, broad Hα emission, and correlations between line width and critical density must be made in large numbers of LINERs. Some initial surveys have already been conducted (e.g., Stauffer 1982; Keel 1983), and much more detailed ones are in progress (Filippenko and Sargent 1984). Preliminary results indicate the presence of these features in many objects, as well as substantial continuity in their prominence, and therefore provide strong support for the photoionization hypothesis.

I am very grateful to Jules Halpern for many illuminating discussions concerning physical conditions in AGNs, and for drawing my attention to MR 2251-178. Observations were made with Steve Shectman's Intensified Reticon at Las Campanas Observatory, where the assistance of Angel Guerra, Fernando Peralta, and Hernan Solis was greatly appreciated. This research represents part of my doctoral dissertation at Caltech. It is supported by a graduate fellowship from the Fannie and John Hertz Foundation, as well as by NSF grant AST-8216544 to my advisor, Wal Sargent.

TABLE 1

Journal of Observations

Object	Date (UT)	Time (s)	g/mm[a]	Ap (")	R (Å)[b]	Δλ (Å)	Standard	Air mass	PA°	See[c]
Pks 1718-649	1983 Aug 09	3600	600	2 x 4	4-5	3490-7170	G158-100	1.24/1.25	180	1
	1983 Aug 14	3000	1200	2 x 4	2-3	3210-5100	G158-100	1.24/1.24	180	1
Pictor A	1983 Aug 11	4200[d]	600	2 x 4	4-5	3890-7580	G24-9	1.49/1.22	90	1.5
MR 2251-178	1983 Aug 14	1200	1200	8 x 8	5-6	3210-5100	G158-100	1.09/1.06	90	1
	1983 Aug 14	1200	1200	8 x 8	5-6	4730-6620	G158-100	1.06/1.04	90	1
IC 4889	1983 Aug 13	2800[d]	600	2 x 4	4-5	3900-7580	G24-9	1.18/1.13	136	1.5
	1983 Aug 14	2400	1200	2 x 4	2-3	3210-5100	G158-100	1.12/1.11	165	1

[a]Number of grooves/mm for each of the two gratings, blazed at ~ λ5000.

[b]Resolution (R) denotes FWHM of unblended emission lines.

[c]Very approximate FWHM of seeing disk, in arc seconds.

[d]Cirrus clouds were present during the integration.

TABLE 2

Relative Intensities of Emission Lines[a]

Line	Pks 1718-649		Pictor A		MR 2251-178	
	F/F(N2)	I/I(N2)[b]	F/F(N2)	I/I(N2)[b]	F/F(N2)	I/I(N2)[b]
[Ne V]λ3346	0.042:	0.059:	—	—	0.032:	0.034:
[Ne V]λ3426	0.118	0.164	—	—	0.123	0.126
[O II]λ3727	0.913	1.181	—	—	0.172	0.175
HI λ3798	...	...	—	—	0.004:	0.004:
HI λ3835	...	...	0.029:	0.031:	0.011	0.011
[Ne III]λ3869	0.192	0.240	0.213	0.225	0.158	0.161
He I + H8 λ3889	0.070	0.087	0.080	0.084	0.050	0.051
[Ne III] + Hε λ3970	0.090	0.111	0.138	0.145	0.082	0.083
[S II]λ4071	0.211	0.254	0.096	0.100	0.010:	0.010:
Hδ λ4102	0.122	0.145	0.172	0.180	0.111	0.112
[Fe II]λ4250 ?[c]	...	...	...	...	0.004:	0.004:
[Fe II]λ4281 ?[c]	...	...	...	...	0.008:	0.008:
Hγ λ4340	0.224	0.254	0.355	0.366	0.328	0.331
[O III]λ4363	0.091	0.103	0.092	0.095	0.132	0.133
He I λ4471	...	...	...	...	0.004:	0.004:
He II λ4686	0.048	0.051	0.136	0.138	0.022[d]	0.022[d]
Hβ λ4861	0.517	0.529	0.847	0.852	1.396[e]	1.398[e]
[O III]λ4959	0.306	0.309	0.350	0.351	0.338	0.338
[O III]λ5007	1.000	1.000	1.000	1.000	1.000[f]	1.000[f]
[Fe VII]λ5159	...	...	0.029	0.029	0.016:	0.016:
[N I]λ5200	0.010:	0.010:	0.019	0.019	0.003:	0.003:
Fe II ~λ5270 ?[g]	...	...	0.045:	0.044:	...	...
[O I]λ5577	...	...	0.022:	0.021:	...	...

(Table 2, continued)

[Fe VII]λ5721	...	...	0.021:	0.020:	—	—
He I λ5876	0.041:	0.036:	0.068	0.066	—	—
[O I]λ6300*	1.101	0.902	0.482	0.459	—	—
[O I]λ6364*	0.376	0.305	0.145	0.138	—	—
[N II]λ6548*	0.185	0.147	0.033	0.031	—	—
Hα λ6563*	2.437	1.930	4.283	4.047	—	—
[N II]λ6583*	0.558	0.441	0.100	0.094	—	—
[S II]λ6716*	0.443	0.345	0.119	0.112	—	—
[S II]λ6731*	0.385	0.299	0.116	0.109	—	—
A_V (mag.)[h]	0.70		0.17		0.05	
F(N2) (erg s^{-1} cm^{-2})[i]	5.06×10^{-14}		6.09×10^{-14}		6.35×10^{-13}	
I(N2) (erg s^{-1} cm^{-2})[j]	1.07×10^{-13}		7.30×10^{-14}		6.70×10^{-13}	

[a]Dashes (—) indicate line not available in data. Dots (...) signify extremely weak or nonexistent line. Colons denote very uncertain measurements (± 100%). Asterisk means flux calibration somewhat affected by second-order contamination.

[b]$A_V = 3.2E_{B-V}$ used to deredden fluxes. A_V given at bottom of table.

[c]Lines identified by Bergeron et al. (1983).

[d]Includes only the well-defined narrow component.

[e]Contains slight contamination from broad component of He II λ4686.

[f]Data affected by coincidence losses. Intensity replaced by 2.96 times F([O III]λ4959).

[g]Possibly Fe II emission, but it is absent elsewhere in the spectrum.

[h]Derived from continuum decomposition in Pks 1718-649 and Pictor A; Galactic reddening in MR 2251-178.

[i]N2 = [O III]λ5007. Flux is absolute only in MR 2251-178. Small (2" x 4") aperture used for other two objects. Reddening not removed.

[j]Same as (i), but with reddening (given by A_V) removed.

TABLE 3

Widths of Forbidden Lines (km s^{-1})[a]

Line[b]	n_e(crit) (cm^{-3})	χ(eV)[c]	Pks 1718-649		Pictor A		MR 2251-178	
			FWHM	FW10	FWHM	FW10	FWHM	FWZI
[S II]λ6716	1.2×10^3	23.3	500	1000	300	650	...	...
[N I]λ5199[d]	1.3×10^3	14.5	...	...	250	400	...	...
[O II]λ3727[d]	3.0×10^3	35.1	450	820	...	...	200	700
[S II]λ6731	3.1×10^3	23.3	500	990	340	720	...	...
[N II]λ6583	9.2×10^4	29.6	500	1000	320	690	...	...
[O III]λ4959	7.9×10^5	54.9	550	1700	470	2020	390	2980
[O III]λ5007	7.9×10^5	54.9	570	1950	480	1820	410	3000
[O I]λ6300	1.4×10^6	13.6	1200	2450	600	2210	...	...
[O I]λ6364	1.4×10^6	13.6	1250	2200	580	1870	...	...
[S II]λ4069	1.7×10^6	23.3	1390	2800	690	2200	...	...
[Ne III]λ3869	1.2×10^7	63.5	950	2450	650	2170	510	3600
[Ne III]λ3967	1.2×10^7	63.5	900	1850	540	1850	570	3300
[Ne V]λ3346	1.9×10^7	126.2	1750	...	...	...	450	2700
[Ne V]λ3426	1.9×10^7	126.2	2050	3100	...	...	640	4000
[O III]λ4363	3.0×10^7	54.9	1300	2900	1000	2600	800	3850

[a] FWHM = full width at half-maximum; FW10 = full width at 10%-intensity; FWZI = full width at zero-intensity. Resolution of spectrograph removed.

[b] Listed in order of increasing critical density.

[c] Ionization potential of species producing the emission line.

[d] Widths refer to each of the two blended components.

TABLE 4

Unweighted Line-width Correlations: $y = A + Bx$

Object	Relation[a]	N[b]	A	B	σ_A	σ_B	r[c]	Prob[d]
Pks 1718-649	FWHM vs. n_e(crit)	13[e]	2.27	0.113	0.16	0.027	0.78	0.998
	FWHM vs. χ	13[e]	2.71	0.131	0.36	0.227	0.17	0.424
	FW10 vs. n_e(crit)	13	2.55	0.122	0.10	0.017	0.91	~1.000
	FW10 vs. χ	13	2.94	0.200	0.32	0.205	0.28	0.651
Pictor A	FWHM vs. n_e(crit)	12	2.11	0.103	0.09	0.015	0.91	~1.000
	FWHM vs. χ	12	2.32	0.242	0.29	0.192	0.37	0.764
	FW10 vs. n_e(crit)	12	2.23	0.161	0.13	0.022	0.92	~1.000
	FW10 vs. χ	12	2.47	0.448	0.44	0.294	0.43	0.841
MR 2251-178	FWHM vs. n_e(crit)	8	1.86	0.125	0.13	0.019	0.94	0.999
	FWHM vs. χ	8	1.77	0.493	0.61	0.331	0.52	0.813
	FWZI vs. n_e(crit)	8	2.36	0.168	0.19	0.029	0.92	0.999
	FWZI vs. χ	8	2.10	0.733	0.80	0.436	0.57	0.856

[a]The common logarithm of each variable is used.

[b]Number of points (see Table 3). All points considered to be independent.

[c]Correlation coefficient.

[d]Probability that the two variables are correlated.

[e][Ne V]λ3346 excluded for consistency with FW10.

TABLE 5

Comparison of Observations with Simple Models

Line	Pks 1718-649	Pictor A	Photoionization			Shock		
			FN[a]	H1[b]	H2[c]	SM(G)[d]	SM(H)[e]	R(D)[f]
[Ne V]λ3426[g]	0.31	...	...	0.01	...	...	...	...
[O II]λ3727[h]	2.23	...	6.4	4.47	5.58	8.55	5.23	8.06
[Ne III]λ3869	0.45	0.26	...	1.01	0.88	...	...	0.38
[O III]λ4363	0.19	0.11	0.03	0.15	0.03	0.25	0.18	0.26
He II λ4686	0.10	0.16	0.17	0.27	0.18	0.12	0.03	<0.01
Hβ λ4861	1.00	1.00	1.00	1.00	1.00	1.00	1.00	1.00
[O III]λ5007	1.89	1.17	2.18	7.95	1.99	5.51	4.10	4.32
[N I]λ5200[h]	0.02	0.02	0.26	1.00	2.36	1.70	0.06	0.03
He I λ5876	0.07	0.08	0.18	0.15	0.17	0.19	0.15	0.11
[O I]λ6300	1.71	0.54	0.96	1.39	2.96	1.82	1.60	0.08
Hα λ6563	3.65	4.75	3.1	3.10	3.08	2.98	3.06	3.25
[N II]λ6583	0.83	0.11	1.6	3.06	4.25	2.96	2.68	1.40
[S II]λ6724[h]	1.22	0.26	2.5	...	...	6.01	4.62	1.05

[a]Ferland and Netzer 1983, Table 3, $\log_{10}U = -3.5$, $\alpha = 1.5$, abundances 0.3 solar.

[b]Halpern 1982, Log U = −2, covering fraction = 0.90, $\alpha = 1.1$, $\log_{10}n = 3.5$ (cm^{-3}).

[c]Halpern 1982, Log U = −2, covering fraction = 0.97, $\alpha = 1.1$, $\log_{10}n = 3.5$ (cm^{-3}).

[d]Shull and McKee 1979, model G, v(shock) = 130 km s^{-1}, n(preshock) = 10 cm^{-3}.

[e]Shull and McKee 1979, model H, v(shock) = 100 km s^{-1}, n(preshock) = 100 cm^{-3}.

[f]Raymond 1979, model D, v(shock) = 81.5 km s^{-1}.

[g]Intensity is ~ 0 in shock models.

[h]Both lines of doublet are included.

REFERENCES

Baldwin, J. A. 1975, Ap. J., 201, 26.

Bergeron, J., Boksenberg, A., Dennefeld, M., and Tarenghi, M. 1983, M.N.R.A.S., 202, 125 (BBDT).

Brocklehurst, M. 1971, M.N.R.A.S., 153. 471.

Burstein, D., and Heiles, C. 1982, A. J., 87, 1165.

Butler, S. E., Heil, T. G., and Dalgarno, A. 1980, Ap. J., 241, 442.

Canizares, C. R., McClintock, J. E., and Ricker, G. R. 1978, Ap. J. (Letters), 226, L1.

Carroll, T. J., and Kwan, J. 1983, Ap. J., 274, 113.

Cox, D. P. 1972, Ap. J., 178, 143.

Danziger, I. J., Fosbury, R. A. E., and Penston, M. V. 1977, M.N.R.A.S., 179, 41P (DFP).

Davidson, K., and Netzer, H. 1979, Rev. Mod. Phys., 51, 715.

De Robertis, M. M., and Osterbrock, D. E., 1984, preprint.

de Vaucouleurs, G., and de Vaucouleurs, A. 1964, Reference Catalogue of Bright Galaxies, Univ. of Texas Press, Austin.

Elvis, M., Soltan, A., and Keel, W. C. 1984, Ap. J., in press.

Ferland, G. J., and Netzer, H. 1983, Ap. J., 264, 105.

Filippenko, A. V. 1982, Pub. A.S.P., 94, 715.

Filippenko, A. V., and Greenstein, J. L. 1984, Pub. A.S.P., in press (July).

Filippenko, A. V., and Halpern, J. P. 1984, Ap. J., in press (Oct. 15). (FH).

Filippenko, A. V., and Sargent, W. L. W. 1984, Ap. J. Suppl.,

submitted.

Fosbury, R. A. E., Mebold, V., Goss, W. M., and Dopita, M. A. 1978, M.N.R.A.S., 183, 549.

Fosbury, R. A. E., Mebold, V., Goss, W. M., and van Woerden, H. 1977, M.N.R.A.S., 179, 89 (FMGW).

Glass, I. 1981, M.N.R.A.S., 197, 1067.

Grandi, S. A. 1978, Ap. J., 221, 501.

Gunn, J. E. 1979, in Active Galactic Nuclei, ed. C. Hazard and S. Mitton (Cambridge: Cambridge Univ. Press), p. 213.

Halpern, J. P. 1982, Ph.D. thesis, Harvard University.

Halpern, J. P., and Filippenko, A. V. 1984, Ap. J., in press (Oct. 15).

Halpern, J. P., and Steiner, J. E. 1983, Ap. J. (Letters), 269, L37.

Heckman, T. M. 1980, Astr. Ap., 87, 152.

Keel, W. C. 1983, Ap. J., 269, 466.

Keel, W. C., and Miller, J. S. 1983, Ap. J. (Letters), 266, L89.

Koski, A. T. 1978, Ap. J., 223, 56.

Koski, A. T., and Osterbrock, D. E. 1976, Ap. J. (Letters), 203, L49.

Krolik, J. H., McKee, C. F., and Tarter, C. B. 1981, Ap. J., 249, 422.

Kwan, J., and Carroll, T. J. 1982, Ap. J., 261, 25.

Kwan, J., and Krolik, J. H. 1981, Ap. J., 250, 478.

Malkan, M. A. 1983, Ap. J., 268, 582.

Malkan, M. A., and Filippenko, A. V. 1983, Ap. J. 275, 477.

Malkan, M. A., and Sargent, W. L. W. 1982, Ap. J., 254, 22.

Marshall, F. E., Boldt, E. A., Holt, S. S., Mushotzky, R. F., Pravdo, S. H., Rothschild, R. E., and Serlemitsos, P. J. 1979, Ap. J. Suppl., 40, 657.

Miller, J. S. 1974, Ap. J., 189, 239.

Oke, J. B., Shields, G. A., and Korycansky, D. G. 1984, Ap. J., 277, 64.

Osterbrock, D. E., and Dufour, R. J. 1973, Ap. J., 185, 441.

Osterbrock, D. E., Koski, A. T., and Phillips, M. M. 1976, Ap. J., 206, 898.

Pelat, D., Alloin, D., and Fosbury, R. A. E. 1981, M.N.R.A.S., 195, 787.

Péquignot, D. 1984, Astr. Ap., 131, 159.

Piccinotti, G., Mushotzky, R. F., Boldt, E. A., Holt, S. S., Marshall, F. E., Serlemitsos, P. J., and Shafer, R. A. 1982, Ap. J., 253, 485.

Phillips, M. M. 1980, Ap. J. (Letters), 236, L45.

Raymond, J. C. 1979, Ap. J. Suppl., 39, 1.

Ricker, G. R. et al., 1979, in X-Ray Astronomy, ed. W. A. Baity and L. E. Peterson (Oxford: Pergammon Press), p. 281.

Ricker, G. R., Clarke, G. W., Doxsey, R. E., Dower, R. G., Jernigan, J. G., Delvaille, J. P., MacAlpine, G. M., and Hjellming, R. M. 1978, Nature, 271, 35.

Rose, J. A., and Tripicco, M. J. 1984, preprint.

Savage, A. 1976, M.N.R.A.S., 174, 259.

Schmidt, M., 1965, Ap. J., 141, 1.

Shectman, S. A. 1981, in Annual Report of the Director, the Mount Wilson and Las Campanas Observatories (Washington: Carnegie Institution of Washington), p. 586.

Shectman, S. A., and Hiltner, W. A. 1976, Pub. A.S.P., 88, 960.

Shuder, J. M., 1981, Ap. J., 244, 12.

Shull, J. M., and McKee, C. F. 1979, Ap. J., 227, 131.

Stauffer, J. R. 1982, Ap. J., 262, 66.

Wilson, A. S. 1979, Proc. Roy. Soc. London, A., 366, 461.

Whitford, A. E. 1958, A. J., 63, 201.

Yee, H. K. C., and Oke, J. B. 1978, Ap. J., 226, 753.

FIGURE CAPTIONS

Figure 1: The smoothed continua of (a) Pks 1718-649 and (b) Pictor A are decomposed into an old stellar population and a nonstellar power law of index α. The absolute flux calibration is uncertain because data were obtained through small entrance apertures. Least-squares fits were used to derive the reddening of the continuum, the contribution of stars at λ5460, and the approximate value of α. At optical wavelengths Pks 1718-649 consists mostly of starlight, whereas Pictor A is dominated by nonstellar radiation.

Figure 2: Spectra of (a) Pks 1718-649, (b) the template galaxy IC 4889, and (c) the emission-line component of Pks 1718-649 are shown on the same ordinate scale but with different zero-point offsets. The nonstellar continuum (Fig. 1a) was removed in (a), and the spectrum dereddened by $A_V = 3.2E_{B-V} = 0.70$ mag. Small adjustments were made to the metallicity and overall shape of IC 4889 to make them match those of Pks 1718-649. In the net spectrum (c), note the faint emission (such as He II λ4686) previously hidden among absorption lines.

Figure 3: Spectra of Pks 1718-649 and Pictor A demonstrate the presence of broad Hα emission and the markedly different profiles of [O I] and [S II]. Stellar and atmospheric absorption was not removed. Balmer emission lines have prominent, roughly logarithmic wings in Pictor A, whereas the broad Hα exhibited by Pks 1718-649 is very weak.

Figure 4: (a) Log_{10}FW10 is plotted against $\log_{10}\chi$ for 13 forbidden lines in Pks 1718-649, where in each case χ is the ionization potential of the emitting species. The scatter is large: there is a 35% chance

that the parent population is uncorrelated. If χ is replaced with n_e(crit) as in (b), the correlation coefficient increases from 0.28 to 0.91 and the probability of an uncorrelated parent population drops to virtually zero. An error bar of $\pm$ 25% indicates probable uncertainties in theoretical calculations of n_e(crit).

Figure 5: A dereddened (A_V = 0.17 mag) spectrum of the central 2" x 4" of Pictor A is shown. The systemic velocity has been removed, as in all other spectra illustrated here. A Gaussian was used to smooth the data to a resolution of ~ 7 Å. Relative fluxes are accurate to ~ 10–15%, except redward of ~ λ6200. The absolute calibration is uncertain due to thin clouds. Note the strong emission lines from neutral as well as highly-ionized species. Stellar absorption lines are weak.

Figure 6: A portion of the spectrum of Pictor A illustrates the wide range of ionization, including lines of [N I] and [Fe VII]. The relative intensity of the broad wings in He II λ4686 and Hβ is much greater than that of the narrow cores, indicating that the ionization parameter is largest in the broad-line region.

Figure 7: (a) A comparison of the FWHM of forbidden lines in Pictor A and the corresponding values of χ reveals the presence of a correlation (probability = 0.76). Different emission lines from the same species (e.g., [S II], [O III]), however, have very disparate widths, suggesting that χ is not the fundamental parameter. As in Pks 1718-649, the correlation is greatly improved (b) if the appropriate critical density, rather than χ, is used for each emission line.

Figure 8: The spectrum of MR 2251-178, obtained through an 8" x 8"

aperture under photometric conditions, is shown. Magnitude $AB = -2.51\log(f_\nu) - 48.6$, where f_ν is in erg s^{-1} cm^{-2} Hz^{-1}. A Galactic A_V of 0.05 mag was used to deredden the data, which were Gaussian-smoothed to a resolution of ~ 7 Å. The Balmer lines are very broad, and a prominent UV excess is visible.

Figure 9: Profiles of five different emission lines, given in order of increasing n_e(crit), illustrate the presence of a range of densities in the NLR of MR 2251-178. The width and relative prominence of the broad base rises with n_e(crit). Marked differences are visible in lines arising from the same species ([O III]), even considering uncertainties in the deblending of [O III]λ4363 from Hγ (Figs. 9e, 9f). This is similar to the observed behavior in Pictor A and Pks 1718-649.

Figure 10: The ratio I([O III]λ4959+5007)/I([O III]λ4363) is plotted against velocity (ie., position in the line profile) for MR 2251-178. The zero-point corresponds to the peak of each line. Using T_e = 15000 K, the derived value of n_e is also given. The ordinate scale at left refers to the [O III] flux ratio, that at right to the density. Low-velocity clouds are clearly the least dense, especially if contamination of the emission-line cores by high-density clouds moving transversely to the line of sight is taken into account.

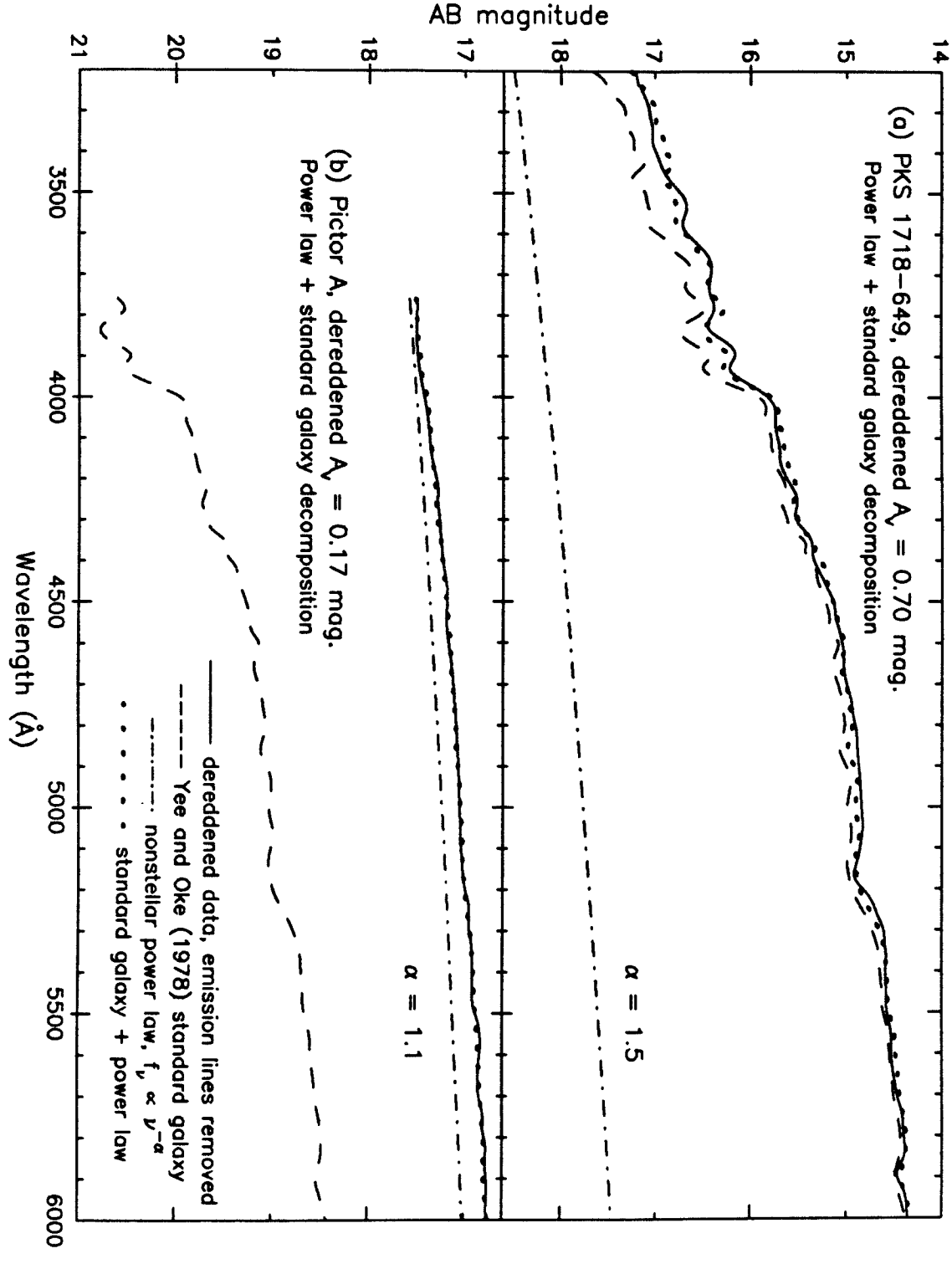
(a) PKS 1718−649, dereddened A_V = 0.70 mag.
Power law + standard galaxy decomposition
α = 1.5
(b) Pictor A, dereddened A_V = 0.17 mag.
Power law + standard galaxy decomposition
α = 1.1
AB magnitude
Wavelength (Å)
dereddened data, emission lines removed
Yee and Oke (1978) standard galaxy
nonstellar power law, $f_\nu \propto \nu^{-\alpha}$
standard galaxy + power law

Figure 1

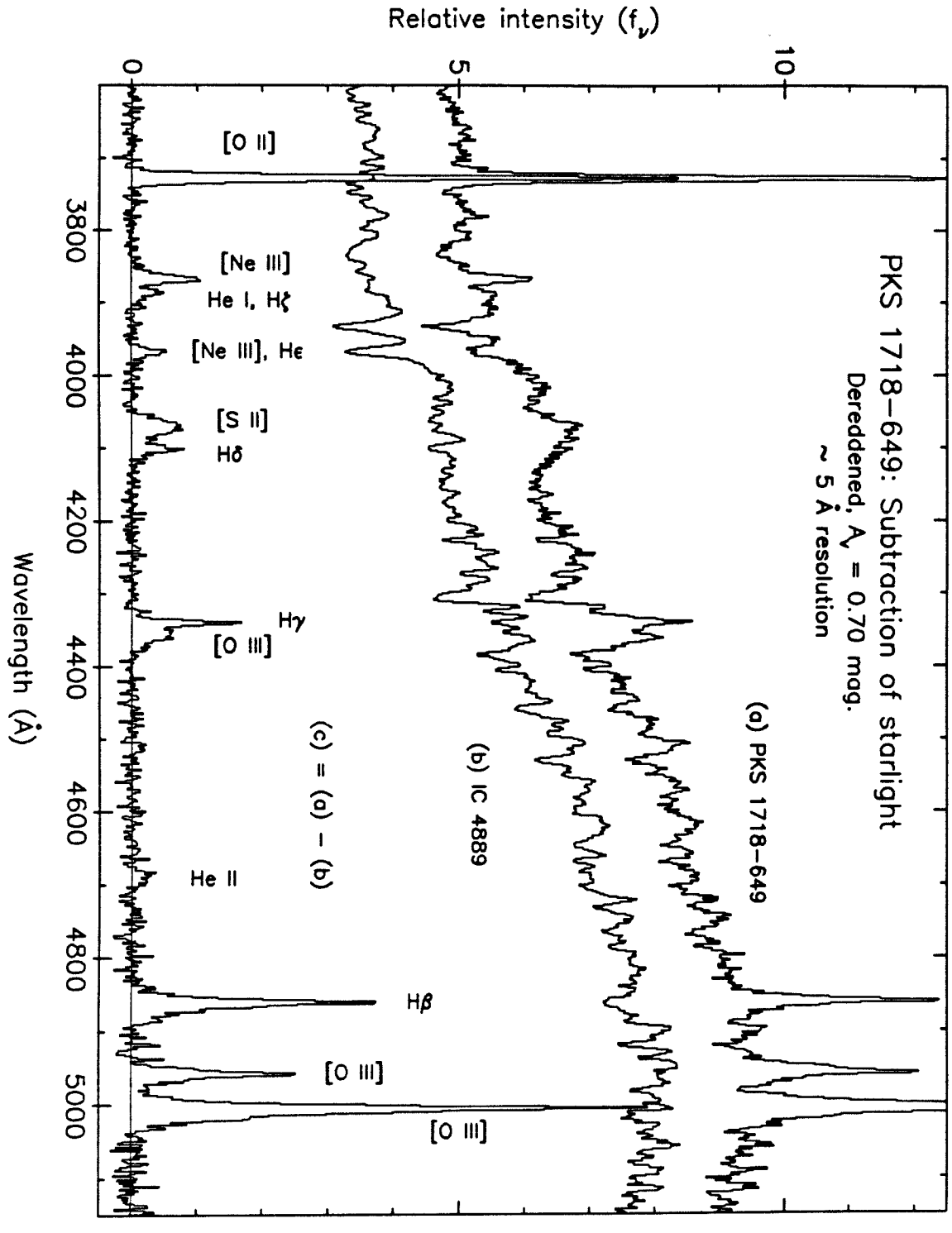
Relative intensity (f_ν)
0
5
10
PKS 1718−649: Subtraction of starlight
Dereddened, A_V = 0.70 mag.
~ 5 Å resolution
(a) PKS 1718−649
(b) IC 4889
(c) = (a) − (b)
[O II]
[Ne III]
He I, Hζ
[Ne III], Hε
[S II]
Hδ
Hγ
[O III]
He II
Hβ
[O III]
[O III]
3800
4000
4200
4400
4600
4800
5000
Wavelength (Å)

Figure 2

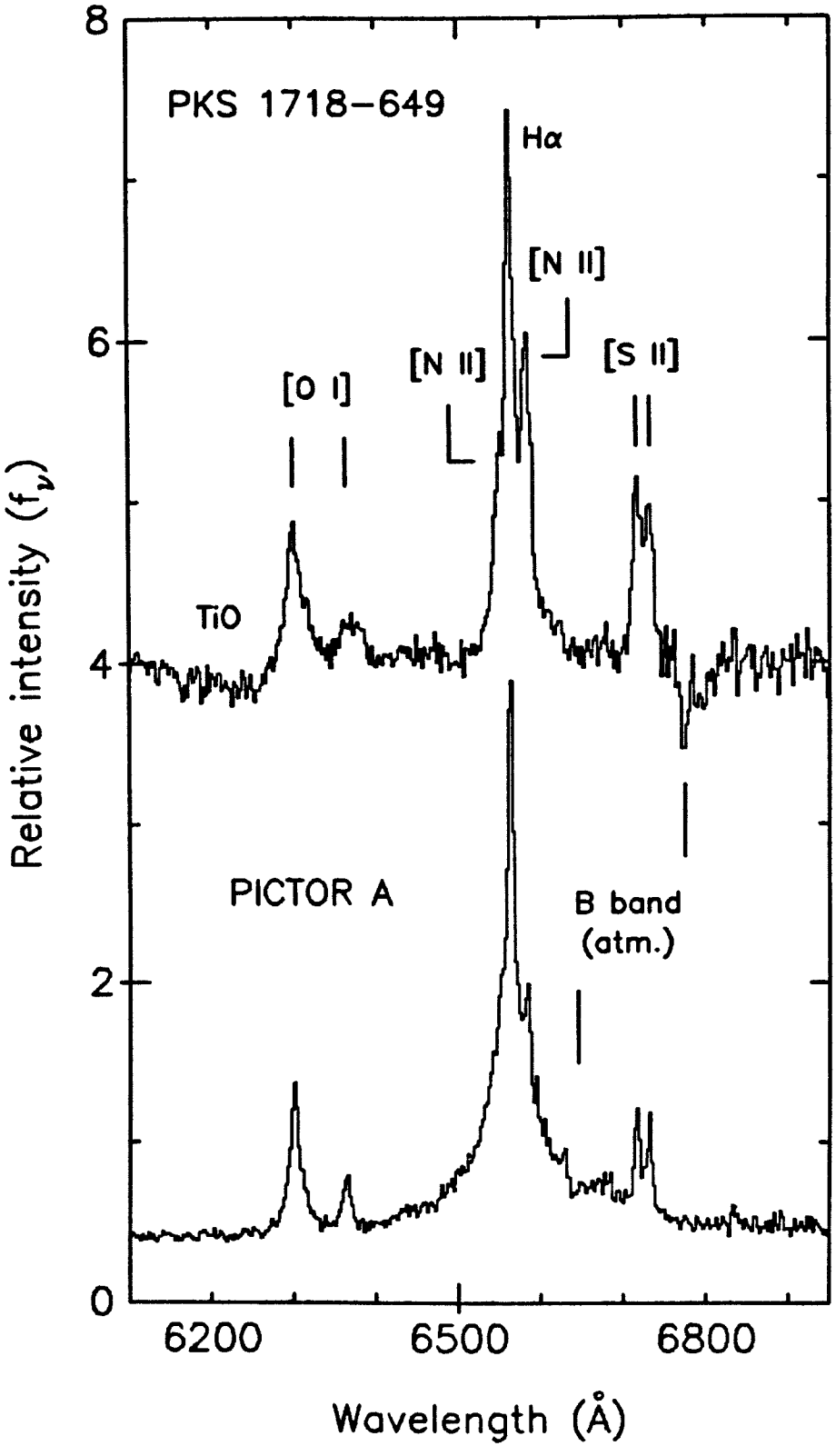
PKS 1718−649
Hα
[N II]
[S II]
[N II]
[O I]
TiO
PICTOR A
B band
(atm.)
Relative intensity (f_ν)
Wavelength (Å)
0
2
4
6
8
6200
6500
6800

Figure 3

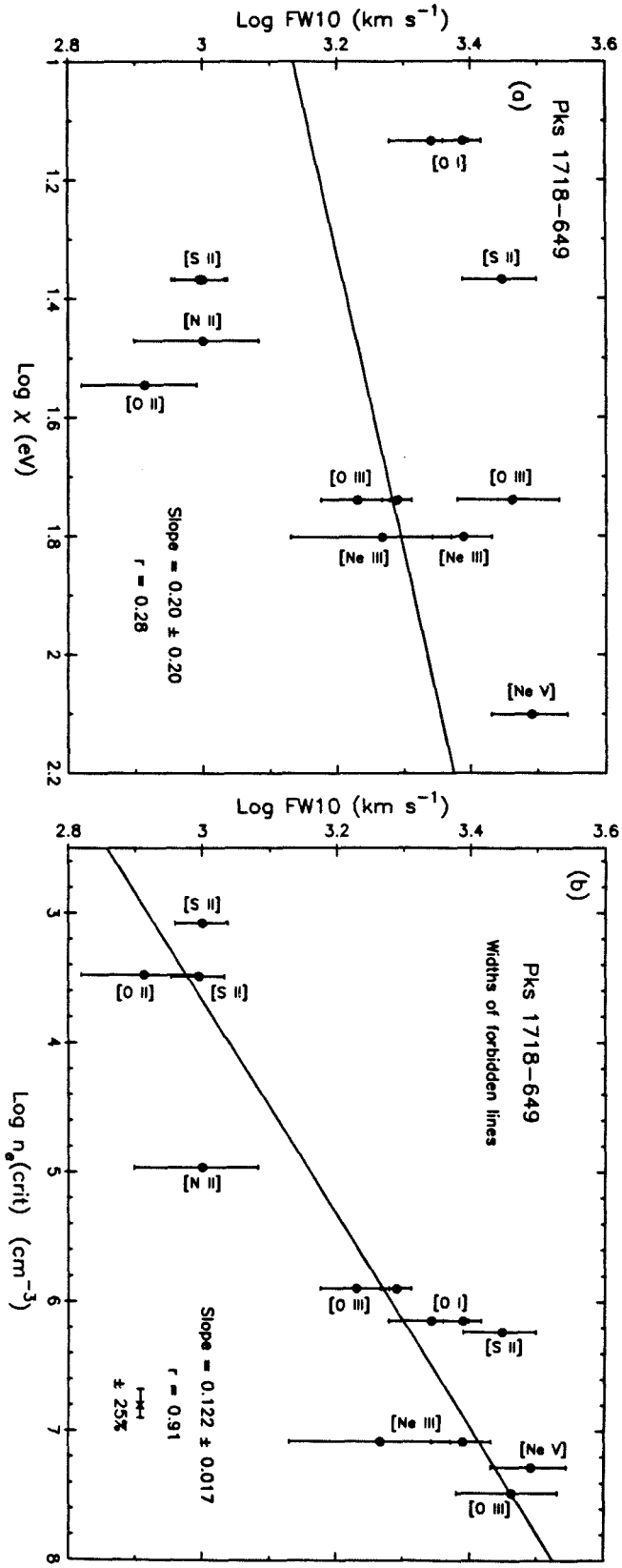
Log FW10 (km s^{-1})
2.8
3
3.2
3.4
3.6
(a)
Pks 1718−649
[O I]
[S II]
[S II]
[N II]
[O II]
[O III]
[O III]
[Ne III]
[Ne III]
[Ne V]
Log χ (eV)
1
1.2
1.4
1.6
1.8
2
2.2
Slope = 0.20 ± 0.20
r = 0.28
Log FW10 (km s^{-1})
(b)
Pks 1718−649
Widths of forbidden lines
[S II]
[O II]
[S II]
[N II]
[O III]
[O I]
[S II]
[Ne III]
[Ne V]
[O III]
Log n_e(crit) (cm^{-3})
3
4
5
6
7
8
Slope = 0.122 ± 0.017
r = 0.91
± 25%

Figure 4

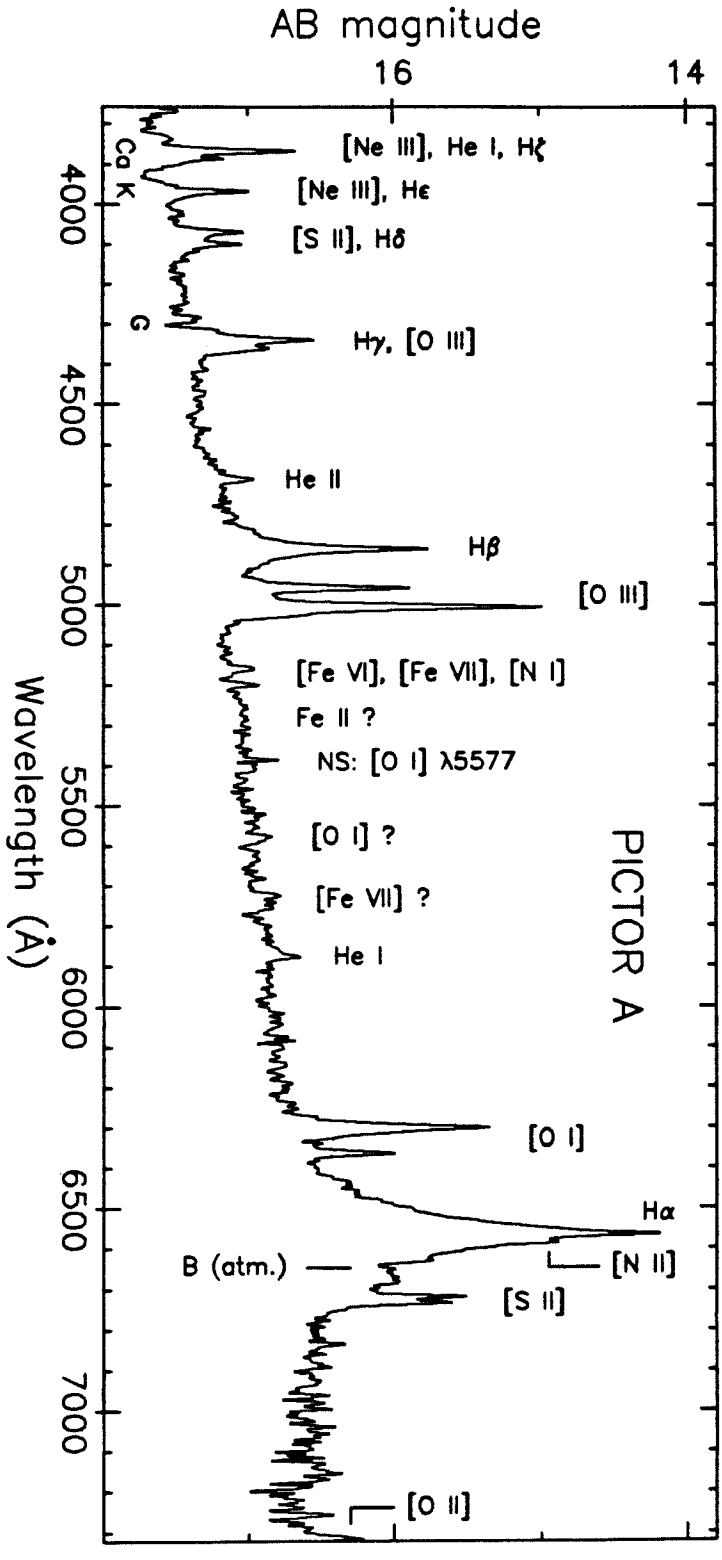
AB magnitude
16
14
Wavelength (Å)
4000
4500
5000
5500
6000
6500
7000
Ca K
G
[Ne III], He I, Hζ
[Ne III], Hε
[S II], Hδ
Hγ, [O III]
He II
Hβ
[O III]
[Fe VI], [Fe VII], [N I]
Fe II ?
NS: [O I] λ5577
[O I] ?
[Fe VII] ?
He I
[O I]
Hα
B (atm.)
[N II]
[S II]
[O II]
PICTOR A

Figure 5

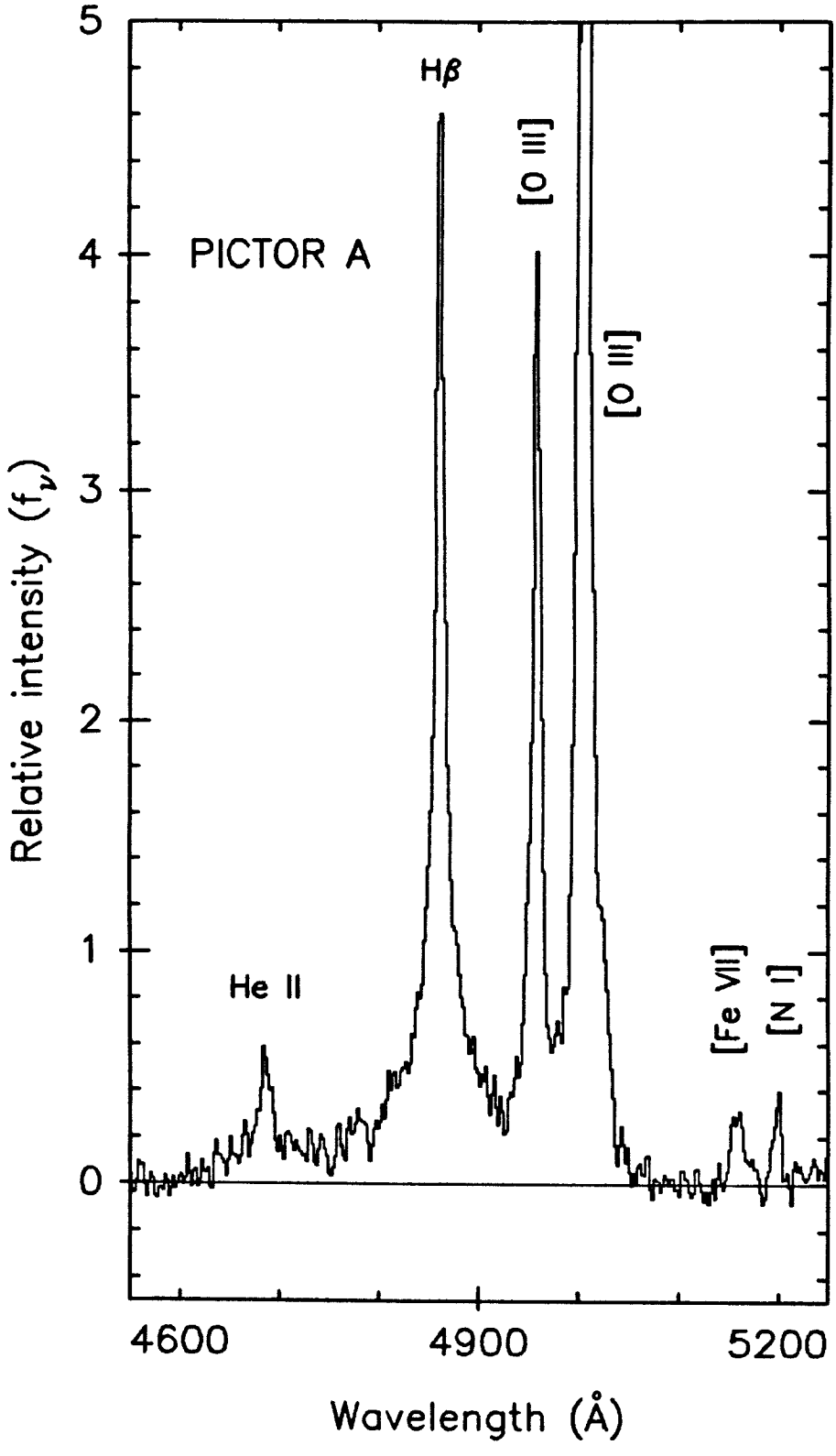
PICTOR A
Hβ
[O III]
[O III]
He II
[Fe VII]
[N I]
Relative intensity (f_ν)
Wavelength (Å)
0
1
2
3
4
5
4600
4900
5200

Figure 6

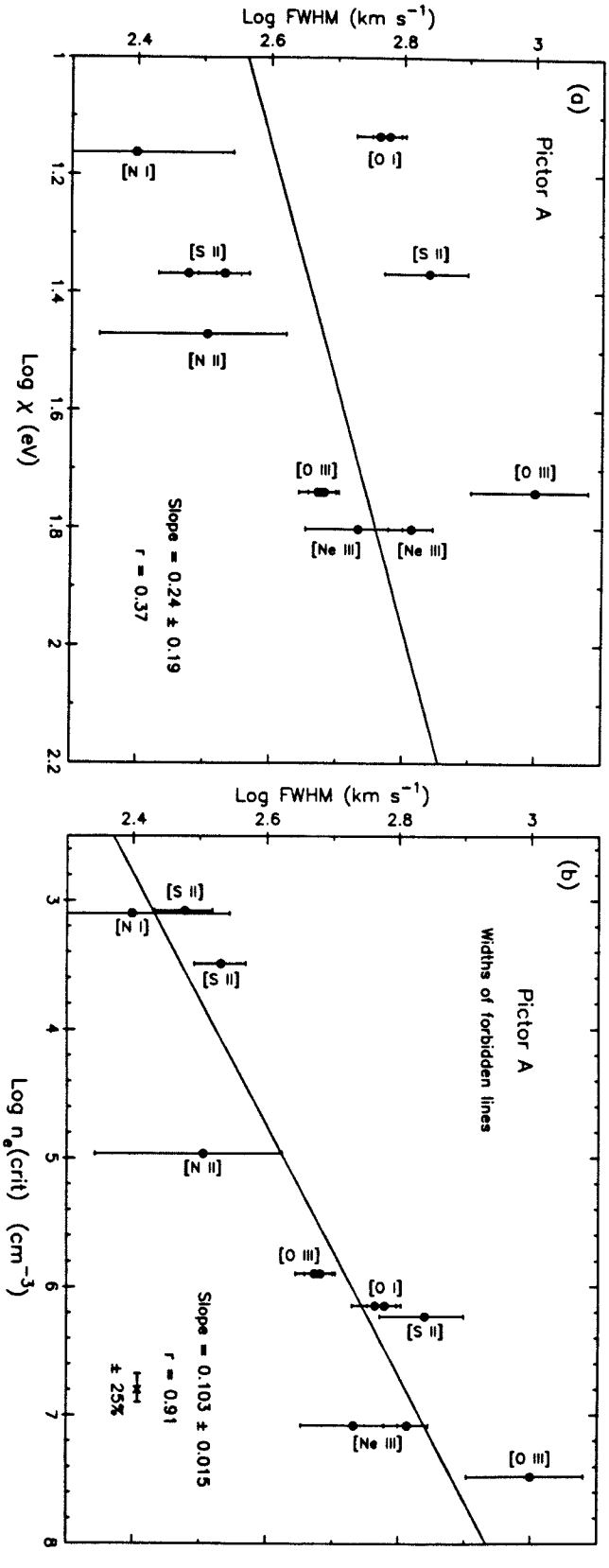
Log FWHM (km s^{-1})
2.4
2.6
2.8
3
(a)
Pictor A
[N I]
[O I]
[S II]
[S II]
[N II]
[O III]
[O III]
[Ne III]
[Ne III]
Log χ (eV)
Slope = 0.24 ± 0.19
r = 0.37
(b)
Pictor A
Widths of forbidden lines
[S II]
[N I]
[S II]
[N II]
[O III]
[O I]
[S II]
[Ne III]
[O III]
Log n$_e$(crit) (cm^{-3})
Slope = 0.103 ± 0.015
r = 0.91
± 25%

Figure 7

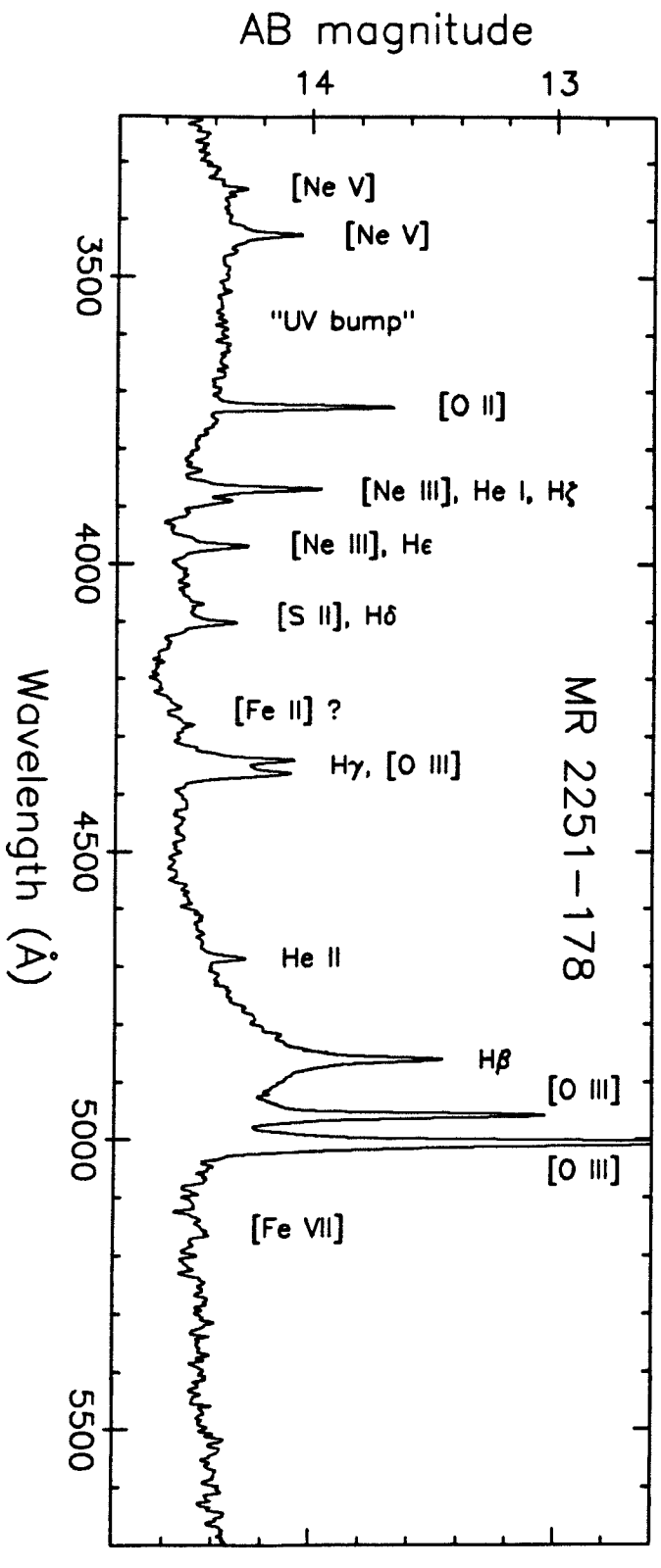
AB magnitude
14
13
[Ne V]
[Ne V]
"UV bump"
[O II]
[Ne III], He I, Hζ
[Ne III], Hε
[S II], Hδ
[Fe II] ?
Hγ, [O III]
He II
Hβ
[O III]
[O III]
[Fe VII]
MR 2251−178
Wavelength (Å)
3500
4000
4500
5000
5500

Figure 8

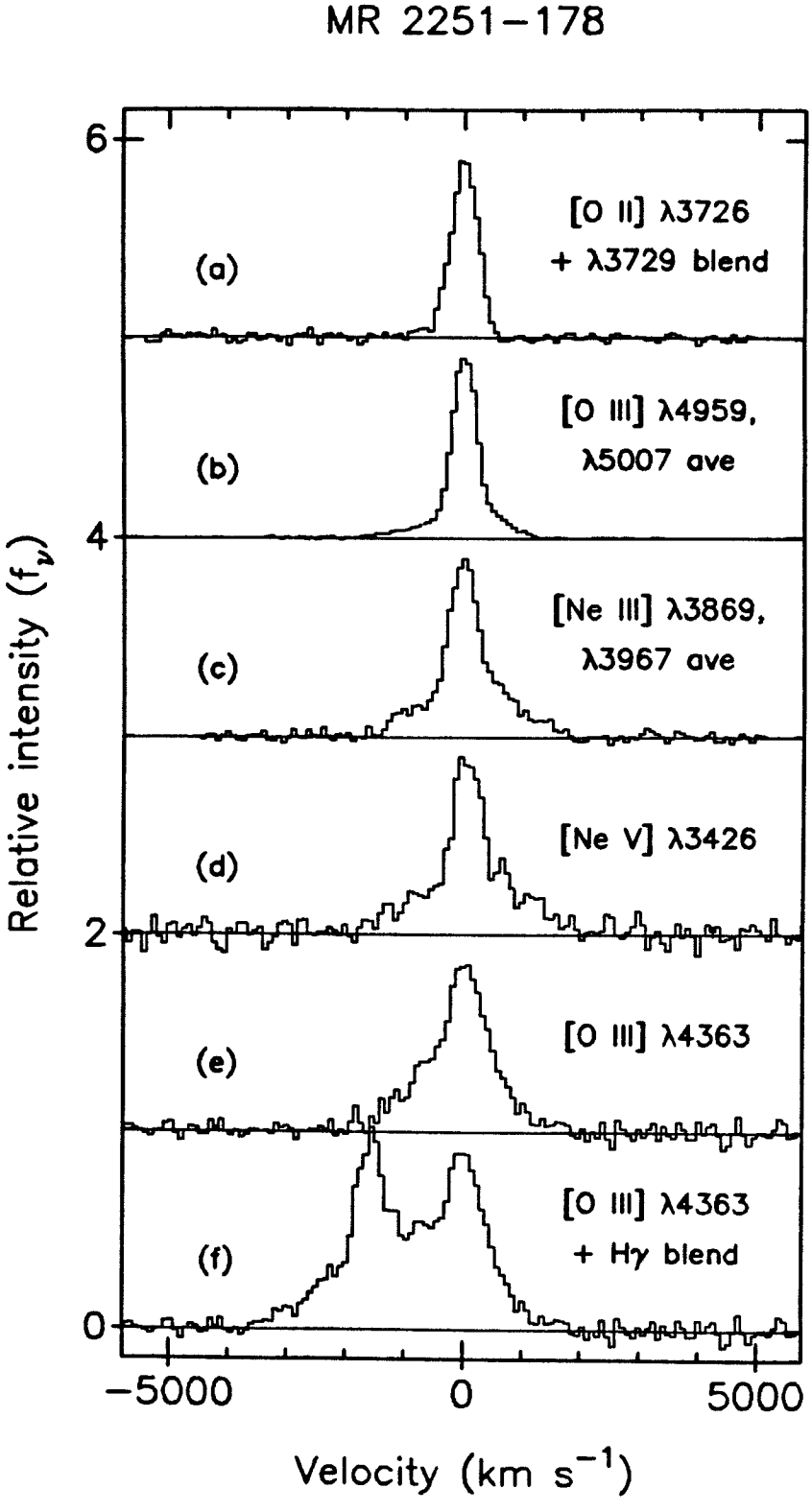
MR 2251−178
Relative intensity (f_ν)
6
4
2
0
(a)
[O II] λ3726
+ λ3729 blend
(b)
[O III] λ4959,
λ5007 ave
(c)
[Ne III] λ3869,
λ3967 ave
(d)
[Ne V] λ3426
(e)
[O III] λ4363
(f)
[O III] λ4363
+ Hγ blend
−5000
0
5000
Velocity (km s^{-1})

Figure 9

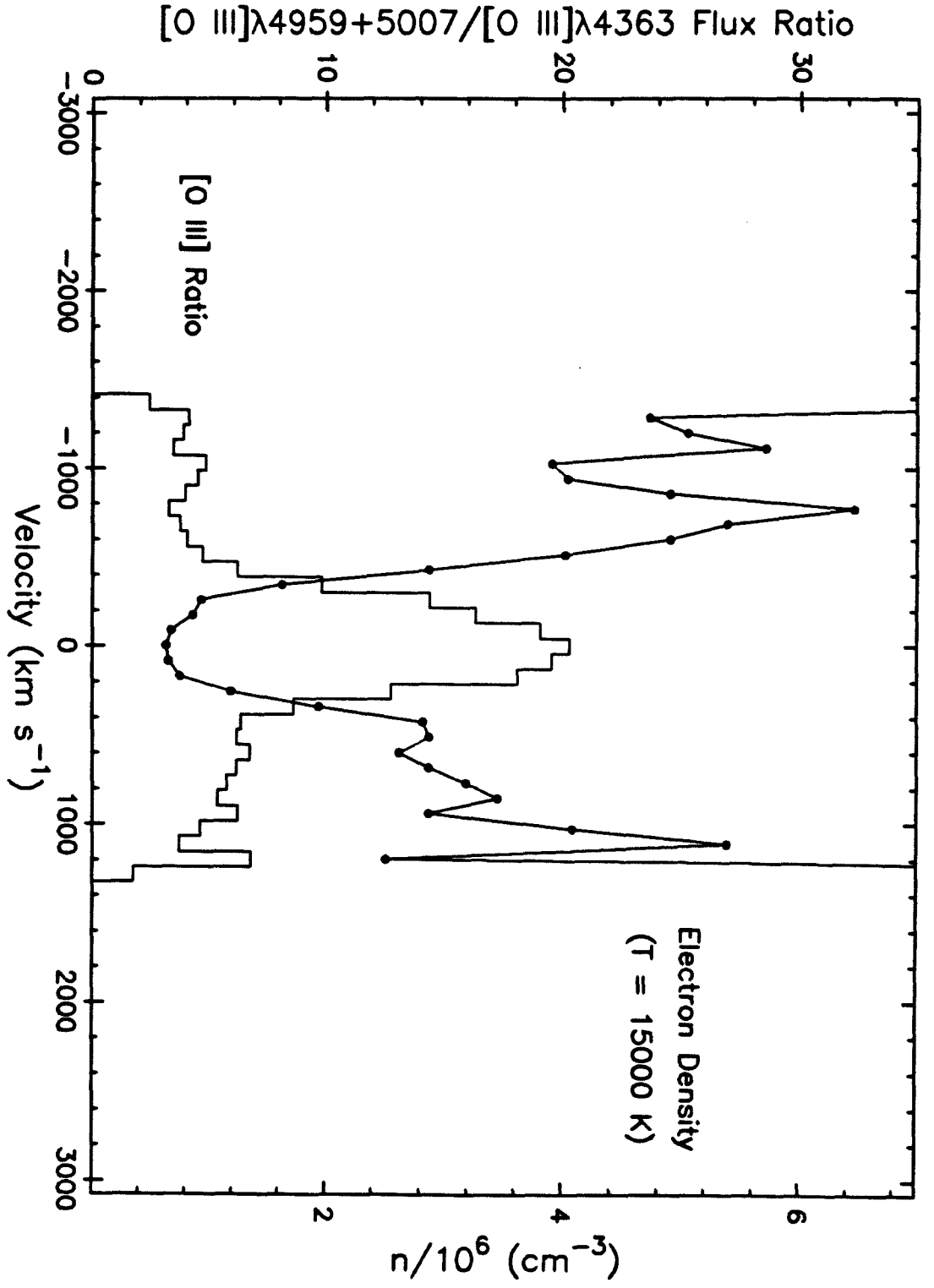
[O III]λ4959+5007/[O III]λ4363 Flux Ratio
0
10
20
30
[O III] Ratio
-3000
-2000
-1000
0
1000
2000
3000
Velocity (km s^{-1})
MR 2251-178
Electron Density
(T = 15000 K)
2
4
6
n/10^6 (cm^{-3})

Figure 10

CHAPTER 5

A Search for "Dwarf" Seyfert 1 Nuclei. I. The Initial Data and Results.

Alexei V. Filippenko and Wallace L. W. Sargent

To be submitted for publication, The Astrophysical Journal Suppl. Series

Now, if I wanted to be one of those ponderous scientific people, and "let on" to prove what had occurred in the remote past by what had occurred in a given time in the recent past, or what will occur in the far future by what has occurred in late years, what an opportunity is here!...

In the space of one hundred and seventy-six years the Lower Mississippi has shortened itself two hundred and forty-two miles. That is an average of a trifle over one mile and a third per year. Therefore, any calm person, who is not blind or idiotic, can see that in the Old Oolitic Silurian Period, just a million years ago next November, the Lower Mississippi River was upward of one million three hundred thousand miles long, and stuck out over the Gulf of Mexico like a fishing-rod. And by the same token any person can see that seven hundred and forty-two years from now the Lower Mississippi will be only a mile and three-quarters long, and Cairo and New Orleans will have joined their streets together, and be plodding comfortably along under a single mayor and a mutual board of aldermen. There is something fascinating about science. One gets such wholesale returns of conjecture out of such a trifling investment of fact.

"Life on the Mississippi" (1874)

Mark Twain

ABSTRACT

A sensitive search for low-luminosity type 1 Seyfert galaxies is being conducted with spectra having ~ 2.5 Å resolution and very high ($\gtrsim$ 100/1) signal-to-noise ratios. Thus far the nuclei of 66 bright, predominantly spiral galaxies (including 26 of the 30 LINERs originally surveyed by Heckman) and 9 well-known Seyferts have been observed with the Palomar 5 m telescope. Four physically independent forbidden lines as well as Hα are included in the spectral region discussed here (λλ 6200-6880). Although a detailed analysis of the data will be given elsewhere, in this paper we present the data and draw some important initial conclusions.

Compared with the forbidden emission, Hα exhibits extended wings in at least 19, and possibly up to 28, of the 75 objects. Of the 26 LINERs listed by Heckman, 8 to 12 show broad Hα. The equivalent width of the broad component ranges from nearly zero to values comparable to those in luminous active galactic nuclei, suggesting the presence of mild nonthermal processes in a significant fraction of all nearby galaxies. Furthermore, the relative intensities of [O I]λ6300, [N II]λ6583, and [S II]λ6716+6731 in these objects are consistent with photoionization by a power-law continuum. This is especially true if the high densities implied by the correlation between line width and critical density (observed in a number of objects) is taken into account. Rotational broadening contributes substantially to the observed widths of lines in many objects. Hα emission often appears narrower than the adjacent [N II] lines; this can partially, but not completely, be explained by the presence of underlying Hα absorption.

These data indicate that the faint end of the luminosity function of active galaxies is much more populated than was previously believed. Given the paucity of nearby QSOs and the growing evidence that they reside in galactic nuclei, it is likely that many of the objects we observed were QSOs in the distant past.

Subject headings: galaxies:general—galaxies:nuclei—
galaxies:Seyfert—line profiles

I. INTRODUCTION

Many of the observed properties of QSOs, Seyfert galaxies, BL Lac objects, and certain radio galaxies are similar, and it is natural to ask whether these objects are in any way related to each other. One fruitful approach to the problem is to quantify the range of values that a given feature exhibits. For example, the discovery of Seyfert nuclei which are as bright as low-luminosity quasars and spectroscopically indistinguishable from them suggests that similar mechanisms of energy generation may be prevalent in many active extragalactic objects (Weedman 1976). Moreover, deep images of almost all relatively low-redshift ($z \lesssim 0.5$) QSOs reveal the existence of extended nebulosity whose properties are similar to those of local ($z \lesssim 0.05$) spiral galaxies and Seyferts (e.g., Wyckoff *et al.*[1981]; Boroson, Oke, and Green 1982; Hutchings 1983). These studies demonstrate that most QSOs are probably the bright nuclei of distant galaxies in which nonthermal processes dominate the stellar component.

Although the gap between QSOs and luminous Seyfert galaxies has now been bridged, that between low-luminosity active galactic nuclei (AGNs) and "normal" nearby galaxies is still prominent. To gain a deeper understanding of the relationship between all these objects, and of the physical processes which occur within them, it is necessary to close this gap. It is particularly important to accurately determine the luminosity function of AGNs which exhibit only mild activity: if a sufficiently large number of galaxies contain a massive central black hole which is deprived of fuel (accreting gas), then it is likely that most galaxies began their lives as QSOs.

In light of this, there has recently been much emphasis on determining the number density and nature of nearby emission-line galaxies. Peimbert and Torres-Peimbert (1981), for example, detected broad Hα emission in the nucleus of M81, and the studies of M51 by Rose and Searle (1982) and by Rose and Cecil (1983) provide evidence for low-level nonthermal activity in an otherwise normal spiral galaxy. Futhermore, Heckman (1980), Stauffer (1982a, b), and Keel (1983a, b) showed that many galactic nuclei ("LINERs") exhibit emission lines whose intensity ratios do not resemble those found in ordinary galactic and extragalactic HII regions.

The exact nature of the activity in these objects, has inspired much debate (e.g., Pagel and Edmunds 1983). Ferland and Netzer (1983) and Halpern and Steiner (1983) independently showed that most of the observed characteristics can be understood in terms of photoionization by a nonstellar continuum, but some of the emission-line intensity ratios nevertheless argue for shock-heating of the gas. Recent investigations, however, strengthen the arguments for photoionization (rather than heating by shocks) as the dominant excitation mechanism. First, the intensity of [O III]λ4363 measured by Koski and Osterbrock (1976) and Fosbury et al. (1978) was probably too large in NGC 1052, the prototypical LINER (Keel and Miller 1983; Rose and Tripicco 1984). Smaller values lead to lower derived temperatures and eliminate some of the conflict with simple photoionization models. Similarly, He II λ4686 has been systematically underestimated in LINERs because of underlying absorption lines (Filippenko and Halpern 1984, hereafter Paper I; Filippenko 1984a, hereafter Paper II).

The second, physically more fundamental, discovery is that

narrow-line clouds of very different density exist in some LINERs, Seyfert galaxies, and QSOs, and that the densest gas can have $n_e \sim 10^7$ cm^{-3} (Papers I and II). Such conditions lead to an enhancement of transauroral and auroral lines such as [O III]λ4363 over the nebular lines, mimicking the effects of high temperatures. Three of the four galaxies in Papers I and II (NGC 7213, MR 2251-178, Pictor A) are clearly photoionized by a nonstellar continuum, indicating that the spectral characteristics of LINERs can easily be produced by mechanisms other than shock heating.

A key to these discoveries was that forbidden lines associated with high critical densities are broader than those with low values of n_e(crit), implying a density stratification among clouds in the narrow-line region (NLR). Moreover, the presence of broad Balmer emission, one of the defining spectroscopic characteristics of QSOs and Seyfert 1 galaxies, suggests a direct link between LINERs and classical AGNs. Clearly, then, one very fruitful approach to determining the faint end of the luminosity function of "dwarf" AGNs is to search for broad Hα emission and differences among the widths of forbidden lines in as many galaxies as possible.

Heckman (1980), Stauffer (1982a, b), and Keel (1983a, b) have already conducted spectral surveys of the region near Hα; the combined number of objects is several hundred. The results have been encouraging. Heckman (1980) noted that [O I]λ6300 is broader than other prominent lines such as [S II]λ6716,6731 in several LINERs, and all three workers detected (or suspected) the presence of a broad component of Hα in a number of objects. Unfortunately, most of the data either are not of sufficient resolution to look for small differences in line

widths, or do not have the high signal-to-noise (S/N) ratios necessary in a sensitive search for weak wings in the profile of Hα. Moreover, these studies have generally concentrated on spiral galaxies because most classical Seyferts are spirals (Adams 1977; Simkin, Su, and Schwartz 1980), thereby precluding the possible discovery of similar activity in elliptical and S0 galaxies.

We have therefore begun a large spectroscopic program to measure the region around Hα (λλ6200-6880) in a complete sample of galaxies, with the hope of eventually determining the luminosity function of AGNs having faint nonstellar activity. This will be achieved by quantifying the intensities and profiles of the physically independent emission lines [O I]λ6300+6364, [N II]λ6548+6583, [S II]6716, [S II]6731, and Hα. The data are of exceptionally high quality: the S/N ratio per resolution element in the continuum of most objects is of order 100/1, and the spectral resolution is ~ 2.5 Å.

Here we present the first results of the survey, which includes a total of 75 galaxies. In order to establish the feasibility and scientific rewards of the project, we concentrated on Heckman's (1980) LINERs and on galaxies from the surveys of Stauffer (1982a, b), Keel (1983a, b), and Filippenko (Palomar 1.5 m telescope, unpublished) which seemed particularly interesting. These objects were among the most likely candidates for "dwarf" Seyfert 1 nuclei, and many were indeed confirmed as such. Also included, for comparison, are 9 bright, "classical" Seyferts from Weedman's (1977) list. As the survey progresses, we will deal with similar results in an analogous manner. In addition, all of the data will be calibrated on an absolute flux scale by obtaining short integrations on the objects during photometric

conditions. It is hoped that a sample of at least 500 galaxies brighter than $B_T \sim 13$ will eventually be published.

Section II discusses the observations and the procedures adopted to reduce the data. The most important conclusions, as well as an atlas of red (Hα) spectra, are presented in § III. Galaxies are discussed on an individual basis in § IV. A detailed analysis of the emission and absorption lines, including information derived from spectra in the range λλ4200–5200 taken simultaneously with the Hα data, will be discussed separately (Filippenko and Sargent 1984a, hereafter FS).

II. OBSERVATIONS AND REDUCTIONS

Two-dimensional data were obtained in July 1982 and February 1984 with the Double Spectrograph (Oke and Gunn 1982) attached to the Cassegrain focus of the Hale telescope at Palomar Observatory. The Journal of Observations is given in Table 1. A grating having 1200 grooves/mm was installed in the "red camera," and a TI CCD (Texas Instruments Charge-Coupled Device) consisting of 800 x 800 square pixels (0.58 x 0.58 arcsec^2) detected and stored photons over the range λλ6300–6900 Å. The "blue camera" was equipped with an RCA CCD in February 1984, and with Shectman's (1982) two-dimensional photon-counting detector in July 1982, but the spectra ($\lambda \lesssim 5200$ Å) will be discussed in greater detail elsewhere (FS). In most cases the slit width was 2″, resulting in a spectral resolution of ~ 2.5 Å. When possible, the slit was aligned along the direction of atmospheric refraction in order to minimize relative light losses (Filippenko 1982). Although the observed galaxies were bright, typical integration times were 900–1200 s to ensure the very high S/N ratios (~ 100/1) necessary

for the detection of faint emission lines.

Bright secondary standards (Oke and Gunn 1983) were used to accurately calibrate the observations obtained in February 1984. During July 1982, on the other hand, the white dwarf LDS 749B (Oke 1974) was observed instead, resulting in a less reliable determination of the overall spectral response. Most of the nights were not photometric, and in many cases thick clouds seriously hampered observations, so absolute fluxes will not be derived here.

The wavelength scale was established by fitting a quartic polynomial to unblended emission lines of Ar and Ne comparison spectra taken throughout each night. Pixel-to-pixel variations in the response of the CCD were removed with exposures of the dome ceiling illuminated by a hot tungsten lamp. The bias level for each data frame was recorded as a single number for every column along the dispersion.

During the reduction procedure, slight tilts and distortions of the spectra with respect to a straight column of pixels were removed with the appropriate cubic polynomial. The spectrum of each object was then obtained by adding together a total of seven pixels centered on the nucleus, and therefore corresponds to a measurement through a 2" x 4.1" effective aperture. These spectra will later be supplemented with data of similar resolution and aperture size, obtained at Las Campanas Observatory for a number of Southern galaxies. In some cases (Table 1) 11 pixels were summed to increase the S/N ratio, giving a 2" x 6.4" aperture.

Subtraction of the sky was accomplished by determining its level in regions distant from the nucleus and interpolating with a constant or linear polynomial. Cosmic rays detected by the CCD were eliminated from

the sky region during this procedure. Since many of the observed galaxies are very extended or have off-nuclear HII regions, the sky was rarely completely free of contamination by the object, but in most cases the resulting errors in equivalent widths of lines are minor. Slight differences in wavelength between the sky and object spectra (primarily caused by poor efficiency of charge transfer in regions containing few counts) sometimes produced imperfect subtraction of [O I]λ6300 and [O I]λ6364, which are almost always much stronger than any other emission features over the observed range of wavelengths. The tell-tale "spikes," as well as those caused by cosmic rays, were found by inspection and deleted where possible.

Absorption at ~ λ6860 due to atmospheric O_2 (the "B band") was removed by dividing the spectrum of each object by that of a sdF star (Oke and Gunn 1983), which are intrinsically nearly featureless (except for Hα) around this region. Differences in air mass were scaled appropriately in this procedure. Nevertheless, in many cases it was obvious that spurious features were introduced by the division, so the data near the B-band were discarded.

III. RESULTS

The spectra of all 75 objects over the range λλ6200-6880 are shown in Figures 1 through 9. In each case the redshift was removed. Heliocentric redshifts were generally taken from Sandage and Tammann (1981), but slight corrections were necessary in a number of objects. Table 1 lists the integration time, position angle, and effective aperture used for each spectrum. The spectra of objects with moderately (or very) strong emission lines were scaled so that the strongest

emission line has approximately the same physical height. Although the intensity scale is linear and represents the flux per unit frequency interval, the actual continuum cannot be determined since zero-point offsets are different for each galaxy.

Casual inspection of the figures reveals the remarkably great variety among the spectra. Section IV provides a description of each galaxy. The equivalent width of the Hα + [N II] blend was measured in each galaxy and listed in Table 1. At best, only a partial removal of Hα absorption was attempted. FS analyze the data in much greater detail by initially subtracting an absorption-line template from each galaxy, as illustrated and described at length for NGC ~~3884~~ 2841 (§ IV; Figure 12).

The main results of our preliminary measurements can be summarized as follows:

1) Out of the 75 galaxies surveyed, 19 definitely have a broad component of Hα. Of these, 10 were known Seyfert galaxies, and in a few others broad Hα was suspected by previous workers in data of poorer quality. Four additional objects probably exhibit a broad Hα component, and five others possibly contain one as well. The detailed analysis by FS may disclose additional candidates, but already it is clear that the number of bright galaxies that are classical type 1 Seyferts or "dwarf" Seyferts is much larger than previously thought.

Heckman (1980) published a list of 30 LINERs (aside from a few which he found in the literature), out of which we observed 26. A very significant result is that 8 to 12 of these (27% - 40%) exhibit broad Hα, indicating that LINERs are indeed a fruitful hunting ground for "dwarf" Seyferts. The statistics become even more impressive when one considers that very few of the surveyed objects which had <u>not</u> been

previously classified as either Seyferts or LINERs were found to have broad Hα emission.

2) At least 30% of Heckman's (1980) LINERs have broader [O I]λ6300 than [S II]λ6716,6731, and in many cases [O I]λ6300 has very extended (almost Lorentzian) wings. It was shown in Papers I and II that this behavior must be interpreted as an increase in the cloud velocities with increasing density, since the critical density of [O I]λ6300 is a factor of 1000 greater than that of [S II]λ6716,6731. A range of densities is present, including values as high as 10^6–10^7 cm^{-3}. When combined with photoionization models involving a low ionization parameter (Halpern and Steiner 1983; Ferland and Netzer 1983), the resulting relative intensities of emission lines are in good agreement with observations, eliminating the necessity of invoking shocks to ionize the gas. In fact, Papers I and II show that shocks cannot explain some of the observed characteristics, so photoionization by a dilute power-law continuum is almost certainly the excitation mechanism. Thus, the "shock" region in the diagrams of Baldwin, Phillips, and Terlevich (1981) have probably been interpreted incorrectly.

With the possible exception of only one or two galaxies, differences in the width of [O I] and [S II] were accompanied by the presence of broad Hα. Papers I and II indicate the same correlation in Pks 1718-649, NGC 7213, and Pictor A. Forbidden emission in the QSO 2251-178 (Paper II) also displays different widths, although the red [O I] and [S II] lines were not available for examination.

3) Rotational broadening often contributes to the observed line widths, and in some cases the increase may be ~ 400 km s^{-1}, depending on the orientation of the observer's entrance aperture. Global rotation of

the nucleus can mask the sometimes effects discussed in (2), which are often subtle. On a related matter, Hα emission appears narrower than the adjacent [N II] lines in a number of galaxies. Not all of this effect is likely to be due to underlying Hα absorption.

IV. NOTES CONCERNING INDIVIDUAL OBJECTS

We will now briefly describe the interesting features of each spectrum. The instrumental resolution has been removed from the quoted line widths with the relation

$$(\mathrm{FWHM})^2_{\mathrm{true}} = (\mathrm{FWHM})^2_{\mathrm{obs}} - (\mathrm{FWHM})^2_{\mathrm{inst}} ,$$

where the subscripts refer to the intrinsic ("true"), observed, and instrumental widths, respectively.

NGC 404: Extremely narrow emission lines are visible in the spectrum (Figure 1a), which was obtained through a 1″ slit. The strong [O I] and [S II] emission puts this object into the LINER class, but it is a peculiar member since the blue continuum and high-order Balmer absorption lines are indicative of a relatively recent episode of star formation (Keel 1983a).

NGC 1052: This is the prototypical LINER, and the primary reason for the classification of similar galaxies as shock-heated (Koski and Osterbrock 1976; Fosbury et al. 1978; Heckman 1980). The [N II] and [S II] lines are very broad (FWHM ~ 400–500 km s^{-1}), and the width of [O I]λ6300 is still greater (750–800 km s^{-1}). Inspection of the two-dimensional CCD spectrum reveals that a significant fraction of the width is produced by rotational broadening: the steep rotation curve covers a velocity difference (Δv_{max}) of 250–300 km s^{-1} over only a few

arc seconds. Extremely weak wings on either side of the [N II] + Hα blend in Figure 1a are probably due to Hα emission similar to that in the broad-line region (BLR) of type 1 Seyfert galaxies. A good comparison may be made with NGC 4051 (Figure 4b), a Seyfert of low luminosity and relatively narrow Balmer lines.

NGC 1068: This famous type 2 Seyfert galaxy (Seyfert 1943; Weedman 1977) has extremely broad emission lines: the FWHM of the uncontaminated [O I] lines is ~ 1100 km s^{-1}, and studies of the [O III]λ5007 profile by Alloin et al. (1983) and others show remarkably complex structure. The emission is clumpy both parallel and perpendicular to the dispersion. Figure 10 shows that no extremely broad Hα is likely to be present, although a broad component corresponding to the one in Hβ possibly detected by Malkan and Filippenko (1983, hereafter MF) may be hidden by the strong [N II].

NGC 1167: [O I]λ6300 (FWHM ~ 700 km s^{-1}) is broader than the [S II] and [N II] lines (FWHM ~ 550 km s^{-1}). A very weak component of even broader Hα emission may be present, but a detailed analysis (FS) is necessary to confirm this. As in many galaxies observed in our survey, the intensity of [O I]λ6364 appears to be less than the theoretical prediction [~ 0.33I([O I]λ6300)] because of strong absorption lines of Fe I at λλ6355, 6359.

NGC 1169: Considerable rotation in the nucleus (Δv_{max} ~ 150-200 km s^{-1}) contributes significantly to the observed widths of emission lines. Underlying absorption decreases the apparent strength of the Hα emission line.

NGC 1275: Figures 1b and 10 reveal weak, remarkably broad wings in the profile of Hα (FWZI ~ 19000 km s^{-1}), considerable differences in the

profiles of [O I] and [S II], and the almost complete absence of stellar absorption lines in this well-known Seyfert galaxy (Seyfert 1943). The extended Hα emission is logarithmic to first order. [O I]λ6300 exhibits a relatively narrow core, a component of intermediate width, and weak, very extended wings (FWZI ~ 6000–7000 km s^{-1}), while the [S II] doublet does not have this complicated structure.

It is often stated (e.g., Weedman 1977) that NGC 1275 should probably never have been classified as a Seyfert since it is a giant elliptical galaxy and has a number of other anomalous properties (Kent and Sargent 1979). Spectra presented here and by MF, however, indicate that in many ways it shares the properties of classical type 1 Seyferts and may contain clues to the nature of other AGNs. The blue color (MF) and Balmer absorption lines (Minkowski 1968) in the nuclear region, for example, are similar to the properties of the underlying galaxy in 3C 48 (Boroson and Oke 1982).

NGC 1358: The spectrum in Figure 1b is the average of two independent integrations. Gaussians adequately represent the relatively narrow (FWHM ~ 250 km s^{-1}) emission except near the continuum, where the observed lines are slightly broader.

NGC 1667: Two separate spectra were combined in Figure 1b to increase the S/N ratio, but no significant differences were visible in the original data. The emission lines are reasonably broad (FWHM ~ 400 km s^{-1}). H II regions define a prominent rotation curve with Δv_{max} ~ 360 km s^{-1}, but rotational broadening in the nucleus itself contributes very little to the observed width (FWHM ~ 360 km s^{-1}) of the emission lines. The profiles have somewhat broader wings than Gaussians, and an accurate subtraction of [N II], using a combination of

the blue and red sides of [S II]λ6716 and [S II]λ6731 (respectively) as a template, is necessary to ascertain the presence of weak, extended Hα emission (FS).

NGC 2146: The faint continuum and the narrow emission lines (FWHM ~ 120 km s^{-1}) derived from the red and blue spectra indicate that H II regions dominate the nucleus of this galaxy (Figure 2a).

NGC 2273: Huchra, Wyatt, and Davis (1982) discovered this type 2 Seyfert galaxy during the course of the Center for Astrophysics (CfA) redshift survey (Huchra *et al.* 1983). Our spectrum (Figure 2a) confirms their classification, since [O III]λ5007 is much more intense than Hβ while [N II] is comparable to Hα. Moreover, He II λ4686 emission is present. The lines are narrow (FWHM ~ 200 km s^{-1}) and predominantly Gaussian, but they exhibit slightly broader wings. Two spatially-resolved knots, one of which is much brighter than the other, are visible in the two-dimensional spectrum of the nucleus.

NGC 2639: A broad component of Hα emission is present in Figure 2a. It was detected by Keel (1983a), and also by Huchra, Wyatt, and Davis (1982) during the CfA redshift survey. Note, however, that the [S II] lines (and hence the [N II] lines as well) have extended wings, so the derived strength of the broad Hα is greatly overestimated if the [N II] + Hα blend is decomposed with Gaussians (FS). The rotation curve contributes a negligible amount to the observed widths of lines.

NGC 2681: The quality of the data obtained in this survey is evident from a careful inspection of two independent spectra of this object (Figure 2a) taken at different positions along the slit; virtually no differences are visible. Balmer absorption is prominent

and greatly decreases the apparent strength of the Hα emission line.

NGC 2685: As in NGC 2681, strong Hα absorption is clearly present (Figure 2a). The equivalent width of [N II]λ6548+6583 is only ~ 2.5 Å, making NGC 2685 only a weak emission-line galaxy.

NGC 2768: Resolved emission lines are present in the nucleus (Figure 2b). There is no broad component of Hα.

NGC 2787: The equivalent widths and relative intensities of the emission lines resemble those in NGC 2768. A faint, broad "bump" is present (Figure 2b), but the discussion of NGC 2841 (see below) shows that this reflects the old stellar population typical of the bulge of early-type spiral galaxies.

NGC 2841: Moderately strong [N II] and Hα emission reside on top of a faint, broad peak (Figure 2b). At first glance it appears as though broad Hα emission may be present, but Figure 12 shows a similar shape for the continuum in the nucleus of NGC 3115, which is devoid of narrow emission. In fact, the spectra of K2 and M0 giants (Figures 12d and 12e) indicate that the broad Hα "bump" is an artifact of the shallow depression near λ6700 produced by TiO in a population of late K and early M stars. The spectrum of an A star, obtained and reduced in the same manner as the other data, is given for comparison (Figure 12f).

In Figure 12a NGC 2841 is dereddened by E_{B-V} = 0.03 mag so that the shape of its continuum agrees with that of NGC 3115. Since differences in the metallicity and velocity dispersion of the two galaxies are minor, subtraction of NGC 3115 from NGC 2841 results in the pure emission-line spectrum of the latter. The benefits of such a subtraction are obvious: aside from the increase in narrow Hα emission and the clear absence of a broad component, [O I]λ6300 appears and

[S II]λ6716 becomes free of contamination by the underlying Ca I λ6718 absorption line. These changes are important, since (a) the strength of [O I]λ6300 is a major diagnostic of physical conditions and supports the classification of NGC 2841 as a LINER, (b) the intensity ratio of the [S II]doublet is an indicator of the gas density, (c)the true equivalent width of narrow Hα emission may be calculated and compared with lines such as [N II], and (d) a reliable upper limit can be derived for the strength of the broad Hα emission which is so crucial in the search for dwarf Seyfert 1 nuclei. FS will apply this technique to other galaxies that contain strong contamination by starlight.

NGC 2911: Gaussian fits to the emission lines indicate that [O I]λ6300 (FWHM ~ 570 km s^{-1}) is somewhat broader than [S II] and [N II] (FWHM ~ 430–500 km s^{-1}), and that a very faint, broad component of Hα may be present (Figure 2b). [O I], [S II], and [N II] emission are all strong, confirming Heckman's (1980) classification as a LINER.

NGC 2985: Deep absorption lines of Ca I and Fe I are visible in the spectrum (Figure 3a). Hα absorption is probably also present. The emission lines are fairly narrow (FWHM ~ 200–250 km s^{-1}).

NGC 3031: Two independent spectra (Figure 3a) demonstrate the presence of the strong, broad (FWZI ~ 4900 km s^{-1}) component of Hα emission discovered by Peimbert and Torres-Peimbert (1981) and confirmed by Shuder and Osterbrock (1981). As noted by Heckman (1980), the Gaussian [S II] lines (FWHM ~ 220 km s^{-1}) are in striking contrast with the profile of [O I]λ6300, which has broad wings similar to those in NGC 7213 (Paper I), Pictor A (Paper II), and Pks 1718-649 (Paper II). This is a clear indication of density stratification in the NLR of NGC 3031. The galaxy exhibits an almost stellar nucleus, as do

classical Seyferts, and it is also an X-ray source (Elvis and Van Speybroeck 1982). [O I]λ6364 appears too weak relative to [O I]λ6300 due to underlying Fe I absorption.

NGC 3115: No emission is visible in the spectrum of this object (Figure 3a), which was selected specifically as an absorption-line template.

NGC 3169: Strong [O I]λ6300, as well as [N II] and [S II] emission, verify that this is a LINER. There appears to be no broad Hα emission. Stellar Hα absorption decreases the apparent strength of the Hα emission line whose width is probably close to that of [S II]λ6716,6731 (FWHM ~ 320 km s^{-1}). Rotational broadening (Δv_{max} ~ 170 km s^{-1}) contributes substantially to the observed widths.

NGC 3185: The emission lines, whose relative intensities resemble those in type 2 Seyfert galaxies, are fairly narrow (FWHM ~ 230 km s^{-1}). Inspection of the two-dimensional spectrum, however, indicates that rotational broadening contributes greatly to the line widths; their intrinsic FWHM is only ~ 100 km s^{-1}. Moreover, the spectrum in Figure 3a contains emission from strong off-nuclear H II regions, where $\underline{I}([N\ II])/\underline{I}(H\alpha) < 1$, as well as the nucleus itself, in which $\underline{I}([N\ II])/\underline{I}(H\alpha) > 1$.

NGC 3227: This galaxy was studied by Seyfert (1943) and shows very broad Hα emission (FWZI ~ 20000 km s^{-1}) as well as narrower components having several different widths (Figures 3b, 10). The two-dimensional spectrum indicates that rotation broadens the narrowest components somewhat. [O I]λ6300 (FWHM ~ 440 km s^{-1}) has a more extended base than a Gaussian. Stellar absorption lines are relatively weak, confirming MF's claim that the very strong Na I D λ5892 doublet is probably

interstellar.

NGC 3379: Only very weak [N II]λ6583 is visible in this object (Figure 3b), which was chosen as an absorption-line template.

NGC 3516: The spectrum of this well-known Seyfert 1 galaxy (Seyfert 1943; Boksenberg and Netzer 1977) exhibits weak forbidden lines in comparison with Hα, whose equivalent width is over 250 Å (Figures 3b, 10). [Fe X]λ6374 is strong relative to [O I].

NGC 3623: Underlying absorption lines are very strong (Figure 3b), and Hα emission is significantly diluted. Rotation may contribute to the line widths (FWHM ~ 330 km s^{-1}). No broad component of Hα is present.

NGC 3627: Once again, Hα absorption affects the emission line (Figure 3b), and rotational broadening increases the apparent widths of lines (FWHM ~ 200 km s^{-1}).

NGC 3642: Very narrow emission lines (FWHM ~ 130 km s^{-1}) are superimposed on weak, significantly broader "triangular" components whose FWZI is ~ 800 km s^{-1}. In addition, there may be a very faint component of Hα which is even broader, similar to (but much weaker than) that in the narrow-line X-ray galaxy NGC 7314 (Filippenko 1984b). Rotation broadens the narrow lines by at least 30% in Figure 4a.

NGC 3718: Weak, broad Hα emission is present, but appears too large in Figure 4a since the continuum has not been removed yet. [O I]λ6300 is strong, broader than the [S II] lines (FWHM ~ 570 km s^{-1} compared with ~ 400 km s^{-1}), and somewhat non-Gaussian.

NGC 3884: This is the only LINER to have been initially discovered as an X-ray source (Reichert et al. 1982). Faint, broad wings are visible in Figure 4a, and are confirmed by a Gaussian decomposition of

the [N II] + Hα blend (as was done for many other objects). In Figure 13a, three Gaussians are used to represent the Hα and [N II]λ6548,6583 lines; oscillations in the residuals indicate that the lines are not exactly symmetrical Gaussians, but more important is the fact that excess emission is visible on the extreme blue and red portions of the blend. Figures 13c and 13d illustrate the absence of this excess emission if a fourth Gaussian is added for a total of 12 free parameters. The fit is physically reasonable, since the derived relative intensity of the [N II] lines agrees with the theoretical prediction of 3, and the widths of the narrow components of Hα and [N II] are all similar. Broad Hα was also suspected by Keel (1983a). [O I]λ6300 (FWHM ~ 600 km s^{-1}) is broader than [N II] (FWHM ~ 510 km s^{-1}). The two-dimensional spectrum shows that a major fraction of the width is probably due to rotational broadening, as the emission is tilted with respect to the continuum.

NGC 3898: Strong Hα absorption decreases the apparent intensity of Hα emission (Figure 4a). Rotational broadening contributes to the line widths.

NGC 3992: The spectrum (Figure 4a) resembles that of NGC 3898, as the emission lines are weak relative to the continuum and absorption is prominent.

NGC 3998: Very prominent, broad wings of Hα are visible on either side of the [N II] + Hα blend (Figures 4a, 11), as was first noticed by Heckman (1980) and confirmed by Blackman, Wilson, and Ward (1983) and Keel (1983a). The FWZI is at least 7000 km s^{-1}. Moreover, [O I]λ6300 (FWHM ~ 850 km s^{-1}) is markedly broader than the individual [S II] lines (FWHM ~ 400 km s^{-1}), and its profile has systematically broader wings

than a Gaussian of the same FWHM. In this way, it resembles NGC 3031, NGC 1275, and the galaxies discussed in Papers I and II. The [S II] lines are also slightly non-Gaussian.

NGC 4036: A Gaussian decomposition of the [N II] + Hα blend similar to that performed on NGC 3884 indicates that a very weak component of broad Hα emission may be present, since the fit in not good with only three Gaussians. On the other hand, [O I] and [S II] are not exactly Gaussian (Figure 4b), so a more detailed removal of [N II] from the blend is required (FS). [O I]λ6300 (FWHM ~ 500 km s^{-1}) is broader than the [S II] lines (FWHM ~ 360 km s^{-1}).

NGC 4051: Figures 4b and 11 illustrate the spectrum of this type 1 Seyfert galaxy (Seyfert 1943; Weedman 1977). The Balmer lines are not very broad compared with those in most Seyfert 1 galaxies, and in fact are comparable to the line widths in NGC 1068 (Figure 1a). Their width is nevertheless more than twice that of the forbidden lines, justifying this object's classification. The FWZI is ~ 5900 km s^{-1}, not much greater than that observed in many of the surveyed galaxies. X-ray variability on short time scales is known to occur.

NGC 4111: Deep Hα absorption is present (Figure 4b). The FWHM of emission lines is ~ 270 km s^{-1}.

NGC 4125: As in NGC 4111, deep Hα absorption dilutes the emission line and makes it appear very narrow. No broad Balmer emission is visible.

NGC 4151: Figures 5a and 11 illustrate the broad, asymmetrical Hα emission in this classical type 1 Seyfert galaxy (Seyfert 1943). In addition to the usual forbidden emission, lines of [S III]λ6312, [Fe X]λ6374, and He I λ6678 are present. The Hα profile has extremely

extended wings, a blueshifted component of intermediate width, and a relatively narrow part which merges smoothly with the narrow core corresponding to the [S II] and [N II] lines.

NGC 4192: The emission lines are strong relative to the continuum (Figure 5a) and have FWHM ~ 310 km s^{-1} (except Hα, which is narrower).

By this time you are probably very tired and wish this thesis would end, but cheer up — having progressed this far, you deserve a reward. To win a beer (or perhaps a glass of milk, Wal?) write "NGC 4192" on a sheet of paper and give it to me at the beginning of the exam.

NGC 4235: This Seyfert galaxy, which might be located in the Virgo cluster, was discovered by Abell, Eastmond, and Jenner (1978). The broad Hα line is very strong and has FWZI ~ 15000 km s^{-1}. A "dip" similar to the one in NGC 7213 (Paper I) is visible redward of [N II]λ6583. [O I]λ6300 (FWHM ~ 500 km s^{-1}) has broader wings than a Gaussian with the same FWHM, and is broader than the [S II] lines (FWHM ~ 420 km s^{-1}). The forbidden lines are asymmetrical in that a significant red shoulder is visible (see [N II]λ6583 in Figure 5a). Figure 11 shows the spectrum in greater detail.

NGC 4258: Beautiful emission lines all along the slit of the two-dimensional spectrum exhibit a very complex velocity field in the disk. Complicated structure is also known to be present in an H I map of the object. A weak, broad component of Hα is present (Figure 5b), and was suspected by Stauffer (1982a). [O I]λ6300, whose profile is similar to that in NGC 3031, NGC 3998, and several other objects, is strong and broader than the Gaussian [S II] lines.

NGC 4274: Emission in the nucleus is produced by H II regions, and the lines are very narrow.

NGC 4278: A weak, broad component of Hα is present in this radio galaxy, whose very strong [O I], [S II], and [N II] make it a classical LINER (Figure 5b). All of the forbidden lines have approximately the same width, which is dominated by rotational broadening (evident in the two-dimensional spectrum).

NGC 4303: H II regions are prominent in the nucleus and all along the slit. Rotational broadening contributes significantly to the line widths, which are nevertheless small (FWHM ~ 100 km s^{-1}). A substantially broader, "triangular" base in each line is evident (Figure 5b), and it is possible that we are seeing a faint type 2 Seyfert nucleus since $I([N\ II])/I(H\alpha) > 1$ and FWZI ~ 800 Å.

NGC 4388: The two-dimensional spectrum shows complicated structure in the emission lines all along the slit. High-excitation emission (including [Ar V] and [Fe X]) is visible in the nucleus itself (Figures 5b, 11, and 14), making this a type 2 Seyfert galaxy (Phillips and Malin 1982). Figure 14 betrays the presence of a very faint, broad (FWZI ~ 7600 km s^{-1}) component of Hα whose equivalent width is only ~ 8 Å. This is much weaker than the component which Stauffer (1982a) claimed to see. In fact, the use of Gaussians in Stauffer's decomposition of the [N II] + Hα blend was clearly unjustified, since the forbidden lines have strong red asymmetries which can mimic broad Hα emission. (These asymmetries may not have been obvious in Stauffer's (1982a) low-resolution spectrum, but they were responsible for the derived relative redshift Δv ~ 300 km s^{-1} of the broad component.) Instead, one must use the observed profile of the [S II] lines to remove the contribution of [N II]. Since NGC 4388 is an X-ray source, our detection of a very faint, broad Hα line supports the belief of Veron et

al. (1980) that all narrow-line X-ray galaxies are actually faint type 1 Seyferts.

NGC 4438: This LINER is interacting strongly with NGC 4435. The emission lines have FWHM ~ 400 km s^{-1} (part of which is due to rotation) and are slightly asymmetrical (blue wings). There is probably no broad component of Hα.

NGC 4450: Each of the emission lines has a broader base than given by a Gaussian with the same FWHM. A faint, even broader component of Hα is probably present, as suspected by Stauffer (1982a).

NGC 4486: The emission lines are broad (FWHM ~ 1000 km s^{-1}) compared with those in most emission-line galaxies and have intensity ratios suggestive of shock-heated gas (Ford and Butcher 1979). Two-dimensional spectra taken across the nucleus at five different position angles exhibit very complicated structure among the emission in the nuclear regions, although the jet is featureless. The velocity field will be examined in detail by Filippenko and Sargent (1984b). In the nucleus itself, Figure 6a shows very faint extensions on either side of the [N II] + Hα blend. This is probably due to broad Hα, since similar wings are not exhibited by the [S II] lines. The FWZI of the broad Hα is ~ 6800 km s^{-1}, and a very rough estimate of its equivalent width is ~ 4-5 Å. The relative strengths of the emission lines can be explained by photoionization models with a low ionization parameter, as in those of Halpern and Steiner (1983) and Ferland and Netzer (1983). Thus, this galaxy may in some ways be a Seyfert (albeit a peculiar one).

NGC 4501: Strong forbidden lines with FWHM ~ 200 km s^{-1} are visible in Figure 6b. As in a number of other galaxies, Hα appears somewhat narrower (FWHM ~ 140 km s^{-1}), possibly due to the presence of

underlying absorption. The lines have broader wings than Gaussians of the same FWHM.

NGC 4569: The emission lines are strong (Figure 6b) and narrow enough not to be blended (FWHM ~ 320 km s^{-1}), although there is slight artificial broadening due to the rotation of the galaxy. No broad component of Hα is evident.

NGC 4579: Hα emission exhibits broad wings (FWZI ~ 5700 km s^{-1}), as noticed by Stauffer (1982a) and Keel (1983a). The profile of [O I]λ6300 is non-Gaussian (Figure 6b) and resembles those in NGC 3031, NGC 3998, and many other galaxies. The [S II] lines also have somewhat extended wings, although not as much so as [O I]λ6300. By analogy with the objects in Papers I and II, the presence of some clouds with very high densities (~ 10^6-10^7 cm^{-3}) can probably account for the anomalously large strength of [O III]λ4363 measured by Stauffer (1982a) and Keel (1983a).

NGC 4594: Very prominent, broad Hα is present (Figure 6b), with FWZI ~ 5400 km s^{-1}. The faint [O I]λ6300 emission (FWHM ~ 800-900 km s^{-1}) is broader than [S II] (FWHM ~ 500 km s^{-1}). Stellar absorption is prominent.

NGC 4736: The spectrum exhibits deep Hα absorption which is partially filled in by a weak emission line (Figure 7a). Other absorption lines are strong as well, while [N II] emission is weak (equivalent width ~ 2.3 Å). Keel and Weedman (1980) pointed out that the galaxy has exceptionally bright inner spiral structure and therefore morphologically resembles NGC 1068. They consider it to be the best candidate for an "ex-Seyfert."

NGC 4826: Strong emission resides in a continuum littered with

fairly narrow absorption lines (Figure 7b). No broad component of Hα emission is present.

NGC 5005: The forbidden lines are broader than normal (FWHM $\geq$ 800 km s^{-1}) and form a striking contrast with those in NGC 4826 (Figure 7a). Inspection of the two-dimensional spectrum, however, indicates an extremely steep rotation curve of large amplitude (Δv_{max} ~ 400 km s^{-1}) which produces a significant fraction of the observed line widths. Over only 1"-1.5" the difference in velocity between the ends of the tilted emission lines is ~ 350 km s^{-1}. This is similar to, but more extreme than, the situation in NGC 3884 and NGC 1052, and shows that rotational broadening can be an important factor in the measured widths of lines.

NGC 5033: This is an X-ray source which Halpern and Steiner (1983) classify as a "transition" object between LINERs and Seyferts. As noticed by Shuder (1980) and confirmed by Stauffer (1982a), however, broad Hα emission (whose FWZI ~ 8000 km s^{-1}) is present. The two spectra in Figure 7a show a remarkable change in the appearance of the broad component, and indicate that the broad-line region can be at most ~ 0.5 pc in extent. Combining this upper limit with a representative velocity of ~ 3000 km s^{-1} (obtained from the FWZI), a mass of $\lesssim 10^9$ $M_\odot$ is estimated for the central object. The very faint wings extending out to the [O I] and [S II] lines in the 1982 spectrum may be artifacts of inaccurate flux-calibration ($\S$ II). Narrow lines in the 1984 spectrum (PA = 165 deg) are slightly affected by rotational broadening.

NGC 5055: Very weak emission lines are visible among a rich absorption-line spectrum (Figure 7b). The line widths are broadened significantly by the galaxy's rotation.

NGC 5077: A weak, broad (FWZI ~ 4200 km s^{-1}) component of Hα is

present, and the narrow lines have FWHM ~ 450-500 km s^{-1}. Deep Ca + Fe λ6495 absorption is visible in Figure 7b.

NGC 5194: Figure 7b displays strong emission lines that have broader wings than expected for single Gaussians with the same FWHM of ~ 220 km s^{-1}. Cecil and Rose (1984) show that the velocity field near the nucleus is complicated. There is no broad Hα component.

NGC 5195: Extremely deep Balmer absorption is produced by a young stellar population in this amorphous companion to NGC 5194. Hα emission partially fills in the underlying absorption line. A cosmic ray hit the CCD between the [S II] lines (Figure 7b). Rotational broadening contributes to the width of emission lines.

NGC 5273: Stauffer (1982a) first noticed the prominent broad Hα emission in this galaxy, and remarked that it is probably variable. Our high-resolution spectra (Figures 8a and 11) show considerably greater detail, and allow a more unambiguous separation of the broad (FWZI ~ 12000 km s^{-1}) and narrow components. The broad Hα line is slightly stronger (relative to the forbidden lines) in the 1984 spectrum than in the 1982 spectrum, although the change is much smaller than in NGC 5033. Since the same slit width was used in both cases (unlike NGC 5033), the equivalent widths of the emission may be directly compared: in 1982, the equivalent width of the entire Hα + [N II] blend was 100 Å, while in 1984 it was 128 Å.

NGC 5371: The emission lines are fairly broad (FWHM ~ 500 km s^{-1}), but a substantial fraction of this (very roughly 200 km s^{-1}) is due to rotational broadening. No broad component of Hα appears to be present.

NGC 5548: This classical Seyfert (Weedman 1977) has a very broad (FWZI ~ 21000 km s^{-1}), bell-shaped Hα emission line whose equivalent

width is ~ 550–600 Å (Figures 8a and 11). [Fe X]λ6374 is present, along with the usual forbidden lines.

NGC 6482: Emission lines are very weak in this object (Figure 8a); the equivalent width of [N II]λ6583 is only ~ 0.2 Å.

NGC 6500: Broad (FWHM ~ 550–600 km s^{-1}), strong emission lines are present. As in NGC 1052, 3884, and 5005, much of the apparent width is due to rotational broadening. [O I]λ6300 is remarkably strong (Figure 8b), like in the prototypical LINER NGC 1052).

NGC 6501: Extremely faint [N II]λ6583 is the only emission line present in the spectrum (Figure 8b).

NGC 6503: The nucleus and disk are dominated by narrow emission from H II regions (Figure 8b).

NGC 6702: As in NGC 6501, extremely faint [N II]λ6583 is the only visible emission line in this galaxy, which was chosen as an absorption-line template (Figure 8b).

NGC 6951: The intensity ratios and profiles of the emission lines (Figure 8b) resemble those in NGC 5194. Away from the nucleus, the strength of [N II]λ6583 relative to Hα rapidly decreases, and is much smaller than Hα in several prominent H II regions.

NGC 7080: Strong, narrow (FWHM ~ 80–90 km s^{-1}) emission lines from H II regions dominate the spectrum (Figure 9a).

NGC 7217: The strong [N II] lines (FWHM ~ 270 km s^{-1}) are noticeably broader than Hα (FWHM ~ 180 km s^{-1}), possibly because of dilution by Hα absorption. No broad component of Hα is visible in the two spectra (Figure 9a), which were taken with the slit oriented along different position angles.

NGC 7331: Very strong absorption lines dominate the spectrum, but

weak emission is present as well. As in other spectra obtained in July 1982 (Figure 9), the shape of the continuum may be slightly erroneous since an accurately-calibrated flux standard was not used in the reductions (§II).

NGC 7479: Visual inspection of two-dimensional spectra taken at different position angles show a very complicated velocity field in the nucleus of this barred spiral galaxy. This is reflected in the double-peaked appearance of Hα in the two spectra shown in Figure 9b. The [N II] lines, on the other hand, do not exhibit two distinct peaks since the emission-line intensity ratios are not constant throughout the nuclear region.

NGC 7742: Strong, relatively narrow absorption contaminates the emission lines (Figure 9b). The profile of [N II]λ6563 is significantly non-Gaussian.

NGC 7743: Prominent emission lines (FWHM ~ 340 km s^{-1}) are visible, but no broad Hα appears to be present. Once again, Hα is narrower (FWHM ~ 280 km s^{-1}) than the forbidden lines.

It is a pleasure to acknowledge the enthusiastic assistance of Skip Staples, Juan Carrasco, Al Lilge, Dave Tennant, Bob Griffith, Bob Thicksten, and Merle Sweet at Palomar Observatory. The data presented here are the direct product of their support during daytime preparations and nighttime observations. We are also grateful to Bev Oke, Jim Gunn, and the Astro-electronics Lab at Caltech for designing and building the Double Spectrograph. We thank Barbara Zimmerman, Todd Boroson, John Biretta, and Peter Young for providing many of the computer programs

necessary during acquisition and reduction of the spectra. Discussions with Jules Halpern were most enjoyable. This research was supported by the Fannie and John Hertz Foundation through a graduate fellowship to A. V. F., and by NSF grant AST-8216544 to W. L. W. Sargent.

TABLE 1

Journal of Observations

NGC	UT Date	Exp (s)	PA	Aper (")	Fig	EW(H+N) (Å)	Ref
404	1982 Jul 18	1800	100	1x4.1	1a	13.4	
1052	1984 Feb 14	1800	30	2x4.1	1a	48.4	
1068	1984 Feb 14	300	40	2x4.1	1a,10	488	W
1167	1984 Feb 15	1200	10	2x4.1	1a(S)	33.7	
1169	1984 Feb 15	1200	90	2x6.4	1a(S)	5.3	
1275	1984 Feb 15	1200	90	2x4.1	1b,10	428	W
1358	1984 Feb 14	900	30	2x4.1	1b	...	
	1984 Feb 15	1000	22	2x4.1	1b	17.9	
1667	1984 Feb 14	1150	18	2x4.1	1b	...	
	1984 Feb 15	1200	10	2x4.1	1b	44.5	
2146	1984 Feb 15	1200	160	2x4.1	2a	88.5	
2273	1984 Feb 15	1200	0	2x4.1	2a	80.5	
2639	1984 Feb 12	900	75	2x4.1	2a	...	
	1984 Feb 13	1200	136	2x4.1	2a	43.4	
2681	1984 Feb 12	600	85	2x4.1	2a	...	H
	1984 Feb 12	900	85	2x4.1	2a	7.0	H
2685	1984 Feb 15	900	30	2x4.1	2b	3.5	H
2768	1984 Feb 13	1200	40	2x4.1	2b	2.7	H
2787	1984 Feb 15	900	20	2x6.4	2b	4.7	H
2841	1984 Feb 12	1200	60	2x4.1	2b,12	6.2	H
2911	1984 Feb 15	1500	155	2x6.4	2b,3a(S)	15.9	H
2985	1984 Feb 12	1200	35	2x4.1	3a	5.1	H
3031	1984 Feb 12	600	65	2x4.1	3a	33.6	H
	1984 Feb 12	1500	65	2x4.1	3a	...	H
3115	1984 Feb 15	1000	180	2x4.1	3a,12	0.0	
3169	1984 Feb 15	1200	180	2x4.1	3a	6.3	
3185	1984 Feb 15	800	135	2x4.1	3a	33.8	
3227	1984 Feb 13	800	160	2x4.1	3b,10	298	W
3379	1984 Feb 15	800	180	2x4.1	3b	0.7	
3516	1984 Feb 15	500	125	2x4.1	3b,10	280	W
3623	1984 Feb 15	900	135	2x6.4	3b(S)	3.5	
3627	1984 Feb 15	900	135	2x4.1	3b	9.5	
3642	1984 Feb 12	1500	60	2x4.1	4a	20.3	H
3718	1984 Feb 12	1200	60	2x4.1	4a(S)	11.5	H
3884	1984 Feb 15	1500	180	2x4.1	4a(S),13	28.6	
3898	1984 Feb 13	590	80	2x6.4	4a	3.1	H

TABLE 1, continued

3992	1984 Feb 15	600	125	2x6.4	4a(S)	3.3	H
3998	1984 Feb 12	1000	60	2x4.1	4a,10	46.5	H
4036	1984 Feb 12	1200	48	2x4.1	4b	16.2	H
4051	1984 Feb 14	820	90	2x4.1	..	...	W
	1984 Feb 15	400	100	2x4.1	4b,10	172	W
4111	1984 Feb 12	1000	70	2x4.1	4b	5.1	H
4125	1984 Feb 15	600	125	2x4.1	4b(S)	4.2	H
4151	1984 Feb 14	600	90	2x4.1	5a,11	799	W
4192	1984 Feb 12	1200	150	2x4.1	5a	12.9	
4235	1984 Feb 12	1500	180	2x4.1	5a,11	115	
4258	1984 Feb 12	900	150	2x4.1	5a	12.2	H
4274	1984 Feb 15	900	180	2x4.1	5b	14.2	
4278	1984 Feb 15	900	180	2x4.1	5b	22.3	H
4303	1984 Feb 15	1000	180	2x4.1	5b	21.0	
4388	1984 Feb 13	1200	91	2x4.1	5b,11,14	405	
4438	1984 Feb 12	1200	25	2x4.1	6a	37.7	
4450	1984 Feb 13	1200	124	2x4.1	6a	10.8	
4486	1984 Feb 12	800	180	2x4.1	..	...	H
4486	1984 Feb 13	1800	138	1x4.1	6a	61.9	H
	1984 Feb 13	2000	110	1x4.1	6a	...	H
	1984 Feb 13	2000	45	1x4.1	..	...	H
	1984 Feb 13	2000	80	1x4.1	..	...	H
	1984 Feb 13	2000	0	1x4.1	..	...	H
4501	1984 Feb 12	1200	35	2x4.1	6b	12.9	
4569	1984 Feb 13	1200	20	2x4.1	6b	18.9	
4579	1984 Feb 12	1000	150	2x4.1	6b	35.1	
4594	1984 Feb 15	600	180	2x4.1	6b	14.6	H
4736	1984 Feb 15	400	100	2x4.1	7a	2.8	H
4826	1984 Feb 15	500	180	2x4.1	7a	8.4	
5005	1984 Feb 12	1200	70	2x4.1	7a	41.9	
5033	1982 Jul 16	2000	77	1x4.1	7a	57.5	
	1984 Feb 15	900	165	2x4.1	7a,11	38.0	
5055	1984 Feb 15	400	90	2x4.1	7b	1.3	H
5077	1984 Feb 15	1000	180	2x6.4	7b(S)	9.4	H
5194	1984 Feb 15	800	120	2x4.1	7b	42.4	H
5195	1984 Feb 15	600	120	2x4.1	7b	3.8	H

TABLE 1, continued

5273	1982 Jul 19	1500	80	2x4.1	8a	100	
	1984 Feb 13	2000	90	2x4.1	8a,11	128	
5371	1984 Feb 12	1200	35	2x4.1	8a	9.5	H
5548	1984 Feb 15	500	180	2x4.1	8a,11	626	W
6482	1982 Jul 19	600	51	2x4.1	8a(S)	1.1	
6500	1982 Jul 17	1500	61	2x4.1	8b	51.2	
6501	1982 Jul 19	1200	55	2x4.1	8b	0.2	
6503	1982 Jul 17	2400	122	2x4.1	8b	15.2	
6702	1982 Jul 16	1500	112	2x4.1	8b	0.3	
6951	1982 Jul 16	2000	90	2x4.1	8b	25.7	
	1982 Jul 18	2100	180	2x4.1	..	...	
7080	1982 Jul 17	2100	96	2x4.1	9a	27.2	
7217	1982 Jul 16	2000	90	2x4.1	9a	13.6	
	1982 Jul 19	800	180	1x4.1	9a	...	
7331	1982 Jul 18	1500	170	1x4.1	9a	1.1	
7479	1982 Jul 16	1800	186	2x4.1	9b(S)	28.4	
	1982 Jul 18	1500	100	2x4.1	9b(S)	...	
	1982 Jul 19	1000	51	2x4.1	..	...	
7742	1982 Jul 17	1850	160	2x4.1	9b	4.0	
7743	1982 Jul 16	1500	90	2x4.1	9b	21.5	

Notes to Table 1

Column 1: NGC identification number.
Column 2: UT date of observation.
Column 3: Integration time, seconds.
Column 4: Position angle of slit (long dimension of aperture), degrees.
Column 6: Figure number containing plot of spectrum. (S) means spectrum was smoothed with 1.5 Å (FWHM) Gaussian before plotting.
Column 7: Equivalent width of Hα plus [N II]λ6548+6583, Angstroms. At best only partially corrected for Hα absorption.
Column 8: References: H = Heckman (1980); W = Weedman (1977).
Column 5: Effective size of rectangular aperture (arc seconds).

REFERENCES

Abell, G. O., Eastmond, T. S., and Jenner, D. C. 1978, Ap. J. (Letters), 221, L1.

Adams, T. F. 1977, Ap. J. Suppl., 33, 19.

Alloin, D., Pelat, D., Boksenberg, A., and Sargent, W. L. W. 1983, Ap. J., 275, 493.

Baldwin, J. A., Phillips, M. M., and Terlevich, R. 1981, Pub. A.S.P., 93, 5.

Blackman, C. P., Wilson, A. S., and Ward, M. J. 1983, M.N.R.A.S., 202, 1001.

Boksenberg, A., and Netzer, H. 1977, Ap. J., 212, 37.

Boroson, T. A., and Oke, J. B. 1982, Nature, 296, 397.

Boroson, T. A., Oke, J. B., and Green, R. F. 1982, Ap. J., 263, 32.

Cecil, G., and Rose, J. A. 1984, preprint.

Elvis, M., and Van Speybroeck, L. P. 1982, Ap. J. (Letters), 257, L51.

Ferland, G. J., and Netzer, H. 1983, Ap. J., 264, 105.

Filippenko, A. V. 1982, Pub. A.S.P., 94, 715.

———. 1984a, Ap. J., submitted (Paper II).

———. 1984b, A. J., submitted.

Filippenko, A. V., and Halpern, J. P. 1984, Ap. J., in press, Oct. 15 (Paper I).

Filippenko, A. V., and Sargent, W. L. W. 1984a, in preparation (FS).

———. 1984b, in preparation.

Ford, H. C., and Butcher, H. R. 1979, Ap. J. Suppl., 41, 147.

Fosbury, R. A. E., Mebold, V., Goss, W., and Dopita, M. A. 1978, M.N.R.A.S., 183, 549.

Halpern, J. P., and Steiner, J. E. 1983, Ap. J. (Letters), 269, L37.

Heckman, T. M. 1980, Astr. Ap., 87, 152.

Huchra, J. P., Davis, M., Latham, D., and Tonry, J. 1983, Ap. J. Suppl., 52, 89.

Huchra, J. P., Wyatt, W. F., and Davis, M. 1982, A. J., 87, 1628.

Hutchings, J. B. 1983, Pub. A.S.P. 95, 799.

Keel, W. C. 1983a, Ap. J., 269, 466.

———. 1983b, Ap. J. Suppl., 52, 229.

Keel, W. C., and Miller, J. S. 1983, Ap. J. (Letters), 266, L89.

Keel, W. C., and Weedman, D. W. 1978, A. J., 83, 1.

Kent, S. M., and Sargent, W. L. W. 1979, Ap. J., 230, 667.

Koski, A. T., and Osterbrock, D. E. 1976, Ap. J. (Letters), 203, L49.

Malkan, M. A., and Filippenko, A. V. 1983, Ap. J., 275, 477 (MF).

Minkowski, R. 1968, A. J., 73, 842.

Oke, J. B. 1974, Ap. J. Suppl., 27, 21.

Oke, J. B., and Gunn, J. E. 1982, Pub. A.S.P., 94, 586.

———. 1983, Ap. J., 266, 713.

Pagel, B. E. J., and Edmunds, M. G. 1983, Nature, 304, 488.

Peimbert, M., and Torres-Peimbert, S. 1981. Ap. J., 245, 845.

Phillips, M. M., and Malin, D. F. 1982, M.N.R.A.S., 199, 905.

Reichert, G. A., Mason, K. O., Thorstensen, J. R., and Bowyer, S. 1982, Ap. J., 260, 437.

Rose, J. A., and Cecil, G. 1983, Ap. J., 266, 531.

Rose, J. A., and Searle, L. 1982, Ap. J., 253, 556.

Rose, J. A., and Tripicco, M. J. 1984, preprint.

Sandage, A. R., and Tammann, G. A. 1981, A Revised Shapley-Ames Catalog of Bright Galaxies. (Carnegie Institution of Washington, Washington, D.C.).

Seyfert, C. K. 1943, Ap. J., 97, 28.

Shectman, S. A. 1982, in Annual Report of the Director, the Mount Wilson and Las Campanas Observatories (Washington: Carnegie Institution of Washington), p. 676.

Shuder, J. M. 1980, Ap. J., 240, 32.

Shuder, J. M., and Osterbrock, D. E. 1981, Ap. J., 250, 55.

Simkin, S. M., Su, H. J., and Schwartz, M. P. 1980, Ap. J., 237, 404.

Stauffer, J. R. 1982a, Ap. J., 262, 66.

———. 1982b, Ap. J. Suppl., 50, 517.

Véron, P., Lindblad, P. O., Zuiderwijk, E. J., Véron, M. P., and Adam, G. 1980, Astr. Ap., 87, 245.

Weedman, D. W. 1976, Ap. J., 208, 30.

———. 1977, Ann. Rev. Astron. Astrophys., 15, 69.

Wyckoff, S., Wehinger, P., and Gehren, T. 1981, Ap. J., 247, 750.

FIGURE CAPTIONS

Figure 1: Spectra of 8 galaxies (λλ6200-6880, rest frame) are shown with different ordinate offsets. As indicated by straight line segments, data are absent at the extreme blue and red ends in most objects. Unless otherwise noted (Table 1), an effective aperture of 2″ x 4.1″ was used and the displayed spectrum was not smoothed. The instrumental resolution (~ 2.5 Å) is indicated by the Ne + Ar comparison arc (2″ x 4.1″ aperture). Note that the [N II] + Hα blend in NGC 1052 exhibits very faint, broad wings attributed to Hα. They may also be present in NGC 1167 and 1667. The profiles of [O I] and [S II] are very different in NGC 1275, which also shows extremely broad Hα emission (Fig. 10).

Figure 2: Same as Fig. 1, for 9 additional galaxies. Two spectra of NGC 2681 were obtained in separate exposures at different locations of the CCD, and indicate that most of the observed features are real. Broad wings of Hα emission are visible in NGC 2639, and possibly in NGC 2911. Fig. 12 demonstrates that the very broad, faint "bump" around Hα in NGC 2841, 2787, and many of the other surveyed objects is due to the underlying stellar continuum. Hα absorption is prominent in several galaxies.

Figure 3: Same as Fig. 1, for 10 additional galaxies. The two spectra of NGC 3031 are independent of each other, but appear virtually identical. Note the great width (especially the FWZI) of [O I]λ6300 in comparison with [S II]λ6716,6731, as well as the broad wings of Hα. NGC 3227 and 3516 are well-known type 1 Seyfert galaxies (Fig. 10). [O I]λ6364 often appears weaker than one-third of [O I]λ6300 due to

strong underlying Fe I absorption.

Figure 4: Same as Fig. 1, for 10 additional galaxies. NGC 3718, 3884 (Fig. 13), and 3998 (Fig. 10) exhibit broad Hα emission; a similar component may be present in NGC 3642 and 4036 as well. NGC 4051 is a known Seyfert 1 galaxy (Fig. 10). [O I]λ6300 is noticeably broader than [N II] and [S II] in NGC 3998.

Figure 5: Same as Fig. 1, for 8 additional galaxies. Broad Hα emission is perceptible in NGC 4258, 4278, and 4388 (Fig. 14). It is very prominent and asymmetrical in the Seyfert galaxies NGC 4151 and 4235 (see also Fig. 11). [O I]λ6300 is broader than the [S II] and [N II] lines in NGC 4235, 4258, and many of the other objects (Figs. 1-9).

Figure 6: Same as Fig. 1, for 7 additional galaxies. Note the weak, extended Hα emission in NGC 4486, 4579, 4594, and possibly 4450. The stellar continuum is very strong in most of the observed galaxies, as indicated by the particularly deep Ca + Fe blend at ~ λ6495 in NGC 4450 and 4594.

Figure 7: Same as Fig. 1, for 8 additional galaxies. Exceptionally strong Hα absorption is visible in NGC 4736 and 5195. A broad component of Hα emission is present in NGC 5033 and 5077. The line profile in the former clearly shows evidence of variability. A cosmic ray was detected by the CCD between the two [S II] lines in NGC 5195.

Figure 8: Same as Fig. 1, for 10 additional galaxies. The broad Hα component in NGC 5273 was slightly larger (relative to the continuum and the forbidden lines) in February 1984 than in July 1982. NGC 5548 is a well-known type 1 Seyfert galaxy (Fig. 11). NGC 6503 is one of the few galaxies in the survey whose emission lines are essentially unresolved and betray the dominance of H II regions in the nucleus.

Figure 9: Same as Fig. 1, for 6 additional galaxies. The two spectra of NGC 7479 differ a little since the slit was not oriented at the same position angles (Table 1) and sampled slightly different regions of the dynamically complex nucleus. Strong stellar absorption is visible in NGC 7331 and 7742, greatly affecting the observed strength and profile of the Hα emission line.

Figure 10: Spectra are shown of four classical Seyfert galaxies as well as NGC 3998 and NGC 1275 (a peculiar Seyfert). All are shifted to zero redshift. The ordinate represents the logarithm of the flux per unit frequency interval, offset by an additive constant so that AB = 0.0 at the peak of the strongest emission line (usually Hα). Very high flux levels are not plotted in order to emphasize the continuum and weak emission lines. Note the very broad component of Hα in NGC 1275, which indicates a resemblance to type 1 Seyferts. A similar, but much weaker, line is evident in the elliptical radio galaxy NGC 3998.

Figure 11: Same as Fig. 10, but for six other Seyfert galaxies. Note the large differences in the profile of Hα among the objects. NGC 5548 and 4388 (see also Fig. 14) represent opposite extremes in the relative strength of the broad Hα emission.

Figure 12: The spectrum of NGC 2841 is shown in (a). It appears as though a faint, very broad component of Hα emission may be present. In (b), however, NGC 3115 exhibits the same broad feature near Hα, but is devoid of other emission lines. NGC 3115 is subtracted from NGC 2841 in (c); note that [O I]λ6300 emission is now visible, and that the intensity ratio of the [S II] lines differs from that in (a) due to the removal of underlying Ca I λ6718 absorption. Spectra (d) and (e) are of 69 ν Gem (M0 III) and 46 τ Gem (K2 III), respectively, showing that the

broad dip near λ6700 which gives rise to the apparent "bump" near Hα in NGC 2841 and 3115 is produced by TiO in late-K and early-M stars. The smooth continuum in the A3 V star 83 φ Gem (f) illustrates the excellent relative flux-calibration achieved in the data.

Figure 13: The Hα + [N II] blend in the X-ray LINER NGC 3884 is decomposed into three independent Gaussians in (a), with the residuals shown in (b). A reasonably good fit is achieved, but broad wings appear to be present in the data. Introducing a fourth, broad Gaussian (presumably Hα emission) in (c) produces substantially better agreement. The oscillatory residuals (d) indicate that the narrow components are actually not exactly symmetrical.

Figure 14: Hα + [N II] emission is shown at two different scales (X1 and X50) for NGC 4388, an X-ray galaxy in the Virgo cluster. The forbidden lines exhibit extended wings. In contrast with most type 2 Seyferts, however, the wings are more prominent redward than blueward of the line peaks. This is especially obvious in the [S II] doublet (Fig. 5b). An extremely weak, fairly symmetrical, broad component of Hα is visible in the expanded (X50) plot.

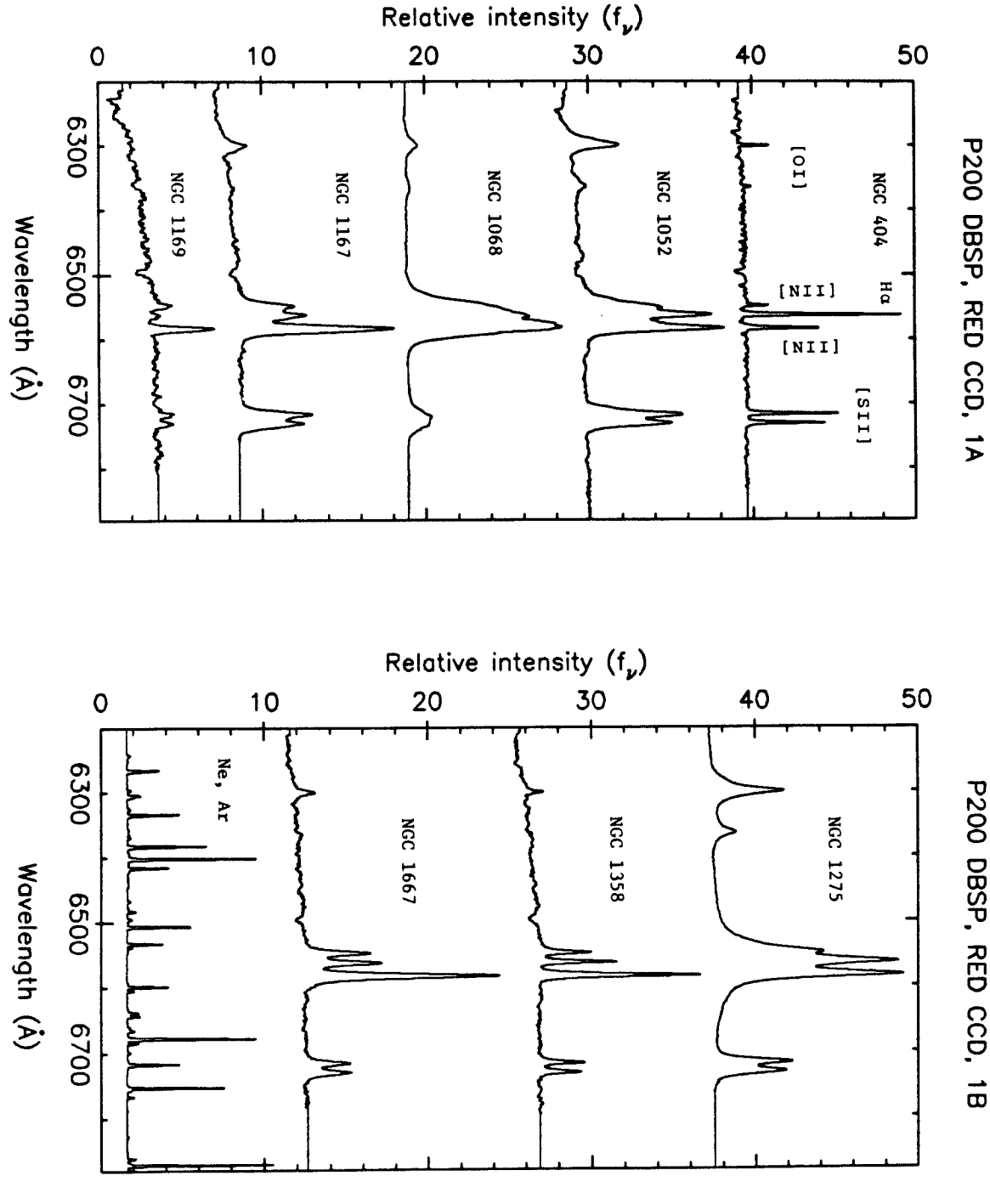
P200 DBSP, RED CCD, 1A
Relative intensity (f_ν)
0
10
20
30
40
50
Wavelength (Å)
6300
6500
6700
NGC 404
Hα
[NII]
[NII]
[SII]
[OI]
NGC 1052
NGC 1068
NGC 1167
NGC 1169
P200 DBSP, RED CCD, 1B
Relative intensity (f_ν)
0
10
20
30
40
50
Wavelength (Å)
6300
6500
6700
NGC 1275
NGC 1358
NGC 1667
Ne, Ar

Figure 1

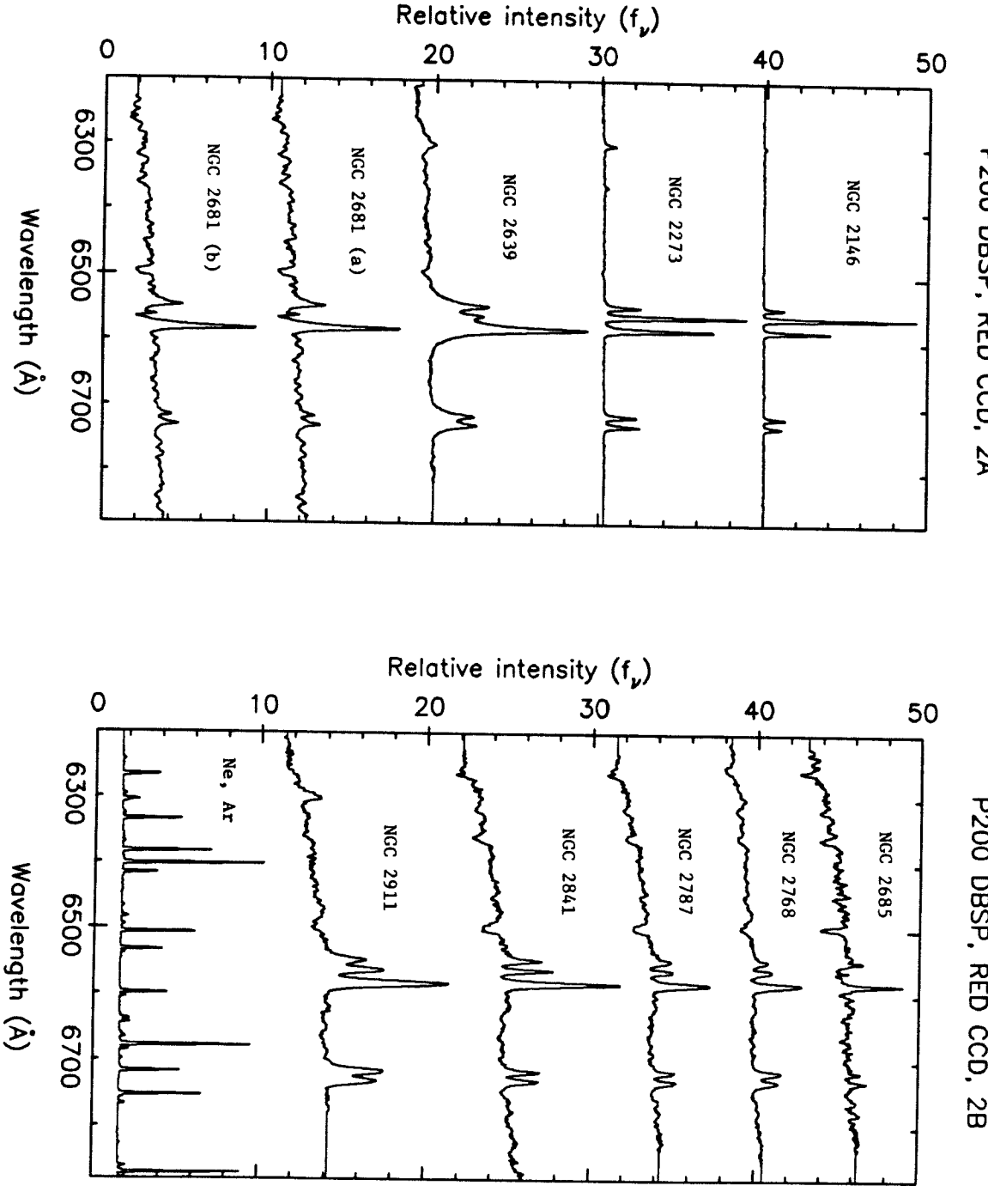
P200 DBSP, RED CCD, 2A
Relative intensity (f_ν)
0
10
20
30
40
50
NGC 2146
NGC 2273
NGC 2639
NGC 2681 (a)
NGC 2681 (b)
6300
6500
6700
Wavelength (Å)
P200 DBSP, RED CCD, 2B
Relative intensity (f_ν)
0
10
20
30
40
50
NGC 2685
NGC 2768
NGC 2787
NGC 2841
NGC 2911
Ne, Ar
6300
6500
6700
Wavelength (Å)

Figure 2

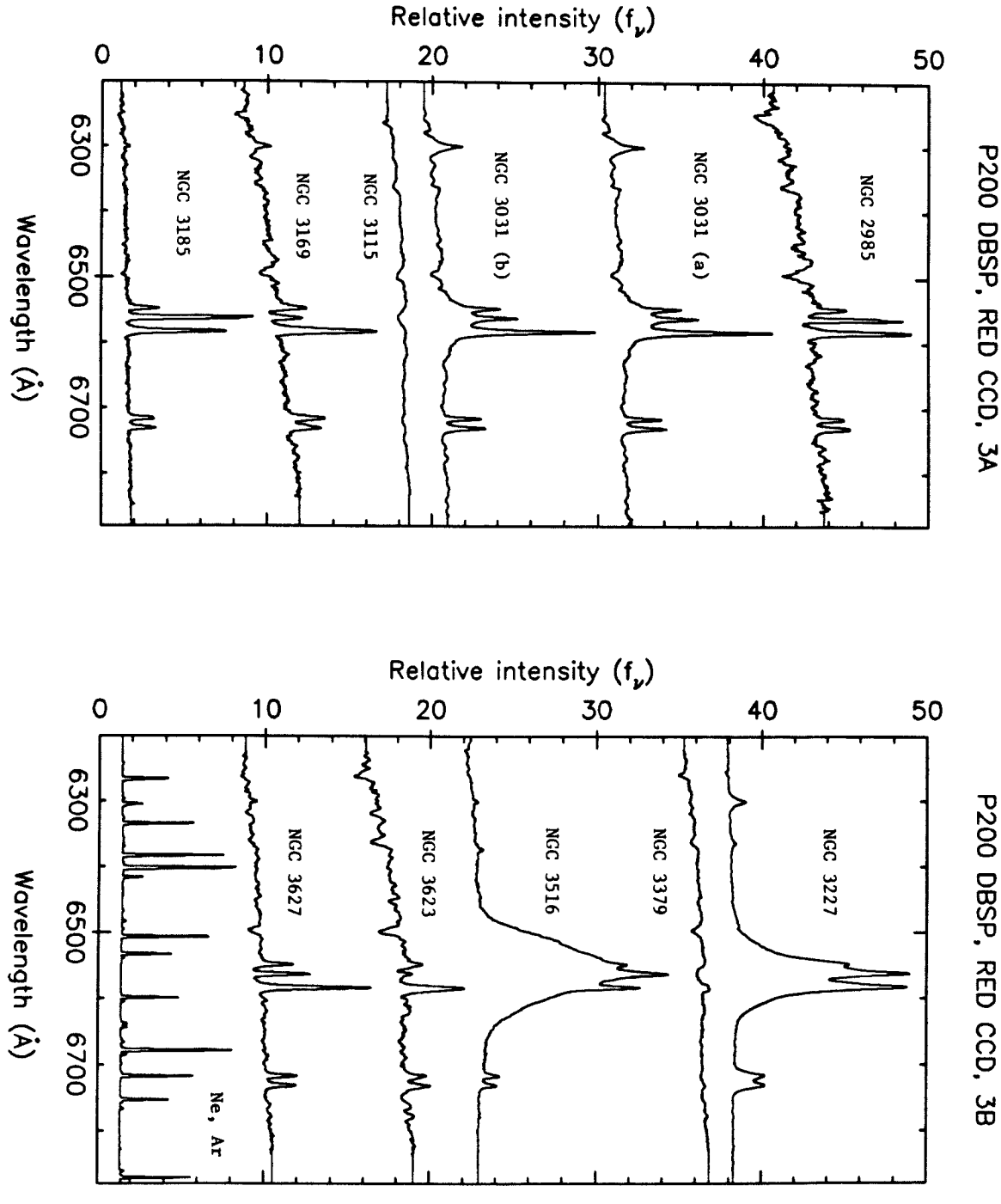
P200 DBSP, RED CCD, 3A
Relative intensity (f_ν)
0
10
20
30
40
50
NGC 2985
NGC 3031 (a)
NGC 3031 (b)
NGC 3115
NGC 3169
NGC 3185
6300
6500
6700
Wavelength (Å)
P200 DBSP, RED CCD, 3B
Relative intensity (f_ν)
0
10
20
30
40
50
NGC 3227
NGC 3379
NGC 3516
NGC 3623
NGC 3627
Ne, Ar
6300
6500
6700
Wavelength (Å)

Figure 3

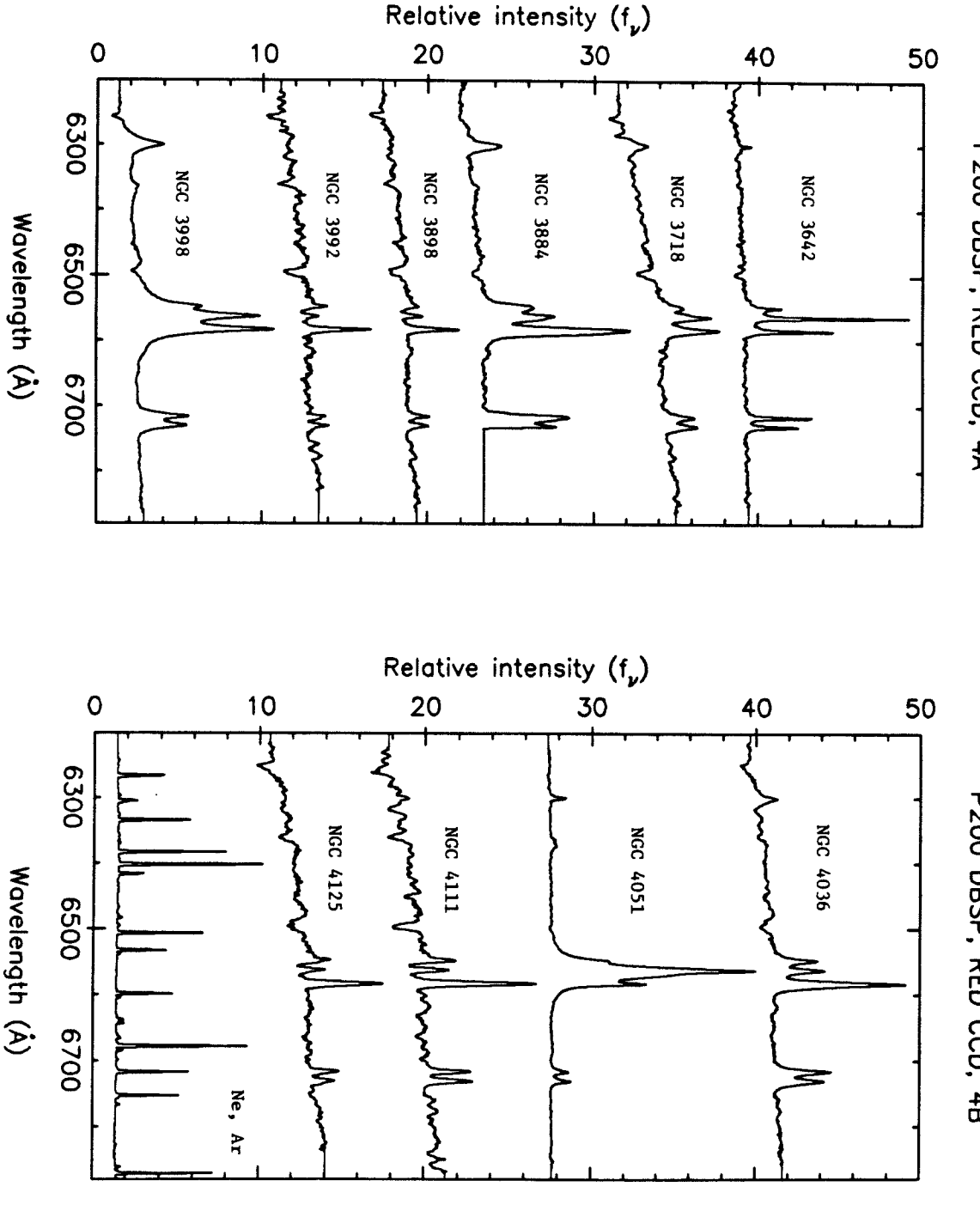
P200 DBSP, RED CCD, 4A
Relative intensity (f_ν)
0
10
20
30
40
50
NGC 3642
NGC 3718
NGC 3884
NGC 3898
NGC 3992
NGC 3998
6300
6500
6700
Wavelength (Å)
P200 DBSP, RED CCD, 4B
Relative intensity (f_ν)
0
10
20
30
40
50
NGC 4036
NGC 4051
NGC 4111
NGC 4125
Ne, Ar
6300
6500
6700
Wavelength (Å)

Figure 4

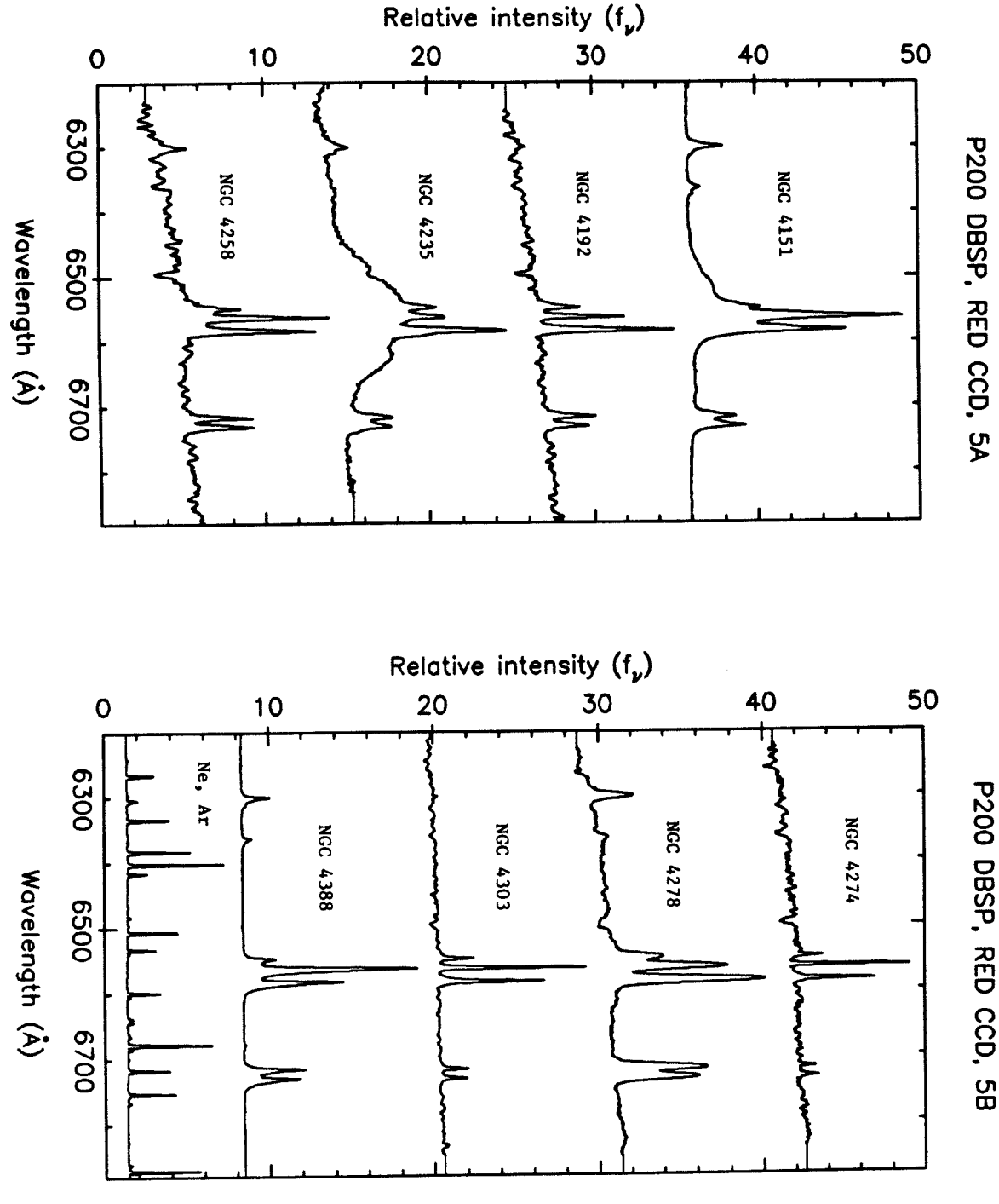
Relative intensity (f_ν)
0
10
20
30
40
50
NGC 4151
NGC 4192
NGC 4235
NGC 4258
6300
6500
6700
Wavelength (Å)
P200 DBSP, RED CCD, 5A
Relative intensity (f_ν)
0
10
20
30
40
50
NGC 4274
NGC 4278
NGC 4303
NGC 4388
Ne, Ar
6300
6500
6700
Wavelength (Å)
P200 DBSP, RED CCD, 5B

Figure 5

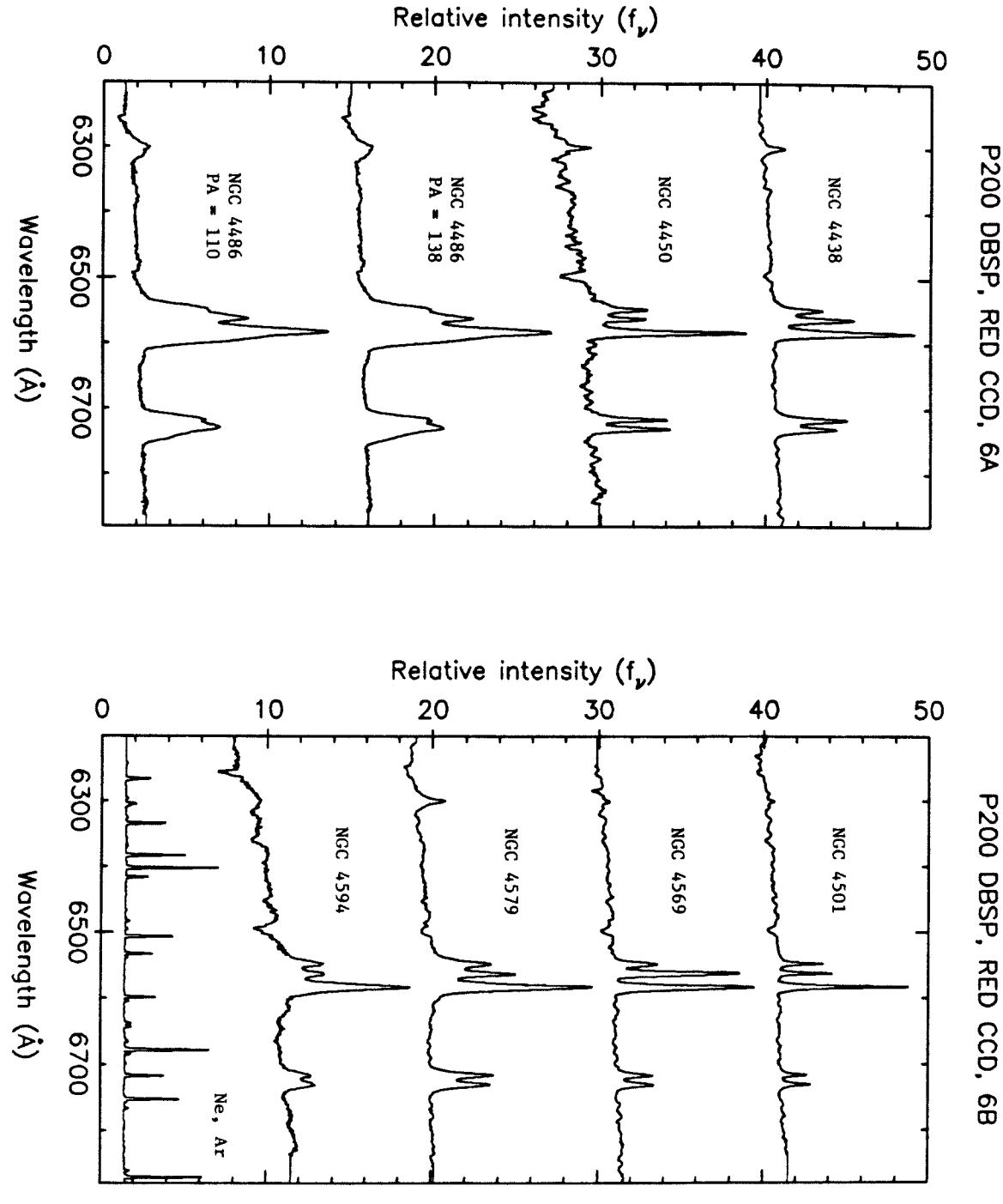
Relative intensity (f_ν)
0
10
20
30
40
50
6300
6500
6700
Wavelength (Å)
NGC 4438
NGC 4450
NGC 4486
PA = 138
NGC 4486
PA = 110
P200 DBSP, RED CCD, 6A
NGC 4501
NGC 4569
NGC 4579
NGC 4594
Ne, Ar
P200 DBSP, RED CCD, 6B

Figure 6

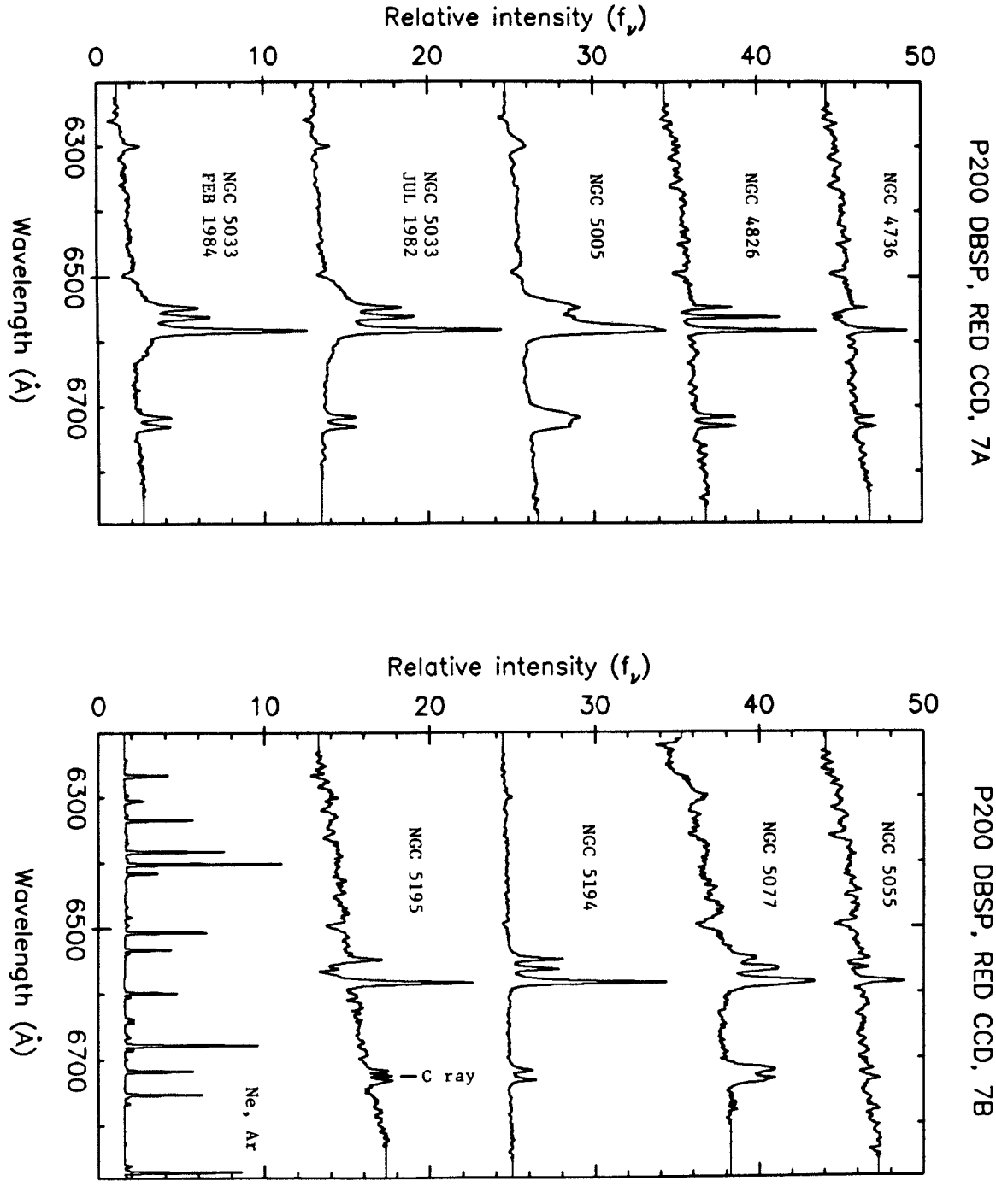
Relative intensity (f_ν)
0
10
20
30
40
50
6300
6500
6700
Wavelength (Å)
NGC 4736
NGC 4826
NGC 5005
NGC 5033
JUL 1982
NGC 5033
FEB 1984
P200 DBSP, RED CCD, 7A
Relative intensity (f_ν)
0
10
20
30
40
50
6300
6500
6700
Wavelength (Å)
NGC 5055
NGC 5077
NGC 5194
NGC 5195
C ray
Ne, Ar
P200 DBSP, RED CCD, 7B

Figure 7

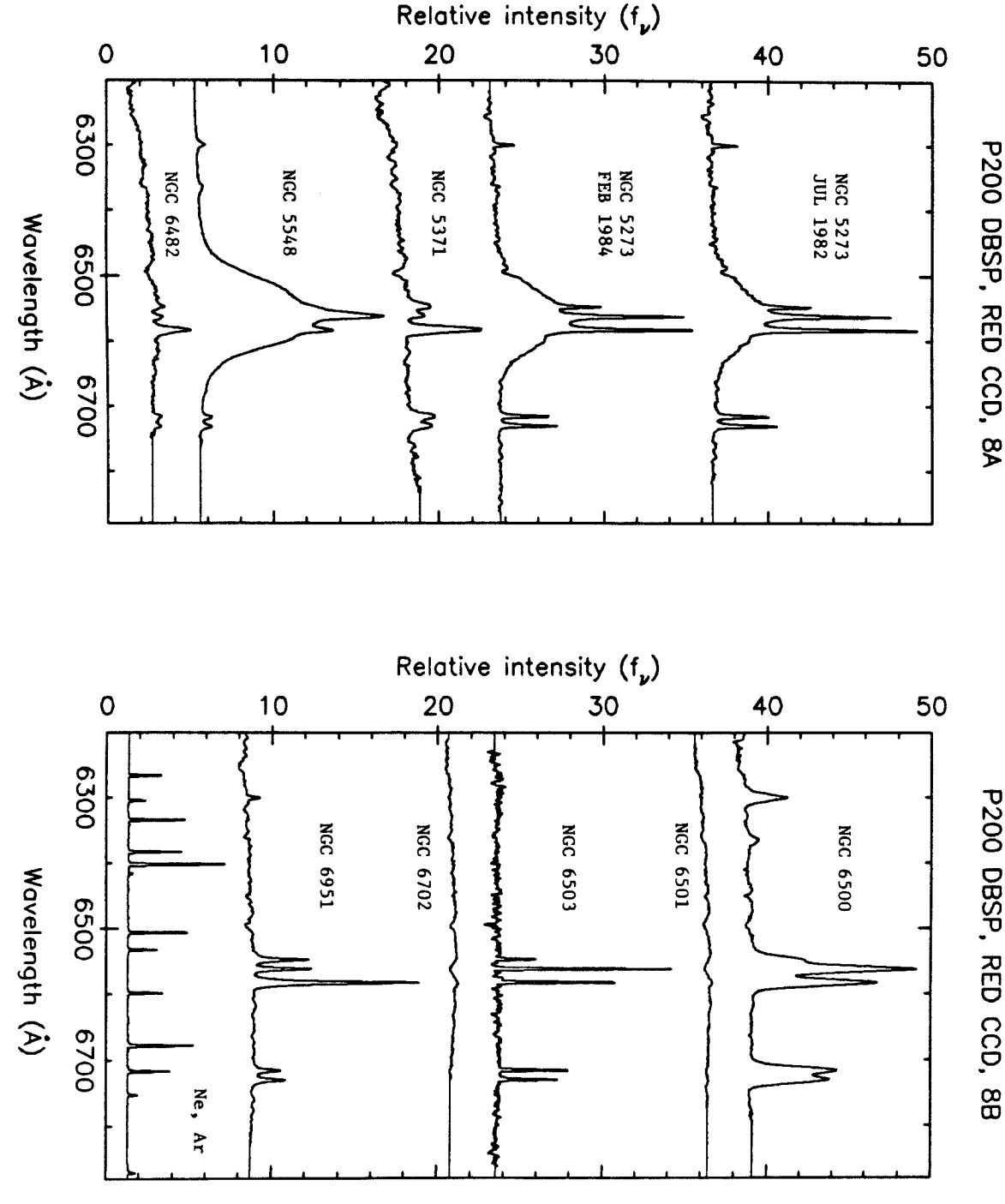
Relative intensity (f_ν)
0
10
20
30
40
50
6300
6500
6700
Wavelength (Å)
NGC 5273
JUL 1982
NGC 5273
FEB 1984
NGC 5371
NGC 5548
NGC 6482
P200 DBSP, RED CCD, 8A
Relative intensity (f_ν)
0
10
20
30
40
50
6300
6500
6700
Wavelength (Å)
NGC 6500
NGC 6501
NGC 6503
NGC 6702
NGC 6951
Ne, Ar
P200 DBSP, RED CCD, 8B

Figure 8

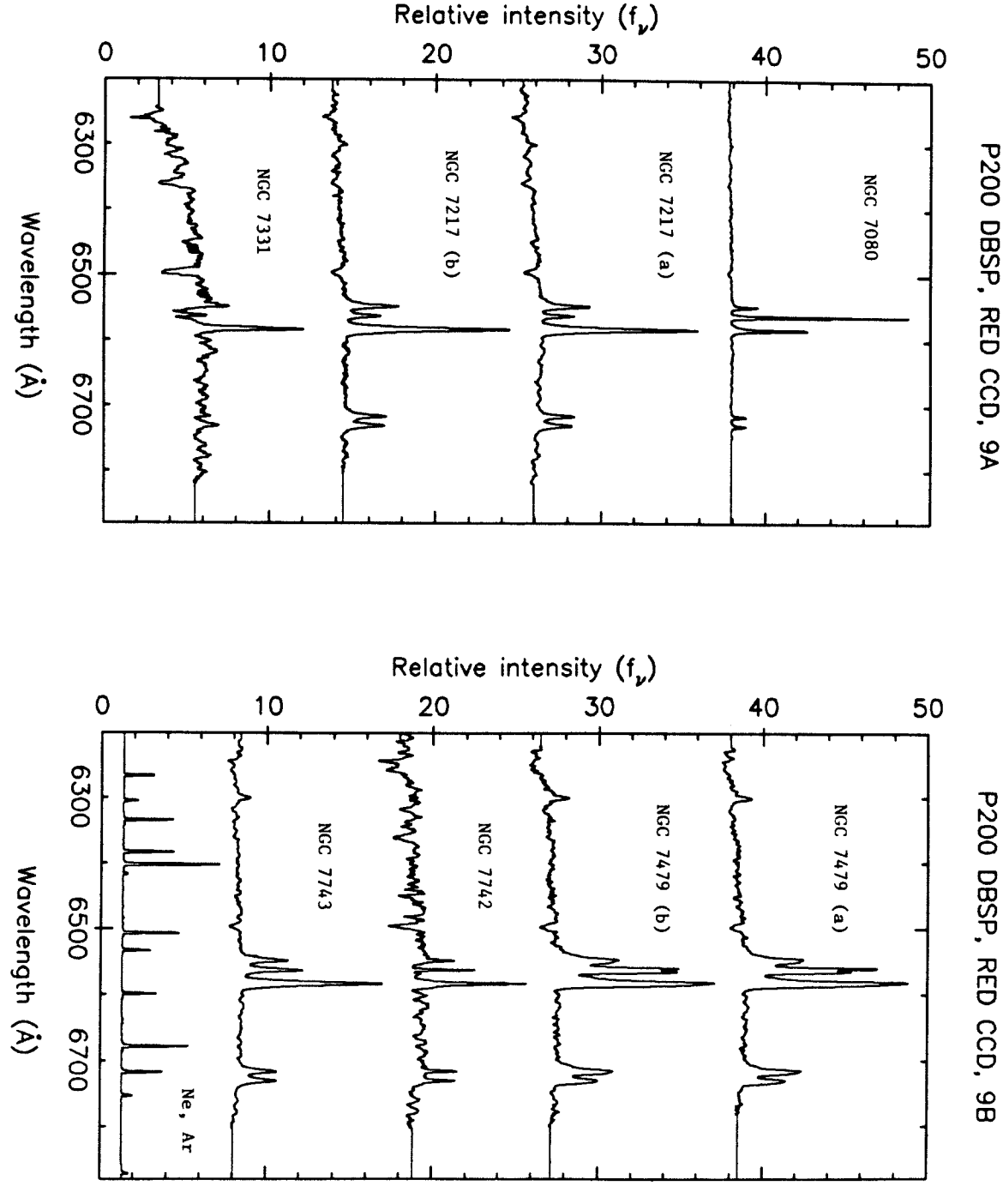
Relative intensity (f_ν)
0
10
20
30
40
50
6300
6500
6700
Wavelength (Å)
NGC 7331
NGC 7217 (b)
NGC 7217 (a)
NGC 7080
P200 DBSP, RED CCD, 9A
Relative intensity (f_ν)
0
10
20
30
40
50
6300
6500
6700
Wavelength (Å)
Ne, Ar
NGC 7743
NGC 7742
NGC 7479 (b)
NGC 7479 (a)
P200 DBSP, RED CCD, 9B

Figure 9

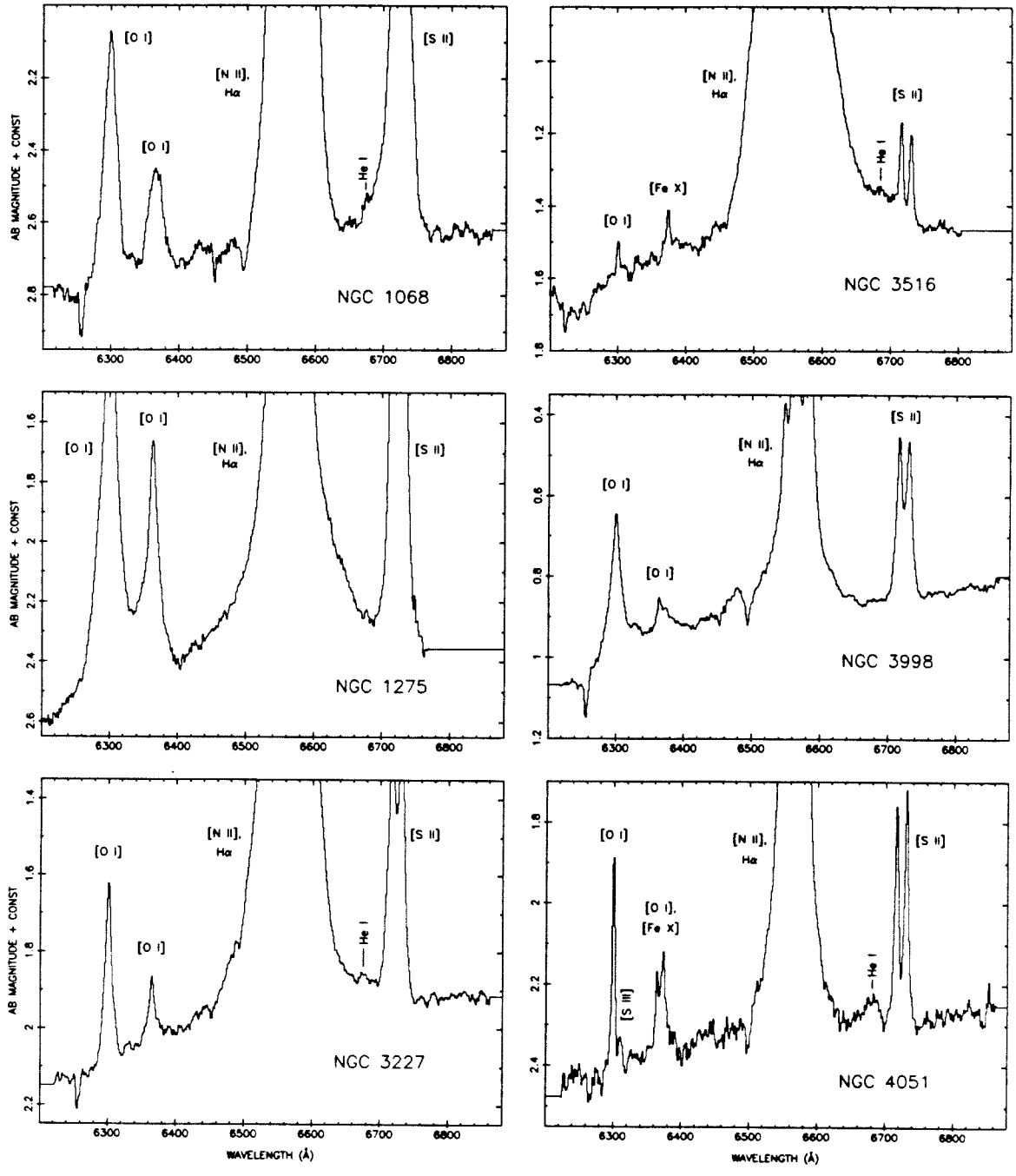
NGC 1068
NGC 3516
NGC 1275
NGC 3998
NGC 3227
NGC 4051
[O I]
[N II], Hα
[S II]
He I
[Fe X]
[S III]
AB MAGNITUDE + CONST
WAVELENGTH (Å)

Figure 10

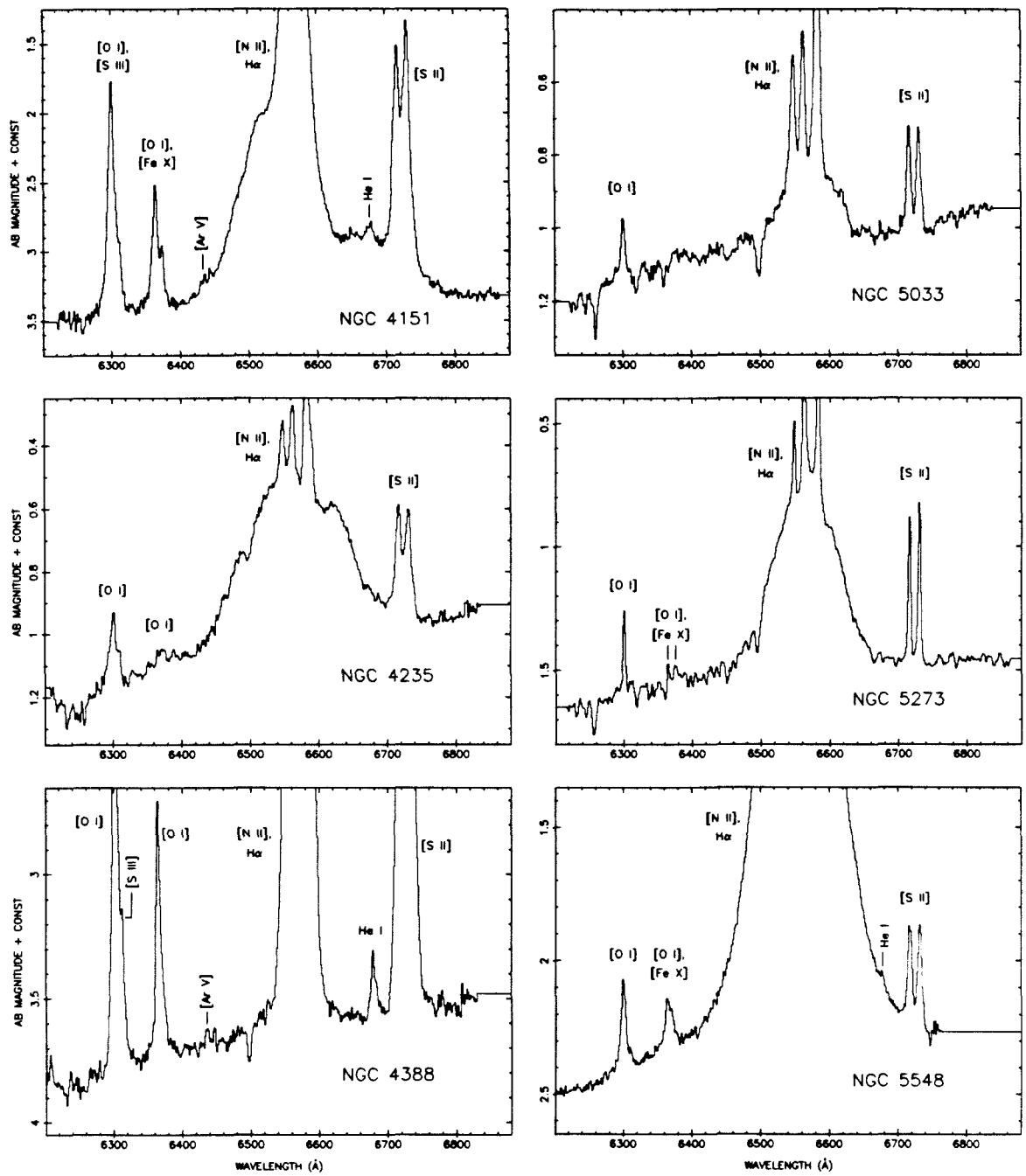
NGC 4151
NGC 5033
NGC 4235
NGC 5273
NGC 4388
NGC 5548
[O I],
[S III]
[O I],
[Fe X]
[Ar V]
[N II],
Hα
He I
[S II]
[O I]
[O I]
[Fe X]
[S III]
AB MAGNITUDE + CONST
WAVELENGTH (Å)

Figure 11

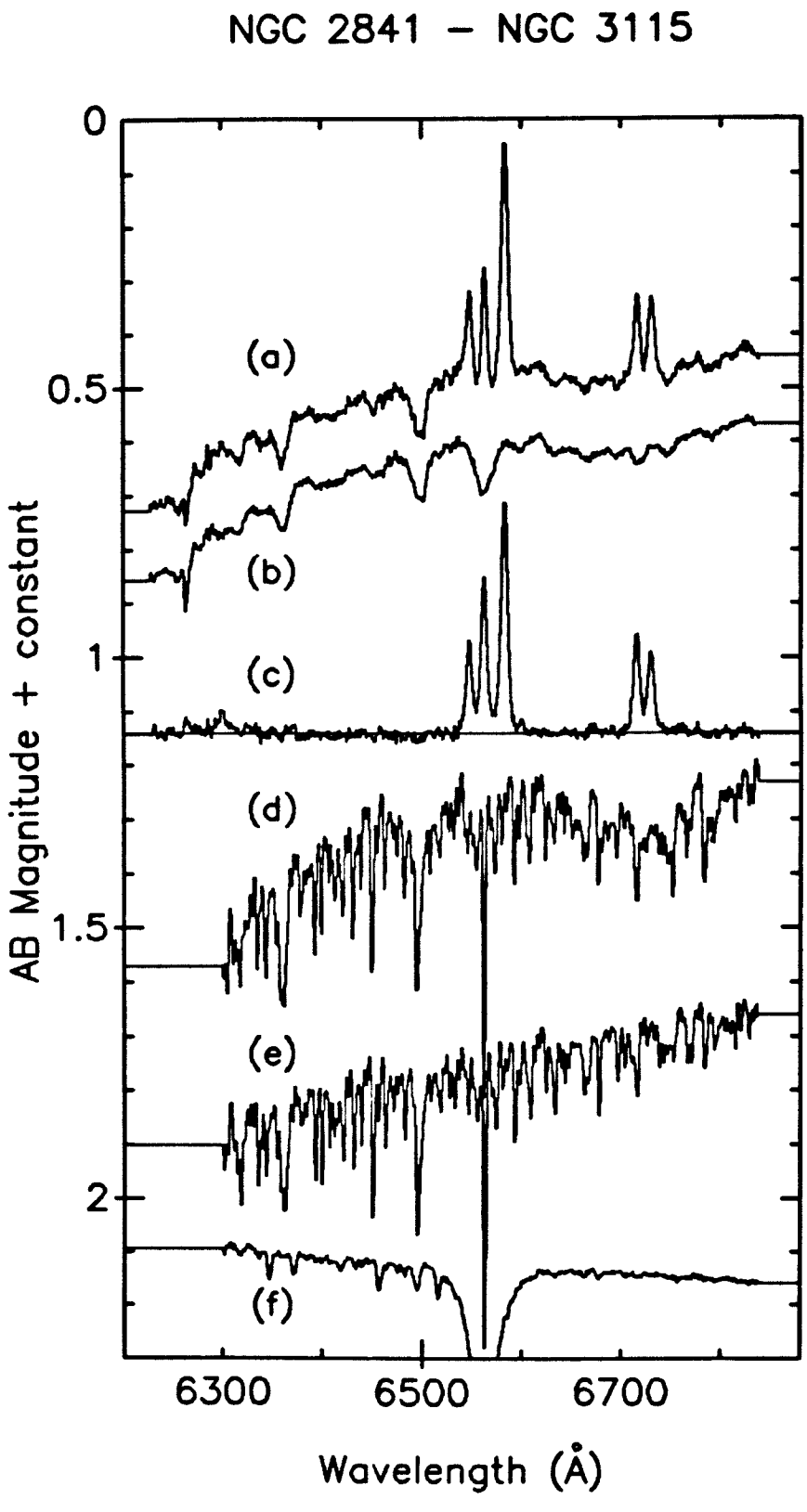
NGC 2841 – NGC 3115
0
0.5
1
1.5
2
AB Magnitude + constant
(a)
(b)
(c)
(d)
(e)
(f)
6300
6500
6700
Wavelength (Å)

Figure 12

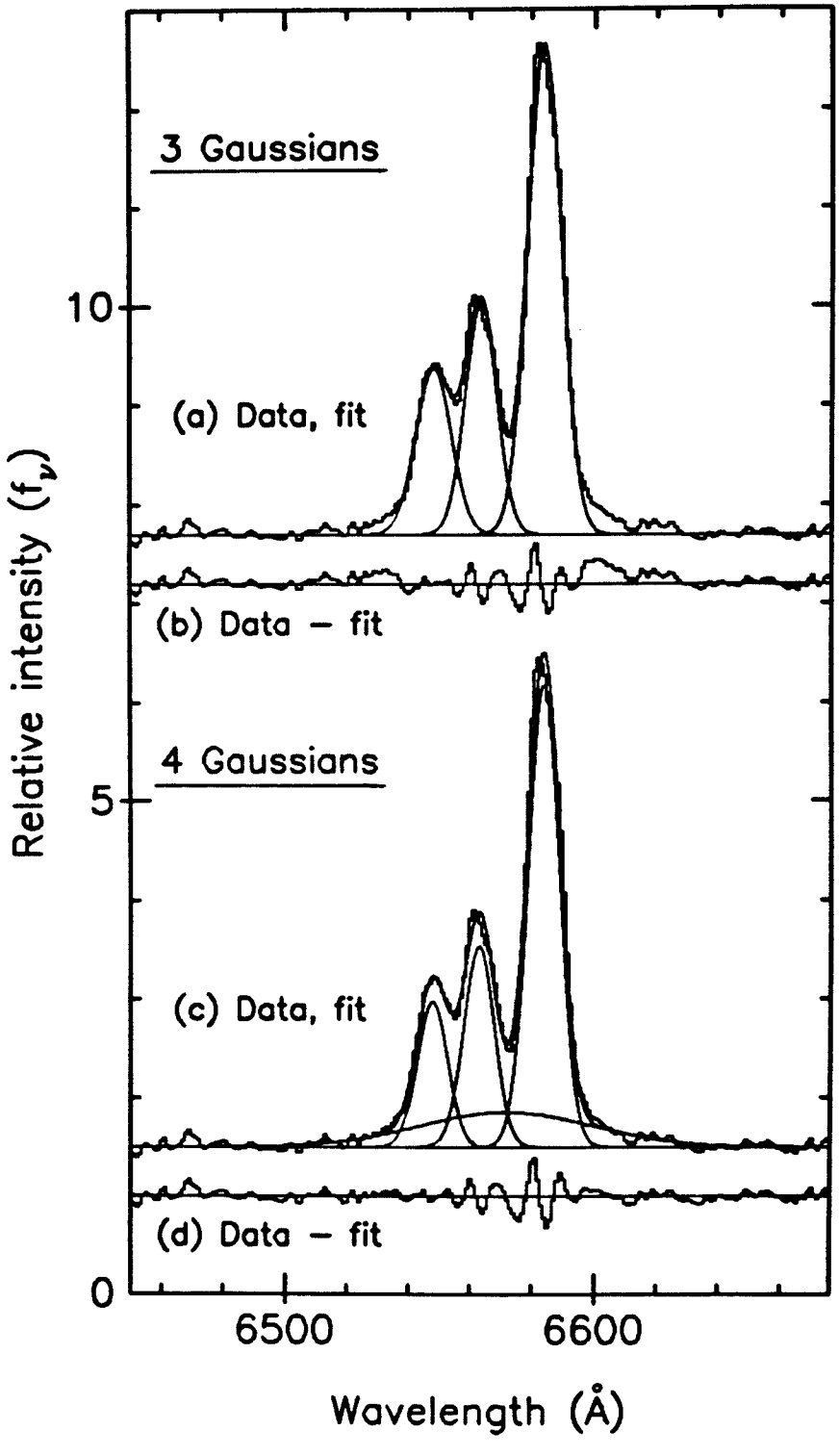
NGC 3884
3 Gaussians
(a) Data, fit
(b) Data − fit
4 Gaussians
(c) Data, fit
(d) Data − fit
Relative intensity (f_ν)
10
5
0
6500
6600
Wavelength (Å)

Figure 13

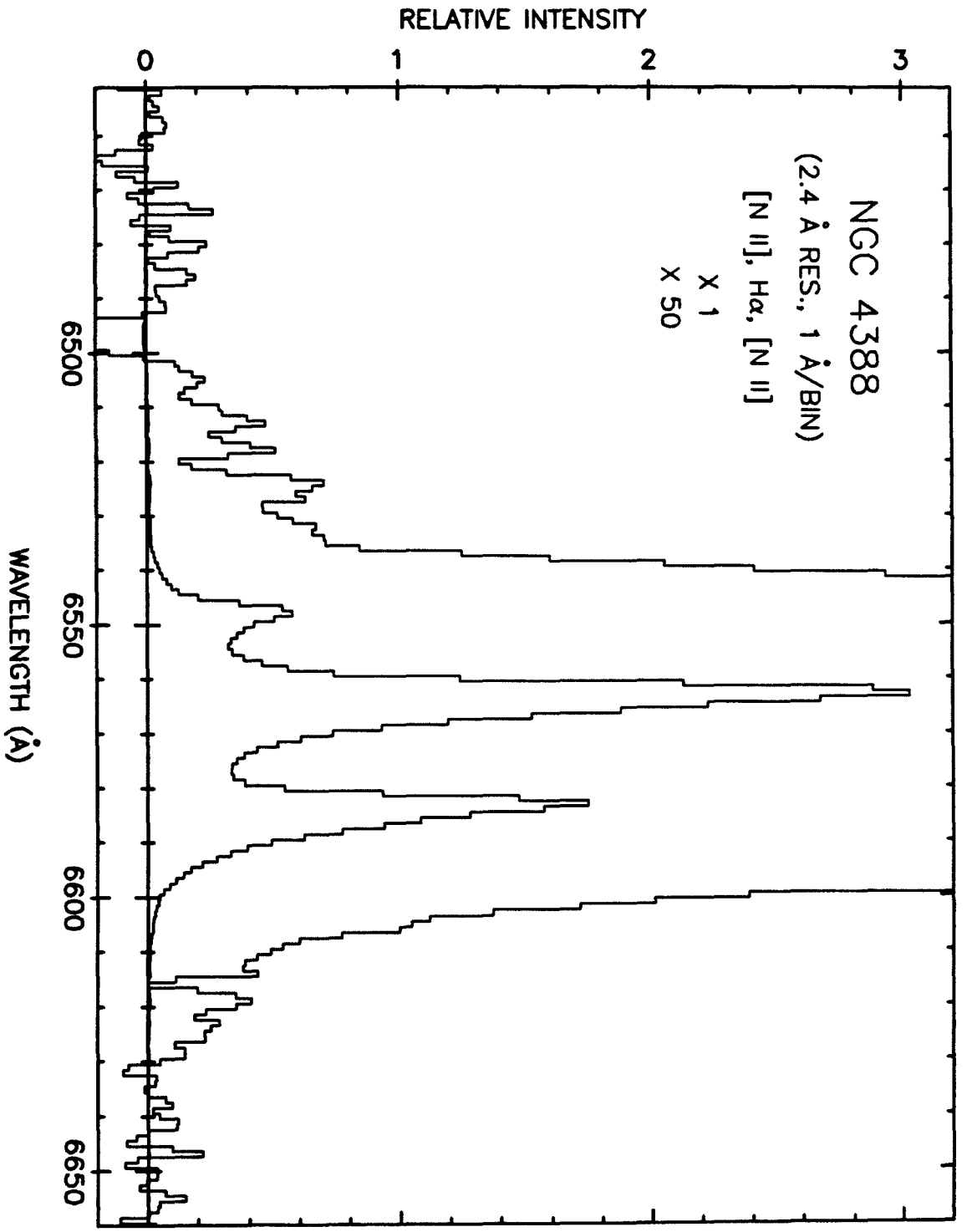
RELATIVE INTENSITY
0
1
2
3
NGC 4388
(2.4 Å RES., 1 Å/BIN)
[N II], Hα, [N II]
X 1
X 50
WAVELENGTH (Å)
6500
6550
6600
6650

Figure 14

CHAPTER 6

Optical Spectrophotometry of the Narrow-Line X-Ray Galaxy NGC 7314.

Alexei V. Filippenko

To be submitted for publication, The Astronomical Journal

In all things of nature

there is something of the marvelous.

Aristotle

ABSTRACT

Optical spectrophotometry of NGC 7314 confirms a previous identification with the X-ray source H2233-261 (2A2237-256) and reveals features which shed light on the remarkable physical conditions near its nucleus.

The relative intensities of emission lines are typical of those seen in type 2 Seyferts, but their widths (FWHM ~ 120-150 km s^{-1}) are smaller than in all other known AGNs. Hence, production of nonstellar ionizing radiation in a galactic nucleus is not necessarily associated with large turbulent or systematic motions among the narrow-line clouds.

A broad (FWZI ~ 5000 km s^{-1}) component is present in the Hα line, and its profile is nearly logarithmic. An even closer approximation is provided by the first exponential integral, which suggests that gas flows radially away from the nucleus in a force-free environment.

The equivalent width (~ 150-200 Å) of the broad Hα emission implies that the covering fraction of broad-line clouds may be large (~ 0.9), and the very weak corresponding component of Hβ ($\underline{I}$(Hα)/$\underline{I}$(Hβ) ~ 50) demonstrates that these lines are severely reddened. However, the power-law slope of the nonstellar UV radiation incident on the narrow-line gas is quite flat ($f_\nu \propto \nu^{-1.1}$), as indicated by the great relative strength of He II λ4686. If this radiation suffers as much reddening as the broad lines, then its initial spectral energy distribution must be considerably flatter than that of luminous quasars, a highly unlikely situation. Therefore, most of the dust is probably located within or near the broad-line clouds rather than in the low-density confining medium, and it does not affect radiation which

passes through holes between the clouds.

Subject headings: galaxies: individual (NGC 7314)—galaxies: nuclei
—galaxies: Seyfert—line profiles—spectrophotometry—
X-rays: sources

I. INTRODUCTION

NGC 7314 is a relatively new member of the rapidly-growing list of interesting emission-line galaxies. Although it is bright, nearby ($\underline{v}$ = 1426 km s^{-1}), and an X-ray source, it received little attention prior to the extensive search for X-ray variability conducted with the Ariel V Sky Survey Instrument (Marshall, Warwick, and Pounds 1981). This is probably due to its southern declination, and to the fact that the Ariel V coordinates (2237-256) differ substantially from its optical position of 2233-263 (epoch 1950.0).

Marshall, Warwick, and Pounds (1981) reported that the X-ray luminosity of 2A2237-256 in the 2-10 keV band was probably constant at a value of 3.3 x 10^{42} erg s^{-1} (H_o = 50 km s^{-1} Mpc^{-1}) during the 5-year period of the Ariel V survey (1974-1979). This luminosity is smaller than that of most type 1 Seyferts and narrow-line X-ray galaxies (Halpern 1982; Mushotzky 1982), but larger than in classical type 2 Seyferts (Kriss 1982).

Piccinotti *et al.* (1982) observed NGC 7314 (H2233-261) as part of the HEAO 1 A-2 experiment. During the first scan, the luminosity in the 2-10 keV range was 4 x 10^{42} erg s^{-1}, whereas 6 months later the value was found to be 5.72 x 10^{42} erg s^{-1}. This represents only a marginally significant increase, so X-ray variability of the source has not been demonstrated conclusively.

The identification of H2233-261 with NGC 7314 is not completely certain, but the X-ray luminosity is above the lower bound chosen by Piccinotti *et al.* (1982) in their luminosity function of active galaxies. Moreover, NGC 7314 (type Sc) was included in a large

spectroscopic survey of bright spiral galaxies conducted by Stauffer (1982b) and he concluded that the gas is photoionized by a nonthermal source (Stauffer 1982a). Also, Stauffer (1982a) mentioned the probable presence of a broad component of Hα having full width at half-maximum (FWHM) ~ 1400 km s^{-1}.

Because of these interesting properties, new optical spectra having moderate resolution (~ 2.5 Å) were obtained as part of an extensive investigation of the physical conditions in emission-line galaxies. The observations and results will be presented in the following sections.

II. THE OPTICAL SPECTRUM

a) Observations

Spectra of NGC 7314 were obtained with the Intensified Reticon Detector (Shectman 1982) at the Cassegrain focus of the 2.5 m du Pont telescope at Las Campanas Observatory (Table 1). Second-order light contaminated the red portions of the low-resolution (~ 5 Å) spectrum, but all other data were unaffected. Various comparison arcs were also measured to determine the wavelength scale, and small spatial irregularities in the sensitivity of the Reticon were removed with the aid of a lengthy exposure to a featureless continuum.

The standard stars GD-248 and G158-100 (Filippenko and Greenstein 1984) were observed to calibrate the spectral response of the system. GD-248 (m_V = 15.08) is a DQ white dwarf with only two or three extremely weak absorption lines at optical wavelengths (making the spectral class almost DC), whereas G158-100 (m_V = 14.87) is a very metal-deficient G subdwarf. Relatively accurate energy distributions were determined with the Multichannel Spectrophotometer (Oke 1969) on the Hale telescope at

Palomar from comparisons with secondary standards (Oke and Gunn 1983). The nearly featureless continua of GD-248 and G158-100 provide greater reliability in flux calibration than the DA and DB stars listed by Oke (1974) and Stone (1974, 1977), and their faintness obviates the necessity of using a neutral-density filter when observing with photon-counting devices on large telescopes.

The nucleus of NGC 7314 and the sky 27.4" away were observed for equal times in each of two rectangular apertures (2" x 4"), so accurate subtraction of atmospheric emission lines was possible. Several lines from H II regions located in the outer sections of the object were detected in the sky spectra, and these were easily eliminated before proceeding with the sky subtraction. Weak continuum radiation from the galaxy proved to be a somewhat greater nuisance in the sky spectra, but it did not affect the measured intensities of emission lines. Relative light losses were minimized by observing the galaxy at small air masses. In addition, the long dimension of the entrance aperture was aligned along the direction of atmospheric refraction (Filippenko 1982) when observing the standards. Some of the data were obtained under photometric conditions, and excellent flux continuity in regions of overlap was produced by applying gray multiplicative factors to spectra taken through thin cirrus clouds.

b) Qualitative Overview

Figures 1a and 1b illustrate the entire optical spectrum rebinned to a resolution of 4 $\mathring{A}$ bin^{-1}. It was obtained by adding together overlapping spectra taken on different nights. The weight assigned to each bin in regions of overlap was proportional to the number of

detected photons in the raw data. Both axes are plotted on a linear scale, and wavelengths refer to the rest frame of the object. The flux per unit frequency interval has not been corrected for reddening.

Despite the modest spectral resolution, it is immediately apparent that the emission lines are extremely narrow, especially in comparison with those in classical Seyferts (Weedman 1977). At first glance, the spectrum resembles those of "isolated extragalactic H II regions" (Sargent and Searle 1970), especially since [O III]λ5007 is so much more intense than Hβ. The gas in these objects is clearly ionized by radiation from hot young stars, however, and their very low metal abundances give rise to very weak [N II]λ6583 relative to Hα, unlike the case in NGC 7314. In fact, Searle (1971) demonstrated that H II regions never exhibit the combination of $\underline{I}$([O III]λ4959+5007)/$\underline{I}$(Hβ) and $\underline{I}$([N II]λ6548+6583)/$\underline{I}$(Hα) which characterizes NGC 7314. The ratios are consistent with photoionization models, on the other hand (Halpern and Steiner 1983).

Numerous faint emission lines are visible in Figure 1$\underline{b}$, which is plotted on an expanded intensity scale. Among these are [Ne V]λ3426, [Fe VII]λ5721, [Fe VII]λ6087, and He II λ4686. Since the ionization potential of neutral helium is only 54.4 eV, He II λ4686 is sometimes visible in galaxies photoionized by hot stars (e.g., Kunth and Sargent 1983), but it is never so intense relative to Hβ. The most direct evidence for photoionization by a nonstellar continuum, however, comes from the strong [Ne V] and [Fe VII] lines, as these cannot be produced by O stars. The central stars in planetary nebulae emit radiation which can give rise to lines of very high excitation, but the number of such stars needed in order to produce the emission in NGC 7314 is large.

Furthermore, [O I]λ6300,6364 is weak in planetary nebulae which exhibit lines from highly-ionized species, since the exponential cutoff of the UV radiation does not provide enough X-rays to produce an extended zone of partially-ionized (~ 10%) hydrogen in which the [O I] lines are formed.

Another significant feature in the optical spectrum is the broad component of Hα emission. Very broad permitted lines are the distinguishing characteristics of Seyfert 1 galaxies and quasars, although NGC 7314's broad Hα is weaker and narrower than that in most active nuclei. Furthermore, the continuum of NGC 7314 is very blue, indicating the presence of a prominent nonstellar component.

III. MEASUREMENTS OF EMISSION LINES

a) The Narrow Lines

To obtain a quantitative understanding of the physical conditions in NGC 7314, the intensity and width of each emission line was measured. Since the continuum is dominated by a featureless component, stellar absorption lines did not significantly affect the results in most cases. Moderate spectral resolution and the narrowness of the emission lines also diminished the difficulty of making accurate measurements. The important Hγ and [O III]λ4363 lines, for example, were easily separated from major absorption lines such as the G-band. On the other hand, the [Ne III]λ3968 + Hε blend was severely affected by Ca II H (λ3968), which was removed to first order by comparison with the strength of Ca II K (λ3934).

The continuum was approximated by a cubic spline drawn through representative points and subsequently subtracted. Line intensities

were calculated by summing the flux in all bins between some chosen endpoints, and also by fitting Gaussians to the observed line profiles. Gaussians provided excellent approximations to the observed profiles, so the agreement between the intensity measurements was generally quite good. In some cases, however, noise and peculiarities in the data clearly indicated that one of the methods was preferable over the other.

The probable error was crudely derived by computing the total number of photons in each line. Moreover, a comparison of this number with the average value of the adjacent continuum provided an estimate of the error due to inaccuracies in defining the continuum level. Finally, the entire measurement procedure was repeated with a new placement of the continuum, and the results compared. Satisfactory agreement was found for most lines.

Each Gaussian fit also provided an estimate of the FWHM. Since the emission lines are so narrow, a major source of error is the uncertainty in the spectral resolution, especially at the blue end where the emission lines are almost unresolved. Figure 2b plots the Gaussian dispersion σ (where FWHM $\sim 2.355\sigma$) of unblended comparison lines as a function of position along the detector for the blue spectrum. Similar curves were constructed for the other spectra, and the intrinsic ("true") σ of each emission line in NGC 7314 was obtained from the observed and instrumental dispersions using

$$\sigma_{true} = (\sigma^2_{obs} - \sigma^2_{inst})^{1/2} \quad .$$

The FWHM of lines from ions such as He^+ and O^{++} is 150 ± 10 km s^{-1}, whereas lines of H^o, N^+, and S^+ are somewhat narrower (FWHM $\sim 120 \pm 10$ km s^{-1}). A similar correlation between line width and ionization

potential was noticed in III Zw 77 by Osterbrock (1981), in NGC 3783 by Pelat, Alloin, and Fosbury (1981), and in several other Seyfert galaxies (De Robertis and Osterbrock 1984). An increase in the velocity of clouds with decreasing distance from the central source of ionizing radiation is the probable cause of the effect. Not enough lines are available to see whether the correlation between width and critical density (Filippenko and Halpern 1984; Filippenko 1984) is even better. Lines from different ions appear at essentially the same redshift in NGC 7314.

Investigations of the physical processes in classical Seyferts have concentrated in part on the unusually broad lines. Even in type 2 Seyferts, typical widths (FWHM) are ~ 500 km s^{-1}, which is greater than in normal H II regions and in galaxies whose nuclei contain aggregates of giant H II regions (FWHM $\lesssim$ 150 km s^{-1}). Consequently, our view of AGNs may have become somewhat biased: broad lines and nonstellar activity accompany each other so frequently that the former is often regarded as a necessary signature of the latter. Indeed, it has been suggested (Balzano and Weedman 1981; Shuder and Osterbrock 1981) that nonthermal activity is absent in galaxies whose nuclei exhibit narrow emission lines (FWHM $\lesssim$ 250–300 km s^{-1}). A number of studies (e.g., Ward et al. 1978; Wilson et al. 1976; Phillips, Charles, and Baldwin 1983) conclusively demonstrate that this cannot be true, since many galaxies exhibiting nonthermal processes have line widths of order 200 km s^{-1}. Lines in NGC 7314 are the narrowest yet reported for a Seyfert, and support the conclusions summarized by Phillips, Charles, and Baldwin (1983).

b) Broad Balmer Emission

Casual inspection of Figure 3a reveals that Hα is blended with [N II]λ6548,6583, and that broad wings are present. An attempt to decompose this blend into four Gaussians was made by performing a least-squares fit with seven free parameters. These were the amplitude, dispersion, and central wavelength of the broad component, as well as the amplitudes of [N II]λ6583 and Hα, the dispersion of the narrow lines, and the central wavelength of [N II]λ6583. The use of a single dispersion for the narrow components is justified by measurements of [S II]λ6716,6731 and Hβ, and by the expectation that [N II]λ6548,6583 is produced in roughly the same region as the sulfur doublet. The exact wavelengths of [N II]λ6548 and Hα were fixed with respect to that of [N II]λ6583. [N II]λ6548 was assumed to be one-third the intensity of [N II]λ6583.

The best fit to the blend is displayed in Figure 3b. It is apparent that the very broad wings cannot be reproduced by the use of only four Gaussian components. Either the broad-line region gives rise to an intrinsically non-Gaussian profile, or it is composed of several cloud distributions having different velocity dispersions. If the latter is correct, then a better fit to the observed blend could be obtained by including additional Gaussian components in the decomposition. However, it is not clear that the results would have great physical significance, especially since the limited signal-to-noise ratio of the data does not allow a unique fit.

On the other hand, the extended wings suggest that the broad component has a Lorentzian profile. The results of a new least-squares fit, consisting once again of seven free parameters, are shown in

Figure 3c. It is clearly more satisfactory than that with four Gaussians, but lacks a solid physical interpretation.

A good fit (not shown in Figure 3) at intermediate velocities in the broad component was obtained by replacing the Lorentzian by a logarithmic profile, in which the flux can be expressed as a function of wavelength shift from the line center by

$$F(\Delta\lambda) = C_1 \log(\Delta\lambda) + C_2 \quad ,$$

where C_1 and C_2 are constants. This is the profile expected for a collection of optically thin, radiatively driven clouds (Blumenthal and Mathews 1975) and in a number of other models as well (Capriotti, Foltz, and Byard 1980), so its physical justification is much better than that of a Lorentzian. On the other hand, it underestimates the flux at large $\Delta\lambda$ (e.g., high velocities).

The first exponential integral combines the good features of the logarithmic and Lorentzian profiles, and gives the best fit of all the functions tested. Figure 3d shows that both the narrow and broad components are represented accurately, except for a slight mismatch in the narrow cores which gives rise to small oscillations in the residuals. Capriotti, Foltz, and Byard (1980) demonstrated that the first exponential integral is the expected functional form if optically thick clouds are flowing away from the nucleus ballistically (that is, in a force-free environment). Note that the broad component of Hα is blueshifted by roughly 150 km s^{-1} with respect to the narrow lines.

Careful examination of the data shows that extremely weak, broad Hβ emission is present in NGC 7314. The great strength of broad Hα compared with the corresponding component of Hβ indicates that the reddening of the broad-line region is very high.

IV. PHYSICAL CONDITIONS

a) Electron Density and Temperature

In a computer program developed by Jules P. Halpern, the formulae given by Kafatos and Lynch (1980) were used to calculate emission-line intensity ratios as a function of electron density and temperature. These formulae assume detailed balance in ions which have five low-lying levels in the ground state configuration. Recent values for collision strengths and transition probabilities were used; the sources are given by Filippenko and Halpern (1984).

The new atomic parameters yield results which differ considerably from old ones. For example, the ratio $\underline{I}$([S II]λ6716)/$\underline{I}$([S II]λ6731) changes most rapidly at densities of ~ 500 cm^{-3} rather than ~ 1100 (Osterbrock 1974). This means that it is most sensitive in roughly the same range of densities as the [O II]λ3726,3729 doublet. While the new calculations are probably more accurate than the old, some of the collision strengths are quite sensitive to the approximations used, so considerable theoretical uncertainty still exists.

In NGC 7314, the electron density derived from the [S II] doublet is $\underline{n}_e$ ~ 250 cm^{-3}. Although the [O II] doublet is not quite resolved, [O II]λ3729 is clearly more intense than [O II]λ3726, indicating a low value of $\underline{n}_e$. The lines were deblended under the assumption of intrinsically Gaussian profiles, giving an $\underline{n}_e$ consistent with the one above. Using the ratio $\underline{I}$([O III]λ4959+5007)/$\underline{I}$([O III]λ4363), the derived electron temperature is ~ 12000 K. No corrections for reddening have been made thus far, however.

b) Reddening

If the Balmer lines are produced purely by recombination at the density and temperature given above, the "Case B" (Baker and Menzel 1938) Balmer decrement is (Brocklehurst 1971)

$$\underline{I}(H\alpha)/\underline{I}(H\beta)/\underline{I}(H\gamma)/\underline{I}(H\delta)/\underline{I}(H\varepsilon) = 2.84/1.00/0.47/0.26/0.16 ,$$

whereas it is observed to be steeper:

$$\underline{I}(H\alpha)/\underline{I}(H\beta)/\underline{I}(H\gamma)/\underline{I}(H\delta)/\underline{I}(H\varepsilon) = 5.08/1.00/0.39/0.17/0.12 .$$

This indicates that the narrow-line region is probably reddened, since at such low densities collisional and optical depth effects probably do not significantly alter the decrement from its Case B value. At most, the intrinsic ratio of Hα to Hβ could be 3.1 (Halpern 1982), and the other ratios remain relatively unchanged.

To determine the amount of reddening, the standard extinction law derived by Whitford (1958) is used. It is normalized relative to Hβ and conveniently tabulated as $\underline{f}(\lambda_i)$ by Lequeux *et al.* (1979), where λ_i are the wavelengths of common emission lines. From the relation

$$\log\left[\frac{I(\lambda)}{I(H\beta)}\right]_{intrinsic} = \log\left[\frac{I(\lambda)}{I(H\beta)}\right]_{observed} + C\,f(\lambda) ,$$

the reddening constant $\underline{C}$ is found to be 0.76 for Hα, 0.63 for Hγ, 0.99 for Hδ, and 0.60 for Hε. The average of these is $\langle\underline{C}\rangle = 0.745$, which is remarkably close to the result obtained for Hα alone. $\underline{C} = 0.75$ is therefore adopted for the narrow-line region.

Since

$$\underline{E}_{\underline{B}-\underline{V}} = 2.5\underline{C}[\underline{f}(\underline{B}) - \underline{f}(\underline{V})] ,$$

the color excess is

$$\underline{E}_{\underline{B}-\underline{V}} \sim 0.655\underline{C} \sim 0.50 \text{ mag},$$

and the corresponding visual extinction is ~ 1.6 mag if dust in NGC 7314

is similar to that found in the solar neighborhood. This value of E_{B-V} includes a contribution due to extinction in the Galaxy, but Burstein and Heiles (1982) show that it is negligible at the galactic longitude (27.14) and latitude (-59.74) of NGC 7314.

An independent estimate of the reddening can be obtained from the ratio $S = I([S\ II]\lambda4069+4076)/I([S\ II]\lambda6716+6731)$. The data indicate $S = 0.031$, and Figure 1 of Malkan (1983) then shows that $E_{B-V} \sim 0.60$ mag. In light of the large uncertainty associated with the measured intensity of [S II]λ4069, it is likely that E_{B-V} is closer to 0.50 mag, the value obtained from the Balmer decrement. This conclusion is supported by the absence of [O II]λ7319,7330, since I([O II]λ7319,7330) decreases with respect to I([O II]λ3726,3729) as the reddening decreases.

Malkan (1983) found that in many Seyfert galaxies the reddening deduced from the [O II] and [S II] line intensities is considerably smaller than that obtained from an analysis of the Balmer decrement, but this is not the case here. It is interesting, however, that in most narrow-line X-ray galaxies the Balmer decrement dereddened using the ([O II], [S II]) method *is* close to the normal case B decrement (Malkan 1983), just as in NGC 7314. Furthermore, NGC 7314 supports Malkan's conclusion that the absolute reddening in these galaxies is much larger than generally found in type 2 Seyferts and in the narrow-line regions of Seyfert 1 galaxies.

Shuder (1980), Véron *et al.* (1980), and others have demonstrated that most narrow-line X-ray galaxies exhibit faint, broad Hα emission. The absence of a similar component of Hβ implies enormous reddening in their broad-line region (BLR), and it is possible that the large

reddening in the narrow-line region is fundamentally related to this. Dust may be distributed throughout a volume whose radius is of order 100 pc, but it is probably concentrated in the broad-line clouds near the nucleus.

The observations reported here support this hypothesis. In NGC 7314 a very faint, broad component of Hβ is detected, so a direct estimate of the reddening in the BLR can be made. Since $\underline{I}(H\alpha)/\underline{I}(H\beta) \sim 48$, the standard (case B) analysis yields $\underline{C} \sim 3.7$ mag, and $\underline{A}_{\underline{V}} \sim 8$ mag. Of course, at high densities there is no guarantee that $\underline{I}(H\alpha)/\underline{I}(H\beta)$ is intrinsically equal to 2.84, but the reddening must be very high even if self-absorption (Netzer 1975) or collisional excitation of Hα from the ground state (Ferland and Mushotzky 1982) are important.

c) The Nonstellar Continuum

Although broad permitted emission lines and strong lines from highly ionized species are the most striking features in the optical spectra of Seyfert galaxies, another important characteristic is the continuum, which is dominated by radiation from a nonstellar source. The presence of a nonstellar continuum in NGC 7314 can be inferred from the strength of lines such as [Ne V]λ3426, [Fe VII]λ6087, and Hα, and it can be measured quantitatively in several ways.

Suppose the broad-line region is composed of small clouds which subtend a fraction $\underline{F}$ of the sky as seen from the nucleus of the galaxy. If the optical and ultraviolet radiation from the central source is described by a power-law ($f_\nu \propto \nu^{-\alpha}$), and if the contribution to the continuum from stars is negligible, then in the absence of reddening the

equivalent width of Hα emission is given by

$$EW(H\alpha) \approx 2200\, F\, \frac{7.2^{-\alpha}}{\alpha} \quad \text{Å} \quad .$$

In NGC 7314, the measured equivalent width of broad Hα is ~ 170 Å, but this is only a lower limit since a portion of the continuum comes from starlight. Such a large value implies that the continuum slope (α) is quite flat and that the covering fraction is large. If $\underline{F} = 0.1$, then $\alpha \lesssim 0.49$, an index which is smaller than that of most Seyfert galaxies; if $\underline{F} = 1.0$, on the other hand, then $\alpha \lesssim 1.2$, which is more typical (Malkan and Sargent 1982; Malkan and Filippenko 1983).

A direct measurement of the nonstellar continuum in the narrow-line region can be obtained by comparing the intensities of He II λ4686 and the narrow component of Hβ. Penston and Fosbury (1978) showed that if the continuum blueward of 912 Å is completely absorbed, then

$$I(\text{He II } \lambda 4686)/I(H\beta) = 1.99/4^{\alpha} \quad .$$

The observed ratio is 0.42 in NGC 7314, indicating $\alpha \sim 1.13$. If the emission lines are dereddened, the ratio becomes 0.45 and $\alpha \sim 1.07$, flatter by $\Delta\alpha \sim 0.8$ than the same spectral region of NGC 4151 (Penston and Fosbury 1978). The exact numerical results are different if NGC 7314 has a significant "UV bump," as do most type 1 Seyfert galaxies (Malkan and Sargent 1982), since the assumption of a constant power-law slope is then obviously incorrect. The qualitative conclusions, however, remain relatively unchanged. Radiation which reaches the narrow-line region experiences far less reddening than the broad Balmer emission; the dust must therefore be concentrated in, or in shells

around, the broad-line clouds themselves, and nonstellar radiation must pass between these clouds on its journey to the narrow-line region.

V. SUMMARY

New optical spectra of the nearby Sc galaxy NGC 7314 confirm its identification as a narrow-line X-ray galaxy (NLXG). Emission-line intensity ratios resemble those in type 2 Seyferts, and broad Hα emission is present. The Hα equivalent width of ~ 170 Å shows that the covering fraction of broad-line clouds may be large. A corresponding component of Hβ is extremely weak, so the broad-line region must be heavily reddened. Relative emission-line strengths, on the other hand, demonstrate that the spectral index of the nonstellar radiation incident on the narrow-line clouds is near unity. It is highly unlikely that this radiation can be reddened as much as the broad Balmer emission. Therefore, dust is probably concentrated within or near the broad-line clouds themselves, and does not seriously affect the nonstellar power law which ionizes the narrow-line gas.

The Intensified Reticon detector and associated paraphernalia were made primarily by Steve Shectman, Gary Yanik, and Ken Clardy. Facilities at Las Campanas Observatory were used as part of the cooperative agreement between the Carnegie Institution of Washington and Caltech. Efficient use of observing time was made possible by the nocturnal assistance of Angel Guerra and Fernando Peralta, as well as by the diurnal efforts of Hernan Solis and Bill Robinson. Discussions with Jules Halpern, Martin Elvis, Martin Gaskell, and Matt Malkan were both

pleasant and informative. Special thanks go to Jules Halpern for the use of his computer code in the calculation of relative line strengths. A graduate fellowship from the Fannie and John Hertz Foundation is greatly appreciated.

TABLE 1

Journal of Observations, NGC 7314[a]

Date (UT)	Time (s)	g/mm[b]	blaze[c]	R (Å)[d]	Δλ (Å)	Air mass[e]	PA[f]	See.[g]	Stan.[h]
1982 Aug 16	3000	1200	6800	2-3	5680-7560	1.00/1.03	0	1	1,2
1982 Aug 17	2400	1200	4600	2-3	3220-4970	1.06/1.14	90	1	1,2
1982 Aug 18	1000	1200	4600	2-3	4470-6350	1.22/1.29	90	1	1,2
1983 Aug 13	3000	600	4600	4-5	3900-7580	1.24/1.10	77	1.5	3
1983 Aug 14	2000	1200	4600	2-3	3210-5100	1.12/1.06	90	1	2

[a]All spectra obtained through 2" x 4" apertures.

[b]Number of grooves/mm in grating.

[c]Approximate blaze (Å) of grating, order 1.

[d]Resolution (FWHM) of unblended emission lines in comparison arc.

[e]Air mass at beginning and end of integration.

[f]Position angle (degrees) refers to long dimension of aperture.

[g]Approximate FWHM of seeing disk (arc seconds).

[h]Standard stars: 1 = GD-248, 2 = G158-100, 3 = G24-9.

REFERENCES

Baker, J. G., and Menzel, D. H. 1938, Ap. J., 88, 52.

Balzano, V. A., and Weedman, D. W. 1981, Ap. J., 243, 756.

Blumenthal, G. R., and Mathews, W. G. 1975, Ap. J., 198, 517.

Brocklehurst, M. 1971, M.N.R.A.S., 153, 471.

Burstein, D., and Heiles, C. 1982, A. J., 87, 1165.

Capriotti, E., Foltz, C., and Byard, P. 1980, Ap. J., 241, 903.

De Robertis, M. M., and Osterbrock, D. E. 1984, preprint.

Ferland, G. J., and Mushotzky, R. F. 1982, Ap. J., 262, 564.

Filippenko, A. V. 1982, Publ. A.S.P., 94, 715.

———. 1984, Ap. J., submitted.

Filippenko, A. V., and Greenstein, J. L. 1984, Publ. A.S.P., in press (July).

Filippenko, A. V., and Halpern, J. P. 1984, Ap. J., in press (Oct. 15).

Halpern, J. P. 1982, Ph.D. thesis, Harvard University.

Halpern, J. P., and Steiner, J. E. 1983, Ap. J. (Letters), 269, L37.

Kafatos, M., and Lynch, J. P. 1980, Ap. J. Suppl., 42, 611.

Kriss, G. A. 1982, Ph.D. thesis, Massachusetts Institute of Technology.

Kunth, D., and Sargent, W. L. W. 1983, Ap. J., 273, 81.

Lequeux, J., Peimbert, M., Rayo, J. F., Serrano, A., and Torres-Peimbert, S. 1979, Astr. Ap., 80, 155.

Malkan, M. A. 1983, Ap. J. (Letters), 264, L1.

Malkan, M. A., and Filippenko, A. V. 1983, Ap. J., 275, 477.

Malkan, M. A., and Sargent, W. L. W. 1982, Ap. J., 254, 22.

Marshall, N., Warwick, R. S., and Pounds, K. A. 1981, M.N.R.A.S.,

194, 987.

Mushotzky, R. F. 1982, Ap. J., 256, 92.

Netzer, H. 1975, M.N.R.A.S., 171, 395.

Oke, J. B. 1969, Publ. A.S.P., 94, 586.

———. 1974, Ap. J. Suppl., 27, 21.

Oke, J. B., and Gunn, J. E. 1983, Ap. J., 266, 713.

Osterbrock, D. E. 1974, Astrophysics of Gaseous Nebulae. (San Francisco: W. H. Freeman and Co.).

———. 1981, Ap. J., 246, 696.

Pelat, D., Alloin, D., and Fosbury, R. A. E. 1981, M.N.R.A.S., 195, 787.

Penston, M. V., and Fosbury, R. A. E. 1978, M.N.R.A.S., 183, 479.

Phillips, M. M., Charles, P. A., and Baldwin, J. A. 1983, Ap. J., 266, 485.

Piccinotti, G., Mushotzky, R. F., Boldt, E. A., Holt, S. S., Marshall, F. E., Serlemitsos, P. J., and Shafer, R. A. 1982, Ap. J., 253, 485.

Sargent, W. L. W., and Searle, L. 1970, Ap. J. (Letters), 162, L155.

Searle, L. 1971, Ap. J., 168, 327.

Shectman, S. A., 1982, in Annual Report of the Director, the Mount Wilson and Las Campanas Observatories (Washington: Carnegie Institution of Washington), p. 676.

Shuder, J. M. 1980, Ap. J., 240, 32.

Shuder, J. M., and Osterbrock, D. E. 1981, Ap. J., 250, 55.

Stauffer, J. R. 1982a, Ap. J., 262, 66.

———. 1982b, Ap. J. Suppl., 50, 517.

Stone, R. P. S. 1974, Ap. J., 193, 135.

———. 1977, Ap. J., 218, 767.

Véron, P., Lindblad, P. O., Zuiderwijk, E. J., Véron, M. P., and Adam, G. 1980, Astr. Ap., 87, 245.

Ward, M. J., Wilson, A. S., Penston, M. V., Elvis, M., Maccacaro, T., and Tritton, K. P. 1978, Ap. J., 223, 788.

Weedman, D. W. 1977, Ann. Rev. Astron. Astrophys., 15, 69.

Whitford, A. E. 1958, A. J., 63, 201.

Wilson, A. S., Penston, M. V., Fosbury, R. A. E., and Boksenberg, A. 1976, M.N.R.A.S., 177, 673.

FIGURE CAPTIONS

Figure 1: The spectrum of NGC 7314 is shown on linear wavelength and intensity scales. In (a), the strong lines are illustrated at full scale, while (b) emphasizes the weaker lines and continuum. Note the presence of prominent low-ionization emission ([O I], [S II]) as well as [Ne V], [Fe VII], and other high-ionization lines. The forbidden lines are remarkably narrow, but Hα exhibits a broad component.

Figure 2: Measurements of emission lines in a comparison arc are used to determine the instrumental resolution (FWHM ~ 2.355σ) as a function of position along the detector. Gaussians represent the lines to high accuracy.

Figure 3: Hα and [N II] are shown in (a). A broad component of Hα is clearly present. Four Gaussians cannot adequately represent the blend (b), but three Gaussians and one Lorentzian are much more satisfactory (c). Replacing the Lorentzian with a logarithmic profile (not shown) results in a better fit at intermediate velocities, but a poorer one in the extreme wings of Hα. The first exponential integral combines the best features of both the Lorentzian and logarithmic profiles, giving an excellent fit at all velocities. Slight asymmetries in the narrow lines produce the oscillations visible in the residuals.

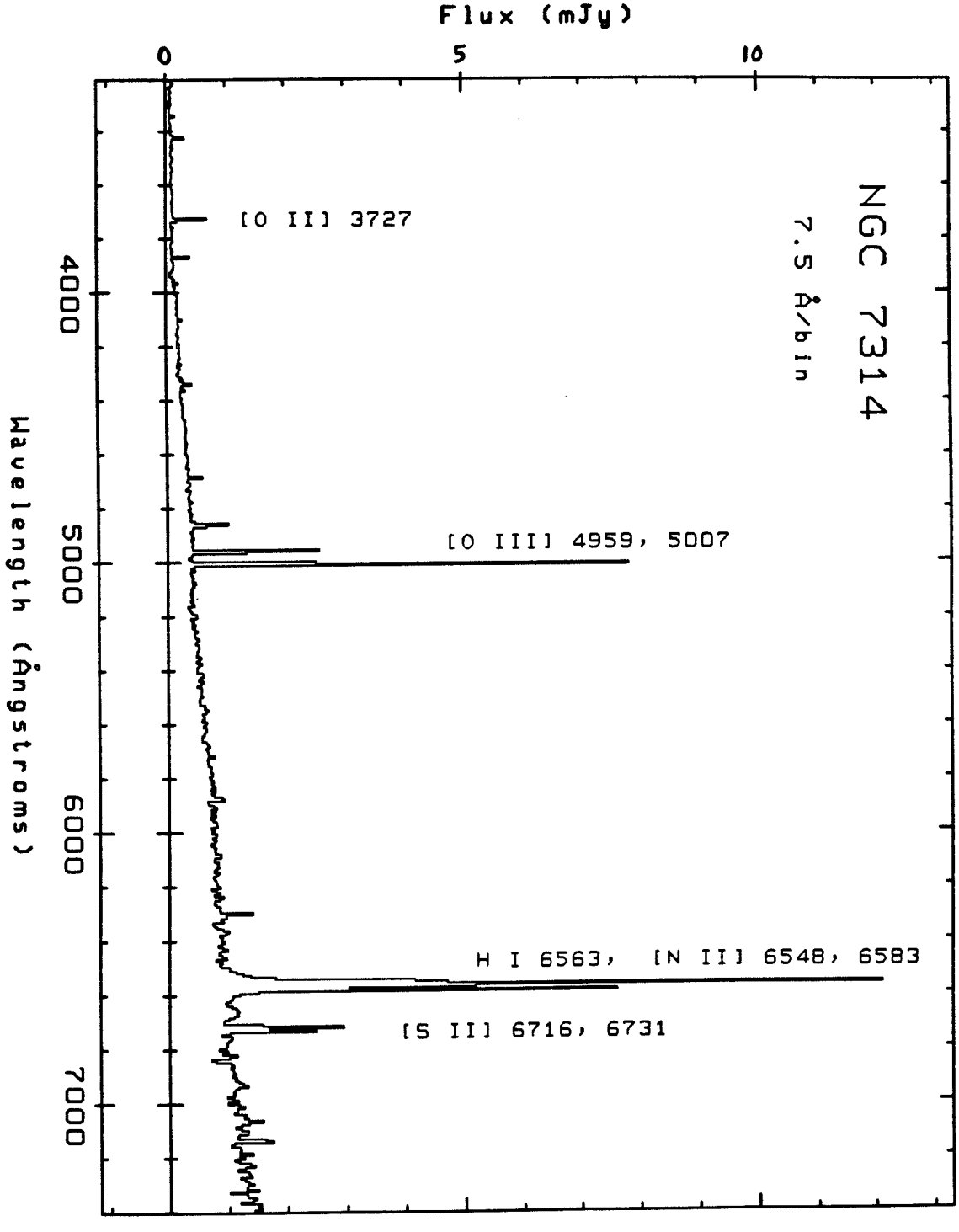
Flux (mJy)
0
5
10
NGC 7314
7.5 Å/bin
[O II] 3727
[O III] 4959, 5007
H I 6563, [N II] 6548, 6583
[S II] 6716, 6731
4000
5000
6000
7000
Wavelength (Ångstroms)

Figure 1a

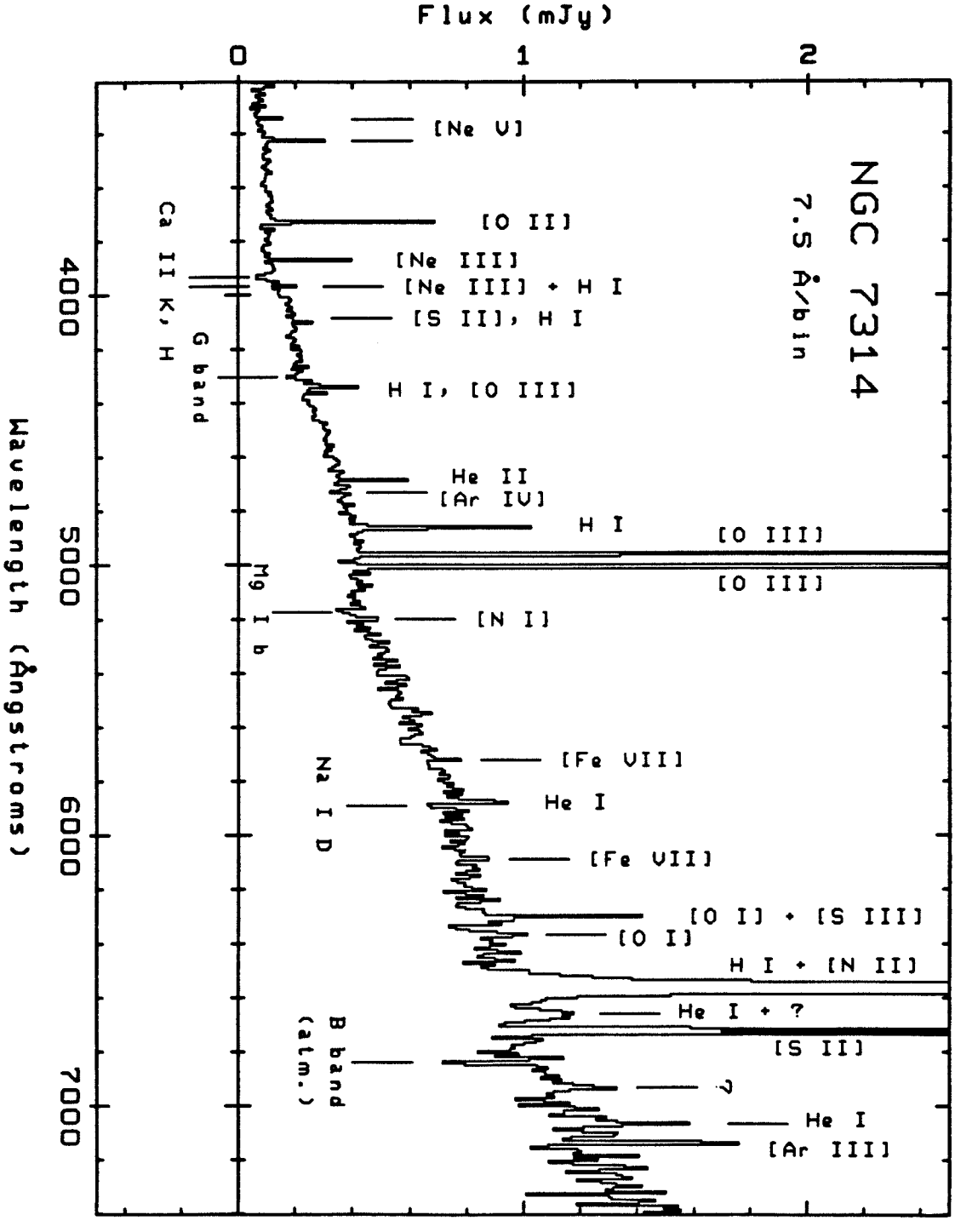
Flux (mJy)
0
1
2
NGC 7314
7.5 Å/bin
[Ne V]
[O II]
[Ne III]
[Ne III] + H I
[S II], H I
H I, [O III]
He II
[Ar IV]
H I
[O III]
[O III]
[N I]
[Fe VII]
He I
[Fe VII]
[O I] + [S III]
[O I]
H I + [N II]
He I + ?
[S II]
?
He I
[Ar III]
Ca II K, H
G band
Mg I b
Na I D
B band
(atm.)
4000
5000
6000
7000
Wavelength (Ångstroms)

Figure 1b

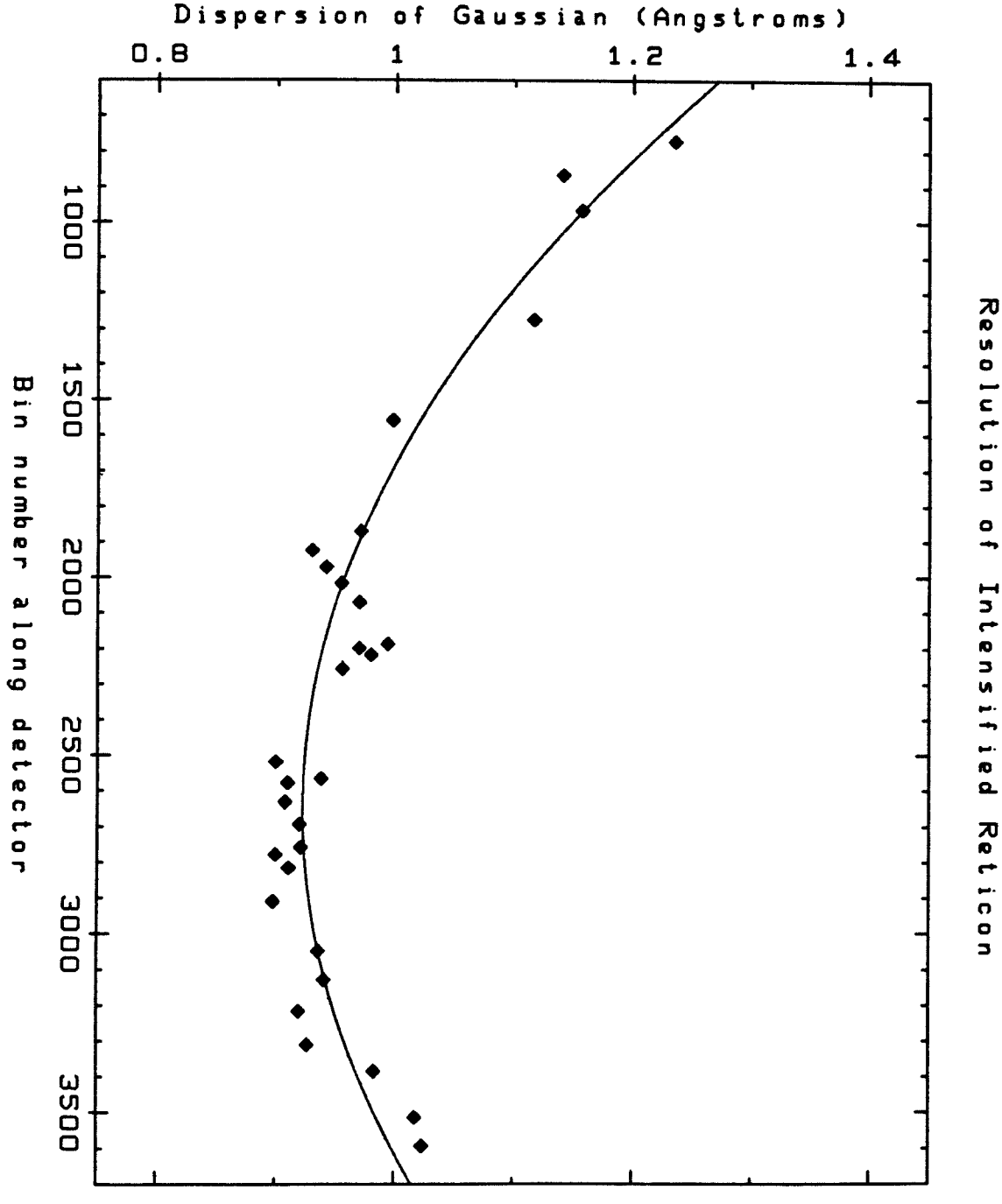
Dispersion of Gaussian (Angstroms)
0.8
1
1.2
1.4
1000
1500
2000
2500
3000
3500
Bin number along detector
Resolution of Intensified Reticon

Figure 2

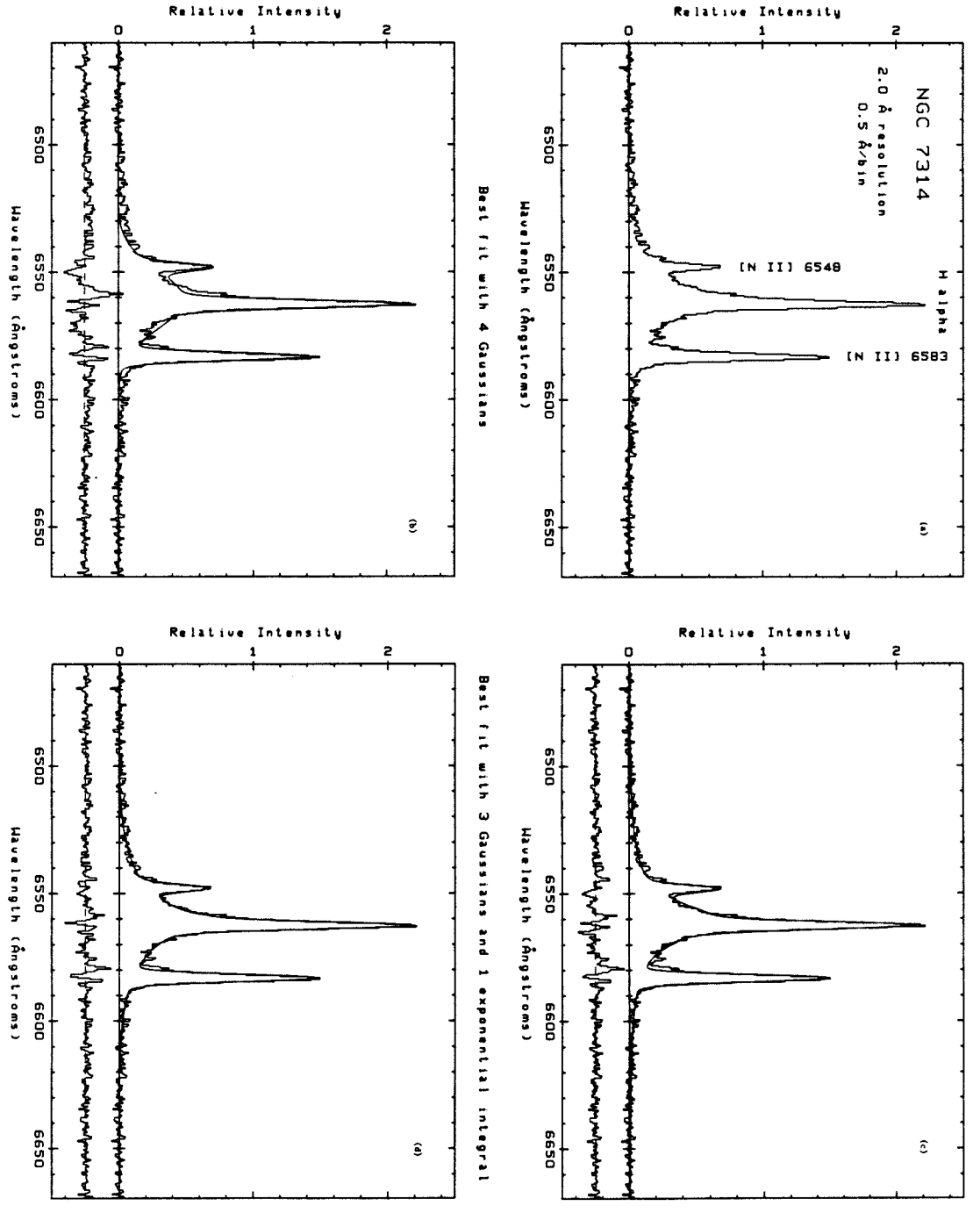
Relative Intensity
Wavelength (Ångstroms)
Data (continuum removed)
NGC 7314
2.0 Å resolution
0.5 Å/bin
H alpha
[N II] 6548
[N II] 6583
(a)
Best fit with 4 Gaussians
(b)
Best fit with 3 Gaussians and 1 Lorentzian
(c)
Best fit with 3 Gaussians and 1 exponential integral
(d)

Figure 3

CHAPTER 7

Summary and the Future.

I. SUMMARY

Physical conditions in the nuclei of emission-line galaxies and low-luminosity Seyferts were investigated by analyzing their continua and optical emission lines. A primary motivation was to determine whether the physical processes are similar to those occurring in QSOs and luminous type 1 Seyfert galaxies. It was found that gas in the nuclear regions of many nearby galaxies is predominantly photoionized by nonstellar radiation, rather than shock-heated. By analogy with active galactic nuclei of high luminosity, the ionizing continuum may be produced through accretion of gas by a massive, central black hole.

Chapter 1 derived the strength and shape of the nonstellar continuum for nine Seyfert galaxies, some of which exhibit only low-level activity. In Seyfert 1 nuclei the Mg I λ5175, Na I λ5892, and Ca II λ8542 stellar absorption lines are extremely weak, indicating that galactic starlight does not contribute a significant fraction of the observed continuum. The starlight measured 5″-30″ from the nucleus generally has colors which are typical of those in the disks of normal spiral galaxies. The nonstellar continuum is similar to that of QSOs — it falls from infrared to visual wavelengths roughly as a power law with slope $\alpha \sim -1.1$ to -1.2, and in the most luminous objects it flattens in the blue. Even at minimum brightness the nonstellar flux has no short-wavelength cutoff near 1 μm, eliminating the possibility that the near-infrared flux is dominated by thermal emission from hot dust grains. These results suggest a continuity between QSOs, bright and faint type 1 Seyferts, and perhaps even nearby galaxies whose relatively faint emission lines are not produced by H II regions.

The next two chapters concentrated on NGC 7213, an S0 galaxy whose optical and X-ray spectra clearly indicate that gas in the vicinity of the nucleus is photoionized by a nonstellar continuum. Curiously enough, NGC 7213 also exhibits spectral characteristics which in "low-luminosity nuclear emission-line regions" (LINERs) have previously been attributed to heating by shocks.

After careful removal of the strong stellar component from the optical spectrum, it was shown that the widths of emission lines range from ~ 200 to ~ 2000 km s^{-1} (FWHM). Large differences were seen even in lines arising from the same species, and a tight correlation was found between line width and critical density ($v \propto n_e(crit)^{1/5}$) for 16 forbidden lines. This indicates that physically distinct clouds having vastly different densities are present and do not contribute in the same proportion to different emission lines. Moreover, the strength of [O III]λ4363 relative to [O III]λ5007 can be reasonably explained only if the density of some clouds in the narrow-line region is of order 10^6–10^7 cm^{-3}. Given the great range of densities (~ 10^3–10^7 cm^{-3}), models involving photoionization by a nonstellar continuum are able to reproduce the observed spectrum better than those invoking shocks. It was conjectured that most LINERs can be explained in the same manner. The observed relationship between cloud velocity and density, which is consistent with clouds in Keplerian orbits and a nearly radius-independent ionization parameter, can be understood in terms of the two-phase model of quasar emission-line regions developed by Krolik, McKee, and Tarter (1981). High velocities and densities are found closer to the nucleus than low values.

X-ray spectra were approximated by a power law with $\alpha = 0.72 \pm 0.12$

and $N_H \leq 2.5 \times 10^{20}$ cm^{-2}. This implies $A_V \lesssim 0.12$ mag, which is less than the value of 0.61 mag derived from a decomposition of the optical continuum into a power law of index 1.1 and the spectrum of a giant elliptical galaxy. The discrepancy might be resolved by the emission of substantial bremsstrahlung radiation at temperatures less than 1 keV from a hot medium which confines the narrow-line clouds.

The analysis was subsequently extended to three additional active nuclei and confirmed numerous results derived from NGC 7213. MR 2251-178, a luminous QSO whose gas is undoubtedly ionized by nonstellar radiation, exhibits some of the same characteristics as NGC 7213. These include a wide range of line widths as well as [O III] intensity ratios which at low densities are incompatible with photoionization. The same can be said for Pictor A, a radio galaxy with features of both type 1 Seyferts and LINERs. The key is that a wide range of densities in the narrow-line region conspire to produce an overall spectrum that cannot be adequately dealt with in simple, single-density models. Pks 1718-649, whose optical emission is less luminous than even that of NGC 7213, also exhibits features which at first glance appear contradictory. Careful subtraction of the stellar continuum was emphasized, since crucial diagnostic lines such as [O III]λ4363 and He II λ4686 cannot be accurately measured otherwise. The observations support the hypothesis that much of the ionizing radiation is produced thermally by a hot ($T \sim 10^4$-10^5 K) accretion disk, rather than by nonthermal processes.

Chapter 5 presented a sensitive search for low-luminosity type 1 Seyfert galaxies with spectra having ~ 2.5 Å resolution and very high ($\gtrsim 100/1$) signal-to-noise ratios. Compared with the forbidden emission,

Hα exhibits broad wings in 30 of 75 objects. Of the 26 LINERs listed by Heckman (1980), 8 to 12 show broad Hα. The equivalent widths range from nearly zero to values comparable to those in previously recognized active nuclei of moderate luminosity. This suggests the presence of activity similar to (but much milder than) that of QSOs in a significant fraction of all nearby galaxies. Furthermore, the emission-line intensity ratios are consistent with photoionization by nonstellar radiation, especially when the high densities implied by the observed correlation between line width and critical density are taken into account. Given the paucity of nearby QSOs and the growing evidence that they reside in galactic nuclei, it is likely that many of the objects surveyed were QSOs in the distant past.

The optical spectrum of NGC 7314, a narrow-line X-ray galaxy, was discussed in Chapter 6. Relative intensities of emission lines are typical of those in type 2 Seyferts, but their widths (FWHM ~ 120-150 km s^{-1}) are smaller than in all other known AGN. This indicates that nonstellar ionizing radiation need not be associated with rapid motions among the narrow-line clouds. A broad component of Hα is present; its profile suggests that gas flows radially away from the nucleus in a force-free environment. Analysis of the emission lines demonstrated that dust, which heavily reddens radiation emitted by the broad-line clouds, is probably located within or near the clouds themselves rather than in the low-density confining medium.

II. THE FUTURE

This thesis demonstrates, among other things, that photoionization by nonstellar radiation is able to explain the spectral characteristics of LINERs, but not that it necessarily is the dominant excitation mechanism in all of these objects. It still must be conclusively determined whether heating by shocks plays an important role in LINERs. To test this, a very sensitive search for weak nonstellar continua, [Ne V]λ3426, broad Hα emission, and correlations between line width and critical density must be made in large numbers of LINERs. The detailed survey I am conducting with W. Sargent, the first results of which were presented in Chapter 5, should resolve some of these questions. It is hoped that a large, complete sample of galaxies will eventually be analyzed.

I am also investigating nearby emission-line galaxies described by Sandage (1978), using the Cassegrain spectrograph on the 2.5 m du Pont telescope at Las Campanas Observatory. Thus far, it appears that many of the objects contain the same physical processes as classical Seyferts. The stellar component is much stronger than in normal Seyfert galaxies, and the emission lines are weaker and narrower, but the physics is fundamentally the same.

Another area which I am pursuing is the relationship between galaxies with extensive star formation in their nuclei and Seyfert galaxies. Weedman (1983) has suggested that "star-burst" galaxies may be the progenitors of Seyferts, and that some objects should exist which exhibit the properties of both phases. Many candidates have already been observed. A particularly interesting example is IC 5135; its

emission lines can be convincingly decomposed into components whose relative intensities and widths are typical of bright H II regions on the one hand, and Seyfert 2 galaxies on the other.

Perhaps the most important work that needs to be done is to quantify the relative intensities and widths of emission lines as a function of distance from the nucleus of a galaxy, using two-dimensional (long-slit) spectra. By comparing the spatial gradients with those predicted by various shock and photoionization models, as was done by Rose and Searle (1982) for M51, one can learn a great deal about the excitation mechanism and galactic dynamics. If an object contains a central source of power-law ionizing radiation, for example, then the relative intensities of the emission lines should vary with distance from the nucleus in a systematic and predictable manner (e.g., due to simple inverse-square dilution of the radiation field). A galactic nucleus dominated by shock heating should show a different set of intensity ratios and radial behaviors.

Two-dimensional spectra are also useful when a galaxy does not exhibit extended emission. Since the objects I am studying are dominated by a normal stellar population, it is difficult to obtain meaningful relative intensities; the strength of an emission line may be affected by underlying stellar absorption. With long-slit spectra, on the other hand, it is possible to remove the undesirable stellar contribution by subtracting an off-nuclear spectrum from that of the nucleus. Of course, the galactic bulge may contain a radial gradient in stellar population, but the method is still applicable (at least to first order) if the metallicity of the galaxy is measured at several positions along the slit and then extrapolated into the nucleus.

W. Sargent, J. Halpern, and I have conducted extensive investigations at Palomar (5 m) and Cerro Tololo (4 m) Observatories with new CCD spectrographs. Figure 1 illustrates the remarkable quantity of information available from even a portion of the optical spectrum obtained through a long slit. In particular, note how the line widths and the ratio I([N II])/I(Hα) differ at various locations in NGC 6951. Analysis of the radial gradient near the nucleus suggests that a central source of nonstellar (power law) ionizing radiation is probably present, while at greater distances the spectrum indicates photoionization by radiation from hot stars. NGC 6500 (Figure 2) presents a more puzzling case. The relative intensities do not exhibit marked radial variations, which may be indicative of heating by shocks (perhaps induced by a dynamical interaction with the companion galaxy, NGC 6501).

These are just a few of the approaches that can be used to study the ionization mechanism in emission-line galaxies. The Space Telescope will open new avenues for this area of research, which in some respects is still in its infancy.

REFERENCES

Heckman, T. M. 1980, Astr. Ap., 87, 152.

Krolik, J. H., McKee, C. F., and Tarter, C. B. 1981, Ap. J., 249, 422.

Rose, J. A., and Searle, L. 1982, Ap. J., 253, 556.

Sandage, A. R. 1978, A. J., 83, 904.

Weedman, D. W. 1983, Ap. J., 266, 479.

FIGURE CAPTIONS

Figure 1: A long-slit spectrum of the nearby spiral galaxy NGC 6951, obtained with the Double Spectrograph on the Palomar 5 m telescope, is shown. The distance (in arc seconds) from the nucleus is given for each individual cut along the dispersion. Strong [O I]λ6300 emission and the great strength of [N II]λ6584 relative to Hα indicate that gas in the nucleus is not photoionized by radiation from ordinary OB stars, unlike the case a few hundred parsecs away from the nucleus. The electron density decreases radially, as do the line widths.

Figure 2: Portions of a two-dimensional spectrum of NGC 6500 show that the emission-line intensity ratios do not change (to first order) at different positions along the slit. It is possible that the main excitation mechanism is heating by shocks. [O I]λ6300 is exceptionally strong, as is the [S II] doublet, making this object a LINER.

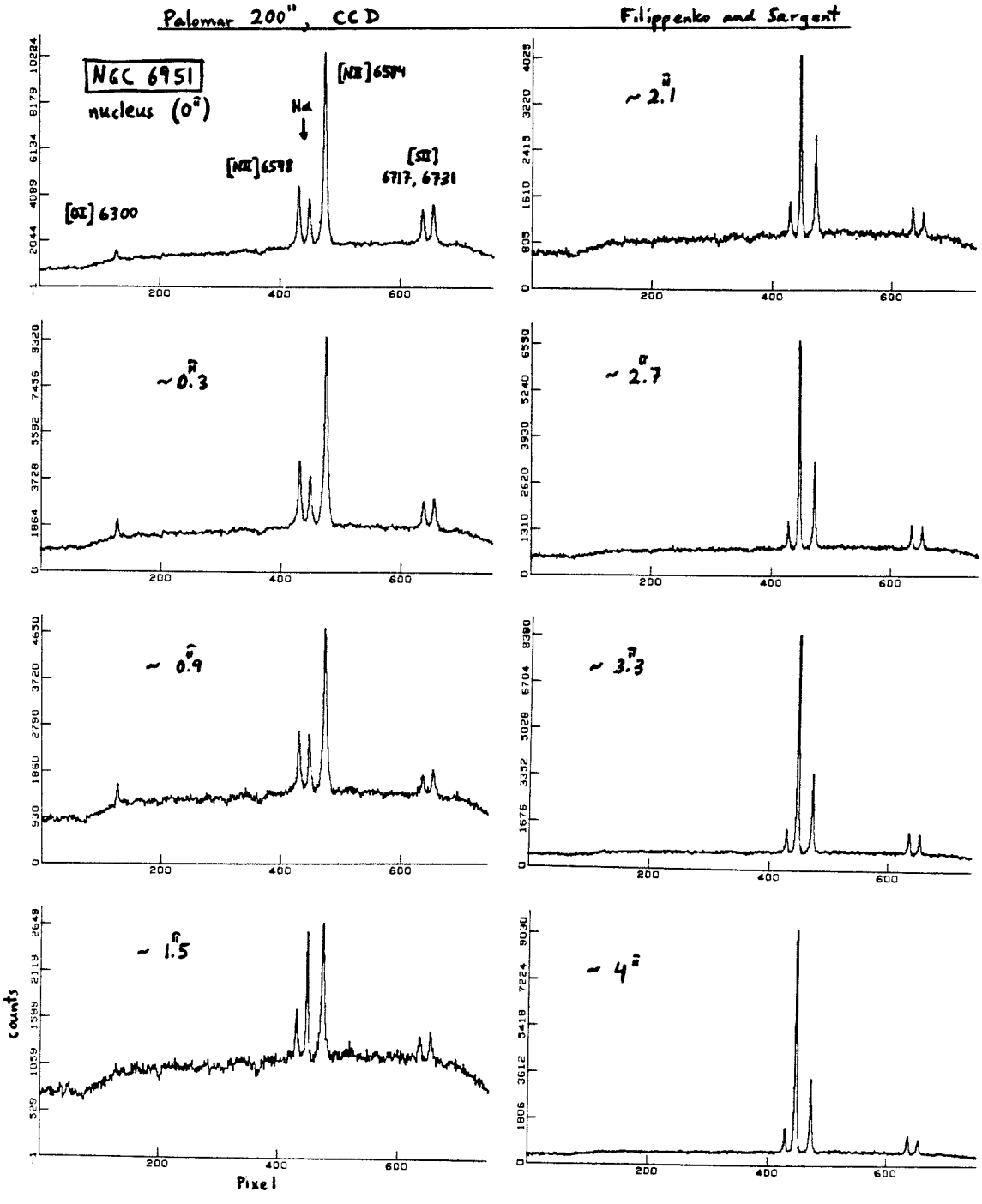

NGC 6951 : $V_0 = 1425$ km s^{-1} $\Rightarrow$ $d = 19$ Mpc if $H_0 = 75$ $\Rightarrow$ 90 pc/″

Note strength of [OI], changing line intensities and widths.

Figure 1

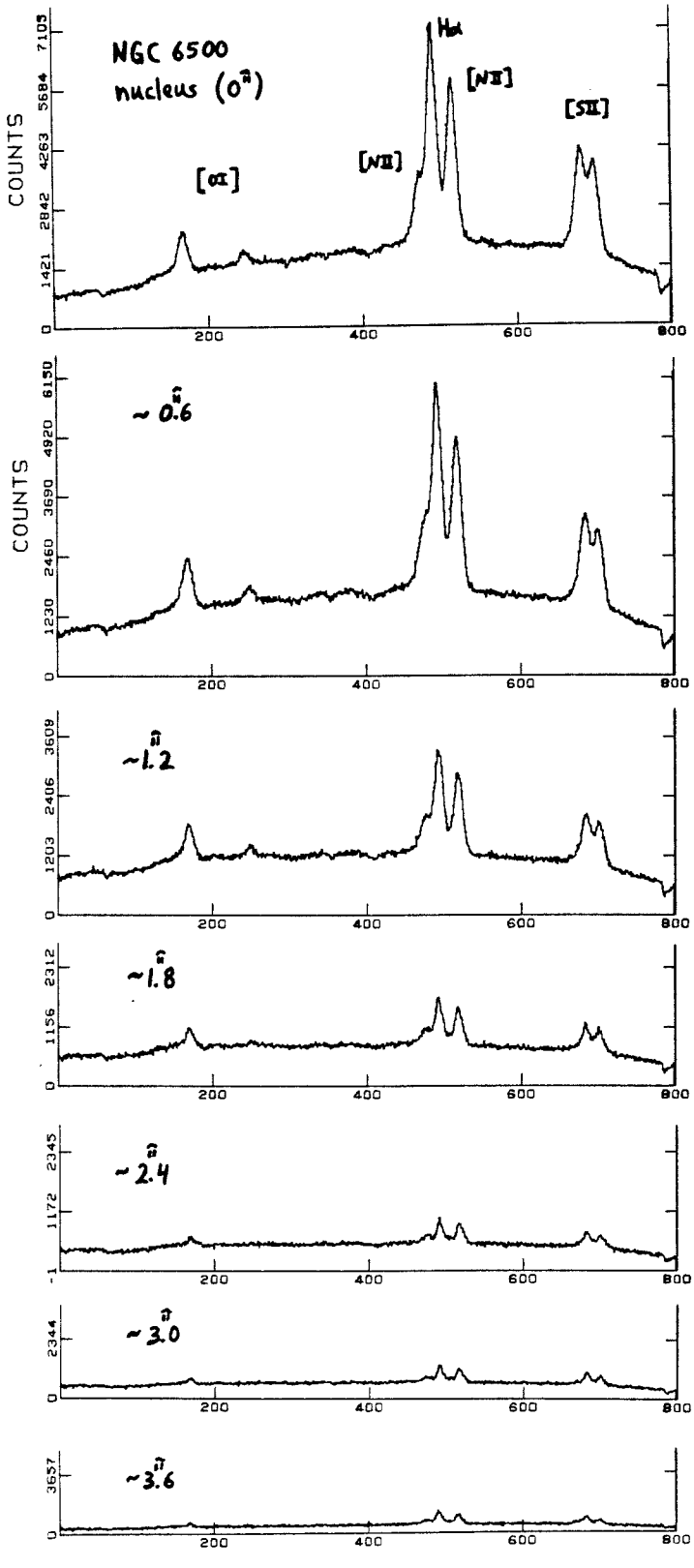

NGC 6500

$V_0 = 2950$ km s^{-1}

$\Rightarrow d = 39$ Mpc ($H_0 = 75$)

$\Rightarrow$ 190 pc/"

Line ratios don't change, to first order.

Figure 2

APPENDIX 1

The Importance of Atmospheric Differential Refraction in Spectrophotometry.

Alexei V. Filippenko

Reprinted from the Publications of the Astronomical Society of the Pacific (1982, 94, 715-721).

When you can measure what you are speaking about, and can express it in numbers, you know something about it; but when you cannot measure it, when you cannot express it in numbers, your knowledge is of a meager and unsatisfactory kind: it may be the beginning of knowledge, but you have scarcely in your thoughts advanced to the stage of <u>science</u>.

Popular lectures and addresses,
William Thomson, Lord Kelvin

PUBLICATIONS OF THE ASTRONOMICAL SOCIETY OF THE PACIFIC
94:715-721, August 1982

THE IMPORTANCE OF ATMOSPHERIC DIFFERENTIAL REFRACTION IN SPECTROPHOTOMETRY

ALEXEI V. FILIPPENKO

Department of Astronomy, California Institute of Technology, 105-24, Pasadena, California 91125

Received 1982 March 15

The effects of atmospheric differential refraction on astronomical measurements are much more important than is generally assumed. In particular, it is shown that relative line and continuum intensities in spectrophotometric work may be erroneous if this phenomenon is neglected. To help observers minimize these errors, the relation between object position and optimal slit or aperture orientation is derived, and practical tables and graphs are presented for use at the telescope.

Key words: instrumentation—observing techniques—spectrophotometry

I. Introduction

Atmospheric differential refraction has long been known to affect the results of a variety of measurement techniques in astronomy. For example, astrometric work requires observations at small zenith angles and comparison of plates taken through similar filter/emulsion combinations—otherwise considerable errors in the derived relative positions of objects may be made (van de Kamp 1967). On the other hand, solar astronomers must often observe through the steady atmosphere shortly after sunrise, and they consequently encounter severe difficulties since different regions of the disk appear along the same line of sight if viewed with a broad-band filter (Simon 1966). Similarly, in spectroscopy a substantial amount of light may be lost at large zenith angles if an object is recorded at a wavelength which differs from the convolution of its energy distribution and the spectral response of the human eye (and/or television guider system).

A related problem at nonzero zenith angles is that more light may be lost from either end of a spectrum than from the center if the object is well-centered in the spectrograph slit at the median wavelengths. This obviously leads to an erroneous measurement of the spectral energy distribution if the wavelength range is large. In view of the recent emphasis placed on relative emission-line intensities in studies of supernovae, planetary nebulae, galactic nuclei, and other objects (e.g., Baldwin, Phillips, and Terlevich 1981), it is important to be aware that even at small air masses the errors may be non-negligible. Although errors can easily be minimized by rotating the spectrograph so that the slit or rectangular aperture is parallel to the direction of atmospheric refraction, a survey of the literature reveals that this practice is generally *not* followed. The purpose of this paper is to remind spectroscopists of the large effects of atmospheric dispersion and to present convenient tables and graphs (for use at the telescope) of optimal slit orientation as a function of object position in the sky.

II. Atmospheric Differential Refraction

A. *Magnitude*

In this section atmospheric differential refraction as a function of wavelength is calculated for the conditions typical of major optical observatories.

At sea level (P = 760 mm Hg, T = 15°C) the refractive index of dry air is given by (Edlén 1953; Coleman, Bozman, and Meggers 1960)

$$(n(\lambda)_{15,760} - 1)10^6 = 64.328 + \frac{29498.1}{146 - (1/\lambda)^2} + \frac{255.4}{41 - (1/\lambda)^2} \quad , \tag{1}$$

where λ is the wavelength of light in vacuo (microns). Since observatories are usually located at high altitudes, the index of refraction must be corrected for the lower ambient temperature and pressure (Barrell 1951):

$$(n(\lambda)_{T,P} - 1) = (n(\lambda)_{15,760} - 1) \times \frac{P[1 + (1.049 - 0.0157\,T)10^{-6}P]}{720.883(1 + 0.003661\,T)} \quad . \tag{2}$$

In addition, the presence of water vapor in the atmosphere reduces $(n - 1)10^6$ by

$$\frac{0.0624 - 0.000680/\lambda^2}{1 + 0.003661T} f \quad , \tag{3}$$

where f is the water vapor pressure in mm of Hg and T is the air temperature in ° C (Barrell 1951). At an altitude of ~ 2 km and a latitude of ~ ±30°, average conditions are (Allen 1973) $P \approx 600$ mm Hg, $T \approx 7$° C, and $f \approx 8$ mm Hg. These values are used in equations (1) through (3) in order to obtain $n(\lambda)$, and atmospheric differential refraction (arc seconds) relative to λ = 5000 Å is then calculated for an object at zenith angle z from (Smart 1931)

$$\Delta R(\lambda) \equiv R(\lambda) - R(5000) \approx 206265\,[n(\lambda) - n(5000)] \tan z \quad . \tag{4}$$

The results are presented in Table I. It is clear that the importance of atmospheric dispersion increases rapidly with increasing zenith angle and decreasing wavelength, and infrared observations are rarely affected.

B. *Effect on Spectrophotometry*

Table I demonstrates that at an air mass ($\sim$ sec z) of only 1.1 the image of a point source viewed at 6500 Å is displaced from that at 3500 Å by three-quarters of an arc second, while at sec z = 1.3 the displacement becomes nearly 1.4 arc seconds. It will now be shown that this leads to considerable relative light losses in low- or moderate-dispersion narrow-aperture spectrophotometry if the aperture or slit is *not* aligned along the direction of atmospheric refraction.

The convolution of guiding errors and seeing produces a point spread function whose surface brightness $\mu(r)$ is a Gaussian with dispersion σ (King 1971):

$$\mu(r) = \frac{1}{2\pi\sigma^2} e^{-r^2/2\sigma^2} \quad . \tag{5}$$

This equation is normalized such that the total intensity at any given wavelength is equal to unity, and σ is assumed to be independent of wavelength. If a star is centered at wavelength λ in a rectangular aperture of width $2a$ and length $2b$ (arc seconds), then the amount of light at λ entering the aperture is given by

$$\begin{aligned} I(\lambda) &= \int_{-b}^{b} \int_{-a}^{a} \mu(r)dxdy \\ &= \frac{1}{2\pi\sigma^2} \int_{-b}^{b} \int_{-a}^{a} e^{-(x^2 + y^2)/2\sigma^2} dxdy \quad , \end{aligned} \tag{6}$$

or

$$\begin{aligned} I(\lambda) = &\left(\frac{1}{\sqrt{2\pi}\,\sigma} \int_{-a}^{a} e^{-x^2/2\sigma^2} dx \right) \\ &\times \left(\frac{1}{\sqrt{2\pi}\,\sigma} \int_{-b}^{b} e^{-y^2/2\sigma^2} dy \right) \quad . \end{aligned} \tag{7}$$

On the other hand, if the star is displaced from the aperture center by x_0 arc seconds along the x direction, then

$$\begin{aligned} I(\lambda) = &\frac{1}{2} \left(\frac{1}{\sqrt{2\pi}\,\sigma} \int_{-(a-x_0)}^{(a-x_0)} e^{-x^2/2\sigma^2} dx \right. \\ &\left. + \frac{1}{\sqrt{2\pi}\,\sigma} \int_{-(a+x_0)}^{(a+x_0)} e^{-x^2/2\sigma^2} dx \right) \\ &\times \left(\frac{1}{\sqrt{2\pi}\,\sigma} \int_{-b}^{b} e^{-y^2/2\sigma^2} dy \right) \quad . \end{aligned} \tag{8}$$

With the aid of standard Gaussian integral tables the above expressions may be easily used to calculate $I(\lambda)$ under various observing conditions.

Suppose, for example, that the spectrum of a star at sec z = 1.1 is obtained with a 2″ × 4″ aperture on a night when 2σ = 1.″5, and that the *small* dimension of the aperture is aligned along the atmospheric dispersion. If the star is centered in the aperture at wavelength 5000 Å, then according to Table I it will be off center by 0.″56 at 3500 Å and by 0.″21 in the opposite direction at 6500 Å. Consequently, equations (7) and (8) show that the percentage of light entering the aperture at 5000 Å, 6500 Å, and 3500 Å is 81.1, 79.5, and 69.7, respectively. Thus, at an air mass of only 1.1 the light loss at 3500 Å is 11.4 percent greater than at 5000 Å, and it is easy to see that the relative light losses grow rapidly with increasing air mass. These errors are particularly alarming in view of the fact that intensity ratios such as I([O III]λ5007)/I([O II]λ3727) are frequently used to distinguish between different ionization mechanisms in galactic nuclei and other objects.

Now suppose that the same conditions apply, except that the *long* dimension of the aperture is oriented along the direction of atmospheric dispersion. Then the percentage of light entering the aperture at 5000 Å, 6500 Å, and 3500 Å is 81.1, 80.9, and 79.5, respectively. The relative light loss has therefore been considerably reduced by proper orientation of the aperture. Furthermore, the losses due to differential refraction disappear entirely if a long slit oriented along the atmospheric refraction is used to obtain widened one-dimensional spectra, since light displaced by different amounts still enters the slit. (Note, however, that problems caused by atmospheric dispersion cannot be completely avoided if unwidened two-dimensional spectra of extended objects are desired.)

III. Optimal Slit or Aperture Position Angle

Since atmospheric differential refraction is perpendicular to the horizon, the slit or rectangular aperture of a spectrograph should be oriented along this direction. When the object is on the meridian, the slit position angle must be 0° or 180°, but as it moves across the sky the angle changes. In this section the optimal slit position angle as a function of object position is derived and tabulated for easy reference. (Following standard practice, the position angle is defined as the angle between the slit and the hour circle through the object, measured from the north through the east from 0° to 360°.)

Consider the spherical triangle whose vertices are defined by the object being observed, the zenith, and the appropriate celestial pole. Application of the law of sines yields

$$\frac{\sin \eta}{\sin (\pi/2 - \phi)} = \frac{\sin h}{\sin z} \quad , \tag{9}$$

where η is the parallactic angle, h is the object's hour angle (h is positive if west of the meridian), z is the object's zenith angle, and ϕ is the observer's latitude. Equa-

Table I

Atmospheric differential refraction at an altitude of 2 km (arcseconds)

	Wavelength (Ångstroms)													
Sec z	3000	3500	4000	4500	5000	5500	6000	6500	7000	7500	8000	8500	9000	9500	10000
1.00	0.00	0.00	0.00	0.00	0.00	0.00	0.00	0.00	0.00	0.00	0.00	0.00	0.00	0.00	0.00
1.05	0.68	0.38	0.20	0.08	0.00	-0.06	-0.11	-0.14	-0.17	-0.19	-0.21	-0.23	-0.24	-0.25	-0.26
1.10	0.97	0.55	0.29	0.12	0.00	-0.09	-0.15	-0.20	-0.24	-0.28	-0.30	-0.32	-0.34	-0.36	-0.37
1.15	1.20	0.68	0.36	0.15	0.00	-0.11	-0.19	-0.25	-0.30	-0.34	-0.38	-0.40	-0.42	-0.44	-0.46
1.20	1.40	0.80	0.42	0.17	0.00	-0.13	-0.22	-0.30	-0.35	-0.40	-0.44	-0.47	-0.50	-0.52	-0.54
1.25	1.59	0.90	0.48	0.20	0.00	-0.14	-0.25	-0.33	-0.40	-0.45	-0.50	-0.53	-0.56	-0.59	-0.61
1.30	1.76	1.00	0.53	0.22	0.00	-0.16	-0.28	-0.37	-0.44	-0.50	-0.55	-0.59	-0.62	-0.65	-0.67
1.35	1.92	1.09	0.58	0.24	0.00	-0.17	-0.30	-0.40	-0.48	-0.55	-0.60	-0.64	-0.68	-0.71	-0.73
1.40	2.07	1.18	0.62	0.26	0.00	-0.19	-0.33	-0.44	-0.52	-0.59	-0.65	-0.69	-0.73	-0.77	-0.79
1.45	2.22	1.26	0.67	0.28	0.00	-0.20	-0.35	-0.47	-0.56	-0.63	-0.69	-0.74	-0.79	-0.82	-0.85
1.50	2.37	1.34	0.71	0.29	0.00	-0.21	-0.37	-0.50	-0.60	-0.68	-0.74	-0.79	-0.84	-0.87	-0.91
1.55	2.51	1.42	0.75	0.31	0.00	-0.23	-0.40	-0.53	-0.63	-0.72	-0.78	-0.84	-0.89	-0.93	-0.96
1.60	2.64	1.50	0.80	0.33	0.00	-0.24	-0.42	-0.56	-0.67	-0.75	-0.83	-0.88	-0.93	-0.98	-1.01
1.65	2.78	1.58	0.84	0.34	0.00	-0.25	-0.44	-0.59	-0.70	-0.79	-0.87	-0.93	-0.98	-1.03	-1.06
1.70	2.91	1.65	0.88	0.36	0.00	-0.26	-0.46	-0.61	-0.73	-0.83	-0.91	-0.97	-1.03	-1.07	-1.11
1.75	3.04	1.73	0.92	0.38	0.00	-0.27	-0.48	-0.64	-0.77	-0.87	-0.95	-1.02	-1.07	-1.12	-1.16
1.80	3.17	1.80	0.95	0.39	0.00	-0.29	-0.50	-0.67	-0.80	-0.90	-0.99	-1.06	-1.12	-1.17	-1.21
1.85	3.29	1.87	0.99	0.41	0.00	-0.30	-0.52	-0.69	-0.83	-0.94	-1.03	-1.10	-1.16	-1.22	-1.26
1.90	3.42	1.94	1.03	0.42	0.00	-0.31	-0.54	-0.72	-0.86	-0.98	-1.07	-1.14	-1.21	-1.26	-1.31
1.95	3.54	2.01	1.07	0.44	0.00	-0.32	-0.56	-0.75	-0.89	-1.01	-1.11	-1.19	-1.25	-1.31	-1.36
2.00	3.67	2.08	1.10	0.45	0.00	-0.33	-0.58	-0.77	-0.92	-1.05	-1.15	-1.23	-1.30	-1.35	-1.40
2.10	3.91	2.22	1.18	0.48	0.00	-0.35	-0.62	-0.82	-0.99	-1.12	-1.22	-1.31	-1.38	-1.44	-1.50
2.20	4.15	2.36	1.25	0.51	0.00	-0.37	-0.66	-0.87	-1.05	-1.18	-1.30	-1.39	-1.47	-1.53	-1.59
2.30	4.38	2.49	1.32	0.54	0.00	-0.40	-0.69	-0.92	-1.11	-1.25	-1.37	-1.47	-1.55	-1.62	-1.68
2.40	4.62	2.62	1.39	0.57	0.00	-0.42	-0.73	-0.97	-1.16	-1.32	-1.44	-1.55	-1.63	-1.70	-1.77
2.50	4.85	2.75	1.46	0.60	0.00	-0.44	-0.77	-1.02	-1.22	-1.38	-1.52	-1.62	-1.71	-1.79	-1.86
2.60	5.08	2.88	1.53	0.63	0.00	-0.46	-0.80	-1.07	-1.28	-1.45	-1.59	-1.70	-1.80	-1.88	-1.94
2.70	5.31	3.01	1.60	0.66	0.00	-0.48	-0.84	-1.12	-1.34	-1.51	-1.66	-1.78	-1.88	-1.96	-2.03
2.80	5.54	3.14	1.67	0.69	0.00	-0.50	-0.88	-1.17	-1.40	-1.58	-1.73	-1.85	-1.96	-2.04	-2.12
2.90	5.76	3.27	1.74	0.71	0.00	-0.52	-0.91	-1.21	-1.45	-1.64	-1.80	-1.93	-2.04	-2.13	-2.20
3.00	5.99	3.40	1.80	0.74	0.00	-0.54	-0.95	-1.26	-1.51	-1.71	-1.87	-2.00	-2.12	-2.21	-2.29
3.10	6.21	3.53	1.87	0.77	0.00	-0.56	-0.98	-1.31	-1.57	-1.77	-1.94	-2.08	-2.19	-2.29	-2.38
3.20	6.44	3.65	1.94	0.80	0.00	-0.58	-1.02	-1.36	-1.62	-1.84	-2.01	-2.15	-2.27	-2.38	-2.46
3.30	6.66	3.78	2.00	0.83	0.00	-0.60	-1.05	-1.40	-1.68	-1.90	-2.08	-2.23	-2.35	-2.46	-2.55
3.40	6.88	3.91	2.07	0.85	0.00	-0.62	-1.09	-1.45	-1.73	-1.96	-2.15	-2.30	-2.43	-2.54	-2.63
3.50	7.10	4.03	2.14	0.88	0.00	-0.64	-1.12	-1.50	-1.79	-2.03	-2.22	-2.38	-2.51	-2.62	-2.72
3.60	7.32	4.16	2.20	0.91	0.00	-0.66	-1.16	-1.54	-1.85	-2.09	-2.29	-2.45	-2.59	-2.70	-2.80
3.70	7.54	4.28	2.27	0.94	0.00	-0.68	-1.19	-1.59	-1.90	-2.15	-2.36	-2.52	-2.66	-2.78	-2.88
3.80	7.76	4.41	2.34	0.96	0.00	-0.70	-1.23	-1.64	-1.96	-2.21	-2.42	-2.60	-2.74	-2.86	-2.97
3.90	7.98	4.53	2.40	0.99	0.00	-0.72	-1.26	-1.68	-2.01	-2.28	-2.49	-2.67	-2.82	-2.95	-3.05
4.00	8.20	4.66	2.47	1.02	0.00	-0.74	-1.30	-1.73	-2.07	-2.34	-2.56	-2.74	-2.90	-3.03	-3.14
4.10	8.42	4.78	2.53	1.04	0.00	-0.76	-1.33	-1.77	-2.12	-2.40	-2.63	-2.82	-2.97	-3.11	-3.22
4.20	8.64	4.90	2.60	1.07	0.00	-0.78	-1.37	-1.82	-2.18	-2.46	-2.70	-2.89	-3.05	-3.19	-3.30
4.30	8.85	5.03	2.67	1.10	0.00	-0.80	-1.40	-1.87	-2.23	-2.53	-2.77	-2.96	-3.13	-3.27	-3.39
4.40	9.07	5.15	2.73	1.12	0.00	-0.82	-1.44	-1.91	-2.29	-2.59	-2.83	-3.04	-3.21	-3.35	-3.47
4.50	9.29	5.27	2.80	1.15	0.00	-0.84	-1.47	-1.96	-2.34	-2.65	-2.90	-3.11	-3.28	-3.43	-3.55
4.60	9.51	5.40	2.86	1.18	0.00	-0.86	-1.51	-2.00	-2.40	-2.71	-2.97	-3.18	-3.36	-3.51	-3.64
4.70	9.72	5.52	2.93	1.21	0.00	-0.88	-1.54	-2.05	-2.45	-2.77	-3.04	-3.25	-3.44	-3.59	-3.72
4.80	9.94	5.64	2.99	1.23	0.00	-0.90	-1.57	-2.09	-2.51	-2.84	-3.10	-3.33	-3.51	-3.67	-3.80
4.90	10.15	5.77	3.06	1.26	0.00	-0.92	-1.61	-2.14	-2.56	-2.90	-3.17	-3.40	-3.59	-3.75	-3.88

tion (9) is equivalent to

$$\sin\eta = \frac{\sin h \cos\phi}{[1 - (\sin\phi \sin\delta + \cos\phi \cos\delta \cos h)^2]^{1/2}}, \tag{10}$$

which gives the parallactic angle, and hence the optimal slit position angle, explicitly as a function of object hour angle and declination δ. In practice, one must be very careful when using equation (10) to calculate the slit position angle, as errors are easily made: if we define $-90° \leq \eta \leq 90°$, then the true position angle may be η, $180° - \eta$, or $-(180° + \eta)$ depending on the hemisphere from which observations are made, on the value of the hour angle, and on whether the object is north or south of the zenith.

In order to minimize relative light losses, it is clearly most desirable to continuously rotate the slit position angle as the object's hour angle changes. Such a system is currently being designed for the 5-m Hale telescope (J. B. Oke 1982). However, for short integrations it is generally sufficient to use the time-averaged value of the optimal position angle.

Tables II and III list the approximate air mass and best position angle as a function of object hour angle and declination. Air masses are included to aid the observer in deciding whether the differential refraction at the object position (as given in Table I) is of sufficient importance to necessitate rotation of the spectrograph. Although Table II is calculated for the latitude of Palomar Observatory ($\phi = +33°21'$), it is also applicable at many other northern observatories; the only large differences occur when an object is near the zenith, in which case the air mass is so small that differential refraction may be neglected. Similarly, Table III refers specifically to Las Campanas Observatory ($\phi = -29°00'$). Figures 1 and 2 display the optimal position angle versus object hour angle for different object declinations. It is seen that the optimal position angle changes very rapidly for objects near the zenith, but usually the spectrograph need not be rotated in such cases.

Table II

(a) Secant z, and (b) Optimal slit position angle at Palomar Observatory

(a) Dec	Hour angle east or west of the meridian 0.0	0.5	1.0	1.5	2.0	2.5	3.0	3.5	4.0	4.5	5.0	5.5	6.0	6.5	7.0	7.5	8.0
-35.0	2.71	2.75	2.89	3.16	3.61	4.39	5.93	9.88									
-30.0	2.23	2.26	2.36	2.54	2.84	3.34	4.23	6.04									
-25.0	1.91	1.93	2.00	2.14	2.36	2.72	3.30	4.38	6.84								
-20.0	1.68	1.69	1.75	1.86	2.03	2.30	2.72	3.45	4.89	8.90							
-15.0	1.50	1.52	1.57	1.66	1.80	2.01	2.34	2.87	3.83	6.01							
-10.0	1.38	1.39	1.43	1.50	1.62	1.79	2.06	2.47	3.17	4.56	8.51						
-5.0	1.28	1.29	1.32	1.39	1.49	1.63	1.85	2.18	2.72	3.70	5.97						
0.0	1.20	1.21	1.24	1.30	1.38	1.51	1.69	1.97	2.39	3.13	4.63	9.17					
5.0	1.14	1.15	1.17	1.22	1.30	1.41	1.57	1.80	2.16	2.73	3.80	6.39					
10.0	1.09	1.10	1.12	1.17	1.24	1.34	1.48	1.68	1.97	2.44	3.24	4.93					
15.0	1.05	1.06	1.09	1.13	1.19	1.28	1.40	1.58	1.83	2.22	2.85	4.04	7.03				
20.0	1.03	1.03	1.06	1.10	1.15	1.23	1.35	1.50	1.72	2.05	2.56	3.44	5.32				
25.0	1.01	1.02	1.04	1.07	1.13	1.20	1.30	1.44	1.64	1.92	2.33	3.02	4.30	7.49			
30.0	1.00	1.01	1.03	1.06	1.11	1.18	1.27	1.40	1.57	1.81	2.16	2.71	3.64	5.54			
35.0	1.00	1.01	1.02	1.06	1.10	1.17	1.25	1.37	1.52	1.73	2.03	2.47	3.17	4.42	7.23		
40.0	1.01	1.01	1.03	1.06	1.10	1.16	1.24	1.35	1.49	1.67	1.93	2.29	2.83	3.71	5.33	9.22	
45.0	1.02	1.03	1.04	1.07	1.11	1.17	1.24	1.34	1.46	1.63	1.85	2.15	2.57	3.21	4.24	6.15	
50.0	1.04	1.05	1.06	1.09	1.13	1.18	1.25	1.34	1.45	1.60	1.79	2.04	2.37	2.85	3.54	4.64	6.55
55.0	1.08	1.08	1.10	1.12	1.16	1.20	1.27	1.35	1.45	1.58	1.74	1.95	2.22	2.58	3.06	3.75	4.74
60.0	1.12	1.12	1.14	1.16	1.19	1.24	1.30	1.37	1.46	1.57	1.71	1.88	2.10	2.37	2.72	3.16	3.74
65.0	1.17	1.18	1.19	1.21	1.24	1.28	1.34	1.40	1.48	1.58	1.70	1.84	2.01	2.21	2.46	2.75	3.11
70.0	1.25	1.25	1.26	1.28	1.31	1.35	1.39	1.45	1.52	1.60	1.69	1.81	1.94	2.09	2.26	2.46	2.68
75.0	1.34	1.34	1.35	1.37	1.39	1.42	1.46	1.51	1.56	1.63	1.70	1.79	1.88	1.99	2.10	2.23	2.36
80.0	1.46	1.46	1.47	1.48	1.50	1.52	1.55	1.59	1.63	1.68	1.73	1.78	1.85	1.91	1.98	2.06	2.13
85.0	1.61	1.61	1.62	1.63	1.64	1.65	1.67	1.69	1.71	1.74	1.77	1.79	1.83	1.86	1.89	1.92	1.96

(b) Dec	Hour angle west of the meridian 0.0	0.5	1.0	1.5	2.0	2.5	3.0	3.5	4.0	4.5	5.0	5.5	6.0	6.5	7.0	7.5	8.0
-35.0	0.0	6.7	13.3	19.7	25.8	31.5	36.8	41.8									
-30.0	0.0	7.0	13.8	20.3	26.5	32.2	37.4	42.2									
-25.0	0.0	7.3	14.4	21.2	27.5	33.2	38.3	42.9	47.0								
-20.0	0.0	7.8	15.3	22.3	28.7	34.4	39.4	43.8	47.6	51.0							
-15.0	0.0	8.3	16.3	23.6	30.2	35.9	40.8	45.0	48.5	51.5							
-10.0	0.0	9.0	17.6	25.3	32.1	37.8	42.5	46.5	49.7	52.3	54.3						
-5.0	0.0	10.0	19.3	27.5	34.4	40.0	44.6	48.2	51.1	53.3	54.9						
0.0	0.0	11.2	21.5	30.2	37.2	42.8	47.1	50.3	52.8	54.5	55.7	56.4					
5.0	0.0	12.9	24.4	33.6	40.8	46.1	50.0	52.8	54.8	56.0	56.8	57.0					
10.0	0.0	15.3	28.3	38.1	45.1	50.0	53.4	55.6	57.1	57.8	58.0	57.8					
15.0	0.0	19.0	33.9	44.0	50.5	54.7	57.4	58.9	59.7	59.8	59.5	58.7	57.6				
20.0	0.0	25.0	41.9	51.7	57.2	60.3	62.0	62.7	62.7	62.2	61.3	59.9	58.3				
25.0	0.0	36.3	54.0	61.7	65.3	66.8	67.2	66.9	66.0	64.8	63.2	61.4	59.2	56.7			
30.0	0.0	60.4	71.4	74.2	74.7	74.1	73.0	71.5	69.7	67.7	65.5	63.0	60.3	57.4			
35.0	180.0	102.8	93.3	88.6	85.2	82.1	79.3	76.5	73.8	70.9	68.0	64.9	61.7	58.2	54.6		
40.0	180.0	135.6	114.3	103.2	96.0	90.5	86.0	81.9	78.1	74.4	70.7	67.0	63.2	59.3	55.2	50.9	
45.0	180.0	151.0	130.1	116.2	106.4	98.9	92.8	87.5	82.6	78.1	73.7	69.4	65.0	60.6	56.1	51.5	
50.0	180.0	158.8	140.8	126.6	115.7	106.9	99.5	93.1	87.4	82.0	76.9	72.0	67.1	62.2	57.3	52.2	47.1
55.0	180.0	163.3	148.0	134.7	123.6	114.1	105.9	98.7	92.1	86.0	80.3	74.7	69.3	64.0	58.6	53.2	47.7
60.0	180.0	166.2	153.0	140.9	130.1	120.5	111.8	104.0	96.8	90.1	83.8	77.7	71.8	66.0	60.2	54.4	48.7
65.0	180.0	168.1	156.6	145.6	135.4	125.9	117.2	109.0	101.4	94.3	87.4	80.8	74.5	68.2	62.0	55.9	49.8
70.0	180.0	169.5	159.2	149.2	139.7	130.5	121.9	113.6	105.8	98.3	91.1	84.1	77.3	70.7	64.1	57.7	51.3
75.0	180.0	170.6	161.3	152.1	143.1	134.4	125.9	117.8	109.8	102.2	94.7	87.4	80.3	73.4	66.5	59.7	53.0
80.0	180.0	171.4	162.8	154.3	145.9	137.6	129.5	121.5	113.6	105.9	98.3	90.8	83.5	76.2	69.1	62.0	55.0
85.0	180.0	172.0	164.0	156.1	148.2	140.3	132.5	124.7	117.0	109.3	101.7	94.2	86.7	79.3	71.9	64.6	57.3

Note: The corresponding position angles for objects east of the meridian are negative.

Many spectrographs capable of being rotated are set by default to a position angle of 90°. Although this minimizes light losses caused by tracking errors, the losses due to atmospheric dispersion may be far larger. Since objects are frequently observed when they are near the meridian, the optimal position angle is often closer to 0° or 180° rather than to the default value. Thus, erroneous relative line strengths pervade the literature and must be viewed with caution. Only the best available data should be incorporated in astrophysical models, as was generally done by Baldwin et al. (1981).

It is a pleasure to thank the Fannie and John Hertz Foundation for financial support, as well as D. P. Schneider, T. A. Boroson, G. Berriman, and J. R. Pier for comments on an earlier version of this paper. Amusing discussions with W. L. W. Sargent are also appreciated.

REFERENCES

Allen, C. W. 1973, *Astrophysical Quantities*, 3rd ed. (London: Athlone Press), pp. 119–22.

Baldwin, J. A., Phillips, M. M., and Terlevich, R. 1981, *Pub. A.S.P.* 93, 5.

Barrell, H. 1951, *J. Opt. Soc. Am.* 41, 295.

Coleman, C. D., Bozman, W. R., and Meggers, W. F. 1960, *Tables of Wavenumbers, N.B.S. Monograph* 3, Washington, p. IV.

Edlén, B. 1953, *J. Opt. Soc. Am.* 43, 339.

King, I. R. 1971, *Pub. A.S.P.* 83, 199.

Oke, J. B. 1982 (private communication).

Simon, G. W. 1966, *A.J.* 71, 190.

Smart, W. M. 1931, *Textbook on Spherical Astronomy*, 6th ed. (1977) (Cambridge: Cambridge University Press), p. 61.

van de Kamp, P. 1967, *Principles of Astrometry* (San Francisco: W. H. Freeman and Co.), chap. 6.

Table III

(a) Secant z, and (b) Optimal slit position angle at Las Campanas Observatory

(a) Dec	Hour angle east or west of the meridian																
	0.0	0.5	1.0	1.5	2.0	2.5	3.0	3.5	4.0	4.5	5.0	5.5	6.0	6.5	7.0	7.5	8.0
35.0	2.28	2.31	2.42	2.61	2.92	3.44	4.38	6.33									
30.0	1.94	1.97	2.04	2.19	2.42	2.79	3.41	4.57	7.34								
25.0	1.70	1.72	1.78	1.90	2.08	2.36	2.81	3.60	5.22								
20.0	1.52	1.54	1.59	1.68	1.83	2.06	2.41	2.99	4.08	6.72							
15.0	1.39	1.40	1.45	1.53	1.65	1.84	2.12	2.57	3.37	5.06							
10.0	1.29	1.30	1.34	1.41	1.51	1.67	1.91	2.27	2.89	4.07	7.21						
5.0	1.21	1.22	1.25	1.31	1.40	1.54	1.74	2.05	2.54	3.43	5.46						
0.0	1.14	1.15	1.18	1.24	1.32	1.44	1.62	1.88	2.29	2.99	4.42	8.76					
-5.0	1.09	1.10	1.13	1.18	1.25	1.36	1.52	1.75	2.09	2.66	3.73	6.41					
-10.0	1.06	1.07	1.09	1.14	1.20	1.30	1.44	1.64	1.94	2.42	3.26	5.09					
-15.0	1.03	1.04	1.06	1.10	1.17	1.26	1.38	1.56	1.83	2.23	2.91	4.24	7.97				
-20.0	1.01	1.02	1.04	1.08	1.14	1.22	1.34	1.50	1.73	2.08	2.64	3.66	6.03				
-25.0	1.00	1.01	1.03	1.07	1.12	1.20	1.31	1.45	1.66	1.97	2.44	3.24	4.88	9.86			
-30.0	1.00	1.01	1.03	1.06	1.11	1.19	1.29	1.42	1.61	1.88	2.28	2.93	4.13	6.97			
-35.0	1.01	1.01	1.03	1.06	1.11	1.18	1.27	1.40	1.57	1.81	2.16	2.69	3.60	5.42			
-40.0	1.02	1.02	1.04	1.07	1.12	1.19	1.27	1.39	1.55	1.76	2.06	2.51	3.21	4.46	7.23		
-45.0	1.04	1.05	1.06	1.09	1.14	1.20	1.28	1.39	1.53	1.73	1.99	2.36	2.92	3.82	5.47	9.42	
-50.0	1.07	1.08	1.09	1.12	1.17	1.22	1.30	1.40	1.53	1.70	1.93	2.25	2.69	3.36	4.43	6.40	
-55.0	1.11	1.12	1.13	1.16	1.20	1.26	1.33	1.42	1.54	1.70	1.90	2.16	2.52	3.02	3.74	4.87	6.84
-60.0	1.17	1.17	1.19	1.21	1.25	1.30	1.37	1.46	1.57	1.70	1.88	2.10	2.38	2.76	3.26	3.96	4.97
-65.0	1.24	1.24	1.26	1.28	1.32	1.36	1.43	1.51	1.60	1.72	1.87	2.05	2.28	2.56	2.91	3.36	3.93
-70.0	1.33	1.33	1.34	1.37	1.40	1.44	1.50	1.57	1.65	1.75	1.88	2.02	2.20	2.40	2.64	2.93	3.27
-75.0	1.44	1.44	1.46	1.48	1.51	1.54	1.59	1.65	1.72	1.80	1.90	2.01	2.14	2.28	2.44	2.62	2.82
-80.0	1.59	1.59	1.60	1.62	1.64	1.67	1.71	1.75	1.81	1.87	1.94	2.01	2.09	2.19	2.28	2.38	2.49
-85.0	1.79	1.79	1.80	1.81	1.82	1.84	1.86	1.89	1.92	1.95	1.99	2.03	2.07	2.11	2.16	2.20	2.25

(b) Dec	Hour angle west of the meridian																
	0.0	0.5	1.0	1.5	2.0	2.5	3.0	3.5	4.0	4.5	5.0	5.5	6.0	6.5	7.0	7.5	8.0
35.0	180.0	172.7	165.6	158.7	152.3	146.2	140.6	135.4									
30.0	180.0	172.4	165.0	157.9	151.3	145.2	139.7	134.7	130.1								
25.0	180.0	171.9	164.1	156.8	150.1	144.0	138.6	133.8	129.5								
20.0	180.0	171.4	163.1	155.4	148.5	142.5	137.2	132.6	128.6	125.2							
15.0	180.0	170.6	161.8	153.7	146.6	140.6	135.5	131.1	127.5	124.5							
10.0	180.0	169.7	160.1	151.6	144.3	138.3	133.4	129.4	126.2	123.5	121.5						
5.0	180.0	168.4	157.9	148.8	141.5	135.6	131.0	127.3	124.5	122.4	120.8						
0.0	180.0	166.7	155.0	145.4	137.9	132.3	128.1	124.9	122.6	121.0	119.8	119.2					
-5.0	180.0	164.3	151.1	140.9	133.6	128.4	124.8	122.2	120.4	119.3	118.7	118.6					
-10.0	180.0	160.7	145.6	135.2	128.3	123.8	120.9	119.0	117.9	117.4	117.4	117.8					
-15.0	180.0	154.9	137.8	127.7	121.9	118.5	116.5	115.5	115.1	115.3	115.9	116.8	118.2				
-20.0	180.0	144.3	126.4	118.2	114.2	112.3	111.5	111.5	112.0	112.9	114.1	115.7	117.5				
-25.0	180.0	122.6	110.0	106.3	105.3	105.3	106.1	107.2	108.6	110.2	112.1	114.3	116.7	119.4			
-30.0	0.0	83.2	89.4	92.7	95.4	97.8	100.1	102.5	104.9	107.4	110.0	112.7	115.6	118.8			
-35.0	0.0	48.7	68.9	78.8	85.1	89.9	93.9	97.5	100.9	104.2	107.6	110.9	114.4	118.1			
-40.0	0.0	31.5	52.8	66.1	75.2	82.0	87.6	92.4	96.8	100.9	105.0	109.0	113.0	117.2	121.5		
-45.0	0.0	22.9	41.6	55.7	66.2	74.5	81.3	87.2	92.5	97.5	102.2	106.8	111.4	116.0	120.8	125.6	
-50.0	0.0	17.9	34.0	47.4	58.4	67.6	75.3	82.1	88.2	93.9	99.3	104.5	109.6	114.7	119.9	125.1	
-55.0	0.0	14.8	28.7	41.1	51.9	61.4	69.7	77.2	84.0	90.3	96.3	102.0	107.6	113.2	118.8	124.4	130.0
-60.0	0.0	12.7	24.8	36.2	46.6	56.0	64.6	72.5	79.8	86.6	93.1	99.4	105.5	111.5	117.4	123.4	129.4
-65.0	0.0	11.1	22.0	32.4	42.2	51.5	60.1	68.2	75.8	83.1	90.0	96.7	103.2	109.6	115.9	122.2	128.4
-70.0	0.0	10.0	19.8	29.4	38.7	47.6	56.1	64.3	72.1	79.6	86.8	93.9	100.7	107.5	114.1	120.7	127.3
-75.0	0.0	9.1	18.1	27.1	35.8	44.3	52.7	60.7	68.6	76.2	83.7	91.0	98.2	105.2	112.2	119.0	125.9
-80.0	0.0	8.4	16.8	25.2	33.5	41.6	49.7	57.6	65.4	73.1	80.7	88.1	95.5	102.8	110.0	117.1	124.2
-85.0	0.0	7.9	15.8	23.7	31.5	39.4	47.1	54.9	62.6	70.2	77.8	85.3	92.8	100.2	107.6	114.9	122.2

Note: The corresponding position angles for objects east of the meridian are negative.

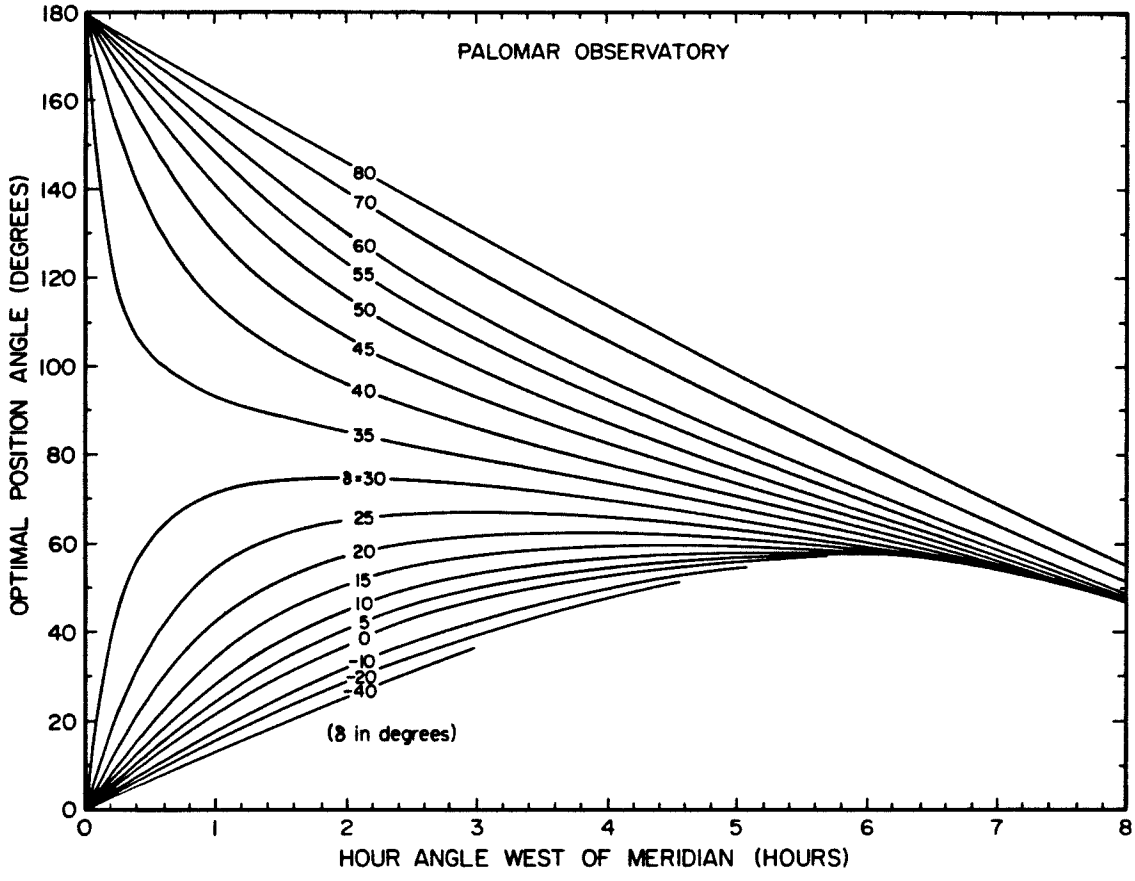

FIG. 1—Optimal slit or aperture position angle as a function of object position west of the meridian, computed for the latitude of Palomar Observatory. The diagram is valid for most other major observatories in the Northern Hemisphere, except at very small air masses. Corresponding position angles for objects east of the meridian are negative.

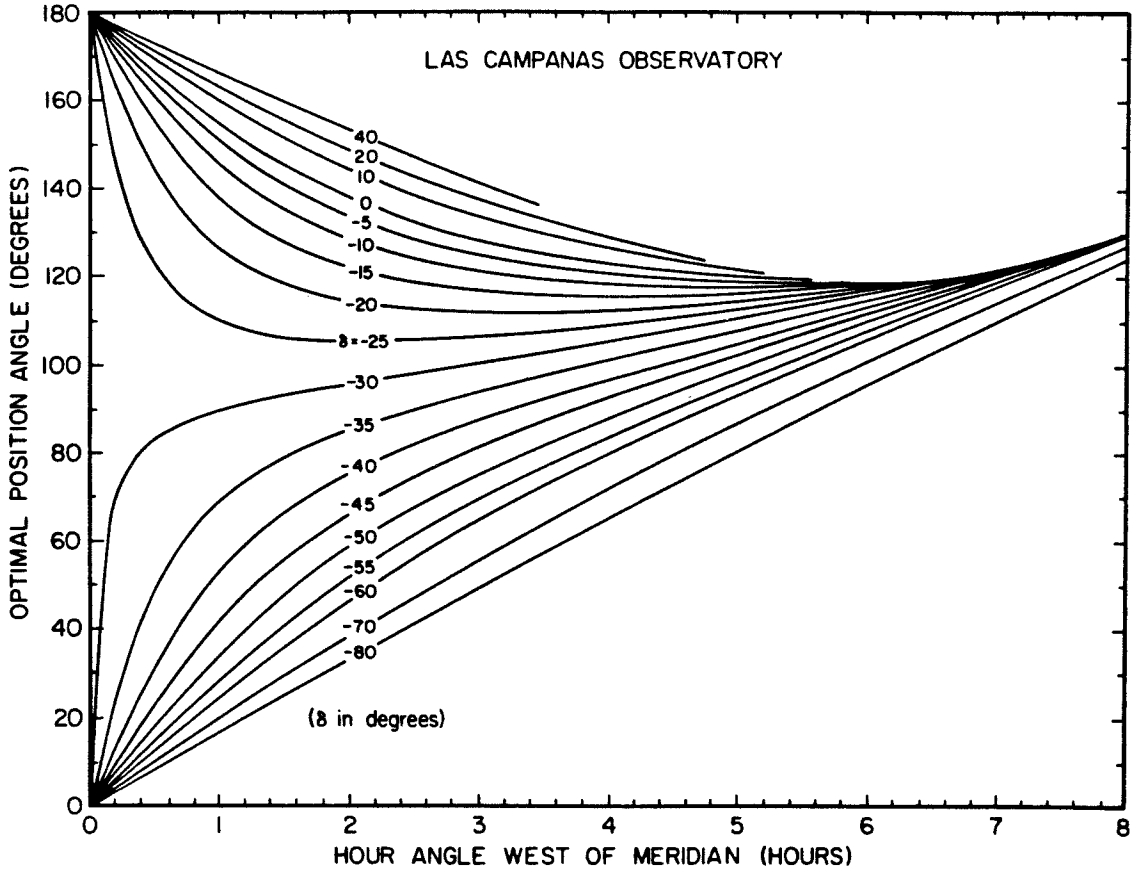

FIG. 2—The same as Figure 1, but computed for the latitude of Las Campanas Observatory. The diagram is valid for most other major observatories in the Southern Hemisphere, except at very small air masses.

APPENDIX 2

Faint Spectrophotometric Standard Stars for Large Optical Telescopes. I.

Alexei V. Filippenko and Jesse L. Greenstein

To be published in the Publications of the Astronomical Society of the Pacific, 1984 July.

Standards? What are they? Why do we need to measure standards if we already know what they look like?

An anonymous astronomer

ABSTRACT

We present spectral energy distributions over the range λλ3300–10000 for a set of five spectrophotometric standards, four of which are white dwarfs. These stars are faint ($m_v \sim 15.5$ mag), equatorial, and exhibit nearly featureless continua, so they can be observed without neutral density filters to calibrate the response of photon-counting spectrographs on large telescopes in both hemispheres.

Key words: spectrophotometry—stars: metal-deficient—stars: white dwarfs

I. INTRODUCTION

Modern electronic detectors on optical astronomical spectrographs can generally be divided into two classes: those in which charge accumulates at a rate proportional to the object's brightness and is measured at the end of an integration, and those that "count" each photon at the time of detection. The main properties of the former group are high quantum efficiency and linearity over an enormous range of incident fluxes, and it includes SIT vidicons (e.g., Kent 1979; Atwood et al. 1979) as well as CCDs (e.g., Oke and Gunn 1982). Reticons (Shectman and Hiltner 1976) and the IPCS (Boksenberg 1972; Boksenberg and Burgess 1973) represent the latter group; they offer real-time monitoring of a spectrum's progress and have no readout noise. On the other hand, they suffer from coincidence losses (Fernie 1976) even at relatively low count rates (~ 1 photon pixel^{-1} s^{-1}), so bright objects cannot be efficiently observed.

It is important to determine the overall spectral response of the spectrograph when reducing data obtained with these detectors. To facilitate this, secondary standards located primarily in the northern hemisphere and calibrated with respect to the absolute energy distribution of α Lyrae (Oke and Schild 1970; Hayes 1970; Hayes and Latham 1975) were established by a number of observers (e.g., Oke 1964; Hayes 1970; Stone 1974, 1977; Breger 1975; Oke and Gunn 1983). In addition, Stone and Baldwin (1983) and Baldwin and Stone (1984) recently provided reliable standards in the southern hemisphere. Most of the stars listed in the above references, however, are too bright to be used with photon-counting systems, since their visual magnitudes are less

than ~ 13. The Intensified Reticon on the 2.5 m duPont telescope at Las Campanas Observatory, for example, detects ~ 1 photon Å^{-1} s^{-1} at $\lambda 5000$ for a star with $m_v \sim 14.5$, so substantial ($\gtrsim 10\%$) coincidence losses occur when a low-dispersion grating is used. Similar problems are evident with stars as faint as $m_v \sim 16$ when using photon-counting spectrometers on the Hale reflector at Palomar Observatory.

Attempts have been made to overcome this problem by adopting as intermediate standards the spectral scans of faint white dwarfs published by Oke (1974). But these objects were not intended to be used as standards; many are unsuitable because of brightness, and the strong, broad absorption lines of H or He visible in the spectra of DA and DB stars prove to be particularly troublesome in reduction programs. It is also best to avoid the use of "neutral density" filters, since their actual transmittance is a function of wavelength and is often difficult to calibrate accurately. Similarly, absolute spectrophotometry is sacrificed if a narrow slit or small aperture is employed to decrease the detected flux, and even relative intensities may be affected because of atmospheric dispersion.

Thus, faint standard stars distributed over the sky are clearly needed for photon-counting detectors on large telescopes. Ideally, these objects should exhibit nearly flat, featureless continua, and at least some of them must be accessible from both hemispheres. In this paper we present an initial set of five stars which come close to satisfying the above requirements. Several of them have already been successfully used by a number of observers; their calibration must be viewed as preliminary, however, since the data have somewhat low signal-to-noise ratios at ultraviolet and near-infrared wavelengths.

With respect to λ5400, relative and absolute uncertainties of roughly ± 0.03–0.04 mag exist from λ4000 through λ8000. The accuracy is worse outside this range, and in some cases the effects of atmospheric dispersion produce substantially greater errors in the UV.

II. OBSERVATIONS AND ANALYSIS

The stars were selected from the extensive catalog of white dwarfs compiled from observations made with the Multichannel Spectrophotometer (MCSP; Oke 1969) on the Palomar 5 m telescope (Greenstein 1984). Apparent magnitude, spectral type, accessibility from Las Campanas during observing runs in August of 1982 and 1983, and the quality of the MCSP data were the primary selection criteria; DA white dwarfs, for example, were generally excluded because of their strong, broad Balmer absorption lines. Table I lists the stars along with their 1950 coordinates, spectral classification on the system of Sion *et al.* (1983), magnitude at λ5400, proper motion, and references. Finding charts reproduced from Palomar Observatory Sky Survey E prints are shown in Figure 1. Plate epochs and the proper motions in Table I can be used to obtain current positions of the stars.

The spectral energy distribution of each object was determined from the MCSP observations. We attempted to use only data taken during nights whose photometric properties could be ascertained with reasonable certainty. At least two secondary standards from Oke and Gunn (1983) were observed each night through a 10″ circular aperture, but spectra of the faint objects were taken through a 7″ aperture in order to decrease contamination by strong moonlight. Under conditions of good seeing ($\lesssim$ 2″), the difference in aperture diameter should introduce negligible

error into the absolute calibration; the possibility of inaccuracies, however, cannot be entirely eliminated.

Reduction of the data included wavelength calibration of the MCSP bandpasses, removal of atmospheric extinction, subtraction of the sky, and determination of the spectral response. Systematic corrections were applied to the derived spectrum of each object in order to account for the recent recalibration (AB_{79}) of the preliminary (AB_{69}) flux distributions of the five sdG secondary standards described by Oke and Gunn (1983). The magnitude and sign of the corrections depended on which of the standards were used on the particular nights of observation.

Several of the MCSP spectra suggest the presence of weak absorption lines. Many of these features are confirmed in spectra having moderate resolution (~ 8–16 Å) obtained with the Intensified Reticon on the duPont 2.5 m reflector at Las Campanas and with the CCD Double Spectrograph (DBSP; Oke and Gunn 1982) on the Palomar Hale telescope. The Reticon spectrum of each star is shown in Figure 2, where $AB = -2.5\log(f_\nu) - 48.6$ at frequency $\nu = c/\lambda$. (Here the units of f_ν are erg s^{-1} cm^{-2} Hz^{-1}; if we wish f_ν in mJy, then $\log(f_\nu) = -0.4AB + 6.56$.)

A smooth curve representing the average continuum was drawn through the MCSP data. Magnitudes were determined at intervals of 100 Å blueward of λ5000 and 200 Å redward of λ5000. These points (listed in Table II and shown as filled circles in Figure 2) ignore the contribution of absorption lines, and are meant to delineate the "featureless" component of each star. Regions containing absorption lines should be excluded in reduction programs when using the stars as spectrophotometric standards; the instrumental response should instead

be estimated by adopting the monochromatic magnitudes in Table II and interpolating across contaminated sections. Note that some weak absorption lines possibly seen in the DBSP data may or may not be visible in the relatively noisy Las Campanas spectra (Figure 2).

III. NOTES CONCERNING INDIVIDUAL STARS

G158-100 (0031-12): This is a very metal-deficient G subdwarf with a nearly featureless spectrum. Weak Balmer absorption is visible, as well as Ca II H (λ3968) and K (λ3934), the G band (λ4304), Mg b (λ5175), Na D (λ5892), and lines of Fe I in the UV. The spectrum is quite similar to those of the Oke and Gunn (1983) secondary standards, although its color temperature is lower (5500-6000 K). G158-100 appears in Greenstein's (1984) catalogue of white dwarfs as a star with uncertain classification; it is also discussed by Greenstein (1976).

G138-31 (1625+09): Narrow Balmer absorption lines having small equivalent widths, and the overall shape of the continuum, indicate that this is a cool white dwarf of spectral type DA. The line profiles are in striking contrast to those found in classical DA stars such as HZ 4 and HZ 7 (Oke 1974), in which the wings of Hβ and Hγ merge. However, the color temperature of ~ 7000 K is far from the zone of hydrogen-driven nonradial oscillations (T ~ 11500 K).

G24-9 (2011+06): The continuum of this white dwarf is almost featureless. There are hints of shallow absorption near λλ4000-4100, λλ4550-4750, and perhaps elsewhere as well, so the spectral class is DQ. At a temperature of ~ 7000 K, the helium-dominated atmosphere is much too cool for the existence of pulsational instabilities, which probably require $T \gtrsim 20000$ K.

G157-34 (2311-06): Moderately strong Swan bands such as λ5165 $C_2(0,0)$ and λ4737 $C_2(1,0)$ are visible, making this a DQ white dwarf with a helium- and carbon-rich atmosphere near T ~ 8000 K. There are additional weaker lines near λ4100 and λ3800 similar to those reported by Wegner and Yackovich (1982) in LHS 262. The region redward of λ7000 may also contain a few weak features.

GD-248 (2323+15): Greenstein (1984) classified this white dwarf as a DC because it exhibits a featureless continuum in the MCSP data. Spectra obtained with the DBSP, however, indicate the possible presence of two or three very weak (depth $\lesssim 0.04$ mag) absorption lines at approximately the same wavelengths as prominent features in G157-34, so the true spectral class may be DQ. The absence of Balmer absorption shows that the atmosphere must be dominated by helium, since the temperature of GD-248 is ~ 9500-10000 K (which is too cool to produce He I lines). Moreover, GD-248 is deficient in carbon compared with most DQ stars; G47-18 (0850+33), an object of similar color temperature, contains very strong C_2 and CI features. Thus, other white dwarfs having helium-rich atmospheres and low C/He abundance ratios may prove to be the most nearly line-free standards in future studies.

IV. ESTIMATE OF ERRORS

The MCSP observations were made with (blue/red) resolution settings of (40/80 Å) or (80/160 Å). Statistical uncertainty in most channels is well below $\pm$ 0.05 mag; true relative errors are undoubtedly smaller, since we smoothed the data when determining the average continuum at each point. Due to the faintness of the objects and to the low sensitivity of the MCSP at ultraviolet and near-infrared wavelengths,

however, the data are of such quality only in the approximate range λλ4000-8000.

A potential source of error is present in the secondary standards (Oke and Gunn 1983) adopted to reduce the MCSP data. These objects are G-type subdwarfs with moderately strong Balmer absorption, and exhibit a marked decrease in brightness at shorter wavelengths than Ca II H and K. Near the Balmer limit they are not well-calibrated relative to the primary standard, α Lyrae. The absorption lines also cause difficulties in the calibration of other objects. Moreover, one of the original stars (HD 140283) is no longer being used as a secondary standard; its spectral energy distribution must therefore be considered less reliable (Oke and Gunn 1983), affecting the calibration of GD-248 and G138-31.

Serious systematic errors in some of our MCSP observations are produced by atmospheric dispersion. Since data for the faint equatorial stars were obtained through a circular aperture of only 7" diameter, substantial UV light was lost. At a given wavelength the loss depends critically on air mass and seeing (Filippenko 1982), but only rough estimates of the latter were recorded. Furthermore, the accuracy with which the aperture is centered on the object, as well as the effective wavelength of the image on the television screen used for guiding, are important factors. Thus, we could not calculate exact corrections for the data, and significant ($\sim \pm 0.1$ mag) uncertainty is present near λλ3300-3500 in G158-100, G157-34, and especially in G24-9. Dispersion corrections at wavelengths longer than ~ 4000 Å were small ($\lesssim 0.03$ mag).

Uncertainties in the average extinction coefficients for Palomar Observatory also decrease the accuracy of our calibrations, particularly at UV wavelengths. Observations of the sdG secondary standards made at

various air masses and checked for consistency, however, indicate that errors are probably small ($\lesssim$ 0.01–0.02 mag) over most of the optical window.

Considering all of the above sources of error, uncertainties relative to λ5400 in the smooth continuum of each star probably do not exceed $\pm$ 0.03–0.04 mag over the range $\lambda\lambda$4000–8000; a comparable error exists in our knowledge of the absolute fluxes. The calibration is less secure ($\pm$ 0.06–0.07 mag) outside these approximate limits, and in a few cases errors at the extreme UV end (λ3300) may be noticeably larger. It would clearly be useful to determine the spectral distributions of these stars with greater accuracy, but the data presented here are sufficient for many observational programs. Other faint standards for large optical telescopes will be published elsewhere.

It is a pleasure to thank the night and day assistants at Palomar and Las Campanas Observatories for their able help during observing runs. Dr. J. B. Oke supplied much useful information and advice, as well as several of the instruments with which the data were obtained. We thank D. P. Schneider for comments on an earlier version of this article. A. V. F. is grateful to the Fannie and John Hertz Foundation for a graduate fellowship. Additional support for this research was provided by NSF grant 83-05504 to J. L. G. Observations at Las Campanas were obtained under the cooperative agreement between the California Institute of Technology and the Carnegie Institution of Washington.

TABLE I

Faint Spectrophotometric Standard Stars

Star	α(1950)	δ(1950)	Type[a]	m(λ5400)	μ("/yr)[b]	PA[b]	Luyten (1957)	Source
G158-100	$00^h31^m22^s$	$-12°24'.4$	sdG	14.87	0.24	136°	LTT 300	3
G138-31	16 25 30	+09 19.3	DA7	16.14	0.47	192	....	1
G24-9	20 11 29	+06 34.1	DQ7	15.72	0.63	203	....	1
G157-34	23 11 51	-06 49.0	DQ6	15.35	0.38	245	LTT 9427	2
GD-248	23 23 36	+15 43.8	DQ5?	15.08	0.10	210	....	4

Sources: 1 = Giclas, Burnham, Thomas (1971)
2 = Giclas, Burnham, Thomas (1978)
3 = Giclas, Burnham, Thomas (1979)
4 = Giclas, Burnham, Thomas (1980)

Notes: [a]From Greenstein (1984), unless otherwise stated in §III. The integer represents an approximate temperature (50400/T).
[b]From Luyten (1979), except for GD-248 (source 4).

TABLE II

Continuum AB_{79} magnitude at selected wavelengths for five faint standards

N	Wavelength (Å)	G158-100	G138-31	G24-9	G157-34	GD-248
1	3300	16.53**	17.08**	16.65***	15.78**	15.21**
2	3400	16.41**	17.00**	16.57***	15.73**	15.18*
3	3500	16.26**	16.93*	16.49**	15.69**	15.16*
4	3600	16.13*	16.87*	16.40**	15.66*	15.14
5	3700	16.01*	16.81*	16.31**	15.62*	15.13
6	3800	15.89*	16.75	16.24**	15.59*	15.12
7	3900	15.78*	16.68	16.18*	15.56	15.10
8	4000	15.67	16.62	16.12*	15.53	15.09
9	4100	15.58	16.57	16.06*	15.50	15.08
10	4200	15.49	16.52	16.02*	15.48	15.07
11	4300	15.41	16.47	15.98*	15.46	15.06
12	4400	15.35	16.42	15.94	15.44	15.06
13	4500	15.28	16.38	15.91	15.42	15.05
14	4600	15.22	16.35	15.88	15.41	15.05
15	4700	15.17	16.31	15.85	15.40	15.05
16	4800	15.12	16.28	15.82	15.39	15.05
17	4900	15.07	16.25	15.80	15.38	15.05
18	5000	15.03	16.22	15.78	15.37	15.06
19	5200	14.95	16.18	15.75	15.36	15.07
20	5400	14.87	16.14	15.72	15.35	15.08
21	5600	14.81	16.11	15.70	15.35	15.10
22	5800	14.76	16.10	15.68	15.35	15.11
23	6000	14.70	16.08	15.66	15.35	15.13
24	6200	14.66	16.07	15.65	15.36	15.15
25	6400	14.61	16.06	15.63	15.36	15.17
26	6600	14.57	16.05	15.62	15.37	15.19
27	6800	14.53	16.04	15.61	15.37	15.21
28	7000	14.50	16.03	15.61	15.38	15.23
29	7200	14.47	16.03	15.60	15.39	15.26
30	7400	14.44	16.03	15.60	15.39	15.28
31	7600	14.41	16.02	15.59	15.40	15.30
32	7800	14.39	16.02	15.59	15.41	15.32
33	8000	14.37	16.02	15.58	15.43	15.34
34	8200	14.35	16.03	15.58	15.44	15.36
35	8400	14.34	16.03	15.58	15.46	15.39
36	8600	14.32	16.03	15.58*	15.47	15.41*
37	8800	14.31*	16.03	15.59*	15.49*	15.43*
38	9000	14.30*	16.04	15.59*	15.51*	15.45*
39	9200	14.29*	16.04*	15.60*	15.52*	15.47*
40	9400	14.28*	16.04*	15.60*	15.54*	15.50*
41	9600	14.27*	16.05*	15.61**	15.56*	15.52*
42	9800	14.26**	16.05*	15.61**	15.58*	15.54*
43	10000	14.25**	16.05**	15.62**	15.59**	15.56**

Notes: Absolute errors are ~ ± 0.03 mag, except G24-9 and G157-34 (± 0.05 mag).
Errors relative to λ5400 are ~ ± 0.03-0.04 mag, unless marked otherwise.
* Probable error relative to λ5400 is ~ ± 0.06 mag.
** Probable error relative to λ5400 is ~ ± 0.09 mag.
*** Probable error relative to λ5400 is ~ ± 0.12 mag.

REFERENCES

Atwood, B., Ingerson, T., Lasker, B. M., and Osmer, P. S. 1979, Pub. A.S.P., 91, 120.

Baldwin, J. A., and Stone, R. P. S. 1984, M.N.R.A.S., 206, 241.

Boksenberg, A. 1972, in Auxiliary Instrumentation for Large Telescopes, Proc. of the ESO-CERN Conference, S. Lausten and A. Reiz, eds., p. 295.

Boksenberg, A, and Burgess, D. E. 1973, in Astronomical Observations with the Television-Type Sensors, J. W. Glaspey and G. A. H. Walker, eds. (Vancouver: University of British Columbia), p. 21.

Breger, M. 1976, Ap. J. Suppl., 32, 1.

Fernie, J. D. 1976, Pub. A.S.P., 88, 969.

Filippenko, A. V. 1982, Pub. A.S.P., 94, 715.

Giclas, H. L., Burnham, R. Jr., and Thomas, N. G. 1971, Lowell Proper Motion Survey, Northern Hemisphere, the G Numbered Stars.

———. 1978, Lowell Obs. Bull. No. 164, Vol. VIII, No. 4.

———. 1979, Lowell Obs. Bull. No. 165, Vol. VIII, No. 5.

———. 1980, Lowell Obs. Bull. No. 166, Vol. VIII, No. 6.

Greenstein, J. L. 1976, Ap. J. (Letters), 207, L119.

———. 1984, Ap. J., 276, 602.

Hayes, D. S. 1970, Ap. J., 159, 165.

Hayes, D. S., and Latham, D. W. 1975, Ap. J., 197, 593.

Kent, S. M. 1979, Pub. A.S.P., 91, 394.

Luyten, W. J. 1957, A Catalogue of 9867 Stars in the Southern Hemisphere with Proper Motions Exceeding 0.2" Annually. (Lund Press, Minneapolis, Minn.).

———. 1979, NLTT Catalogue. (Univ. of Minnesota,

Minneapolis, Minn.).

Oke, J. B. 1964, Ap. J., 140, 689.

———. 1969, Pub. A.S.P., 81, 11.

———. 1974, Ap. J. Suppl., 27, 21.

Oke, J. B., and Gunn, J. E. 1982, Pub. A.S.P., 94, 586.

———. 1983, Ap. J., 266, 713.

Oke, J. B., and Schild, R. E. 1970, Ap. J., 161, 1015.

Shectman, S. A., and Hiltner, W. A. 1976, Pub. A.S.P., 88, 960.

Sion, E. M., Greenstein, J. L., Landstreet, J. D., Liebert, J., Shipman, H. L., and Wegner, G. A. 1983, Ap. J., 269, 253.

Stone, R. P. S. 1974, Ap. J., 193, 135.

———. 1977, Ap. J., 218, 767.

Stone, R. P. S., and Baldwin, J. A. 1983, M.N.R.A.S., 204, 347.

Wegner, G., and Yackovich, F. H. 1982, A. J., 87, 155.

FIGURE CAPTIONS

Figure 1: Finding charts (12′ x 12′) are given for the new standard stars. North is at the top, and east to the left. The number and epoch of each Palomar plate is as follows: G158-100 (E-1203, 1954); G138-31 (E-1372, 1955); G24-9 (E-805, 1953); G157-34 (E-306, 1951); GD-248 (E-320, 1951).

Figure 2: Spectra of faint spectrophotometric standards are shown. A smooth curve ($\lambda\lambda$3240-10060), derived from MCSP observations, represents the featureless continuum of each star, and filled circles correspond to the values listed in Table II. Optical spectra having moderate resolution demonstrate the presence of weak absorption lines. The feature (B band) at ~ λ6860 is due to atmospheric oxygen molecules.

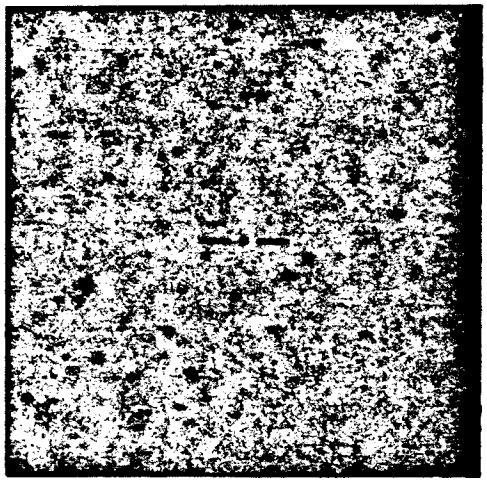

G158-100

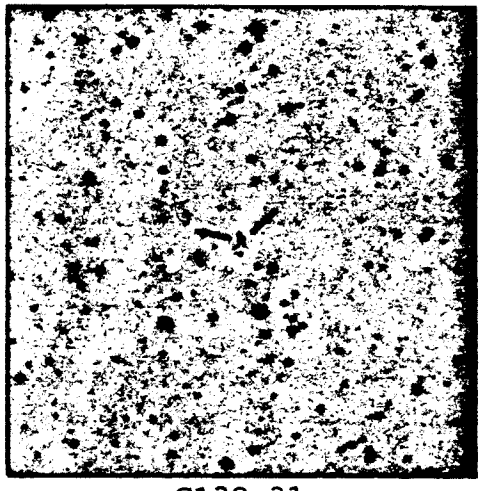

G138-31

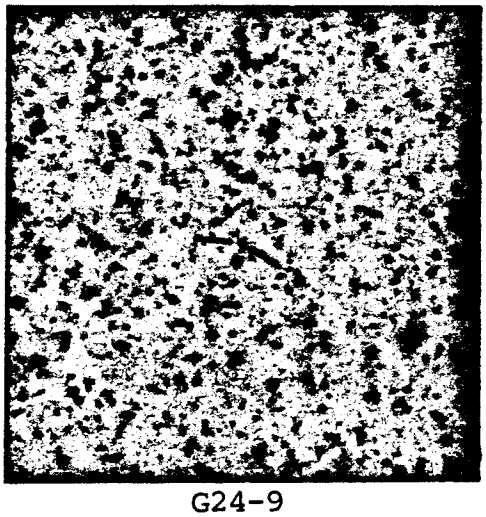

G24-9

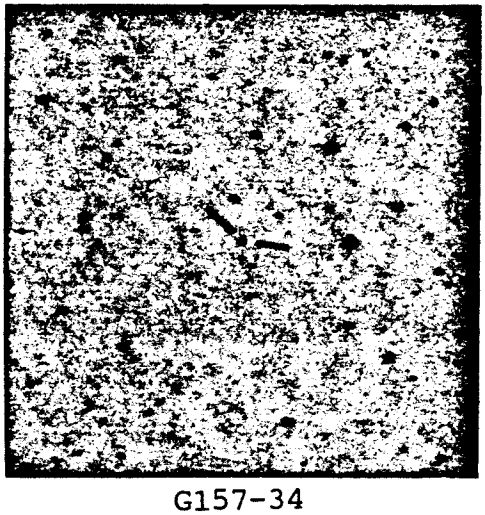

G157-34

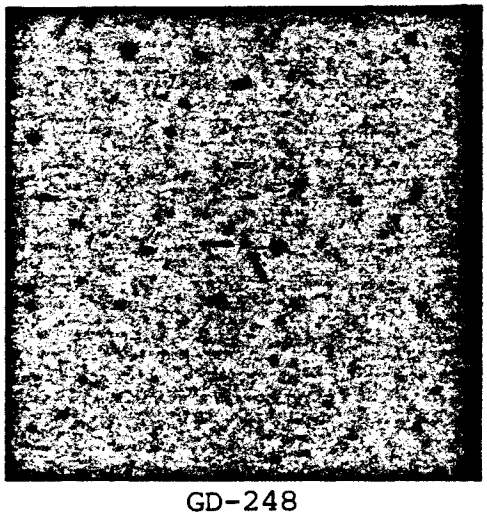

GD-248

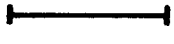

4 ARCMIN

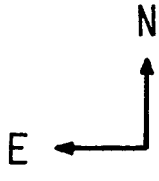

POSS E

Figure 1

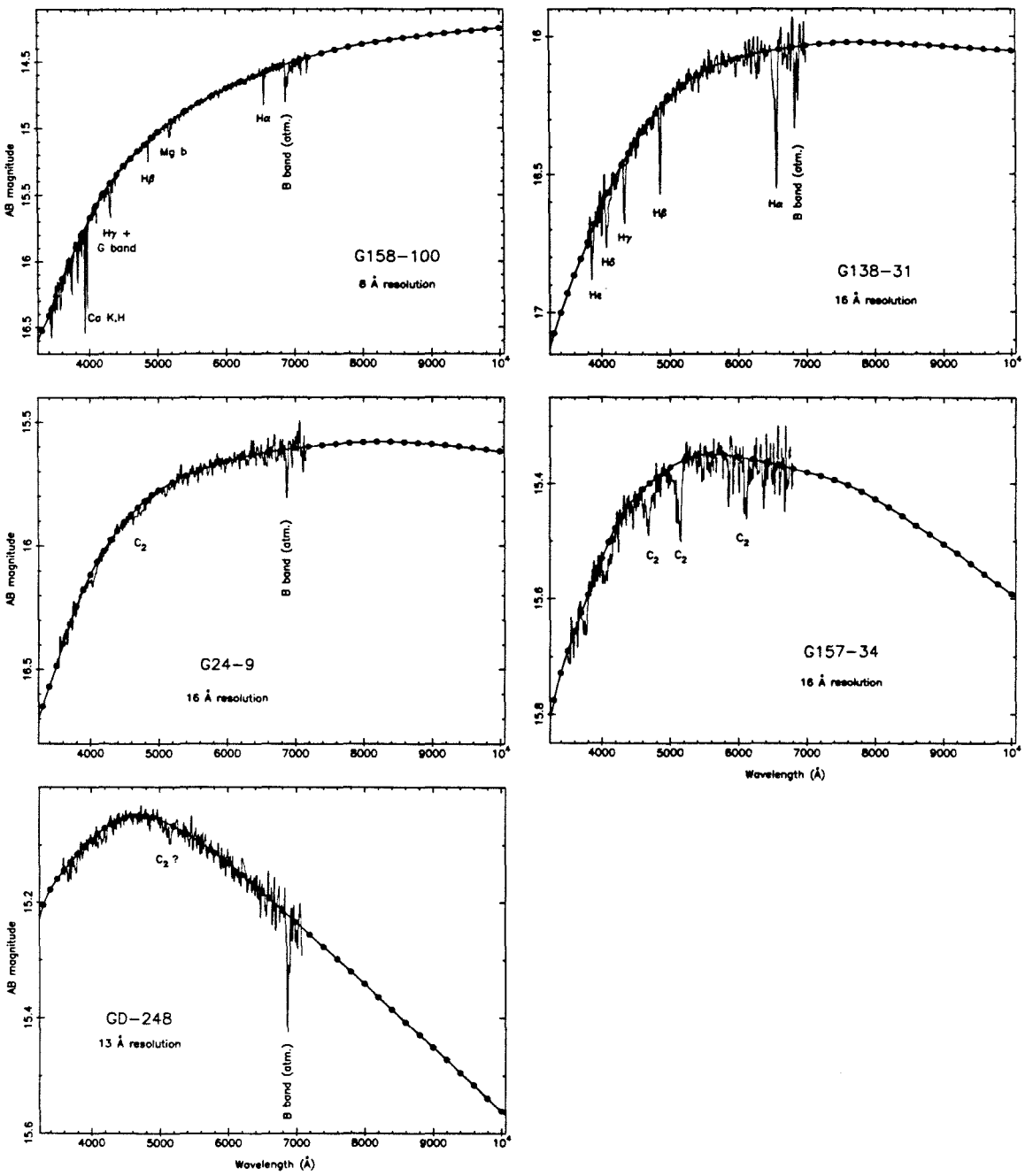
G158-100
8 Å resolution
Ca K,H
Hγ + G band
Mg b
Hβ
Hα
B band (atm.)
G138-31
16 Å resolution
Hε
Hδ
Hγ
Hβ
Hα
B band (atm.)
G24-9
16 Å resolution
C2
B band (atm.)
G157-34
16 Å resolution
C2
C2
C2
GD-248
13 Å resolution
C2 ?
B band (atm.)
AB magnitude
Wavelength (Å)

Figure 2

And thus we die,

Still searching, like poor old astronomers

Who totter off to bed and go to sleep

To dream of untriangulated stars.

Octaves, XI

Edwin Arlington Robinson